Advanced Thin Layer Deposition of Materials for Li-ion Batteries via Electrospray

Proefschrift

ter verkrijging van de graad van doctor
aan de Technische Universiteit Delft,
op gezag van de Rector Magnificus
Rector Magnificus, Prof. ir. K.C.A.M. Luyben
voorzitter van het College voor Promoties,
in het openbaar te verdedigen op

vrijdag 31 january 2014 om 10:00 uur

door

Esteban GARCIA-TAMAYO

Ingeniero Físico
Universidad EAFIT - Medellín

geboren te Medellín, Colombia

Dit proefschrift is goedgekeurd door de promotoren:

Prof. dr. S.J. Picken

Copromotor:

Dr. ir. E.M. Kelder

Samenstelling promotiecomissie:

Rector Magnificus	Technische Universiteit Delft, voorzitter
Prof. dr. S.J. Picken	Technische Universiteit Delft, promotor
Dr. ir. E.M. Kelder	Technische Universiteit Delft, copromotor
Prof. dr. E.H. Brück	Technische Universiteit Delft
Prof. dr. B. Dam	Technische Universiteit Delft
Prof. dr. M. Koper	Universiteit Leiden
Prof. dr. K. Edstrom	Uppsala Universitet
Prof. dr. A. Chadwick	University of Kent
Prof. dr. F.M. Mulder	Technische Universiteit Delft, reservelid

Cover design by Stefania Masuino

ISBN 978-94-6186-251-8

Advanced Thin Layer Deposition of Materials for Li-ion Batteries via Electrospray

Thesis

presented for the degree of doctor
at Delft University of Technology,
under the authority of the Vice-Chancellor,
Rector Magnificus, Prof. ir. K.C.A.M. Luyben
Chairman of the Board of Doctorates,
to be defended in public in the presence of a committee on

Friday, January 31st, 2014 at 10:00 o'clock

by

Esteban GARCIA-TAMAYO

Degree in Engineering Physics
Universidad EAFIT - Medellín

Born in Medellín, Colombia

This thesis is approved by the promoters:

Prof. dr. S.J. Picken

Supervisor:

Dr. ir. E.M. Kelder

Composition of Examination Committee:

Rector Magnificus	Technische Universiteit Delft, chairman
Prof. dr. S.J. Picken	Technische Universiteit Delft, promoter
Dr. ir. E.M. Kelder	Technische Universiteit Delft, supervisor
Prof. dr. E.H. Brück	Technische Universiteit Delft
Prof. dr. B. Dam	Technische Universiteit Delft
Prof. dr. M. Koper	Universiteit Leiden
Prof. dr. K. Edstrom	Uppsala Universitet
Prof. dr. A. Chadwick	University of Kent
Prof. dr. F.M. Mulder	Technische Universiteit Delft, reserve member

Cover design by Stefania Masuino

ISBN 978-94-6186-251-8

A mi querida Familia and to my dear Friends

What an astonishing thing a book is. It's a flat object made from a tree with flexible parts on which are imprinted lots of funny dark squiggles. But one glance at it and you're inside the mind of another person, maybe somebody dead for thousands of years. Across the millennia, an author is speaking clearly and silently inside your head, directly to you. Writing is perhaps the greatest of human inventions, binding together people who never knew each other, citizens of distant epochs. Books break the shackles of time. A book is a proof that humans are capable of working magic

---

Carl E. Sagan, *Cosmos*, 1980

Contents

List of Figures

List of Tables

Chapter 1

Introduction

> Good people drink good beer
>
> Hunter S. Thompson, *Fear and Loathing in Las Vegas*, 1971

This chapter gives an introduction to the subject of Li-ion batteries. At first, a discussion on current issues such as sustainabily will be covered in order to put the topic of energy storage into perspective. This will be followed by a historical review of how and when Li-ion batteries came to be, stopping briefly to describe how an electrochemical cell works. Further, a comparison will be shown between existing battery technologies and where that of Li-ion stands in terms of volumetric and gravimetric energy densities, as well as in specific power and energy (Ragone plot). This will then lead to what will be the main topic of this thesis, 'Thin Film and 3D (micro) Batteries'. Finally, a description of materials for Li-ion batteries for both positive and negative electrodes will be described.

1.1 Thoughts on Sustainable Energy

The scientific consensus about the reality of anthropogenic climate change is clearly expressed in the reports of the Intergovernmental Panel on Climate Change (IPCC). This scientific body "*was established by the United Nations Environment Programme (UNEP) and the World Meteorological Organization (WMO) in 1988 to provide the world with a clear scientific view on the current state of knowledge in climate change and its potential environmental and socio-economic impacts*" [1]. In its most recent assesment report (2007), this panel states, unquestionably, a summary of main findings taken from the scientific consensus, from which only a couple of items will be extracted:

- "Observational evidence from all continents and most oceans shows that many natural systems are being affected by regional climate changes, particularly temperature increases."
- "A global assessment of data since 1970 has shown it is likely that anthropogenic warming has had a discernible influence on many physical and biological systems"

Nowadays, the main energetic source used by mankind are fossil fuels. According to the International Transport Forum, "*Transport-sector CO_2 emissions represent 23% (globally) and 30% (OECD) of overall CO_2 emissions from Fossil fuel combustion. The sector accounts for approximately 15% of overall greenhouse gas emissions*" [2]. One of the main drawbacks of fossil fuels, is that they are not sustainable as the amount of time needed for the fossilization of the organic matter is extraordinarily large compared with the time involved in the combustion proccess. This means that the oil deposits are going to end while the energy demand will continue to rise [3].
Sustainability is a concept that accounts for the intimate relationship between the development of our modern society and the quantity of raw materials available on the planet. *Energy* is a wide term that comprises more than one meaning. The one that will mainly be used in this thesis, unless otherwise stated, is that of the word used in economics to describe the part of the market where it is used as a resource that is harnessed and sold to consumers. In an attempt to bring objectivity in the discussion around the topic of *sustainable energy*, several institutions have formulated definitions of the term. The British Renewable Energy and Efficiency Partnership, for example, defines it as: *'The provision of energy such that it meets the needs of the future without compromising the ability of future generations to meet their own needs'* [4].

According to this institution, 'Sustainable Energy' has two key components, namely Renewable Energy and Energy Efficiency.

The first term accounts to the production of energy and can be divided in three categories: *1st Generation*, or *Old Technologies*, are those that have been used already for more than a century, e.g. hydroelectrical, hydrothermal or geothermal plants; *2nd Generation*, or *Current Technologies*, are those that have already proven their concept, but are still a major subject of research and development. Nonetheless, these techonologies are currently under implementation and their market is considered to experience strong growth in the next couple of decades. Some examples include wind turbines, photovoltaic solar cells, biomass and biofuels; finally, *3rd Generation*, or *Future Technologies*, do not yet have a fully proven concept, but are expected to contribute significantly to future clean energy production. Hot dry rock geothermal energy, ocean energy and nuclear fusion, are some examples [5].

The second term covers the correct utilisation of the energy in terms of its consumption, production and storage. Therefore, the *Reduction of energy dependency*, to start with, can be achieved by optimising the energy use of appliances and installations. The replacement of ordinary light sources for energy efficient LED lights, the improvement of house insulation or strong policies on food production and consumption, especially meat, are some examples of such strategies. Secondly, the *Optimization of energy production* can achieve large improvements in efficiency by, for instance, capturing and (re) using the heat, which is produced as by-product when electricity is generated, to process steam, heating or other industrial purposes. This 'cogeneration', used to describe combined use of heat and power, can increase the plant's efficiency drastically [5]. Finally, the intermittent nature intrinsically found in renewable energy production sources such as wind turbines or solar cells, imperatively calls for the neccesity to store the energy at times of high-production, to ensure a reliable supply at times of low-production. It is important to remark that in this thesis I will restrict the term 'energy storage' to 'electricity storage', taking into consideration the existance of other methods to store energy.

The most familiar electricity storage devices are batteries. Compared to other mechanisms, the energy capacity of batteries is relatively low but its efficiency is high (>95%). This makes batteries an ideal energy storage system for small scale applications. To exemplify this, the International Energy Agency reports that over 180.000 passenger car Electric Vehicles (EVs) sold worldwide trough 2012 and though represent only 0.02% of the total passenger car stock at present, they expect a global deployment of at least 20 million passenger car EVs, including plug-in hybrids and fuel-cell electric vehicles, by 2020 [6]. Since the use of cars accounts for a large portion of the daily energy consumption, a continuous increase of EV adoption might lead to improved grid stabilization.

In order to continue the discussion, it is important to briefly define what

batteries are. The main purpose of these electrochemical energy-conversion devices is to take advantage of the chemical processes occurring within the system (which are translated into potential energy in the form of chemical energy) and convert it into electrical energy. According to Dell and Rand [7], the convenience of batteries lies in the wide range of sizes in which they may be manufactured or assembled into packs, their ability to supply electrical power instantly, their portability (for smaller sizes), and the option of single-use or multiple-use units. The last two items provide the terms accepted for the classification of batteries and can be summarized into two broad categories: (i) 'primary batteries', which can be used only once, spending all their 'chemical fuel' during the first (and only) discharge; (ii) 'secondary batteries', which have the possibility to be recharged and used again with the help of an electrical energy source connected to the system.

1.2 A brief historical review on Li-ion batteries

There have been more than 200 years of battery technology improvement, starting with Alessandro Volta in 1800 with his famous letter to the Royal Society of London where he described his famous experiment, continuing with John Daniell who invented the cell that carries his name (consisting in the famous couple copper/zinc electrodes), and going through a series of huge developments in the field made by French chemists Leclanche (who invented the first primary cell that bears his name, in 1866), Plante (who developed the first effective secondary rechargeable battery named "lead acid battery", in 1859) and Faure (who in 1888, showed how to increase the capacity and reduce the time of plate formation of Plante's battery), led the Swedish scientist Waldemar Junger, around the turn of the 19th century, to patent the first work on batteries with alkaline solutions named as "nickel-cadmium battery. At about the same time, Thomas Edison in the USA developed the "nickel-iron battery". These systems were similar in principle, except that in the first case a cadmium-iron mixture was used as negative electrode, while in the second one an all-iron electrode was used instead.

The 20th century began and Quantum Mechanics was born bringing with it a new field of knowledge: electronics. In just a few decades humanity faced an almost incredible development of new devices, each of them surprising. Between them the transistor takes, by far, the first place. Even more incredible than these inventions was the pace at which they were developing and it was Moore, in 1965, who described this trend. Battery science could not keep this pace even though completely new technologies in primary and (rechargeable)

secondary batteries were developed and commercialized. The most remarkable ones were the nickel-metal hybrid and lithium ion batteries. Several reviews and accounts on the historical developments in Li-battery research can be found on the literature [8, 9].

Li-ion batteries, which will be the subject of this thesis, followed a previous technology which used metallic lithium as one of its electrodes (anode) and was firstly investigated in the 1970s [10]. The motivation for using a battery technology based on Li metal as anode relied initially on the fact that Li is the most electropositive (-3.04 V versus standard hydrogen electrode) as well as the lightest (equivalent weight M = 6.94 g mol^{-1}, and specific gravity $\rho = 0.53$ g cm^{-3}) metal, thus facilitating the design of storage systems with high energy density. The so-called intercalation compounds started to appear in the scientific radar over the same period and their discovery was crucial in the development of high-energy rechargeable Li systems. Initial demonstrations of such batteries proofed them to be energetically successful [10, 11], but they soon encountered safety issues due to the Li-metal/liquid electrolyte combination which lead to Li dendrites growing as the metal was replated over subsequent charge and discharge. While some groups were substituting metallic lithium with an Al alloy to circumvent these safety issues [12], research on intercalation materials, specially oxides, were giving higher capacities and voltages [13]. A particular breakthrough proposed by Goodenough, at the beginning of the 1980s, with his family of intercalation transition metal oxides Li_xMO_2 (where M = Co, Ni, or Mn) [14], would pave the way to what is found, almost exclusively, in the Li-ion battery technology, even at present.

The principle of rocking-chair, which already existed for the Ni-MeH batteries, was proposed first by Murphy [15] and then by B. Scrosati et al. [16]. It consisted in the substitution of metallic lithium for another insertion material, initially with rutiles, as was the case in the former at Bell laboratories, and later with a Li_xWO_2 /Li_yTiS_2 system, as was the case in the latter. These preliminary findings led in the late 1980's to the discovery of the highly reversible, low-voltage Li intercalation-deintercalation process in carbonaceous material [17] and with it, at the beginning of the 1990's, to the creation of the C/$LiCoO_2$ rocking-chair cell commercialized by Sony Corporation in June 1991 [18]. This type of Li-ion cell, having a potential exceeding 3.6 V (three times that of alkaline systems) and gravimetric energy densities as high as 120-150 Wh kg^{-1} (two to three times those of usual Ni-Cd batteries) [8], revolutionized portable electronics and is found in most of today's portable devices.

It is well accepted that a battery, no matter which type, consists basically in a distribution of electrochemical cells in tandem. Depending on the application these arranges, and the connection between them, varies. In order to

understand how a battery works, the description of its elemental building block will be given in the next section.

1.3 Electrochemical Cell

An electrochemical cell communicates with the external world through the connection of two (conductive) contacts, one with the negative and the other one with the positive electrode. These electrodes are commonly (but inaccurately[1]) referred to as anode and cathode, respectively. In spite of this, these terms will be interchangeably used throughout this thesis. A schematic illustration of the setup can be observed in Figure 1.1.

The process shown in the schematic occurs during cell discharge. When

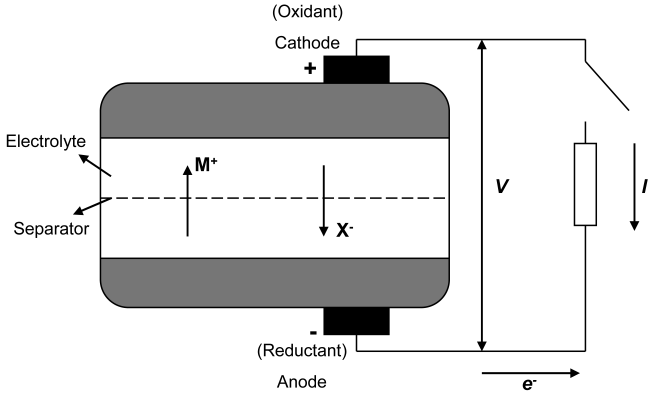

Figure 1.1 – Elements of an Electrochemical Cell Direction of the arrows correspond to the discharge.

an electrical load (i.e. electronic devices or household appliances) is plugged

[1]This misconception arises in the fact that, in a galvanic cell (this is, a discharging battery), a cathode acts always as positive since it is where the current flows out of the device, leaving the anode as the negative electrode. But, when a cell works as a power consuming device (i.e, during charging cycle) the cathode acts as the negative terminal, because it sends current back to the external source, leaving the anode as the positive electrode

and the circuit closed, electrons flow from anode to cathode creating an electronic current I, in the direction shown. In the case of Li-ion batteries, ions are flowing in the same direction (from anode to cathode) in order to convert chemical energy into electrical energy. Ions move between the electrodes by means of an electrolyte which has the property to be good electronic insulator and good ionic conductor. As a liquid electrolyte is used in most of the cases, a separator is placed in the middle in order to maintain an even spacing between both electrodes. This separator must provide blocking of electronic current and permeation of its ionic analogue.

During charge, an external voltage is applied to the circuit forcing electrons and ions to flow from cathode to anode. This process is performed to convert electrical energy back to chemical energy. The chemical produced at the anode during charge, or consumed while discharging, is the reductant of the chemical reaction. Likewise, the chemical produced on charge at the cathode, and consumed while discharging, is the oxidant. The maximum voltage provided by an electrochemical cell is given by the division of the energy, produced by the reaction between reductant and oxidant, over the electronic charge passed in the reaction. This value is also the minimum voltage required to charge the cell.

1.4 Rechargeable Batteries

As mentioned before, the increase in the demand of rechargeable batteries in order to power portable electronic devices as well as applications such as wireless sensors, high-power consumption tools and HEVs/EVs, among others, require the optimization of the available technologies or the discovery of novel ones. The goal thus is to obtain an energy storage system in which the amount of energy stored in a given mass or volume unit is as high as possible. To compare the energy content of cells, the terms specific energy (Wh kg^{-1}) and energy density (Wh L^{-1}) are widely accepted. Figure 1.2 [9], shows a comparison of different rechargeable battery technologies and where they stand in terms of their volumetric and gravimetric energy density. When moving upward in the *'y'* axis, batteries tend to become more compact due to the fact that a larger amount of energy can be stored in a smaller volume. Correspondingly, when going forward in the *'x'* axis, batteries become lighter because a larger amount of energy can be stored in a smaller amount of mass.

It is clear from Figure 1.2 that Li-ion technology, whatever its form (standard Li-ion, Li Polymer or thin film Li-ion), currently outperforms its homologous in terms of both volumetric and gravimetric energy density. Moreover,

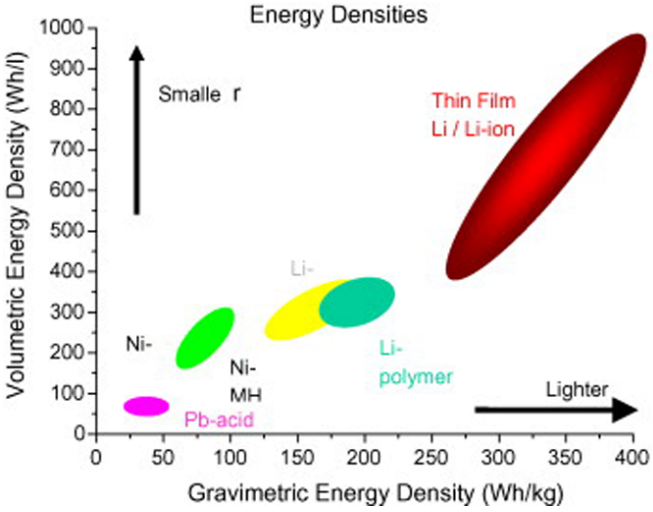

Figure 1.2 – Comparison of (rechargeable) battery technologies in terms of volumetric and gravimetric energy density. This particular graph excludes other technologies like lithium-sulphur and metal-air batteries. Adapted from [Patil et al., 2008]

it is clear that to achieve higher energy density, especially for portable electronics and small-scale applications such as MEMS or wireless sensors, this industry relies in the success of achieving optimized thin films Li-ion systems. It is important to remark that this plot does not include novel and promising technologies like Li-sulfur or Li-air which are currently under intensive research but without practical applications at present.

Batteries are the most commonly used power source for complementary

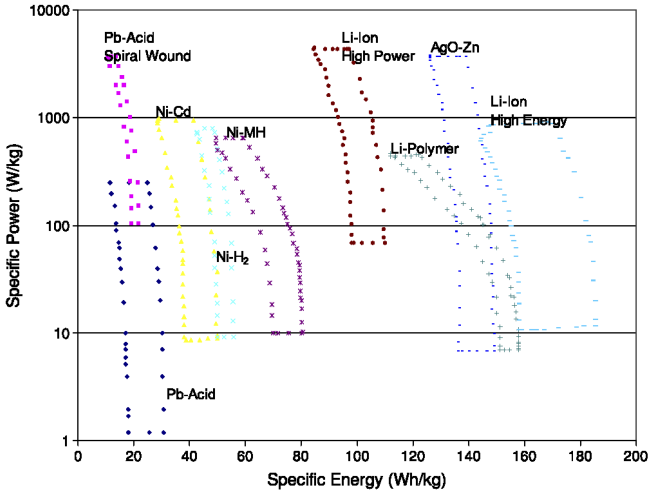

Figure 1.3 – Ragone plot comparing the performance of various battery electrochemistries. Note also that the various time intervals, in which the energy is being delivered, are indicated by the dotted lines. Adapted from [Cook-Chennault et al., 2008]

metal-oxide semiconductor (CMOS) based MEMS. They can be used for both power generation and energy storage, provide continuous energy, have relatively high energy and power densities, and can generally be easily replaced without substantial modifications to a device. Moreover, they also provide direct and continuous current and therefore do not require complex signal conditioning for conversion of alternating current to direct current, as do regenerative power supplies, such as photovoltaic, electromagnetic and piezoelectric generators [19]. A Ragone plot comparing battery technologies is shown in Figure 1.3.

The power supply in the majority of portable electronics, no matter in

which electrochemistry is based, is several times larger than the size of the device itself [20]. The disparity between battery and host device size results from the nonlinear scaling of battery size with the diminishing sizes of transistors [21] in CMOS-based MEMS. For example, mobile phone batteries account for up to 36% of the mass of the entire phone [19]. The difficulty in reducing battery size is based on the inherent specific energy and energy densities of commonly used primary and secondary batteries and the inability of these batteries to meet growing life cycle demands of portable electronics and biomedical devices. Therefore a number of workers have developed lithium-ion thin-film, thick-film and 3D batteries [22–38] for powering MEMS based portable electronics.

1.5 Thin Film and 3D (micro) Batteries

In the previous subsection it was shown how Li-ion ion batteries are one of the most promising energy storage systems for a wide range of applications due to their high energy density and how, for the development of autonomous integrated systems within the field of small-scale applications, Li-ion microbatteries are even of greater interest. The possibility to include the energy storage device into integrated electronic circuits will lead to autonomous functionality [39] (smart autonomous sensors, radio frequency identification tags, smart cards). The purpose of this section is to discuss the historical background/context and design of thin film batteries and it is of great importance as this will be the subject of most of experimental work presented in this thesis. Chapters 4, 5 and 6 will deal with the implementation of novel deposition techniques for the production of thin films for battery applications.

Chapter 5, in particular, examines the results obtained during a large European project where thin film cathode layers of high voltage $LiNi_{0.5}Mn_{1.5}O_4$ are deposited on especially customized silicon wafers for the development of a novel 3D Li-ion microbattery. The synthesis technique employed, allows the production of layers with capacities up to the required capacity per square centimeter, by adjusting its thickness. The method in that respect also show acceptable homogeneity within the ”holes” or ”grooves” of an etched Si wafer and demonstrates its potential in the production of 3D all solid state Li-ion batteries. A complete thin film battery stack was done in collaboration with an European Consortium. The role of the TU Delft and scope of my work, which will be throughly described in Chapter 5, was to synthesise and deposit positive electrode materials on flat and textured substrates, which were then

delivered to the partners for the completion of the stack.

In roder to have a clearer discussion, the similarities and differences between regular Li-ion and thin film Li-ion batteries will be shown in the next subsection.

1.5.1 Historical background and Context

Thin film batteries started, in practice, in 1982, when Hitachi Co. in Japan announced their solid-state thin film battery. It was composed by a TiS_2 cathode prepared by Chemical Vapour Deposition (CVD), a $Li_{3.6}Si_{0.6}P_{0.4}O_4$ glass electrolyte by Radio Frequency (RF) sputtering, and metallic lithium as anode deposited via a vacuum evaporation technique. Around the mid 1980s, a $WO_3V_2O_5$ cathode prepared by sputtering in H_2-Ar plasma, was also combined with the above battery [40].

NTT Co. Group in Japan had developed thin film batteries by using $Li_{3.4}V_{0.6}Si_{0.4}O_4$ glass as electrolyte and $LiCoO_2$ [41] and $LiMn_2O_4$ [42] for cathodes by using RF sputtering. The battery size was about 1 cm^2 and the thickness was 1-5 μm of cathode, 1 μm of electrolyte and 4-8 μm of lithium anode. Over the same period, Bellcore Co. presented its lithium cell consisting of $LiMn_2O_4$ cathode, a lithium borophosphate (LiBP) glass or lithium phosphorus oxynitride glass (LiPON) for electrolyte and metallic lithium as anode. The cell had a 4.2 OCV and operated between 3.5 - 4.3 V, with an areal capacity of 70 $\mu A/cm^2$ for more than 150 cycles. The LiPON was prepared by RF sputtering of Li_3PO_4 target in nitrogen gas. This electrolyte is rather stable in comparison with other lithium oxide or sulfide based glasses, in spite of moderate ionic conductivity of 2.3 x 10^{-6} S cm^{-1} at room temperature and activation energy of 0.55 eV [43]. The stability range of LiPON was from 0 to 5.5 V with respect to Li electrode. Lithium metal anode was prepared by vacuum evaporation, and LiPON electrolyte and cathodes of $LiCoO_2$, $LiMn_2O_4$, etc., were made by RF sputtering. LiPON is now recognized as a standard solid electrolyte for thin film lithium batteries and has been used by many groups.

In 1999, Bellcore researchers introduced polymeric electrolytes in a liquid Li-ion system. They developed the first reliable and practical rechargeable Li-ion hybrid polymer electrolyte (HPE) battery, referred to as plastic Li-ion, which differs considerably from the usual coin-, cylindrical- or prismatic-type cell configurations. Such a thin-film battery technology, offers shape, versatility, flexibility and lightness. Contemporary to this, important technological innovations emerged from the field of microelectromechanical systems (MEMS) and other small devices such as medical implants, micro sensors and self pow-

ered integrated circuits [44]. However, this increase in miniaturization, not to mention their integration and energy autonomous performance, is today limited by the low energy density of batteries. Such devices need rechargeable batteries with dimensions on the scale of 1-10 mm^3 including all the components and all the associated packaging [45].

Several reviews on the historical developments, concepts, materials and progress in planar and 3D Li-ion microbattery research can be found in the References [44–48].

1.5.2 Design

There are no fundamental differences between the physics and the chemistry of thin layer batteries and other Li-ion batteries: they also consist of two current collectors, two electrodes, an electrolyte in between and a packaging unit. The main difference consists in their architecture and in the fact that they typically have a solid electrolyte like LiPON [49] or a polymer [50, 51]. When such electrolyte is utilised, in the literature this cell is usually referred to as an 'All-Solid-State Microbattery'. Therefore, most of the electrode materials' used in normal Li-ion batteries are also employed in their thin film counterparts. Historically, the idea of reducing the internal resistance of the cell was the first reason for the use of thin film electrodes. The drawback of this concept is the low capacity as this is proportional to the surface area and thickness of the electroactive layer. Recently, the development of 3D-architectured systems has shown a new horizon for micro battery applications [46, 52, 53]. Due to a higher surface-to-volume ratio, the layered thin film structure exhibits higher energy densities [45–47, 52, 54].

One immediate advantage over conventional Li-ion technology is demonstrated theoretically by the decrease of diffusion path length for both charge carriers, namely electrons and ions. The diffusion time (τ) is directly proportional to the square of the diffusion lenght (l), as described by:

$$\tau \approx l^2/D \tag{1.5.1}$$

where D is the diffusion coefficient.

Therefore the decrease in thickness of all active layers, namely anode, cathode and electrolyte, directly yields a reduction of ionic and electronic transference time, enhancing the power delivery.
Solid state lithium batteries have been studied for about 50 years. Their advantages compared to those using a liquid electrolyte are the ease of utilization, resistance to shocks and vibrations, absence of possible pollution due to liquid

electrolyte, thermal stability, absence of self-discharge (owing to the very low electronic conductivity of the solid electrolytes generally used) and miniaturization. The current densities obtained with these batteries were generally low because of the high internal resistance of the cell, which mainly results from the low ionic conductivity of the electrolyte [55]. Over the last 20 years thin film Li-ion microbatteries have emerged as surface mountable devices up to about 10 μm thick [26, 56]. Despite the many achievements gained over these years in terms of energy density and miniaturization, the evolution of modern MEMS constantly imposes a challenge in the energy sources because of the limited energy and power available per area of footprint on the substrate. In this regard, the conventional path usually followed in battery design, which consists on increasing the thickness of the layers to get higher gravimetric energy, does not solve this problem in a thin film cell because it also increases the current path length, leading to a reduction in power density. Therefore, the concept of capacity per footprint area (mAh cm^{-2}) becomes a key consideration for the construction of microbatteries where the limitation is the area available, contrary to the typical concept in larger battery technologies where charge storage is defined in terms of gravimetric (mAh g^{-1}) and volumetric capacities (units mAh cm^{-3}) [46].

These microbatteries can be manufactured with a footprint area of less than a few square millimeters. Moreover, as mentioned before, their thickness can also be greatly decreased, especially because solid-state electrolytes have a typical thickness of approximately 1 μm, whereas the separator in liquid electrolyte-based cells typically has a thickness of 20 μm. This technology also provides the feasibility to use almost any material as a substrate, i.e. glasses [45], ceramics [28, 45], metals [28], polymers [28] or paper. More important, the usage of film deposition, especially for the electrolyte, opens the possibility to directly write or print onto substrates of interest (including electrodes with complex geometries). A schematic representation of such architecture is presented in Figure 1.4. It consists of a positive and a negative electrode, separated by a solid thin film electrolyte, each of them connected to independent current collectors. On top of them all, a packaging structure must be employed to provide protection against external chemical and physical phenomenon, hence reducing parasitic reactions of the active components [45].

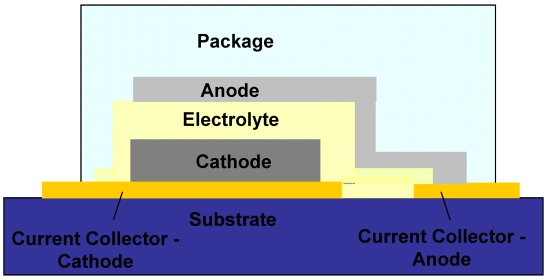

Figure 1.4 – Schematic representation of a planar solid-state thin film battery

1.6 Materials for Li-ion Batteries

In order to maximize volumetric and gravimetric energy densities, two requirements must be met: (i) increase in the specific capacity (Ah kg^{-1}) and charge density (Ah L^{-1}); (ii) high difference of potential between positive and negative electrodes inside the batteries.

A wide range of materials for both negative and positive electrodes is shown in Figure 1.5 [8]. In this scheme, the y axis represents the potential (in units of volts) of each material compared to metallic lithium (which has the most electropositive standard potential compared to hydrogen) and in the x axis the capacity (Ah kg^{-1}).

1.6.1 Materials for positive electrodes

Typical materials for positive electrodes are intercalation compounds made from Li-metal oxides, which provides a source of lithium stable in air and with a relatively high potential. They consist mostly of layered structures such as $LiCoO_2$ and $LiNiO_2$ that allow Li ions to move back and forth between their lattice planes. Safety concerns associated with these materials prevent its use in transportation and stationary storage applications. Their chemical instability, and the consequential safety concerns, arising from an overlap of the $M^{3+/4+}$: 3d band with the top of the O^{2-}:2p band, have been widely studied [57, 58]. This feature is more pronounced for the $Co^{3+/4+}$ couple and, hence, both the Ni and $Mn^{3+/4+}$ couples offer better safety. As a consequence, layered solid solutions like the $LiNi_{1/3}Mn_{1/3}Co_{1/3}O_2$ cathode [59, 60] are replacing $LiCoO_2$ in portable electronics due to better safety and lower cost [61].

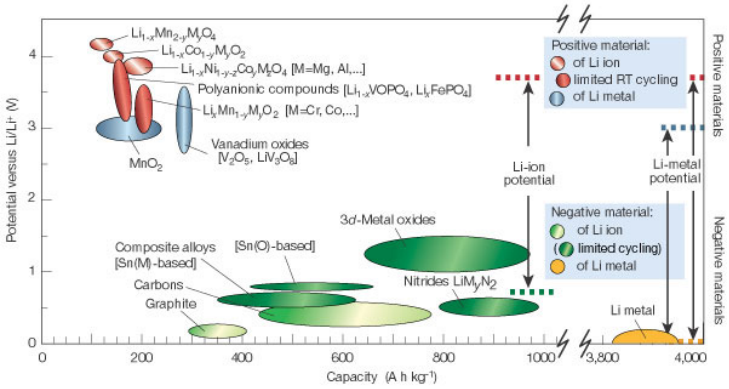

Figure 1.5 – Voltage versus capacity for positive- and negative-electrodes of rechargeable Li-based cells. Adapted from [Tarascon et al., 2001]

Because of the safety concerns and high cost, alternative materials like the spinel $LiMn_2O_4$ and the olivine $LiFePO_4$ have become appealing. Besides, the materials are interesting for its environmental friendliness. Still, they need to show good structural and chemical stabilities, and high charge-discharge rate capability. For the $LiMn_2O_4$, its three dimensional cubic spinel structure also provides wider 3D-pathways for Li [62], but it also present intrinsic disadvantages in terms of structural changes and limited cycle life, as well as Mn dissolution due to disproportionation of Mn^{3+} into Mn^{4+} and Mn^{2+} at high potentials [63, 64]. These issues could be suppressed significantly by cationic and anionic substitution, or by surface modifications [61]. In the case of the olivine $LiFePO_4$, it yields a very stable potential up to its full capacity (i.e. 170 mAh g^{-1}, it is stable at elevated temperatures (up to 85 °C) over prolonged cycling [65], however the major issue with $LiFePO_4$ is the poor lithium ion and electronic conduction. Further development of this material by carbon coating [66, 67] or even using non-coated nanoparticles makes it possible to fabricate operational electrodes, but it involves high processing cost associated with its manufacturing under controlled atmosphere.

1.6.2 Materials for negative electrodes

As pointed out earlier, to overcome certain safety issues, intercalation materials were preferred over metallic lithium for the negative electrode. In that respect, graphite is an interesting material as it accepts and donates Li ions, while being an excellent electronic conductor [68]. Despite its interesting properties, the ratio between Li-ions and carbon atoms, i.e. 1:6, which yields a theoretical capacity of 372 mAh g^{-1}, is rather low. Another commonly used anode material is the spinel $Li_4Ti_5O_{12}$, which shows attractive characteristics in terms of stable potential around 1.55 V versus metallic lithium up to about 90% of its theoretical capacity (i.e. 175 mAh g^{-1}) [69]. Moreover it has a negligible volume variation (i.e. $< 0.1\%$) of the host lattice during Li uptake and removal, resulting in a 'zero strain' material [70]. However, the capacities of the abovementioned examples are low as they have reached the top of their Lithium storage capacity.

It is important to mention that the practical values for the overall capacity in Li-ion batteries are ultimately limited by the positive materials. The real breakthrough should come from the discovery of new Li-rich sources for positive electrodes, which could provide much higher capacities than those mentioned above. Still, increasing the capacity of the negative electrode materials is an issue. This means that a reduced amount of negative electrode material is needed to obtain a definite capacity value, and more material on the positive side can be added at the same time to match the needed energy density figures.

In order to find materials with much higher storage capacity, materials which can form alloys with lithium are of great interest [71]. Lithium metal alloys are formed when lithium ions are inserted into a metal matrix. Their advantage relies in their ability to store large amounts of lithium, resulting in huge theoretical capacities as compared to graphite. Tin and silicon, are promising candidates to replace graphite, as a Sn or Si atom can host up to 4.4 Li atoms forming $Li_{22}Sn_5$ and $Li_{22}Si_5$, with theoretical capacities of up to 993 mAg g^{-1} and 4200 mAh g^{-1} [72]. A silicon or tin - based negative electrode would reduce significantly the battery energy density in terms of Wg kg^{-1} and Wh L^{-1}. However, the adoption of this technology is held back by its large volumetric expansion during lithium uptake, and once it is being removed it leads to electrode cracking and crumbling, which becomes serious by successive charging and discharging, leading to huge fading in battery performance [73].

The last alternative material to carbon I will cover here is that is that of transition metal oxides (TMOs). In this reaction mechanism, proposed almost ten years ago [74, 75] and termed 'conversion', metal oxides with rock salt structures such as CoO, CuO or FeO, present a reversible reaction with

lithium by storing lithium in the form of Li_2O. The very nature of the electrochemical reaction of Li with TMO is responsible for the formation of a complex nanostructured system in which non-active metal nanoparticles are dispersed in an active matrix of Li_2O. However, in spite of the large capacities these materials provide (from 600 - 1200 mAh g^{-1}, depending on the TMO), they also suffer from a number of shortcomings, such as a limited cycle life due to volume changes of the host and a big hysteresis in their characteristic voltage profiles [76].

1.7 Outlook and Scope of this thesis

The remarkable physicist Richard P. Feynman once said, more than fifty years ago: "the principles of physics, as far as I can see, do not speak against the possibility of maneuvering things atom by atom. It is not an attempt to violate any laws; it is something, in principle, that can be done; but in practice, it has not been done because we are too big" [77]. Since then (1959), human creativity and innovation have led to a paramount number of developments, opening the possibility to study, design and fabricate novel materials not only with top-down techniques, but also with bottom-up methods.

Nanostructured materials and their applications to various technological fields (i.e. thin film production) are literally booming during the last decades. This is not surprising, because the search for new materials with special properties is a key point to overcome the limitations posed by conventional materials and their current technological use. Nanostructures are interesting systems, since their properties often vary strongly from those of the bulk. Their reduced size influences the physical and chemical properties of the original materials.

This thesis focuses on the deposition and (electro) chemical characterisation of electrode films synthesised via an aerosol-assisted route, based on electrospraying liquid precursors. Electrospray, also referred to as Electrospraying or Electrohydrodynamic Atomization (EHDA), is a versatile technique for the production of nearly-monodispersed, highly-charged droplets that, when coupled with a reaction mechanisms (i.e. pyrolysis), allows the production of a wide variety of nanostructured functional films and materials. When pyrolysis is used as reaction mechanism, the technique is usually referred to in the literature as Electrostatic Spray Pyrolysis (ESP) or Deposition (ESD), terms that will be used interchangeably throughout this thesis. Therefore, the main focus of this thesis is related to the synthesis and deposition of nanostructured thin films as electrode materials in Li-ion batteries. It will also deal with various

aspects, including the effects of the deposition parameters on the properties of the deposited layers.

The structure of the thesis consists of seven chapters that describe the main ideas developed in this work and that are summarized in the final conclusions. The experimental chapters that form the heart of this thesis (Chapters 4, 5, 6 and 7) are mainly based on papers published [78–80] or submitted for publication [81, 82]. As a consequence, there might be some overlap in parts of the introduction of each chapter. A brief outline of the chapters is given below.

Chapter two describes the general theory of electrospraying and its modes of operation. The attractive features of generating charged, nearly-monodispersed droplets with tunable sizes, as well as the challenges related to the increase of their production rate are discussed. Applications in the field of Li-ion batteries, i.e. cathode and anode materials, electrolytes are also described.

Chapter three provides an account of the different electrospray equipment used for the experiments that will be described throughout this thesis, as well as which are their main differences. Moreover, a short description of a new experimental setup designed with the purpose of handling big substrates, i.e. silicon wafers, is illustrated.

Chapter four focuses on the synthesis and deposition of Fe_2O_3 and CuO nanostructured electrodes in one step via Electrostatic Spray Pyrolysis (ESP). It also offers some insight on possible shortcomings deriving from the conventional electrode fabrication, where the active materials (i.e. nanopowders) need to be processed in multi-step processes with polymeric binders/additives in order to cast laminated electrodes. During the processing, solutions containing precursor metal salts dissolved together with Polyvinylidene Fluoride (PVdF) binder are electrosprayed on a heated substrate where the generated submicron-sized droplets undergo pyrolysis. The oxide nanoparticles generated via pyrolysis of the metal precursors are in intimate contact with the binder contained in the emitted droplets during the electrospray process. The reacted droplets are at the same time directly driven on selected areas to form nanocomposite coated electrodes. Electrochemical tests demonstrate that the conversion reactions in these electrodes enable large initial discharge capacities, but also reveal that capacity retention needs further improvements. It is, therefore, proposed that it is a viable approach to synthesize and assemble in one step thin nanocomposite coatings of negative electrodes at low temperature.

Chapter five examines the results obtained during a large European project where thin film cathodes of high voltage $LiNi_{0.5}Mn_{1.5}O_4$ are deposited on especially customized silicon wafers for the development of a novel 3D Li-ion microbattery. ESP, which is employed as synthesis and deposition technique, allows the production of layers with capacities up to the required capacity per

square centimeter, by adjusting its thickness. Besides, when having a three-dimensional substrate surface, the thickness can be significantly reduced, according to the actual received surface area. The method in that respect also show acceptable homogeneity within the "holes" or "grooves" of an etched Si wafer and demonstrates its potential in the production of 3D all solid state Li-ion batteries. The influence of the synthesis parameters on the structure, texture and electrochemical behaviour of the produced electrode is investigated using different characterisation techniques.

Chapter six proposes the synthesis of pure $LiNi_{0.5}Mn_{1.5}O_4$ thin films followed by the application of surface modification in the form of Cr_2O_3 catalytic active sites, or 'islands'. ESP is used as synthesis technique for both materials. The film morphology and structural characterisation is discussed and special attention is given to the electrochemical performance. These measurements demonstrate that, although the coating does not alter the initial spinel structure of $LiNi_{0.5}Mn_{1.5}O_4$, it influences the electrochemical behaviour of the bare spinel cathode as it act as a catalyst for electrochemical processes occurring at the interface while, at the same time, improves the ionic exchange from the electrolyte into the active material enhancing the battery performance.

Chapter seven describes some preliminary results at building a modified AFM for in situ electrochemical characterisation of Lithium-ion battery electrode surfaces on a nanometre scale. A specific application of such technique is to know if a catalytic active site on battery electrodes, like the ones that are described in Chapter six, would render faster charge transfer.

References

[1] Intergovernmental Panel on Climate Change, "Climate Change 2007: Impacts, Adaptation and Vulnerability." http://www.ipcc.ch/pdf/assessment-report/ar4/wg2/ar4-wg2-ts.pdf, 2007. Accessed: 14 October 2013.

[2] International Transport Forum, "Reducing Transport Greenhouse Gas Emissions Trends & Data - 2010." http://www.internationaltransportforum.org/Pub/pdf/10GHGTrends.pdf, May 2010. Accessed: 14 October 2013.

[3] D. Munao, *Si nano-particles for a Sustainable Mobility*. PhD thesis, Delft University of Technology, Delft, The Netherlands, May 2012.

[4] X. Lemaire, "Renewable Energy and Energy Efficiency Partnership: Glossary of Terms in Sustainable Energy Regulation." http://www.reeep.org/glossary-terms-sustainable-energy-regulation, September 2010. Accessed: 21 Augustus 2013.

[5] W. Borghols, *Lithium insertion in nanostructured titanates*. PhD thesis, Delft University of Technology, Delft, The Netherlands, March 2010.

[6] International Energy Agency, "Global EV Outlook - Understanding the Electric Vehicle Landscape to 2020." http://www.iea.org/topics/transport/electricvehiclesinitiative/EVI_GEO_2013_FullReport.pdf, April 2013. Accessed: 21 Augustus 2013.

[7] R. Dell and D. Rand, *Understanding Batteries*. Royal Society of Chemistry, 2001. ISBN 0-85404-605-4.

[8] J. Tarascon and M. Armand, "Issues and challenges facing rechargeable lithium batteries," *Nature*, vol. 414, pp. 359–367, 2001.

[9] A. Patil, V. Patil, D. Shin, J.-W. Choi, D.-S. Paik, and S.-J. Yoon, "Issue and challenges facing rechargeable thin film lithium batteries," *Materials Research Bulletin*, vol. 43, no. 8-9, pp. 1913–1942, 2008.

[10] M. Whittingham, "Electrical Energy Storage and Intercalation Chemistry," *Science*, vol. 192, no. 4244, pp. 1126–1127, 1976.

[11] M. Whittingham, "Chalcogenide battery. Patent. US4009052 A." `http://www.google.com/patents/US4009052`, February 1977.

[12] B. Rao, R. W. Francis, and H. Christopher, "Lithium-Aluminum Electrode," *Journal of The Electrochemical Society*, vol. 124, no. 10, pp. 1490–1492, 1977.

[13] D. Murphy and P. Christian, "Solid State Electrodes for High Energy Batteries," *Science*, vol. 205, no. 4407, pp. 651–656, 1979.

[14] M. Thackeray, W. David, P. Bruce, and J. Goodenough, "Lithium insertion into manganese spinels," *Materials Research Bulletin*, vol. 18, no. 4, pp. 461–472, 1983.

[15] D. Murphy, F. Di Salvo, J. Carides, and J. Waszczak, "Topochemical reactions of rutile related structures with lithium," *Materials Research Bulletin*, vol. 13, no. 12, pp. 1395–1402, 1978.

[16] M. Lazzari and B. Scrosati, "A Cyclable Lithium Organic Electrolyte Cell Based on Two Intercalation Electrodes," *Journal of The Electrochemical Society*, vol. 127, no. 3, pp. 773–774, 1980.

[17] M. Mohri, N. Yanagisawa, Y. Tajima, H. Tanaka, T. Mitate, S. Nakajima, M. Yoshida, Y. Yoshimoto, T. Suzuki, and H. Wada, "Rechargeable lithium battery based on pyrolytic carbon as a negative electrode," *Prog. Batteries Solar Cells*, vol. 26, no. 3-4, pp. 545–551, 1989.

[18] T. Nagaura and K. Tozawa, "Lithium ion rechargeable battery," *Prog. Batteries Solar Cells*, vol. 9, p. 209, 1990.

[19] K. Cook-Chennault, N. Thambi, and A. Sastry, "Powering MEMS portable devices - a review of non-regenerative and regenerative power supply systems with special emphasis on piezoelectric energy harvesting systems," *Smart Materials and Structures*, vol. 17, no. 4, pp. 1–33, 2008.

[20] S. Roundy and P. Wright, "A piezoelectric vibration based generator for wireless electronics," *Smart Materials and Structures*, vol. 13, no. 5, pp. 1131–1142, 2004.

[21] International Technology Roadmap for Semiconductors, "ITRS 2006 Update: Overview and Working Group Summaries (European Semiconductor Industry Association, Japan Electronics and Information Technology Industries Association, Korea Semiconductor Industry Association, Taiwan Semiconductor Industry Association, Semiconductor Association)." `http://www.itrs.net/Links/2006Update/2006updatefinal.htm`, 2006. Accessed: 7 Augustus 2013.

[22] J.-S. Do, S.-H. Yu, and S.-F. Cheng, "Preparation and characterization of thick-film Ni/MH battery," *Biosensors and Bioelectronics*, vol. 20, no. 1, pp. 60–67, 2004.

[23] C. Wang, L. Taherabadi, G. Jia, M. Madou, Y. Yeh, and B. Dunn, "C-MEMS for the Manufacture of 3D Microbatteries," *Electrocehmical and Solid State Letters*, vol. 7, no. 11, pp. A435–A438, 2004.

[24] J. Harb, R. LaFollette, R. Selfridge, and L. Howell, "Microbatteries for self-sustained hybrid micropower supplies," *Journal of Power Sources*, vol. 104, no. 1, pp. 46–51, 2002.

[25] J. Bates, N. Dudney, G. Gruzalski, R. Zuhr, A. Choudhury, C. Luck, and J. Robertson, "Electrical properties of amorphous lithium electrolyte thin films," *Solid State Ionics*, vol. 53-56, no. 1, pp. 647–654, 1992.

[26] J. Bates, N. Dudney, N. Dudney, G. Gruzalski, B. Kwak, X. Yu, and R. Zuhr, "Thin-film rechargeable lithium batteries," *Journal of Power Sources*, vol. 54, no. 1, pp. 58–62, 1995.

[27] C. Branci, N. Benjelloun, J. Sarradin, and M. Ribes, "Vitreous tin oxide-based thin film electrodes for Li-ion micro-batteries," *Solid State Ionics*, vol. 135, no. 1-4, pp. 169–174, 2000.

[28] J. Bates, N. Dudney, N. Dudney, B. Neudecker, A. Ueda, and C. Evans, "Thin-film lithium and lithium-ion batteries," *Solid State Ionics*, vol. 135, no. 1-4, pp. 33–45, 2000.

[29] P. Birke, W. Chu, and W. Weppner, "Materials for lithium thin-film batteries for application in silicon technology," *Solid State Ionics*, vol. 93, no. 1-2, pp. 1–15, 1996.

[30] N. Dudney, "Addition of a thin-film inorganic solid electrolyte (Lipon) as a protective film in lithium batteries with a liquid electrolyte," *Journal of Power Sources*, vol. 89, no. 2, pp. 176–179, 2000.

[31] N. Dudney and B. Neudecker, "Solid state thin-film lithium battery systems," *Current Opinion in Solid State and Materials Science*, vol. 4, no. 5, pp. 479–482, 1999.

[32] P. Humble, J. Harb, and R. LaFollette, "Development and performance of a rechargeable thin-film solid-state microbattery," *Journal of Power Sources*, vol. 54, no. 1, pp. A1357–A1361, 2001.

[33] S. Jones and J. Akridge, "Microscopic Nickel-Zinc Batteries for Use in Autonomous Microsystems," *Journal of Power Sources*, vol. 148, no. 12, pp. 63–67, 1995.

[34] S. Jones and J. Akridge, "A microfabricated solid-state secondary Li battery," *Solid State Ionics*, vol. 86-88, no. 2, pp. 1291–1294, 1996.

[35] B. Neudecker, N. Dudney, and J. Bates, "'Lithium-Free' Thin-Film Battery with In Situ Plated Li Anode," *Journal of The Electrochemical Society*, vol. 147, no. 2, pp. 517–523, 2000.

[36] B. Neudecker, R. Zuhr, and J. Bates, "Lithium silicon tin oxynitride (Li_ySiTON): high-performance anode in thin-film lithium-ion batteries for microelectronics," *Journal of Power Sources*, vol. 81-82, pp. 27–32, 1999.

[37] K. Park, Y. Park, M. Kim, J. Son, H. Kim, and S. Kim, "Characteristics of tin nitride thin-film negative electrode for thin-film microbattery," *Journal of Power Sources*, vol. 103, no. 1, pp. 67–71, 2001.

[38] A. Shukla, S. Venugopalan, and B. Hariprakash, "Nickel-based rechargeable batteries," *Journal of Power Sources*, vol. 100, no. 1-2, pp. 125–148, 2001.

[39] E. Torres and G. Rincon-Mora, "Energy-Harvesting System-in-Package Microsystem1," *Journal of Energy Engineering*, vol. 134, no. 4, pp. 121–129, 2008.

[40] K. Kanehori, K. Matsumoto, K. Miyauchi, and T. Kudo, "Thin film solid electrolyte and its application to secondary lithium cell," *Solid State Ionics*, vol. 9-10, no. 2, pp. 1445–1448, 1983.

[41] H. Ohtsuka and J.-I. Yamaki, "Preparation and Electrical Conductivity of Li_2O-V_2O_5-SiO_2 Thin Films," *Japanese Journal of Applied Physics*, vol. 28, pp. 2264–2267, 1989.

[42] H. Ohtsuka, S. Okada, and J.-I. Yamaki, "Solid state battery with Li_2O-V_2O_5-SiO_2 solid electrolyte thin film," *Solid State Ionics*, vol. 40-41, no. 2, pp. 964–966, 1990.

[43] X. Yu, J. Bates, G. Jellison Jr., and F. Hart, "A Stable Thin-Film Lithium Electrolyte: Lithium Phosphorus Oxynitride," *Journal of The Electrochemical Society*, vol. 144, no. 2, pp. 524–532, 1997.

[44] J. Long, B. Dunn, D. Rolison, and H. White, "Three-Dimensional Battery Architectures," *Chemical Reviews*, vol. 104, no. 10, pp. 4463–4492, 2004.

[45] J. Oudenhoven, L. Baggetto, and P. Notten, "All-Solid-State Lithium-Ion Microbatteries: A Review of Various Three-Dimensional Concepts," *Advanced Energy Materials*, vol. 1, no. 1, pp. 10–33, 2011.

[46] M. Roberts, P. Johns, J. Owen, D. Brandell, K. Edstrom, G. El-Enany, C. Guery, D. Golodnitsky, M. Lacey, C. Lecoeur, H. Mazor, E. Peled, E. Perre, M. M. Shaijumon, P. Simon, and P. Taberna, "3D lithium ion batteries-from fundamentals to fabrication," *Journal of Materials Chemistry*, vol. 21, pp. 9876–9890, 2011.

[47] D. Golodnitsky, M. Nathan, V. Yufit, E. Strauss, K. Freedman, L. Burstein, A. Gladkich, and E. Peled, "Progress in three-dimensional (3D) Li-ion microbatteries," *Solid State Ionics*, vol. 177, no. 26-32, pp. 2811–2819, 2006.

[48] T. Arthur, D. Bates, N. Cirigliano, D. Johnson, P. Malati, J. Mosby, E. Perre, M. Rawls, A. Prieto, and B. Dunn, "Three-dimensional electrodes and battery architectures," *MRS Bulletin*, vol. 36, no. 7, pp. 523–531, 2011.

[49] R. Salot, S. Martin, S. Oukassi, M. Bedjaoui, and J. Ubrig, "Microbattery technology overview and associated multilayer encapsulation process," *Applied Surface Science*, vol. 256, no. 3, Supplement, pp. S54–S57, 2009.

[50] G. El-Enany, M. Lacey, P. Johns, and J. Owen, "In situ growth of polymer electrolytes on lithium ion electrode surfaces," *Electrochemistry Communications*, vol. 11, no. 12, pp. 2320–2323, 2009.

[51] S. Tan, S. Walus, J. Hilborn, T. Gustafsson, and D. Brandell, "Poly(ether amine) and cross-linked poly(propylene oxide) diacrylate thin-film polymer electrolyte for 3D-microbatteries," *Electrochemistry Communications*, vol. 12, no. 11, pp. 1498–1500, 2010.

[52] S. Cheah, E. Perre, M. Rooth, M. Fondell, A. Harsta, L. Nyholm, M. Boman, T. Gustafsson, J. Lu, P. Simon, and K. Edstrom, "Self-Supported

Three-Dimensional Nanoelectrodes for Microbattery Applications," *Nano Letters*, vol. 9, no. 9, pp. 3230–3233, 2009.

[53] A. Jeyaseelan and RohanJ.F, "Fabrication of three-dimensional substrates for Li microbatteries on Si," *Applied Surface Science*, vol. 256, no. 3, Supplement, pp. S61–S64, 2009.

[54] D. Golodnitsky, M. Nathan, V. Yufit, E. Strauss, K. Freedman, L. Burstein, A. Gladkich, and E. Peled, "Progress in three-dimensional 3D Li-ion microbatteries," *Solid State Ionics*, vol. 177, pp. 2811–2819, 2006.

[55] A. Levasseur, M. Menetrier, R. Dormoy, and G. Meunier, "Solid state microbatteries," *Materials Science and Engineering: B*, vol. 3, no. 1-2, pp. 5–12, 1989.

[56] Bates, J.B. and Dudney, N.J. and Gruzalski, G.R. and Zuhr, R.A. and Choudhury, A. and Luck, C.F. and Robertson, J.D, "Fabrication and characterization of amorphous lithium electrolyte thin films and rechargeable thin-film batteries," *Journal of Power Sources*, vol. 43, no. 1-3, pp. 103–110, 1993.

[57] R. Chebiam, A. Kannan, F. Prado, and A. Manthiram, "Comparison of the chemical stability of the high energy density cathodes of lithium-ion batteries," *Electrochemistry Communications*, vol. 3, no. 11, pp. 624–627, 2001.

[58] J. Choi, E. Alvarez, T. A. Arunkumar, and A. Manthiram, "Proton Insertion into Oxide Cathodes during Chemical Delithiation," *Electrochemical and Solid State Letters*, vol. 9, no. 5, pp. A241–A244, 2006.

[59] Z. Lua, D. MacNeilb, and J. Dahn, "Layered $Li[Ni_xCo_{1-2x}Mn_x]O_2$ Cathode Materials for Lithium-Ion Batteries," *Electrochemical and Solid State Letters*, vol. 4, no. 12, pp. A200–A203, 2001.

[60] T. Ohzuku and Y. Makimura, "Layered Lithium Insertion Material of $LiNi_{1/3}Mn_{1/3}Co_{1/3}O_2$ for Lithium-Ion Batteries," *Chemistry Letters*, vol. 30, no. 7, pp. 642–643, 2001.

[61] A. Manthiram, "Materials Challenges and Opportunities of Lithium Ion Batteries," *Solid State Ionics*, vol. 2, no. 3, pp. 176–184, 2011.

[62] M. Thackeray, L. de Picciotto, A. de Kock, P. Johnson, V. Nicholas, and K. Adendorff, "Spinel electrodes for lithium batteries - A review," *Journal of Power Sources*, vol. 21, no. 1, pp. 1–8, 1987.

[63] R. Gummow, A. de Kock, and M. Thackeray, "Improved capacity retention in rechargeable 4 V lithium/lithium-manganese oxide (spinel) cells," *Solid State Ionics*, vol. 69, no. 1, pp. 59–67, 1994.

[64] D. Jang, Y. Shin, and S. Oh, "Dissolution of Spinel Oxides and Capacity Losses in 4V $Li/Li_xMn_2O_4$ Cells," *Journal of The Electrochemical Society*, vol. 148, no. 7, pp. 2204–2211, 1996.

[65] P. Prosini, M. Carewska, S. Scaccia, P. Wisniewski, and M. Pasquali, "Long-term cyclability of nanostructured $LiFePO_4$," *Electrochimica Acta*, vol. 48, no. 28, pp. 4205–4211, 2003.

[66] S.-Y. Chung, J. Bloking, and Y.-M. Chiang, "Electronically conductive phospho-olivines as lithium storage electrodes," *Nature Materials*, vol. 1, pp. 123–128, 2002.

[67] B. Ellis, W. Kan, W. Makahnouk, and L. Nazar, "Synthesis of nanocrystals and morphology control of hydrothermally prepared LiFePO4," *Journal of Materials Chemistry*, vol. 17, no. 30, pp. 3248–3254, 2007.

[68] S. Megahed and B. Scrosati, "Lithium-ion rechargeable batteries," *Journal of Power Sources*, vol. 51, no. 1-2, pp. 79–104, 1994.

[69] T. Ohzuku, A. Ueda, N. Yamamoto, and Y. Iwakoshi, "Factor affecting the capacity retention of lithium-ion cells," *Journal of Power Sources*, vol. 54, no. 1, pp. 99–102, 1995.

[70] S. Scharner, W. Weppner, and P. Schmid-Beurmann, "Evidence of Two-Phase Formation upon Lithium Insertion into the $Li_{1.33}Ti_{1.67}O_4$ Spinel," *Journal of The Electrochemical Society*, vol. 146, no. 3, pp. 857–861, 1999.

[71] M. Winter and J. Besenhard, "Electrochemical lithiation of tin and tin-based intermetallics and composites," *Electrochimica Acta*, vol. 45, no. 1-2, pp. 31–50, 1999.

[72] M. Winter, J. Besenhard, M. Spahr, and P. Novak, "Insertion Electrode Materials for Rechargeable Lithium Batteries," *Advanced Materials*, vol. 10, no. 10, pp. 725–763, 1998.

[73] N. Ding, J. Xu, G. Yao, Y. amd Wegner, I. Lieberwirth, and C. Chen, "Improvement of cyclability of Si as anode for Li-ion batteries," *Journal of Power Sources*, vol. 192, no. 2, pp. 644–651, 2009.

[74] P. Poizot, S. Laruelle, S. Grugeon, L. Dupont, and J.-M. Tarascon, "Nano-sized transition-metal oxides as negative-electrode materials for lithium-ion batteries," *Nature*, vol. 407, pp. 496–499, 2000.

[75] S. Laruelle, S. Grugeon, P. Poizot, M. Dolle, L. Dupont, and J.-M. Tarascon, "On the Origin of the Extra Electrochemical Capacity Displayed by MO/Li Cells at Low Potential," *Journal of the Electrochemical Society*, vol. 149, no. 5, pp. A627–A634, 2002.

[76] M. Valvo, *Electrospray-assisted synthesis methods of nanostructured materials for Li-ion batteries*. PhD thesis, Delft University of Technology, Delft, The Netherlands, November 2010.

[77] Feynman, R.P., "Plenty of Room at the Bottom." `http://www.its.caltech.edu/~feynman/plenty.html`, December 1959. Accessed: 21 Augustus 2013.

[78] E. Garcia-Tamayo, M. Valvo, U. Lafont, C. Locati, D. Munao, and E. Kelder, "Nanostructured Fe_2O_3 and CuO composite electrodes for Li ion batteries synthesized and deposited in one step," *Journal of Power Sources*, vol. 196, no. 15, pp. 6425–6432, 2011.

[79] U. Lafont, A. Anastasopol, E. Garcia-Tamayo, and E. Kelder, "Electrostatic spray pyrolysis of $LiNi_{0.5}Mn_{1.5}O_4$ films for 3D Li-ion microbatteries," *Thin Solid Films*, vol. 520, no. 9, pp. 3464–3471, 2012.

[80] Valvo, M. and Garcia-Tamayo, E. and Lafont, U. and Kelder, E.M, "Direct synthesis and coating of advanced nanocomposite negative electrodes for li-ion batteries via electrospraying," *Journal of Power Sources*, vol. 196, no. 23, pp. 10191–10200, 2011.

[81] E. Garcia-Tamayo and E. Kelder, "Electrostatic spray pyrolysis as viable method for the production of 3D Li-ion microbatteries: Thin film $LiNi_{0.5}Mn_{1.5}O_4$ as cathode," *Submitted to Journal of Power Sources*, 2013.

[82] E. Garcia-Tamayo, R. Fredon, J. Ross, and E. Kelder, "Effects of chromium oxide coating on the performance of $LiNi_{0.5}Mn_{1.5}O_4$ thin films," *Submitted to Journal of Power Sources*, 2013.

Chapter 2

Electrospray in Li-ion batteries: An overview of a novel thin film synthesis and deposition method

> (it appeared) probable that the progenitors of man, either the males or females or both sexes, before acquiring the power of expressing mutual love in articulate language, endeavoured to charm each other with musical notes and rhythm
>
> Charles Darwin, *Descent of Man*, 1871

This chapter presents a novel method for the production of thin films called 'electrospray'. At first, a small introduction will be made presenting the wide range of applications. Further, a brief account on the fundamentals of this method, especially its behaviour in the cone-jet mode and the scaling laws related to it will be shown. Finally, a review on its application in the fabrication of thin films for Li-ion battery components will be given.

2.1 Introduction

Electrospraying, also known in literature as electrospray or electrohydrodynamic atomisation (EHDA), is a technique where a liquid precursor, flowing out of a capillary nozzle, is atomised and dispersed into fine droplets by means of a high electric potential. The disruption of droplets occurs through Rayleigh instabilities and Coulombic interaction of charges in the liquid, which involves a build-up of charge and a further break-up into tiny charged droplets [1]. The size of the droplets spans from hundreds of micrometres down to several tens of nanometres. Droplet generation can be manipulated by changing the flow rate of the precursor and the voltage at the nozzle. In this way, droplet size and droplet size distribution can be controlled to some extent. Electrospraying can be widely applied to both industrial processes and scientific instrumentations. Over the last years, it has opened new routes to nanotechnology and it is being used, among many other applications, for micro- and nano-thin-film deposition and particle production. Different reactions (i.e. pyrolysis, hydrolysis, condensation, etc.) can be also coupled to the electrospray in order to produce functional materials for ceramics, lithium batteries, fuel cells, solar cells and MEMS, among many others. Thin film deposition technique using electrospray is frequently called 'electrostatic spray deposition' (ESD) or 'electrostatic assisted vapour deposition' (ESAVD) [2]. When pyrolysis, which involves the use of a heat source in order to promote the evaporation of the solvent or to decompose the precursors and synthesize different materials at higher temperatures, is used as reaction mechanism, the technique is usually referred to in the literature as 'electrostatic spray pyrolysis' (ESP)[1].

In the previous chapter, a discussion was carried out mainly on the importance of energy storage systems, in particular Li-ion batteries. Special attention was given to thin film batteries for applications in small electronic systems like MEMS, medical devices, wireless sensors, among others. In this chapter a brief description will be given of the fundamentals of EHDA and its application for the production of thin films. Furthermore, numerous examples will be shown on the application of this technique in materials for Li-ion battery anodes, cathodes and electrolytes.

[1]The terms electrospraying, electrospray and EHDA will be used interchangeably throughout this thesis. The same will happen with the terms ESD and ESP, as electrospray was coupled with pyrolysis so as to obtain thin films

2.2 Fundamentals

The different names how this technique is referred to in the literature, contain terms that are important to define in order to avoid misconceptions. *Atomisation* is the breakdown of a liquid into droplets, while the suspension of droplets and/or solid in a surrounding gas is defined *spray* or *aerosol* [3–5]. In this regard, EHDA, or electrospray, is the dispersion of liquid into fine droplets by the influence of a strong electric field.

The formation of a liquid droplet is a phenomenon known and studied for centuries that involves the influence of two forces, surface tension and gravity. The earliest attempt to formulate a theory of the break-up of electrified jets and drops was that of Lord Rayleigh [6, 7]. He analysed the balance between the repulsive electrical forces due to the charge on the drop or jet and the surface tension restoring forces. An important concept developed in his studies is know today as the 'Rayleigh limit', and it refers to the maximum amount of charge that can be carried by a charged droplet [6]. It has been suggested that the charge on the droplets can eventually approach half of this limit [8]. When the repulsive electrical force due to interaction of charges in a droplet wins over the cohesive force from the surface tension, it disrupts into smaller droplets. The limiting charge, q_R, for a liquid droplet of radius a is given by:

$$q_R = 8\sqrt{\pi\epsilon\gamma a^3} \tag{2.2.1}$$

where γ is the surface tension of the liquid and ϵ_0 is the permittivity of free space. Rayleigh's analysis is important to this day, because it has been a starting point in the analysis of many experimental observations.

Liquid flowing out of a capillary forms a meniscus that, when subjected to electrical stresses from an electric field may become elongated and eventually cause disruption of the jet into droplets. The interaction between two groups of forces governs the phenomena of the eventual break-up of the liquid jet (see Figure 2.1): normal and tangential stresses at the liquid surface and bulk forces on the jet.

Among the stresses of the liquid, which deform the jet shape, the electrodynamic stress tensor (Λ), that results from the surface charge density (q) and the local electric field (E), probably plays the major role. The bulk forces on the jet include the electrodynamic force (F_e), which is proportional to the electric field and to the space charge of any previously emitted droplet (F_Q); the gravitational force (F_g); the drag force (F_η), which is proportional to the surrounding gas viscosity and jet velocity; and the surface tension (F_σ).

With the description of these forces and stresses it is sufficient to illustrate that, under certain conditions, the interaction between these forces will cause

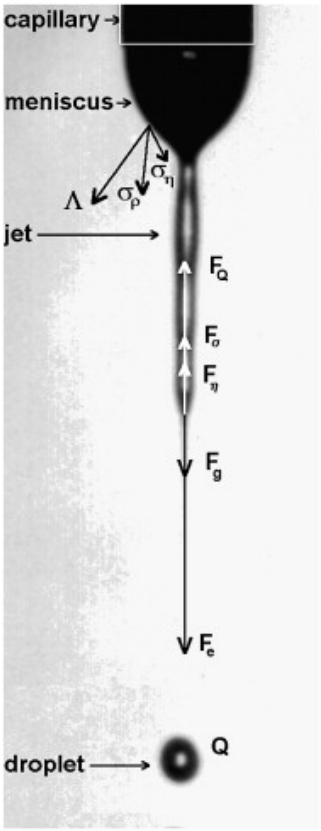

Figure 2.1 – Schematic illustration of stresses and forces on a liquid jet (spindle mode) flowing out from a capillary nozzle. Adapted from [Jaworek et al., 2008]

the meniscus to elongate into a jet, which eventually disintegrates into droplets. The mathematical description of this phenomena can be found in the literature [8, 9] and is beyond the scope of this chapter.

It is well known, for example, that the interaction between electric field, surface tension and kinetic energy of the liquid jet leaving the nozzle (flow rate), promotes the formation of different *spraying modes* [1]. Several studies have been performed to identify and classify such modes [1, 8, 10–16] and, as a general rule, they are divided in two groups: discontinuous and continuous modes. The description of both groups presented in this thesis is mainly based on the clear and succinct description made by Valvo, 2010 [17] and Jaworek et al., 2008 [9] in which they categorize these modes based on the geometrical properties of the jet and meniscus, and on the type of jet behaviour in its disintegration into droplets. The first group, comprises the modes in which only fragments of the liquid are ejected from the nozzle and do not exhibit a continuous flow through the meniscus. These modes are called dripping (large drops), microdripping (fine drops) and (multi) spindle modes (elongated spindles). The second includes the modes in which the liquid flows out the capillary nozzle in the form of a long, continuous jet that disintegrates into droplets only over a certain distance from the tip of the capillary. The modes comprised in this group are cone-jet (smooth and stable), oscillating-jet mode (oscillates in its plane), precession mode (rotates around the capillary axis) and multi-jet mode (few jets on the circumference of the capillary). These modes of electrospraying are schematically shown in Figure 2.2.

As mentioned before, these modes arise due to changes in the force diagram. A careful selection of an electric potential (electric stress), flow rate (kinetic energy) and precursor solution (surface tension), renders a change on the classical spherical shape of the pendant droplet into a conical shape. The use of diagrams to represent the different spraying modes is quite common [1, 5, 18] and it becomes useful as it describes how they are formed related to the electric potential (V) and flow rate (Q). In Figure 2.3, a diagram adapted from Agostinho, 2013, is presented. For certain window values of both Q and V, a stable cone-jet appears. In this mode the round meniscus take the shape of a Taylor cone from which a jet emerges breaking up into fine droplets due to Plateau-Rayleigh instabilities, i.e. varicose breakup [5]. Inside the same cone-jet window, if the potential is increased, the varicose breakup is influenced by kink instabilities, i.e. whipping breakup [19]. It is important to mention that not all the modes occur for all liquids [1, 5].

Most research about electrospraying, especially those devoted to the production of nearly-monodisperse droplets and thin films, have been focused on the so-called cone-jet mode in which the meniscus adopts a conical shape with

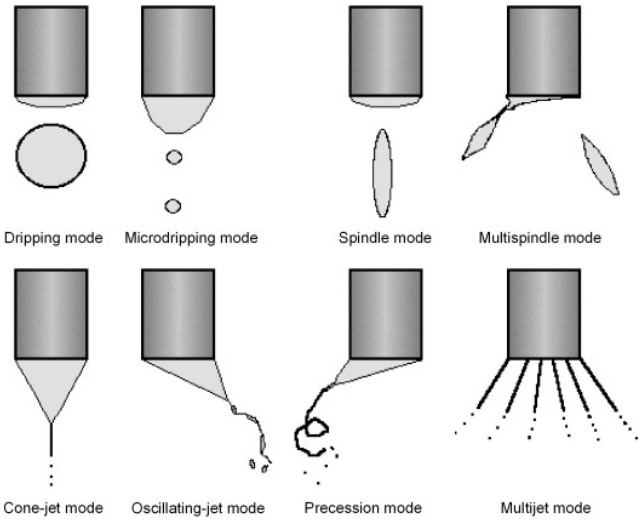

Figure 2.2 – Main modes of electrospraying. Adapted from [Jaworek et al., 2008]

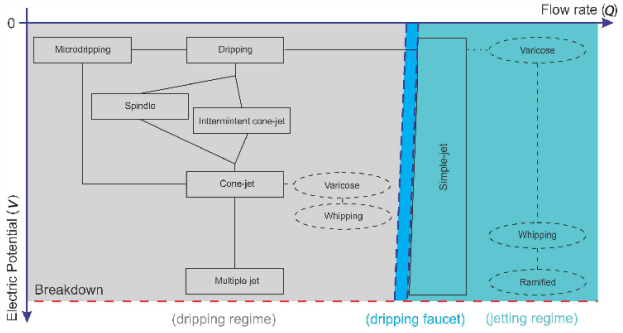

Figure 2.3 – Electrospraying modes as a function of the applied potential and flow rate. Adapted from [Agostinho, 2013]

a thin (< 100 μm) jet at its apex. This feature is referred as 'Taylor cone' in the literature, named after the scientist who, in 1964, studied the phenomenon extensively [20].

2.2.1 EHDA in the cone-jet mode

The reason why electrospray systems usually operate in the cone-jet mode are mainly because the charge distribution of the produced particles is narrow, and the probability of producing monodispersed droplets, as well as their emission frequencies, is higher. Moreover, the average size-range of the droplets may reach that of few nanometres up to micrometres, depending on intrinsic (i.e. the chosen precursor) and extrinsic (i.e. flow rate) properties. These characteristics become relevant for applications where a narrow size distribution is crucial, as is the case of thin film production.

Albeit film deposition efficiency is higher for electrospraying as compared to mechanical and conventional atomisers, the liquid throughput of the system is relatively low for applications at an industrial level. Many studies have been done on out-scaling electrospraying in the cone-jet mode and such approaches have been summarised recently [5]. It could be expected that a simple increase in the flow rate would render higher production rates but, as mentioned above and as it will be described more in detail in Subsection 1.2.2, this would alter the spray mode and thus change the size and charge distribution of the generated droplets. It is yet possible to electrospray in the simple-jet mode, which operates at much higher flow rates [1, 11]. This mode is not commonly used as it produces larger droplets than that of the cone-jet, however it has been recently shown that it is a good option for applications which require high throughput with droplets on the hundreds of micrometers range [21]. On the other hand, out-scaling might be possible to achieve by the usage of multinozzle systems (multiple jets) in a linear array [22] or rim-emission mode [23]. Another explored approach is via multiplexed nozzle systems, which enables parallel electrospray [24]. An array of multiple nozzles, no matter the geometry, requires a sound delivery of the precursor solution in order to ensure that the required flow rate will fed to all the nozzles. Although satisfactory results have been achieved with these systems and an increase in the production has been reported in all cases, factors such as electrical interferences between neighbouring nozzles that destabilizes the overall process still need to be circumvented. Recently, a multinozzle system consisting of four nozzles placed in a circular geometry plus a central nozzle, all of them electrospraying in the simple-jet mode, has been developed. They successfully placed an insulating

layer between the nozzles and counter electrodes achieving a stable operation and high throughputs of 2.2 L h^{-1} [25].

Despite these limitations, electrospraying in the cone-jet mode continues to be the main focus. In the case of fundamental studies the stability achieved in this mode, as compared to the others, makes it feasible to analyse and characterise its behaviour [5, 26, 27]. This has lead to the numerical modelling of droplet generation and the creation of the so-called scaling laws.

2.2.2 Scaling laws for current and droplet size

Several studies have been devoted to the analysis of charge droplets in the cone-jet mode [11, 19, 28, 29]. An overview of the current classification reported in the literature and the corresponding behaviour of the liquid meniscus has been reported recently [26]. These scaling laws relate the size of the produced droplets, d, or the current through the system, I, to several material properties of the liquid being sprayed and the applied flow rate. These mathematical correlations are especially useful when developing new applications. It is important to mention that a large amount of equation have been proposed, which indicates not only that the mathematical model of EHDA is complex, but that it is far from complete. Extensive measurements on the atomisation of liquids with different physical properties, based on both experimental and theoretical results, show that d and I are strongly dependent on the viscosity and the conductivity of the liquid, and present basically two different scaling behaviours. The values assumed by a dimensionless number, $\delta_\mu \delta^{1/3}$, allow the distinction between these two behaviours [17, 30]:

$$\delta_\mu \delta^{(\frac{1}{3}} = \left(\frac{\gamma^3 \epsilon^2}{\mu^3 \kappa^2 Q} \right)^{\frac{1}{3}} \tag{2.2.2}$$

This number represents the ratio of the change in the kinetic energy of the liquid jet in the axial direction and the change in viscous stress in the radial direction. Liquids with high conductivities and viscosities exhibit a flat profile for the axial velocity in the jet ($\delta_\mu \delta^{1/3} < 1$) and behave differently from liquids with low conductivity and viscosity ($\delta_\mu \delta^{1/3} > 1$). Ganan-Calvo et al., found out that, in particular, flat profiles of the velocities are known to yield currents scaling as I $Q^{1/2}$, while non-flat profiles generally follow I $Q^{1/4}$ [30]. Hartmann et al., on its turn, independently derived a scaling law for the current, which was extended for all Newtonian liquids with low conductivities and viscosities [31]. They noted that when $\delta_\mu \delta^{1/3} < 1$:

$$I \approx 2 \left(\gamma \kappa Q \right)^{\frac{1}{2}} \tag{2.2.3}$$

Which was then used to calculate the average droplet for the different mechanisms of jet break-up, varicose, $d_{d,v}$:

$$d_{d,v} = c_d \left(\frac{\rho \epsilon_0 Q^4}{I^2} \right)^{\frac{1}{6}} \tag{2.2.4}$$

And whipping, $d_{d,w}$:

$$d_{d,w} = \left(0.8 \frac{288 \epsilon_0 \gamma Q^2}{I^2} \right)^{\frac{1}{3}} \tag{2.2.5}$$

Substituting Equation 2.2.3 in Equations 2.2.4 and 2.2.5, and taking c_d constant (approx. 2):

$$d_{d,v} \approx \left(\frac{16 \rho \epsilon_0 Q^3}{\gamma \kappa} \right)^{\frac{1}{6}} \tag{2.2.6}$$

$$d_{d,w} \approx \left(0.8 \frac{72 \epsilon_0 Q}{\kappa} \right)^{\frac{1}{3}} \tag{2.2.7}$$

These physical models should be used carefully as real measurements on the droplet size show deviations of up to 30%, although they are very useful as a first estimate on the average droplet size.

2.3 Thin films

Thin film are layers ranging from sub-nanometre to several micrometres in thickness. They are used to improve surface properties, such as in mechanical and tribological systems, for electronic semiconductor devices and as optical coatings, among many others. A number of deposition techniques have been developed to deposit thin-films on a substrate and to fabricate ceramic layers. They can be widely classified in three categories, as suggested by Chen (1998) [32], depending on the type of precursors used and the reactors in which the films are formed:

- Gas-phase deposition
- Liquid-phase deposition
- Aerosol deposition

These will be discussed in more detail below.

Gas-phase deposition

Physical and chemical vapour deposition (PVD) and (CVD), respectively, are the most used and well known methods in this category. PVD includes sputtering, evaporation, and laser ablation techniques which vaporise solid precursors usually under vacuum conditions and deposit thin films on a substrate. Advantages of PVD include good quality of the films obtained in terms of high density and smoothness, with a good adhesion to the substrate. Some disadvantages consist of the cost of the equipment involved, difficulties in controlling film compositions and up-scaling. CVD process, on its turn, usually involves the presence of more than one gaseous precursor led by a carrier gas to a reaction zone where deposition takes place on or above the surface of a substrate. Advantages of CVD include lower equipment costs than PVD, relatively easy up-scaling, and a large number of available precursors. Some disadvantages are the difficulty in obtaining a good reproducibility, as well as in controlling the compositions of thin-films of ternary and more complex materials, and the fact that a large amount of material is lost to the chamber walls. Both CVD [33–35] and PVD [36–38] have been used to prepare various components for lithium-ion microbatteries.

Liquid -phase deposition

This category includes a widely used set of techniques such as sol-gel processes, hydrothermal growth and electrodeposition. A sol-gel process is a versatile route to prepare fine powders and ceramic coatings and it can be either a polymeric or an aqueous process. The polymeric sol-gel is normally used in combination with spin- or dip-coating for thin film production. Hydrothermal method is the production of powders by the crystallisation of substances from high-temperature aqueous solutions at high vacuum pressures. It can also be used for the deposition of in autoclaves under hydrothermal conditions. Electrodeposition is a process that uses electrical current to reduce dissolved metal cations so that they form a metal coating on an electrode. The system media usually consist on aqueous solutions. All these routes usually present advantages such as low cost of the equipment and an easy control on the composition. Electrodeposition [33, 39, 40] and hydrothermal [41, 42] examples as successful methods for the production of thin films in batteries are more common. Sol-gel processes have been reported before [43], but its usage is not widely documented.

Aerosol deposition

Often referred as 'spray deposition techniques' in literature, these methods consist in the generation of an aerosol, from a liquid precursor, which is subsequently directed towards a substrate or target in order to form thin-films. These techniques are usually attributed with advantages such as the low cost of the equipment involved, as well as its simplicity; the wide choice of precursors; relatively easy control on the composition; a wide range of film morphologies are easily achievable; some of them may be easily scaled-up. Different sprayers or atomizers, such as pneumatic, ultrasonic or electrostatic, are used to generate the aerosol and, as such, they differ in droplet size, rate of atomization, and droplet velocity [32]. Some disadvantages include, in the case of mechanical atomisers, the layer is not sufficiently homogeneous and of the same thickness on the entire surface.

The quality of thin film formed on a substrate strongly depends on the size of particles or droplets forming the layer, their monodispersity, and their uniform distribution on the surface. Smaller particles, of narrow size distribution should be generated in order to reduce the number and size of voids, flaws and cracks in the film. The droplets ought to be uniformly dispersed over the substrate to ensure the layer to be even and of the same thickness. The electrospray is a promising tool for production of high quality layers and films because it fulfils all these requirements. The electrostatic forces disperse the droplets homogeneously in the space between the nozzle and the substrate. The electrospray process is also easy to control by adjusting liquid flow rate and the voltage applied to the nozzle, and it is less expensive in production of thin films than chemical or physical vapour deposition, or plasma spraying requiring high vacuum installations. The film thickness can be simply controlled by varying the concentration and flow rate of the precursor solution [2].

Electrospraying has been used in a wide variety of applications, such as the production of pharmaceutical particles [44–47] and tailor-made, reacting or encapsulated particles [48, 49]. It has been also used to create emulsions [50], for crop spraying [18] and, of particular interest in this thesis, for thin film production.

In this respect, several studies on thin film deposition by means of electrospray (ESD or ESP), in numerous applications, have been presented [51–61] and, as a focus in this thesis, it has been studied also in the field of lithium-ion batteries [62–74] as it will be mentioned in more detail in the following section. Finally, several important and complete reviews have been performed by Jaworek et al., [2, 9], Salata [75] and Valvo (2010) [17].

The process of thin films deposition via ESP is usually done at lower tem-

peratures than conventional solid-state reactions. The temperature of the substrate, besides being needed as a synthesis parameter to obtain the desired material, is critical for the control of the layer uniformity and porosity [54, 59, 71]. The porosity is a result of fast evaporation of the solvent, and increases with the substrate temperature [63, 76]. Optimal tuning of the temperature so as to obtain the desired structure without compromising the layer quality can be achieved by choosing a solvent with higher boiling temperature or by mixing several solvents.

In his PhD work, Chen (1998) [32] gave, apart from an overview of the theoretical background of the processes involved in the ESD technique, experimental descriptions of the most important properties in thin film generation, including general set-up, nozzle design, substrate temperature, concentration of precursor solution, electric field strength, effect of the substrate, solvents and different additives to enhance conductivity. He concluded that even if the morphology is influenced by all these factors, including the spray droplet size, the spreading rate of solution droplets on the substrate and the solution chemistry, the factor playing the main role in the properties of the layer is the substrate temperature. The higher it is, the more porous the layer. At moderate temperatures the deposited layer is relatively dense but becomes porous with the increase in thickness.

The precursor concentration is also an important parameter. Studies on ESP production of TiO_2 (anatase) films, from a precursor solution of titanium diisopropoxide bis 2,4-pentanedionate dissolved in 2-propanol, at low precursor concentrations (0.05 M) resulted in amorphous layers, while those made at higher concentrations (0.2 M) formed crystalline anatase [77].

Other studies have been reported on parameters intrinsic to the liquid precursor such as the increase of the conductivity by using additives, i.e. acetic acid [78], or the change of surface tension by mixing water and methanol in the same precursor [79]. In the first case, the morphology of the layer changed from cracked to crack-free reticular and it was attributed to the smaller droplets generated when acetic acid was added. The increase of surface tension caused the film to become rough and porous, attributed to the dispersion into large number of droplets. A wider study on the effect of liquid physical properties such as viscosity, surface tension, conductivity, and molecular weight on the morphology of thin films prepared by ESD has been presented by Morota et al. [80]. As a result, layers formed by building particles such as nanospheres, nanospindles and nanofibers were achieved by changing these properties and the applied voltage.

The layer formation is a complex and multi-step process, and, therefore, numerous explanations can be met in the literature. A complete and chronological

description of the different categorisations has been proposed by Jaworek [2]. An initial description was made by Chen et al. [62], where he distinguished four types of layer morphologies, but following results performed by other groups showing different morphologies [54, 63, 76, 81–84], indicated that other structures should be incorporated in this categorisation. Jaworek classifies these layer morphologies in two main groups: dense and porous. The dense layer can be amorphous, crystalline (of different structures) or amorphous with incorporated particles (intrusions). The porous layer can be reticular, grainy, or fractal-like. These structures are schematically shown in Figure 2.4.

It can be concluded that electrospray based methods are a versatile op-

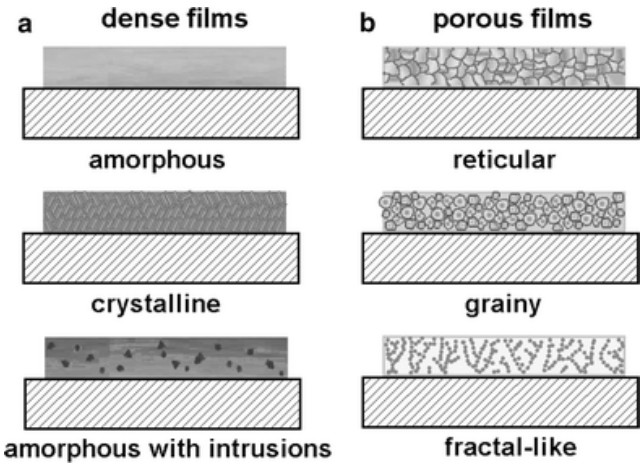

Figure 2.4 – Film structure morphologies: dense (a), porous (b). Adapted from [Jaworek, 2007]

tion for thin film production. Layer morphology, thickness and structure can be controlled in a relatively easy way by tuning the parameters involved in the process, including those of the system as a whole (nozzle design, distance nozzle-to-substrate, applied voltage, flow rate, temperature of the substrate, etc), as well as those involved in the precursor solution (concentration of the constituting salts, boiling temperature of the solvent, conductivity, surface tension, viscosity, etc). Moreover, the equipment required is cheap and easy to acquire, and the process is flexible and easily tuneable. Compared to other methods like CVD or PVD, its main advantage is that the growth rate of the layer is relatively high. The process can be carried out in an ambient atmosphere, in air

or other gas, and at low temperature, without the need for a complex reactor and vacuum system.

Although each research group reports the successful film deposition and fabricated device operation, most of them suggest that further development is required. Despite many experimental data, the definitive explanation of the electrospray mechanisms and film formation processes is not yet available [2].

After this account on the fundamentals of the technique, especially its behaviour in the cone-jet mode and the scaling laws related to it, and showing the wide variety of studies and examples on ESD as a tool for thin films deposition, a brief review on the application of electrospray in the fabrication of Li-ion battery components will be mentioned in the following section.

2.4 ESD in Li-ion batteries

ESD has been used in the field of Li-ion batteries for almost 20 years. Van Zomeren et. al were probably the first who employed it to produce materials for positive electrodes, i.e. $LiMn_2O_4$, in 1994 [85]. Since then more attention has been paid to this process as a feasible process for thin film battery components, most likely due to the interest in production of electrodes for lithium microbatteries [2]. The demand for production of microbatteries is an effect of miniaturisation of electronic devices and a reduction of their power consumption. A survey of open publications related with electrostatic spray deposition and lithium batteries in the past 20 years is given in Figure 2.5, together with a distribution of where the research from those publications took place. These literature data were obtained based on Scopus and Google Scholar search systems. The data shows that, over the past decade, electrospray has maintained over five articles per year with and steady increase in the last lustrum.

Several studies have been carried out and promising results have shown the potential of these techniques for developing both positive and negative electrodes, as well as solid electrolytes. The possibility of direct synthesis or deposition of nanostructured electrode materials onto current collectors is particularly attractive, especially for thin films, where no binders or electronically conductive additives are usually required for effective operation.

2.4.1 Cathode materials

Thin film deposition of materials for positive electrodes is usually obtained by the pyrolysis of precursors containing lithium and other metal salts (i.e. acetates or nitrates) so as to obtain metal-oxides. The choice of solvents mostly depends on the solubility of the salts. The boiling point of the solvent plays an

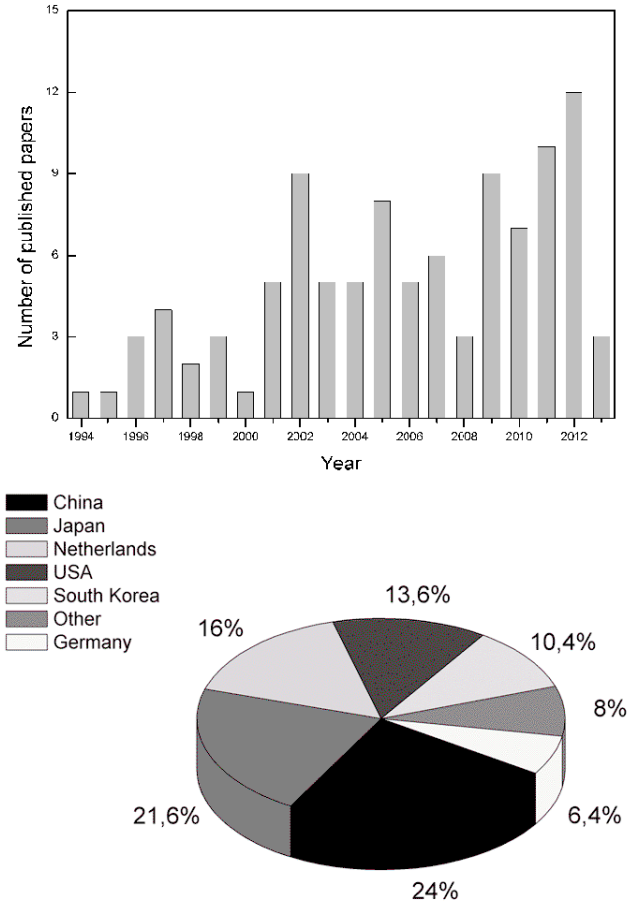

Figure 2.5 – Comparison of the annual number of scientific publications since the first publication in 1994 and publication distribution around the world. Data analysis of publications was done using the Scopus and Google Scholar search systems with the terms 'electrostatic spray' AND 'lithium batteries', on 2 September 2013.

important role as it used to tune the morphology of the layer.

Positive electrode materials such as $LiCoO_2$ [62, 64, 71, 76, 86], $LiCo_xMn_{2-x}O_4$ [87], $LiNi_xMn_{2-x}O_4$ [87], $LiNiO_2$ [86, 88], $LiAl_yNi_{1-y}O_2$ [88], $LiCo_yNi_{1-y}O_2$ [88], $LiCo_{0.5}Ni_{0.5}O_2$ [89], $LiAl_{0.25}Ni_{0.75}O_2$ [89], $Li_4Mn_5O_{12}$ [89], $Li_4Ti_5O_{12}$ [66], $LiMn_2O_4$ [86, 90–92], $LiNi_{0.5}Mn_{1.5}O_4$ [67, 93] have been obtained, and different morphologies ranging from dense to porous layers have been reported. In most cases, the synthesis process took place at relatively low temperatures between 250 - 500 °C. Some studies however showed that an extra step of annealing was required in order to obtain the desired structure [67], the complete reaction to happen or the crystallisation of the materials. Electrochemical tests demonstrate that these electrodes undergo Li^+ intercalation/de-intercalation similar to conventional laminated electrodes and that porous structures favor efficient charge transfer [17].

2.4.2 Anode materials

In a similar way as for the positive electrode materials, thin film deposition of negative electrode materials uses pyrolysis, especially when transition metal oxides are desired. In this case, no lithium is added to the precursor solution, but a similar choice of salts (i.e. acetates or nitrates) and solvents (i.e. ethanol, methanol, 2-propanol, ethylene glycol, etc) is made. In particular, nanostructured negative materials such as SnO_2 [17, 86, 94, 95] and transition metal oxides (i.e. M_xO_y) such as Fe_2O_3 [17, 74, 94, 96], CoO [17, 86, 94, 97], MnO_2 [86], CuO [96], Cu_2O [98], NiO, ZrO_2 [99], Al_2O_3 [99], ZnO [99], TiO_2 [86, 100], are receiving increasing attention as alternative negative electrodes. Specific capacities much larger than those of carbonaceous materials can be achieved in such systems via alloying mechanisms or reversible conversion reactions, especially when they occur at the nanoscale [17].

A similar approach can be applied for the production of homogeneous layers from previously synthesised (nano) powders. In this case, the particles are suspended in a particular solvent so as to form an ink. This precursor is then electrosprayed onto a substrate, most of the time partially heated in order to promote adhesion. In our group, we have been focusing on this during the past years paying especial attention on Si nanoparticles. As de/lithiation of Si causes strong mechanical stresses, a polymeric binder, and therefore conductive additive to increase electronic conduction, is needed to obtain a functioning battery. Recently a number of articles have been published in this respect showing the versatility and advances of this technique for the production of thin films [17, 94, 101].

2.4.3 Solid Electrolytes

A couple of studies have been reported on the usage of ESD for the production of solid electrolytes in the form of thin films. A study by Chen et al. where they synthesised several ceramic materials for battery components, among which $Li_{0.1}BPO_4$ [86] was included, led to the implementation of a two-layer structure comprising a cathode ($Li_xMn_2O_4$) and solid electrolyte (Li_xBPO_4), prepared from lithium acetate and manganese acetate precursors [63].

Although the production of solid electrolytes using this technique has not been broadly studied, the versatility is clear with a wide choice of possible materials, using this relatively easy and cheap process. The possibility remains open for the development of an all-solid-state thin-film battery produced only with ESD.

2.5 Conclusions

Electrospraying was proved to be a versatile tool for various material processing technologies. This chapter intended to show the interest in industrial and laboratory applications with regard to this technique, which allows the generation of sub-micrometric droplets while working in the cone-jet and multi-jet modes. The goal of this review was to provide a summary of electrospray applications in thin solid film deposition.

The temperature of the substrate, besides being needed as a synthesis parameter to obtain the desired material (i.e. by means of pyrolysis), is critical for the control of the layer uniformity and porosity. The porosity is a result of fast evaporation of the solvent, and increases with the substrate temperature. Optimal tuning of the temperature so as to obtain the desired structure without compromising the layer quality can be achieved by choosing a solvent with higher boiling temperature or by mixing several solvents.

Electrospray has advantages of uniform coating of large areas, inexpensive equipment, operation at atmospheric conditions, and easy control of deposition rate and film thickness by adjusting voltage and flow rate. Utilisation of this technique in the field of thin film battery production will surely continue to rise, and new achievements in this field can be expected in the near future.

References

[1] J. Grace and J. Marijnissen, "A review of liquid atomization by electrical means," *Journal of Aerosol Science*, vol. 25, no. 6, pp. 1005–1019, 1994.

[2] A. Jaworek, "Electrospray droplet sources for thin film deposition," *Journal of Materials Science*, vol. 42, no. 1, pp. 266–297, 2007.

[3] D. Michelson, *Electrostatic Atomization*. IOP Publishing Ltd, 1990. ISBN 0-85274-235-5.

[4] J. Eggers and E. Villermaux, "Physics of liquid jets," *Reports on Progress in Physics*, vol. 71, no. 3, pp. 1–80, 2008.

[5] L. Agostinho, *Electrohydrodynamic Atomization in the Simple-Jet Mode*. PhD thesis, Delft University of Technology, Delft, The Netherlands, February 2013.

[6] F. Rayleigh, "On the equilibrium of liquid conducting masses charged with electricity," *Philosophical Magazine Series 5*, vol. 14, no. 87, pp. 184–186, 1882.

[7] F. Rayleigh, "On the capillary phenomena of jets," *Proceedings of the Royal Society of London*, vol. 29, no. 196-199, pp. 71–97, 1879.

[8] A. Jaworek and A. Krupa, "CLASSIFICATION OF THE MODES OF EHD SPRAYING," *Journal of Aerosol Science*, vol. 30, no. 7, pp. 873–893, 1999.

[9] A. Jaworek and A. Sobczyk, "Electrospraying route to nanotechnology: An overview," *Journal of Electrostatics*, vol. 66, no. 3-4, pp. 197–219, 2008.

[10] G. Joffre, B. Prunet-Foch, S. Berthomme, and M. Cloupeau, "Deformation of liquid menisci under the action of an electric field," *Journal of Electrostatics*, vol. 13, no. 2, pp. 151–165, 1982.

[11] M. Cloupeau and B. Prunet-Foch, "Electrohydrodynamic spraying functioning modes: a critical review," *Journal of Aerosol Science*, vol. 25, no. 6, pp. 1021–1036, 1994.

[12] L. de Juan and J. Fernandez de la Mora, "Charge and Size Distributions of Electrospray Drops," *Journal of Colloid and Interface Science*, vol. 186, no. 2, pp. 280–293, 1997.

[13] A. Gomez and K. Tang, "Charge and fission of droplets in electrostatic sprays," *Physics of Fluids*, vol. 6, no. 1, pp. 404–415, 1994.

[14] A. Ganan-Calvo, "The size and charge of droplets in the electrospraying of polar liquids in cone-jet mode, and the minimum droplet size," *Journal of Aerosol Science*, vol. 25, no. 1, pp. S309–S310, 1994.

[15] A. Ganan-Calvo, A. Barrero, and C. Pantano-Rubino, "The electrohydrodynamics of electrified conical menisci," *Journal of Aerosol Science*, vol. 24, no. 1, pp. S19–S20, 1993.

[16] S. Shiryaeva and A. Grigor'ev, "The semiphenomenological classification of the modes of electrostatic dispersion of liquids," *Journal of Electrostatics*, vol. 34, no. 1, pp. 51–59, 1995.

[17] M. Valvo, *Electrospray assisted synthesis methods of nanostructured materials for Li-ion batteries.* PhD thesis, Delft University of Technology, Delft, The Netherlands, November 2010.

[18] K. Geerse, *Applications of Electrospray: from people to plants.* PhD thesis, Delft University of Technology, Delft, The Netherlands, May 2003.

[19] R. Hartman, D. Brunner, D. Camelot, J. Marijnissen, and B. Scarlett, "Jet break-up in electrohydrodynamic atomization in the cone-jet mode," *Journal of Aerosol Science*, vol. 31, no. 1, pp. 65–95, 2000.

[20] G. Taylor, "Disintegration of Water Drops in an Electric Field," *Proceedings of The Royal Society A*, vol. 280, no. 1382, pp. 383–397, 1964.

[21] L. Agostinho, G. Tamminga, C. Yurteri, S. Brouwer, E. Fuchs, and J. Marijnissen, "Morphology of water electrosprays in the simple-jet mode," *Physical Review E*, vol. 86, no. 6, pp. 066317–1–6, 2012.

[22] R. Bocanegra, D. Galan, M. Marquez, I. Loscertales, and A. Barrero, "Multiple electrosprays emitted from an array of holes," *Journal of Aerosol Science*, vol. 36, no. 12, pp. 1387–1399, 2005.

[23] Y. Arnanthigo, Y. C.U., G. Biskos, J. Marijnissen, and A. Schmidt-Ott, "Out-scaling electrohydrodynamic atomization systems for the production of well-defined droplets," *Powder Technology*, vol. 214, no. 3, pp. 382–387, 2011.

[24] W. Deng, C. Waits, B. Morgan, and A. Gomez, "Compact multiplexing of monodisperse electrosprays," *Journal of Aerosol Science*, vol. 40, no. 10, pp. 907–918, 2009.

[25] L. Agostinho, C. Yurteri, J. Wartena, S. Brouwer, E. Fuchs, and J. Marijnissen, "Insulated multinozzle system for electrohydrodynamic atomization in the simple-jet mode," *Applied Physics Letters*, vol. 112, no. 19, pp. 194103–1–5, 2013.

[26] S. Verdoold, *ElectroHydroDynamic Atomisation: Unipolar and bipolar characterisation and modelling*. PhD thesis, Delft University of Technology, Delft, The Netherlands, April 2012.

[27] U. Stachewicz, *Analysis of Electrospraying as an On-demand Deposition Method*. PhD thesis, Delft University of Technology, Delft, The Netherlands, May 2010.

[28] J. Fernandez de la Mora and I. Loscertales, "The current emitted by highly conducting Taylor cones," *Journal of Fluid Mechanics*, vol. 260, pp. 155–184, 1994.

[29] A. Ganan-Calvo, "The surface charge in electrospraying: its nature and its universal scaling laws," *Journal of Aerosol Science*, vol. 30, no. 7, pp. 863–872, 1999.

[30] A. Ganan-Calvo, J. Davila, and A. Barrero, "Current and droplet size in the electrospraying of liquids. Scaling laws," *Journal of Aerosol Science*, vol. 28, no. 2, pp. 249–275, 1997.

[31] R. Hartman, D. Brunner, D. Camelot, J. Marijnissen, and B. Scarlett, "Electrohydrodynamic atmisation in the cone-jet mode physical modeling of the liquid cone and jet," *Journal of Aerosol Science*, vol. 30, no. 7, pp. 823–849, 1999.

[32] C.-H. Chen, *Thin-film components for lithium-ion batteries*. PhD thesis, Delft University of Technology, Delft, The Netherlands, September 1998.

[33] A. van Zomeren, *Thin films of lithium intercalation compounds.* PhD thesis, Delft University of Technology, Delft, The Netherlands, November 1993.

[34] A. van Zomeren, J.-H. Koegler, J. Schoonman, and P. v.d. Put, "Charge transport phenomena in thin-film cathodes," *Solid State Ionics*, vol. 53-56, pp. 333–338, 1992.

[35] J. Oudenhoven, *Deposition and Characterization of Thin Films for 3D Lithium-ion Micro-Batteries.* PhD thesis, Eindhoven University of Technology, Eindhoven, The Netherlands, November 2011.

[36] C. Julien, L. El-Farh, M. Balkanski, O. Hussain, and G. Nazri, "The growth and electrochemical properties of metal-oxide thin films: lithium intercalation," *Applied Surface Science*, vol. 65-66, pp. 325–330, 1993.

[37] G. Amatucci, A. Safari, F. Shokoohi, and B. Wilkens, "Lithium scandium phosphate-based electrolytes for solid state lithium rechargeable microbatteries," *Solid State Ionics*, vol. 60, no. 4, pp. 354–365, 1993.

[38] C. Liquan and J. Schoonman, "Polycrystalline, glassy and thin films of $LiMn_2O_4$," *Solid State Ionics*, vol. 67, no. 1-2, pp. 17–23, 1993.

[39] M. Chapeau-Poinso, J. Bouteillon, and J. Poignet, "Cathodic codeposition of alloyed materials for use in lithium battery negative electrodes," *Journal of Applied Electrochemistry*, vol. 24, no. 1, pp. 66–71, 1994.

[40] K. Naoi, K. Ueyama, and T. Osaka, "Electrochemical Study on Charge-Discharge Performance of Lithium/Polyazulene Battery," *Journal of The Electrochemical Society*, vol. 136, no. 9, pp. 2444–24449, 1989.

[41] J. Guo, Y. Li, and M. Whittingham, "Hydrothermal synthesis of electrode materials pyrochlore tungsten trioxide film," *Journal of Power Sources*, vol. 54, no. 2, pp. 461–464, 1995.

[42] M. Whittingham, R. Chen, T. Chirayil, and P. Zavalij, "The intercalation and hydrothermal chemistry of solid electrodes," *Solid State Ionics*, vol. 94, no. 1-4, pp. 227–238, 1997.

[43] J. Livage, G. Guzman, F. Beteille, and P. Davidson, "Optical properties of sol-gel derived vanadium oxide films," *Journal of Sol-Gel Science and Technology*, vol. 8, no. 1-3, pp. 857–865, 1997.

[44] J.-P. Borra, D. Camelot, J. Marijnissen, and B. Scarlett, "A new production process of powders with defined properties by electrohydrodynamic atomization of liquids and post-production electrical mixing," *Journal of Electrostatics*, vol. 40-41, pp. 633–638, 1997.

[45] R. Hartman, *Electrohydrodynamic atomization in the cone-jet mode: From Physical Modeling to powder production.* PhD thesis, Delft University of Technology, Delft, The Netherlands, November 1998.

[46] T. Ciach, "Microencapsulation of drugs by electro-hydro-dynamic atomization," *International Journal of Pharmaceutics*, vol. 324, no. 1, pp. 51–55, 2006.

[47] D. DePaoli, C. Tsouris, and M.-C. Hu, "EHD micromixing reactor for particle synthesis," *Powder Technology*, vol. 135-136, pp. 302–309, 2003.

[48] M. Alexander, "Pulsating electrospray modes at the liquid-liquid interface," *Applied Physics Letters*, vol. 92, no. 14, pp. 144102–144105, 2008.

[49] M. Alexander, M. Paine, and J. Stark, "Pulsation Modes and the Effect of Applied Voltage on Current and Flow Rate in Nanoelectrospray," *Analytical Chemistry*, vol. 78, no. 8, pp. 2658–2664, 2006.

[50] J. Abu-Ali and S. Barringer, "Method for electrostatic atomization of emulsions in an EHD system," *Journal of Electrostatics*, vol. 63, no. 5, pp. 361–369, 2005.

[51] J. Gaury, E. Kelder, E. Bychkov, and G. Biskos, "Characterization of Nb-doped WO_3 thin films produced by Electrostatic Spray Deposition," *Thin Solid Films*, vol. 534, pp. 32–39, 2013.

[52] D. Perednis, O. Wilhelm, S. Pratsinis, and L. Gauckler, "Morphology and deposition of thin yttria-stabilized zirconia films using spray pyrolysis," *Thin Solid Films*, vol. 474, no. 1-2, pp. 84–95, 2005.

[53] S. Kim, K. Choi, J. Eun, H. Kim, and HwangC.S, "Effects of additives on properties of MgO thin films by electrostatic spray deposition," *Thin Solid Films*, vol. 377-378, pp. 694–698, 2000.

[54] T. Nguyen and E. Djurado, "Deposition and characterization of nanocrystalline tetragonal zirconia films using electrostatic spray deposition," *Solid State Ionics*, vol. 138, pp. 191–197, 2001.

[55] S. Youssef, R. Al Asmar, J. Podlecki, M. Abdallah, D. Zaouk, and A. Foucaran, "Preliminary study on pyroelectric lithium tantalite by a novel electrostatic spray pyrolysis technique," *Microelectronics Journal*, vol. 39, no. 5, pp. 792–796, 2008.

[56] N. Stelzer, A. Goossens, and J. Schoonman, "Synthesis of terbia doped yttria stabilized zirconia thin films by using the electrostatic spray deposition (esd) technique," *MRS Proceedings*, vol. 453, no. 6, pp. 429–438, 1996.

[57] J. Jeong, Y. Jeon, K. Jeon, K. Hwang, and B. Kim, "Preparation of zinc oxide films by an electrostatic spray deposition process," *Ceramic Processing Research*, vol. 7, no. 1, pp. 70–74, 1993.

[58] O. Wilhelm, L. Madler, and S. Pratsinis, "Electrospray evaporation and deposition," *Journal of Aerosol Science*, vol. 34, pp. 815–836, 2003.

[59] H. Huang, X. Yao, X. Wu, M. Wang, and L. Zhang, "Ferroelectric $PbTiO_3$ thin films prepared by electrostatic spray deposition (ESD)," *Microelectronic Engineering*, vol. 66, no. 1-4, pp. 688–694, 2003.

[60] D. Zaouk, Y. Zaatar, R. Asmar, and J. Jabbour, "Piezoelectric zinc oxide by electrostatic spray pyrolysis," *Microelectronics Journal*, vol. 37, no. 11, pp. 1276–1279, 2006.

[61] K. Hwang, K. Jeon, Y. Jeon, and B. Kim, "Hydroxyapatite forming ability of electrostatic spray pyrolysis derived calcium phosphate nano powder," *Journal of Materials Science*, vol. 41, pp. 4159–4162, 2006.

[62] C. Chen, E. Kelder, P. Van Der Put, and J. Schoonman, "Morphology control of thin $LiCoO_2$ films fabricated using the electrostatic spray deposition (ESD) technique," *Journal of Materials Chemistry*, vol. 6, no. 5, pp. 765–771, 1996.

[63] C. Chen, E. Kelder, and J. Schoonman, "Electrode and solid electrolyte thin films for secondary lithium-ion batteries," *Journal of Power Sources*, vol. 68, pp. 377–380, 1997.

[64] C. Chen, E. Kelder, and J. Schoonman, "Unique porous $LiCoO_2$ thin layers prepared by electrostatic spray deposition," *Journal of Materials Science*, vol. 31, no. 20, pp. 5437–5442, 1996.

[65] H. Ryu, J. Kim, Z. Guo, H. Liu, K. Kim, J. Ahn, and H. Ahn, "Electrochemical properties of Fe_2O_3 thin film fabricated by electrostatic spray deposition for lithium-ion batteries," *Physica Scripta*, vol. T139, p. 014066, 2010.

[66] Y. Yu, J. Shui, and C. Chen, "Electrostatic spray deposition of spinel $Li_4Ti_5O_{12}$ thin films for rechargeable lithium batteries," *Solid State Communications*, vol. 135, no. 8, pp. 485–489, 2005.

[67] U. Lafont, A. Anastasopol, E. Garcia-Tamayo, and E. Kelder, "Electrostatic spray pyrolysis of $LiNi_0.5Mn_1.5O_4$ films for 3D Li-ion microbatteries," *Thin Solid Films*, vol. 520, no. 9, pp. 3464–3471, 2012.

[68] C. Hsu and B. Hwang, "Microstructure and Properties of the $La_{0.6}Sr_{0.4}Co_{0.2}Fe_{0.8}O_3$ Cathodes Prepared by Electrostatic-Assisted Ultrasonic Spray Pyrolysis Method," *Journal of The Electrochemical Society*, vol. 153, no. 8, pp. A1478–A1483, 2006.

[69] D. Zaouk, Y. Zaatar, A. Khoury, C. Llinares, J. Charles, and J. Bechara, "Fabrication of tin oxide (SnO_2) thin film by electrostatic spray pyrolysis," *Microelectronic Engineering*, vol. 51-52, pp. 627–631, 2000.

[70] C. Chen, F. Yuan, and J. Schoonman, "Spray pyrolysis routes to electroceramic powders and thin films," *European Journal of Solid State and Inorganic Chemistry*, vol. 35, no. 2, pp. 189–196, 1998.

[71] C. Chen, A. Buysman, E. Kelder, and J. Schoonman, "Fabrication of $LiCoO_2$ thin film cathodes for rechargeable lithium battery by electrostatic spray pyrolysis," *Solid State Ionics*, vol. 80, no. 1–2, pp. 1–4, 1995.

[72] A. Subramania, S. Karthick, and N. Angayarkanni, "Preparation and electrochemical behaviour of $LiMn_2O_4$ thin film by spray pyrolysis method," *Thin Solid Films*, vol. 516, no. 23, pp. 8295–8298, 2008.

[73] D. Zaouk, R. Al Asmar, J. Podlecki, Y. Zaatar, A. Khoury, and A. Foucaran, "X-ray diffraction studies of electrostatic sprayed SnO_2:F films," *Microelectronics Journal*, vol. 38, no. 8-9, pp. 884–887, 2007.

[74] L. Wang, H. Xu, P. Chen, D. Zhang, C. Ding, and C. Chen, "Electrostatic spray deposition of porous Fe_2O_3 thin films as anode material with improved electrochemical performance for lithium-ion batteries," *Journal of Power Sources*, vol. 193, no. 2, pp. 846–850, 2009.

[75] O. Salata, "Tools of Nanotechnology: Electrospray," *Current Nanoscience*, vol. 1, pp. 25–33, 2005.

[76] C. Chen, E. Kelder, M. Jak, and J. Schoonman, "Electrostatic spray deposition of thin layers of cathode materials for lithium battery," *Solid State Ionics*, vol. 86-88, pp. 1301–1306, 1996.

[77] K. Choy, "Processing-structure-property of nanocrystalline materials produced using novel and cost-effective ESAVD-based methods," *Materials Science and Engineering: C*, vol. 16, no. 1-2, pp. 139–145, 2001.

[78] C. Chen, E. Kelder, and J. Schoonman, "Effects of additives in electrospraying for materials preparation," *Journal of the European Ceramic Society*, vol. 18, no. 10, pp. 1439–1443, 1998.

[79] R. Chandrasekhar and K. Choy, "Innovative and cost-effective synthesis of indium tin oxide films," *Thin Solid Films*, vol. 398-399, pp. 59–64, 2001.

[80] K. Morota, H. Matsumoto, T. Mizukoshi, Y. Konosu, M. Minagawa, A. Tanioka, Y. Yamagata, and K. Inoue, "Poly(ethylene oxide) thin films produced by electrospray deposition: morphology control and additive effects of alcohols on nanostructure," *Journal of Colloid and Interface Science*, vol. 279, no. 2, pp. 484–492, 2004.

[81] M. Cich, K. Kim, H. Choi, and S. Hwang, "Deposition of $(Zn,Mn)_2SiO_4$ for plasma display panels using charged liquid cluster beam," *Applied Physics Letters*, vol. 73, no. 15, pp. 2116–2119, 1998.

[82] H. Gourari, M. Lumbreras, R. Van Landschoot, and J. Schoonman, "Elaboration and characterization of SnO_2-Mn_2O_3 thin layers prepared by electrostatic spray deposition," *Sensors and Actuators B: Chemical*, vol. 47, no. 1-3, pp. 189–193, 1998.

[83] E. Diagne and M. Lumbreras, "Elaboration and characterization of tin oxide-lanthanum oxide mixed layers prepared by the electrostatic spray pyrolysis technique," *Sensors and Actuators B: Chemical*, vol. 78, no. 1-3, pp. 98–105, 2001.

[84] I. Taniguchi, R. van Landschoot, and J. Schoonman, "Fabrication of $La_{1-x}Sr_xCo_{1-y}Fe_yO_3$ thin films by electrostatic spray deposition," *Solid State Ionics*, vol. 156, no. 1-2, pp. 1–13, 2003.

[85] A. van Zomeren, E. Kelder, J. Marijnissen, and J. Schoonman, "The production of thin films of LiMn2O4 by electrospraying," *Journal of Aerosol Science*, vol. 25, no. 6, pp. 1229–1235, 1994.

[86] C. Chen, E. Kelder, and J. Schoonman, "Functional Ceramic Films with Reticular Structures Prepared by Electrostatic Spray Deposition Technique," *Journal of The Electrochemical Society*, vol. 144, no. 11, pp. L289–L291, 1997.

[87] K. Dokko, N. Anzue, Y. Makino, M. Mohamedi, T. Itoh, M. Umeda, and I. Uchida, "Fabrication of Thin Film Electrodes of $LiM_xMn_{2-x}O_4$ (M = Ni, Co) for 5 Volt Lithium Batteries," *Electrochemistry*, vol. 71, no. 12, pp. 1061–1063, 2003.

[88] K. Yamada, N. Sato, T. Fujino, C. Lee, I. Uchida, and J. Selman, "Preparation of LiNiO2 and LiM y ?Ni1- y ?O2 (M=Co,Al) films by electrostatic spray deposition," *Journal of Solid State Electrochemistry*, vol. 3, no. 3, pp. 148–153, 1999.

[89] K. Yamada, N. Sato, T. Fujino, M. Nishikawa, and I. Uchida, "Preparation of Li Containing Mixed Metal Oxide Films by Electrostatic Spray Deposition and Their Stabilities in Molten Alkali Carbonates," *Electrochemistry*, vol. 67, no. 1, 1999.

[90] J. Shui, G. Jiang, S. Xie, and C. Chen, "Thin films of lithium manganese oxide spinel as cathode materials for secondary lithium batteries," *Electrochimica Acta*, vol. 49, no. 13, pp. 2209–2213, 2004.

[91] M. Mohamedi, D. Takahashi, Y. Makino, K. Dokko, T. Itoh, M. Umeda, and I. Uchida, "ESD Fabricated Thin Films of Spinel $LiMn_2O_4$ for Lithium Microbatteries: I. Effects of Thickness," *Journal of The Electrochemical Society*, vol. 149, no. 1, pp. A19–A25, 2002.

[92] F. Cao and J. Prakash, "A comparative electrochemical study of $LiMn_2O_4$ spinel thin-film and porous laminate," *Electrochimica Acta*, vol. 47, no. 10, pp. 1607–1613, 2002.

[93] M. Mohamedi, Y. Makino, K. Dokko, T. Itoh, and I. Uchida, "Electrochemical investigation of $LiNi_{0.5}Mn_{1.5}O_4$ thin film intercalation electrodes," *Electrochimica Acta*, vol. 48, no. 1, pp. 79–84, 2002.

[94] Valvo, M. and Garcia-Tamayo, E. and Lafont, U. and Kelder, E.M, "Direct synthesis and coating of advanced nanocomposite negative electrodes for li-ion batteries via electrospraying," *Journal of Power Sources*, vol. 196, no. 23, pp. 10191–10200, 2011.

[95] M. Mohamedi, S.-J. Lee, D. Takahashi, T. Nishikawa, T. Itoh, and I. Uchida, "Amorphous tin oxide films: preparation and characterization as an anode active material for lithium ion batteries," *Electrochimica Acta*, vol. 46, no. 8, pp. 1161–1168, 2001.

[96] E. Garcia-Tamayo, M. Valvo, U. Lafont, C. Locati, D. Munao, and E. Kelder, "Nanostructured Fe_2O_3 and CuO composite electrodes for Li ion batteries synthesized and deposited in one step," *Journal of Power Sources*, vol. 196, no. 15, pp. 6425–6432, 2011.

[97] Y. Yu, C. Chen, J. Shui, and S. Xie, "Nickel-Foam-Supported Reticular CoO-Li_2O Composite Anode Materials for Lithium Ion Batteries," *Angewandte Chemie International Edition*, vol. 44, no. 43, pp. 7085–7089, 2005.

[98] Y. Yu, Y. Shi, and C. Chen, "Nanoporous cuprous oxide/lithia composite anode with capacity increasing characteristic and high rate capability," *Nanotechnology*, vol. 18, no. 5, p. 055706, 2007.

[99] C. Chen, M. Emond, E. Kelder, B. Meester, and J. Schoonman, "Electrostaic Sol-Spray deposition of nanostructured ceramic thin films," *Journal of Aerosol Science*, vol. 30, no. 7, pp. 959–967, 1999.

[100] C. Chen, E. Kelder, and J. Schoonman, "Electrostatic sol-spray deposition (ESSD) and characterisation of nanostructured TiO_2 thin films," *Thin Solid Films*, vol. 342, no. 1-2, pp. 25–41, 1999.

[101] Munao, D and van Erven, J.W.M and Valvo, M and Garcia-Tamayo, E and Kelder, E.M, "Role of the binder on the failure mechanism of si nano-composite electrodes for li-ion batteries," *Journal of Power Sources*, vol. 196, pp. 6695–6702, 2011.

Chapter 3

Electrospray equipment used including a new experimental setup

> Además, todo el mundo cree que nos marchamos para disfrutar de una vida más fácil. No saben lo difícil que es abrirte camino en un mundo ajeno
>
> Milan Kundera, *La Ignorancia*, 2000

3.1 Introduction

In the previous chapter a detailed description of the Electrospraying process, with emphasis on its application to the field of Li-ion batteries, was conducted. Although a brief description of the experimental equipment which is generally used in the literature to perform such research was discussed in Sections 2.1, 2.2 and 2.3, more attention was paid to the fundamentals and the application of electrospray.

In this chapter, an account will be given of the different electrospray equipment used for the experiments that will be described throughout this thesis, as well as which are their main differences. Moreover, a short description of a new experimental setup designed with the purpose of handling big substrates, i.e. silicon wafers, will be illustrated.

3.1.1 Background

Electrospraying is a technique where a liquid precursor, flowing out of a capillary nozzle, is atomized and dispersed into fine droplets by means of a high electric potential. The size of the droplets spans from hundreds of micrometres down to several tens of nanometres. Droplet generation can be manipulated by changing the flow rate of the precursor, the voltage at the nozzle and nozzle to substrate distance. In this way, droplet size and droplet size distribution can be controlled to some extent. Electrospraying can be widely applied to both industrial processes and scientific instrumentations. Over the last years, it has opened new routes to nanotechnology and it is being used, among many other applications, for micro- and nano-thin-film deposition and particle production. Different reactions (i.e. pyrolysis, hydrolysis, condensation, etc.) can be also coupled to the electrospray in order to produce functional materials for ceramics, lithium batteries, solar cells, among many others. Typically, Electrostatic Spray Deposition (ESD) and Pyrolysis (ESP) involve the use of a heat source in order to promote the evaporation of the solvent or to decompose the precursors and synthesize different materials at higher temperatures.

In the ESP a capillary plate configuration is adopted (the orientation between these two elements varies throughout the literature). The precursor solution is contained inside a syringe which is placed in a syringe pump that permits the user to control the volume of precursor and time of spraying. The syringe is connected, via a polymer hose, to a metal capillary nozzle. A high voltage (HV) is applied between the metallic nozzle and the substrate holder creating an electric field across this region. When the HV source and the pump

are turned on, this field also penetrates the liquid surface and interacts with ions in the solution causing them to disperse, leading to atomization of the liquid precursor. The droplets generated in this way will eventually land on the substrate which is placed on top of the substrate holder under a mask used to select the area wanted for the deposition. The temperature of the substrate can be controlled and tuned in such a way that pyrolysis will take place. As mentioned in the previous chapter, several parameters play crucial roles in the droplet generation and the film formation processes. To mention a few:

- Distance between nozzle and substrate: by changing it, the time of flight of the droplets varies.
- Temperature of the substrate holder: influences multiple processes like pyrolysis, drying of the droplet, temperature gradient of the reactor chamber, adhesion on the substrate, etc.
- Voltage: can be easily tuned to achieve different phenomena.
- Spraying volume: the amount of precursor to be sprayed.
- Flow rate: it can also be tuned in order to achieve different phenomena, but is basically used to release the volume of precursor in a desired time.

Apart from the parameters related to the system, the physical and chemical properties of the solution play an important role on the process:

- Electrical conductivity
- Absolute permittivity
- Viscosity
- Surface tension

3.1.2 Experimental equipment used

The system consists mainly of three units, namely: (1) a high voltage power supply (HCN14-12500, FUG) connected to a nozzle and a heated substrate holder (grounded) that is attached to a temperature controller; (2) a pumping unit, where a precursor solution, loaded in a glass syringe (Fortuna Optima), can be injected in a controlled manner via a syringe pump (KD Scientific KDS120, 8950); (3) a reaction chamber, where the sample is positioned and the nozzle (EFD® Ultra) is fed via a chemically-resistant hose (Watson-Marlow) with the precursor to produce a fine aerosol that will be followed by pyrolysis reactions after the droplets land on the heated substrate, and a high intensity

halogen lamp. Additionally, the system comprises other supporting elements, including electronic connection cables suitable for high voltage operation and a digital calliper to measure the nozzle to substrate distance. The necessity of using the high-intensity lamp is stressed because it helps to determine the mode of spraying.

The different setups used for the experiments described in this thesis were composed of these three main units, using the same equipment. The only difference was in the reaction chamber (3) in the sense that the vertical configuration of the nozzle to substrate-holder was varied, i.e. the atomization was in the same direction as the gravitational force (downwards, for experiments in Chapter 4) and in the direction opposite to it (upwards, for experiments in Chapters 5 and 6). These equipments, however, have constraints in terms of the size of the substrate they can handle. A new equipment was thus constructed in order to support the usage of samples of up to 20 cm, i.e. for deposition of thin films on 8" silicon wafers (experiments in Chapter 5).
This system will be briefly described now.

Downwards configuration (Chapter 4)

In Chapter 4, a direct, one-step approach for the synthesis and coating of nanocomposite electrodes based on metal oxides as active materials and PVdF as polymeric binder will be presented. Therefore, the parameters used for such experiments and the results obtained will be discussed later. The paragraph at hand will deal with the description of the setup used.

Different configurations regarding the position of the capillary and the substrate can be found in the literature. Perhaps the most commonly used is that with a vertical orientation in which the capillary is facing downwards and the substrate rests on the holder) [1–7]. In this case the gravitational force (F_g) is in the same direction as the electrohydrodynamic force (F_e), as depicted in Figure 2.1 in Chapter 2. A schematic drawing of the equipment used for the synthesis and assembly of the coated electrodes is shown in Figure 3.1(a), while a picture of the electrospray in operation is shown in Figure 3.1(b).

Upwards configuration (Chapters 5 and 6)

In Chapter 5, high voltage $LiNi_{0.5}Mn_{1.5}O_4$ thin film electrodes for 3D Li-ion microbattery application will be discussed. Likewise, Chapter 6 will deal with the application of surface modification, i.e. partial coatings via a short-time deposition, on previously synthesised layers.

For the experiments that will be described in the above mentioned chapters,

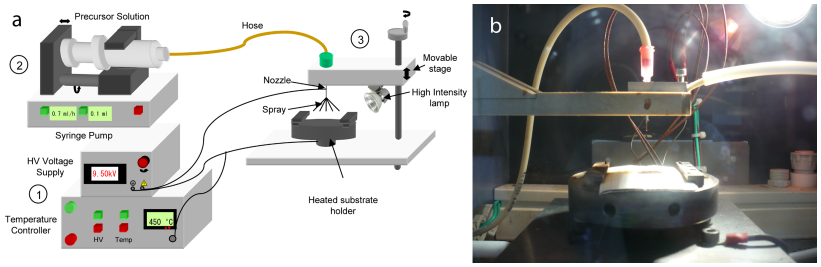

Figure 3.1 – Schematic drawing (a) and photo (b) of the electrostatic spray deposition setup used for the direct synthesis and assembly of coated nanocomposite electrodes, as will be discussed in Chapter 4.The nozzle, feeding hose and the heated substrate holder are clearly visible. The halogen lamp helps with the visualisation of the spraying mode.

ESP was used as synthesis technique using almost the same setup as the one described before, except that the nozzle is directed towards the substrate facing upwards. Such orientation has been regularly used in the literature for several applications [8–13]. In this case, the gravitational force (F_g) is in opposite direction to that of the electrohydrodynamic force (F_e). It is important to stress the fact that the gravitational force may be neglected in the case of electrostatic spraying because droplets produced in this way are very small [14]. A schematic drawing of the equipment used for the synthesis and coating of cathode electrodes as well as their subsequent surface modification is shown in Figure 3.2. It also shows the system during spraying. This particular configuration is just one of many possibilities. It is also possible to spray upwards (as described above) or even horizontally [15–17]. In our case, spraying upwards has the advantage that excess solution does not drip on the sample, but then follows simply along the nozzle downwards. This may look trivial at first but when dealing with expensive and/or scarce substrates it becomes a relevant aspect.

New equipment for large samples (Chapter 5)

As could be observed in the images of the experimental setups shown above, the size of the samples was restricted to about 4 cm (the diameter of the masks employed, as shown in Figures 3.1(b) and 3.2(b), are 1.5 cm). As mentioned before, a new equipment was thus constructed in order to support the usage of

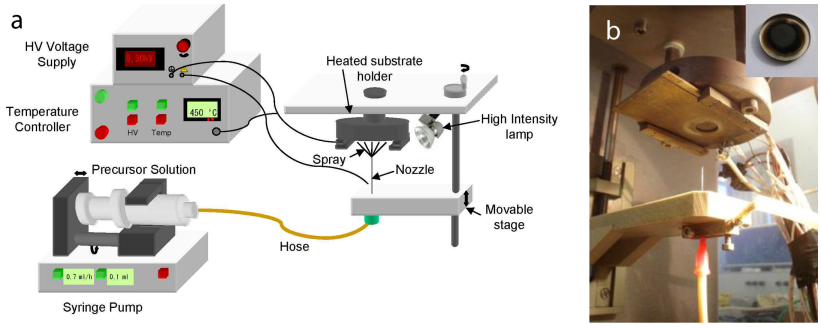

Figure 3.2 – Schematic drawing (a) and photo (b) of the electrostatic spray deposition setup used for the synthesis and coating of cathode electrodes, as will be discussed in Chapters 5 and 6. The picture on the right shows the circular mask used and the resulting film sprayed on a CR2320 coin cell cap.

samples of up to 20 cm, i.e. for deposition of thin films on 8" silicon wafers. In Chapter 5, a full description of the substrates will be made. For the purpose of this chapter, it is enough to say that the system has an upward configuration as described above and that it has a much bigger size.
A schematic drawing of the designed equipment is shown in Figure 3.3a). The system is composed by the same components as its smaller counterparts with the exception of the reaction zone. Here, the nozzle is mounted on a movable 'x, y, z' table, whose motion is controlled by a computer. This movable table is composed of two independent linear actuators (PBC Linear-MLB Series [18]), each with a linear speed of 1.2 mm s^{-1}. A photograph of the setup, shown during spraying, is shown in Figure 3.3(b), where it is possible to identify the two separate linear actuators which hold, on their turn, a separate vertical arm where the nozzle is attached to. This arm includes an optical ruler and a knob that permits the control of the 'z' direction. The substrate holder can be also observed in Figure 3.3(b). This massive component consists of two separate parts, namely a heating plate and an isolation element. The heating plate, clearly seen in the central part actually holding a metallic mask and having the nozzle directly pointed at it, is made of stainless steel and it is composed of two separate heating elements (HotSet-Hotspring®, max. temp. 750 °C), one for the inner part and the other one for the outer part, as shown in the technical drawing in Figure 3.4(a). Each heating spring has its own port to connect a thermocouple, hence the temperature can be separately controlled.

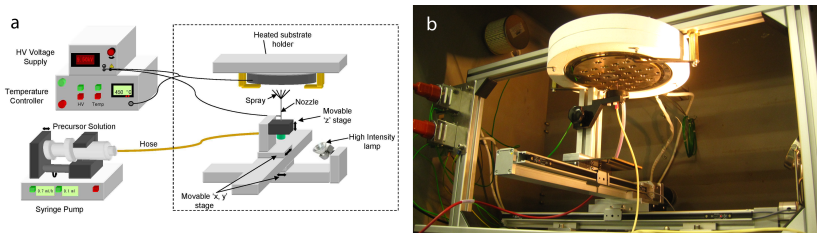

Figure 3.3 – Schematic drawing (a) and photo (b) of the new experimental ESP setup designed and built for thin film synthesis on large substrates, as will be discussed more in detail in Chapters 5.

The thermal isolation element (MONOLUX® 800), present in Figure 3.3(b) as the white ceramic component surrounding the heating plate, is a 30 cm cylindrical piece machined with a 23 cm hole in the centre part where the heating plate is placed, as it can be observed in Figure 3.4(b). Finally, the substrate is held against the holder via two stainless steel springs which not only play the role of mechanically pressing the substrate against the plate, but are also the electrical pole which is grounded in order to close the high voltage circuit.

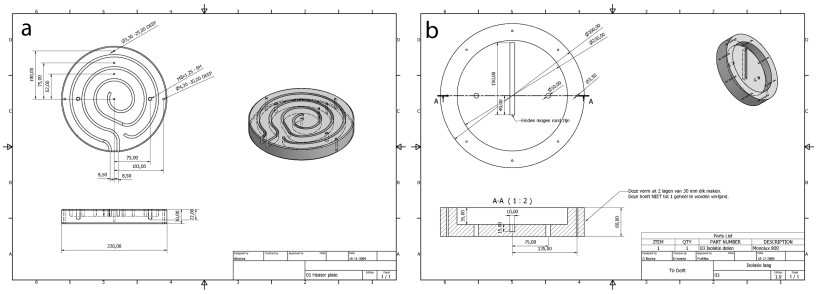

Figure 3.4 – Technical drawings of: (a) the heating plate containing two separate heating elements; and (b) the thermal isolation component.

3.2 Conclusions and Outlooks

Electrospraying is a versatile tool for liquid atomization that has the advantage of uniform droplet generation from relatively inexpensive equipment. These systems can operate under atmospheric conditions, and the rate of particle production is easy to control via voltage and flow rate. In particular for the field of Li-ion batteries, it is an easy, cost-effective approach for the direct synthesis and coating of advanced (composite) electrodes, as it will be shown in the coming chapters of this manuscript.

As mentioned in a recent article published by our group, e.g. Valvo et al. [7], the various products, with desired compositions, thicknesses, morphologies and textures can be obtained by using dedicated precursors, solvents, polymers, additives, gas atmospheres and so forth. The method combines the powerful aerosol tool of electrospray deposition (i.e. generation of highly charged droplets with tuneable size, large area coverage, etc.) with the intrinsic versatility of wet chemistry and polymers, in order to form functional materials with peculiar structures and textures. Embracing in a single step the various stages required by conventional electrode preparation (i.e. blending of slurries, paste casting and coating consolidation) is extremely useful and effective in minimizing time and energy needed for electrode fabrication. Even more important is the fact that the active nanoparticles are generated in situ, while being inter-dispersed with the polymer binder and directly attached to the substrate, thus not separating the processes of materials synthesis, mixing and assembly. Moreover, the control over the morphology, the coverage and the thickness of the coatings by electrospraying can be controlled in a more accurate manner than in conventional laminated electrodes. Obviously, all these features are attractive not only for the fabrication of electrodes for Li-ion batteries, but also for other applications that may require deposition of functional nanocomposite structures.

In his PhD dissertation Valvo, 2010 [19], described the potential implementation of this procedure into a continuous, larger scale process for full fabrication of advanced nanocomposite electrodes in a roll-to-roll process by convenient upscaling of electrospray via multiple nozzle systems [20] or equivalent equipments. One of his analyses included the one shown in the schematic drawing in Figure 3.5 which compares the typical manufacturing process of laminated electrodes with the proposed concept of direct synthesis and assembly. The main advantage of the electrospray is that the thickness of the coatings can be controlled with higher precision than by conventional casting and the entire process can be performed in a one-step, continuous mode. Deposition times for electrode coating can be drastically reduced by means of multiple-

nozzle systems, especially when low flow rates are required on single spraying points in order to generate homogenously-sized droplets. In such a way, these nanocomposite materials that have been synthesized by a simple equipment, like the one shown in Figures 3.1, 3.2 and 3.3, could be produced on a larger scale via a roll-to-roll process.

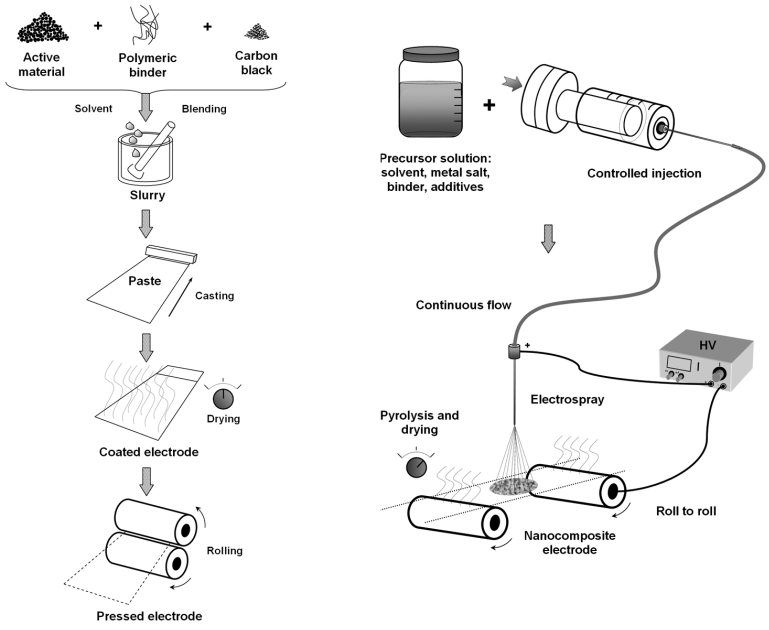

Figure 3.5 – Schematic drawing of (a) a typical manufacturing process of coated electrodes; and (b) the proposed on-step fabrication process. Adapted from Valvo, 2010 [19]

In this regard, besides the new experimental set-up built for the deposition of various coatings on large substrates (i.e. as that one on the E-STARS project [21]), which will be described in detail in Chapter 5) as shown in Figure 3.3, this set-up will soon be adjusted for the formation of layers on aluminium - roll-to-roll system, which preliminary versions of the setup are shown in Figure 3.6. The method will be further optimized together with a Dutch Small Medium Enterprise with governmental support.

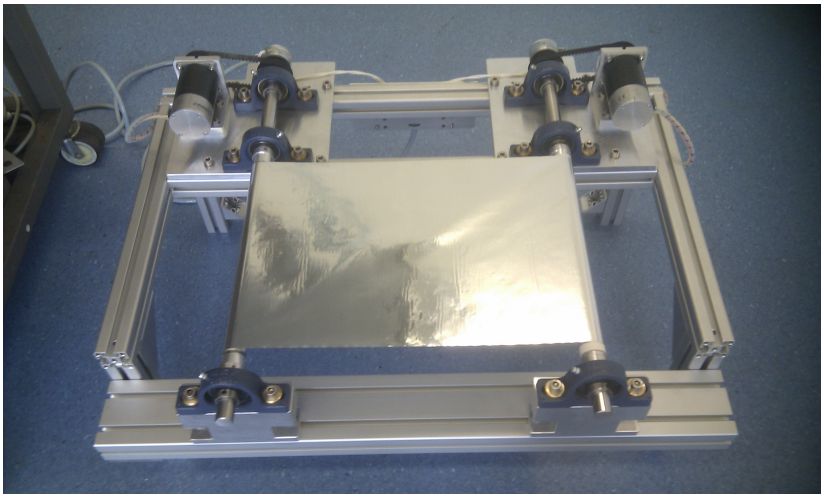

Figure 3.6 – Preliminary design of a roll-to-roll system to be coupled with ESP coating device for the production of advanced electrodes.

As these kinds of technologies are more advanced, and thus still at a laboratory scale, transfer to industrial manufacturing level will require development works with industrial equipment supplier. Nevertheless, advances in electrospray applications in nanotechnology will certainly continue in the near future, and new achievements in this field can be expected.

References

[1] W.-S. Yoon, S.-H. Ban, K.-K. Lee, K.-B. Kim, M. Kim, and J. Lee, "Electrochemical characterization of layered $LiCoO_2$ films prepared by electrostatic spray deposition," *Journal of Power Sources*, vol. 97-98, pp. 282–286, 2001.

[2] E. Garcia-Tamayo, M. Valvo, U. Lafont, C. Locati, D. Munao, and E. Kelder, "Nanostructured Fe_2O_3 and CuO composite electrodes for Li ion batteries synthesized and deposited in one step," *Journal of Power Sources*, vol. 196, no. 15, pp. 6425–6432, 2011.

[3] Munao, D and van Erven, J.W.M and Valvo, M and Garcia-Tamayo, E and Kelder, E.M, "Role of the binder on the failure mechanism of si nano-composite electrodes for li-ion batteries," *Journal of Power Sources*, vol. 196, pp. 6695–6702, 2011.

[4] J. Gaury, E. Kelder, E. Bychkov, and G. Biskos, "Characterization of Nb-doped WO3 thin films produced by Electrostatic Spray Deposition," *Thin Solid Films*, 2013.

[5] K. Hwang, K. Jeon, Y. Jeon, and B. Kim, "Hydroxyapatite forming ability of electrostatic spray pyrolysis derived calcium phosphate nano powder," *Journal of Materials Science*, vol. 41, pp. 4159–4162, 2006.

[6] H. Huang, X. Yao, X. Wu, M. Wang, and L. Zhang, "Morphology control of ferroelectric lead titanate thin films prepared by electrostatic spray deposition," *Thin Solid Films*, vol. 458, no. 1-2, pp. 71–76, 2004.

[7] Valvo, M. and Garcia-Tamayo, E. and Lafont, U. and Kelder, E.M, "Direct synthesis and coating of advanced nanocomposite negative electrodes for li-ion batteries via electrospraying," *Journal of Power Sources*, vol. 196, no. 23, pp. 10191–10200, 2011.

[8] A. A. van Zomeren, E. M. Kelder, J. C. M. Marijnissen, and J. Schoonman, "The production of thin films of $LiMn_2O_4$ by electrospraying," *Journal of Aerosol Science*, vol. 25, no. 6, pp. 1229–1235, 1994.

[9] C. Chen, M. Emond, E. Kelder, B. Meester, and J. Schoonman, "Electrostatic sol-spray deposition of nanostructured ceramic thin films," *Journal of Aerosol Science*, vol. 30, no. 7, pp. 959–967, 1999.

[10] U. Lafont, A. Anastasopol, E. Garcia-Tamayo, and E. Kelder, "Electrostatic spray pyrolysis of $LiNi_{0.5}Mn_{1.5}O_4$ films for 3D Li-ion microbatteries," *Thin Solid Films*, vol. 520, no. 9, pp. 3464–3471, 2012.

[11] S. Youssef, R. Al Asmar, J. Podlecki, M. Abdallah, D. Zaouk, and A. Foucaran, "Preliminary study on pyroelectric lithium tantalite by a novel electrostatic spray pyrolysis technique," *Microelectronics Journal*, vol. 39, no. 5, pp. 792–796, 2008.

[12] D. Zaouk, Y. Zaatar, R. Asmar, and J. Jabbour, "Piezoelectric zinc oxide by electrostatic spray pyrolysis," *Microelectronics Journal*, vol. 37, no. 11, pp. 1276–1279, 2006.

[13] J. Jeong, Y. Jeon, K. Jeon, K. Hwang, and B. Kim, "Preparation of zinc oxide films by an electrostatic spray deposition process," *Ceramic Processing Research*, vol. 7, no. 1, pp. 70–74, 2000.

[14] C. Chen, E. Kelder, P. Van Der Put, and J. Schoonman, "Morphology control of thin $LiCoO_2$ films fabricated using the electrostatic spray deposition (ESD) technique," *Journal of Materials Chemistry*, vol. 6, no. 5, pp. 765–771, 1996.

[15] C. Chen, A. Buysman, E. Kelder, and J. Schoonman, "Fabrication of $LiCoO_2$ thin film cathodes for rechargeable lithium battery by electrostatic spray pyrolysis," *Solid State Ionics*, vol. 80, no. 1–2, pp. 1–4, 1995.

[16] C. Chen, E. Kelder, M. Jak, and J. Schoonman, "Electrostatic spray deposition of thin layers of cathode materials for lithium battery," *Solid State Ionics*, vol. 86-88, no. 2, pp. 1301–1306, 1996.

[17] M. Mohamedi, M. Makino, K. Dokko, T. Itoh, and I. Uchida, "Electrochemical investigation of $LiNi_{0.5}Mn_{1.5}O_4$ thin film intercalation electrodes," *Electrochimica Acta*, vol. 48, no. 1, pp. 79–84, 2002.

[18] STOGRA Antriebstechnik GmbH, "Stepper motors: Sm 56.2.18j3 manual 2009." http://www.stoegra.de/pdf/sm56_2_e.pdf, July 2009. Accessed: 20 July 2013.

[19] M. Valvo, *Electrospray-assisted synthesis methods of nanostructured materials for Li-ion batteries*. PhD thesis, Delft University of Technology, Delft, The Netherlands, November 2010.

[20] L. L. F. Agostinho, *Electrohydrodynamic Atomization in the Simple-Jet Mode*. PhD thesis, Delft University of Technology, Delft, The Netherlands, February 2013.

[21] Efficient Smart sysTems with enhAnced eneRgy Storage, "Newsletter I." http://www.estars-project.eu/home/liblocal/docs/NewsletterI.-V0.pdf, November 2009. Accessed: 26 May 2013.

Chapter 4

One step synthesis and assembly of Fe_2O_3-, CuO-PVdF nanocomposite electrodes

> The Human Genome Project took about ten years, representing many person-centuries. [...] Like the Apollo moon landings, and like the Large Hadron Collider (the gigantic scale of this international endeavour moved me to tears when I visited), the complete deciphering of the human genome is one of those achievements that makes me proud to be human
>
> Richard Dawkins, *The Greatest Show on Earth*, 2009

A direct approach for the synthesis and coating of advanced nanocomposite electrodes based on iron and copper oxides as active materials, is presented in this chapter. The Metal-oxide/PVdF electrodes are directly formed by electrospraying precursor solutions containing metal salts, dissolved in N-methylpyrrolidone (NMP), together with Polyvinylidene Fluoride (PVdF) as binder. In this way, sub-micrometric deposits are formed as a composite of

oxide nanoparticles of a few nanometers dispersed in situ in a PVdF polymer matrix, creating nanocomposite structures that are being coated at once as thin electrode layers on stainless steel coin cell cans. The intimate contact between the nanoparticles and the binder favours enhanced adhesion of the materials in the overall electrode structure and adequate electrochemical performances are obtained without any conductive additive. Electrochemical tests demonstrate that the conversion reactions in these electrodes enable large initial discharge capacities, but also reveal that capacity retention needs further improvements. In a more general view, the results show that this approach is suitable, not only for the fabrication of nanocomposite electrodes for Li-ion batteries, but also for other novel applications.

This chapter is based on the published articles:

- **E. Garcia-Tamayo**, M. Valvo, U. Lafont, C. Locati, D. Munao, E.M. Kelder. *"Nanostructured Fe_2O_3 and CuO composite electrodes for Li ion batteries synthesized and deposited in one step"*. Journal of Power Sources 196 **(2011)** 6425-6432
- M. Valvo, **E. Garcia-Tamayo**, U. Lafont, E.M. Kelder. *"Direct synthesis and coating of advanced nanocomposite negative electrodes for Li-ion batteries via electrospraying"*. Journal of Power Sources 196 **(2011)** 10191-10200.

4.1 Introduction

Li-ion batteries are one of the most popular power sources that are currently used to power up a wide range of portable electronic devices. However, the increasing miniaturization of these devices implies that they become thinner, smaller and lighter, therefore requiring batteries with enhanced energy and power densities. Furthermore, high-power applications (e.g. EVs, HEVs, Power tools) require even higher volumetric and gravimetric energy densities, which can be eventually achieved by employing new materials in order to improve the existing Li-ion battery technology based on bulk, micrometer-sized materials. Intercalation represents the reaction mechanism on which rechargeable Li-ion batteries have always relied since their first commercial release by Sony [1]. Intercalation reactions in negative electrodes and their characteristic properties have been widely discussed and reviewed [2, 3]. The major drawback of this mechanism is related to its limited capacities. In the case of graphite, it is possible to reversibly store only one atom of lithium per 6 atoms of carbon (i.e. LiC_6), corresponding to a theoretical capacity of about 370 $mAhg^{-1}$.

It has been shown that lithium can react with a range of transition metal-oxides (TMO) by a process referred to as conversion [4]. The main advantage of TMO over carbonaceous materials in negative electrodes is that their capacities are noticeably higher (i.e. up to 1000 $mAhg^{-1}$), due to their ability to incorporate more than one Li atom per MO. Moreover, these type of materials in general, and Copper and Iron oxides in particular, are of interest because they can be produced using low-cost precursors with a limited impact on the environment. However, negative electrodes based on these materials suffer from mechanical volume changes during Li uptake and removal, even though not as severe as those of Li-alloys [5]. This disadvantage confers an important role to the process of particle synthesis and electrode assembly, where the active particles are mixed with other inactive components (i.e. binders and additives). Apart from that issue, they present intrinsic shortcomings of large separation of the voltage on charge and discharge [6]. In fact, incorporation of larger amount of Li ions, whatever the mechanism of reaction, results in a volume increase at the host material which causes mechanical stresses and may even produce cracking of the electrodes upon subsequent Li extraction and uptake.

In this respect, the use of nanostructures and nanocomposites is a prerequisite to accommodate better the strains and to obtain longer cycle life for these negative electrodes [7, 8]. Moreover, they can also significantly improve charge transfer and power delivery in the electrodes because of larger surface contact with the electrolyte and shorter diffusion lengths for the charge carriers (i.e. Li+ ions and electrons). In particular, the presence of small nanoparticles and

extended interfaces is decisive in transition metal oxides to have almost fully-reversible reactions [9, 10], as well as extra charge storage at the boundaries in a pseudo-capacitive way [11, 12]. Previous works adopting this approach have been reported [9, 13–16], pointing out the crucial role that nanostructured materials can play in these systems, as well as in other energy conversion and storage applications [6, 8, 10, 12, 17].

Nevertheless, exploiting the features of nanomaterials in practical negative electrodes in most of the cases is not a trivial task. Their favourable characteristics can be easily masked by improper incorporation into the ultimate electrode structures. This holds especially when these materials are processed in a powder form and their dispersion and assembly in coated electrodes become more difficult.

Various strategies have been proposed to address this issue and they have been succinctly described by M. Valvo, with whom I worked closely during the last part of his PhD. Some of the novel methods he mentions in his dissertation [18], include well-designed and advanced methods for fabrication of negative electrodes such as the dispersion of nanoparticles in a supporting carbon matrix [19], the embedment of active (nano) material in carbon microspheres [20–22], as well as carbon-encapsulated hollow structures [23]. Their studies on cycle life show enhanced performance due to an improved mechanical stability that prevents particle agglomeration and the increase of electronic conductivity of the entire electrode.

Nevertheless, these methods present shortcomings such as the use of expensive precursors and the fact that the syntheses are usually multi-step processes. Even in one-step syntheses, high temperatures (i.e. 700 °C) are usually necessary for the preparation of such nanocomposites. Moreover, the electrode is still not present at its final stage as the as-produced active material still needs to be mixed with the inactive components (binder and conductive additives) to form a slurry which will be finally coated on the current collector.

Several groups have used alternative processes to reduce the steps required for the fabrication of electrodes. Their strategy generally consists in combining, simultaneously, the synthesis and growth/deposition of the active materials directly on the current collectors. Techniques such as electrodeposition [24], template-synthesis [25, 26], physical vapour deposition [27], sputtering [28], vapour-solid-liquid (VLS) [29] or vapour-solid (VS) growth [30] have been widely used yielding interesting results. In all these cases, binders and conductive additives (i.e. carbon black) are not included in the final electrodes. However, most of these methods are highlighted as very interesting and promising alternatives for applications where only the active material is required, such as in the field of microbatteries [31].

In this respect, their ability for the production of different nano-architectures (i.e. 3D self-supported nanowires or nanotubes arrays, etc.) are particularly attractive in terms of achievable capacities and rate capabilities, offering enhanced surface areas in contact with the electrolyte [32–34].

Among the reported morphologies some are mechanically favourable as they can better sustain with the strain caused by Li (de) insertion. Examples of these 3D nano-architectures include rods, wires or tubes. Each structure has its own contact with the substrate, contributing directly to the overall electrochemical reaction without any additional material needed for operation. However, the fabrication methods applied so far (i.e. template-assisted syntheses, VLS, VS, etc.) are quite cumbersome and, even in the most favourable cases, there are obvious limitations arising, for example, from pre-treatments needed for the substrates, the size of the template membranes, the use of expensive catalysts, the limited area coverage and the scarce amount of active material effectively grown. Moreover, the risk of breaking the structures during fabrication should be also taken into account. Such circumstance results in a direct loss of capacity, since the electrical contact of the individual structures with the substrate is definitively lost. Therefore, the role of polymer binders and eventual additives in practical coated electrodes becomes important, even though they account for inactive mass added to the entire structure. Active metal or metal-oxide nanoparticles need a suitable "glue" to holds them together and to reinforce the entire electrode during the electrochemical processes. Particles must adhere to the current collector and not move far apart from each other in order to ensure percolation. Additionally, the binder adhesion to the surface of the nanoparticles should be optimal, promoting the transport of the charge carriers to and from the particles, while preventing them from agglomeration and coalescence.

In this scenario, the possibility of direct synthesis and coating of nanocomposite layers, containing the active nanoparticles dispersed in a binder with eventual additives, is obviously attractive. More important, it is convenient to generate in situ the active nanoparticles already mixed with the binder, rather than dispersing them in a separate step. Indeed, the process of synthesis of the active materials does not need to be separated from their assembly in composite coated electrodes with other components.

Electrospray-based methods (i.e. electrospray pyrolysis and deposition, electrospinning) are powerful tools to perform such a one-step synthesis and coating of nanocomposite electrodes. They have been conveniently applied to the synthesis and deposition of various functional coatings like MgO [35], ZrO_2 [36], as well as thin film electrodes for Li-ion batteries. Different materials have been synthesized, e.g. $Li_{1.2}Mn_2O_4$ [37], $LiMn_2O_4$ [38], $LiCoO_2$ [39, 40], $Li_4Ti_5O_12$ [41] for positive electrodes and Fe_2O_3 [42], SnO_2 [43] for negative

electrodes. However, all these materials do not include any polymer for binding purposes. The presence of the binder promotes the mutual adhesion of the deposits, as well as their overall contact with the underlying substrate to obtain a reinforced composite electrode coating. This circumstance should be also addressed when internal and external mechanical stresses are present. A similar approach using a precursor ink consisting of a solution of polymer binder with a suspension of previously synthesized silicon nanoparticles and commercial carbon additive has been recently reported [44].

This chapter is focused on the synthesis and deposition of Fe_2O_3 and CuO nanostructured electrodes in one step via Electrostatic Spray Pyrolysis (ESP). During the processing, solutions containing precursor metal salts dissolved together with Polyvinylidene Fluoride (PVdF) binder, were electrosprayed on a heated substrate where the generated sub-micron sized droplets underwent pyrolysis. The oxide nanoparticles are generated and thereby mixed immediately with the binder (i.e. PVdF) so as to form the composite electrodes and hence avoiding powder mixing and paste casting. It is, therefore, proposed that it is a viable approach to synthesize and assemble in one step thin nanocomposite coatings of negative electrodes at low temperature.

4.2 Materials and Methods

As described in Chapter 3, Paragraph 3.1.2, a schematic of the equipment used for the production of the Fe_2O_3 and CuO nanostructured composite electrodes is shown in Figure 3.1.

The precursor solutions were prepared from Iron (II) Acetate Anhydrous, $Fe(C_2H_3O_2)_2$ (Alfa® GmbH) and Copper (II) Nitrate trihydrate, $Cu(NO_3)_2.3H_2O$ (AnalaR® BDH). These salts were independently mixed with Polyvinylidene fluoride (PVdF SOLEF 1015) in a weight ratio (Metal:PVdF wt%) of 5:1 and were respectively dissolved in 15 ml of N-Methyl-2-pyrrolidone (NMP MERCK-Schuchardt). Vigorous stirring was applied in order to achieve a complete dissolution of the PVdF and the precursor salts. The solution obtained was relatively viscous and concentrated. No carbon black was added to the precursor solutions for the experiments. A precision dispense tip (EFD® Nordson) with inner diameter 0.61 mm was utilized in order to facilitate a continuos flow and avoid clogging. The solutions were fed to the electrified nozzle at a constant flow rate in order to undergo electrospraying and direct reaction so as to deposit electrodes on coin cell cans. The high electrical field applied between the nozzle and the substrate holder caused the formation and acceleration of tiny, highly-charged droplets towards the substrate. The atomization process

was accompanied by the evaporation of the solvent and subsequent pyrolysis of the precursor salts, enabling the direct formation of coated nanocomposite electrodes without any "doctor-blading" method [45, 46]. All the experiments were performed in air. The distance between the tip of the nozzle and the support was kept constant at 20 mm during the electrode deposition, as well as the injection flow rate (values are reported in Table 4.1). The applied voltage was tuned in each experiment in order to reach a stable electrospray in the so-called cone-jet mode (see Chapter 2.2.1), which was observed by means of a high intensity lamp. The temperature of the substrate was kept constant at 280 °C to ensure complete evaporation of the solvent (i.e. NMP evaporates around 200 °C) and to obtain pyrolysis of the precursors, as well as good adhesion of the PVdF to the coin cell can substrates. Furthermore, it was far from the threshold for decomposition of PVdF in air (i.e. >315 °C). Some possible pyrolysis reactions at 280 °C in air for the precursor salts are the following:

$$Cu\,(NO_3)_2 \cdot 3H_2O + O_2 \overset{280^\circ C}{\longrightarrow} CuO + CO \nearrow + 3CO_2 \nearrow + 3H_2O \nearrow \quad (4.2.1)$$

$$2Fe\,(CH_3COO)_2 + 8O_2 \overset{280^\circ C}{\longrightarrow} Fe_2O_3 + CO \nearrow + 7CO_2 \nearrow + 6H_2O \nearrow \quad (4.2.2)$$

The mass percentage of the oxide materials in the composite electrodes was calculated by means of the weight ratio of the PVdF/ precursor salts and their respective pyrolysis reactions, yielding approximately 60-70%.

Control of the morphology, thickness and texture (i.e. porosity) of the deposited layers can be achieved by adjusting the physical parameters of the ESP. The electrode thickness can be controlled, for example, by adjusting the deposition time on the substrate. The morphology and texture can be influenced by adjusting flow rate, voltage, distance from nozzle to sample, as well as by taking into account properties of the solvent, like its temperature of evaporation, viscosity, conductivity, etc. A mask was used to control the area of deposition on the coin cell cans in order to obtain circular coatings of approximately 150 mm^2. It is worth mentioning that the resulting electrodes do not need any further treatment and that they can be directly sealed in a full battery assembly by adding the remaining parts (i.e. electrolyte-soaked separator, lithium disk, spring, gasket and stainless steel lid).The deposited mass and thickness of the PVdF-oxide composites were determined by carrying out measurements on the coin cell cans before and after the process of electrode coating. For this purpose a digital balance (Sartorius) with an accuracy of 10^{-2} mg and a digital caliper (Mitutoyo Absolute, 10^{-3} mm accuracy) were employed.

Table 4.1 – Experimental parameters and characteristics of the reacted materials.

Precursor	Voltage (kV)	Current (mA)	Flow rate (mLh^{-1})	Nozzle (mm)	Temperature (°C)	Expected Material	Estimated % of active material
$Cu(NO_3)_2$+ PVdF+NMP	8.4	0.002	0.2	20	280	CuO +PVdF	62
$Fe(Ac)_2$+ PVdF+NMP	8.0	0.001	0.4	20	280	Fe_2O_3 +PVdF	69

Galvanostatic and Cyclic Voltammetry (CV) measurements were performed in order to assess the electrochemical performance of the coated electrodes on CR2320-type coin cells assembled in an Ar-filled (H_2O<2ppm) glove box (MBraun). The nanostructured coatings were directly tested as working electrodes, while lithium metal disks were used as reference and counter electrodes with polyethylene separators (Solupor) soaked with an electrolyte solution of 1M $LiPF_6$ in EC:DMC 2:1 (Mitsubishi Chemical). The cells were discharged and charged on a Maccor S-4000 cycler with a cut-off voltage between 0.05 V and 3.0 V at gravimetric current densities of 124 mAg^{-1} for Fe_2O_3/PVdF and 337 mAg^{-1} for CuO/PVdF, respectively. Likewise, voltammograms were carried out with an Autolab (Ecochemie, The Netherlands) between 0.02 V and 3.0 V, at scan rate of 0.1 mVs^{-1}. Atomic Force Microscopy (AFM) was performed on the coated samples by a NT-MDT NTEGRA scanning probe microscope in semi-contact mode by a Si cantilever and tip (NT-MDT, Silicon: NSG 03). A Philips CM30T transmission electron microscope operated at 300kV was used to investigate the morphology, size and crystallinity of the as-deposited nanocomposites. An EDX probe (Oxford) coupled to the TEM was further used to perform an elemental analysis of the materials. Their composition and crystalline structure were also studied by means of X-ray diffraction on a Bruker (AXS D8 Advance) diffractometer equipped with a Cu-K_α radiation source (α=1.5418 Å).

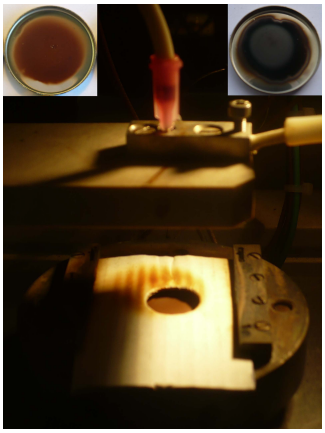

Figure 4.1 – Photo of the reaction chamber were the direct synthesis and assembly of coated nanocomposite electrodes takes place. Examples of composite coatings with PVdF are shown as insets in the photo. Fe_2O_3 in the top left-hand corner and CuO in top right-hand corner.

4.3 Results and Discussions

4.3.1 General characterization

A close up picture of the reaction chamber of this system is observed in Figure 4.1, together with images of the as-deposited layers on coin cell cans. It is seen that the resulting coatings are fairly homogeneous and their colors indicate the different metal oxide particles inter-dispersed within the PVdF. The dark reddish-brown and black hues match with the characteristic colors of the oxides produced, namely Fe_2O_3 and CuO, respectively.

The measured values of thickness and mass obtained in correspondence of different sprayed volumes for the precursors are shown in Figure 4.2. As expected, increasing the thickness of the coating results in a growth of the mass deposited on the coin cell cans following a linear trend.

4.3.2 Structural and morphological characterization

The morphology of the coated materials was investigated by AFM. The images of the scanned areas for the composite CuO/PVdF and Fe_2O_3/PVdF electrodes

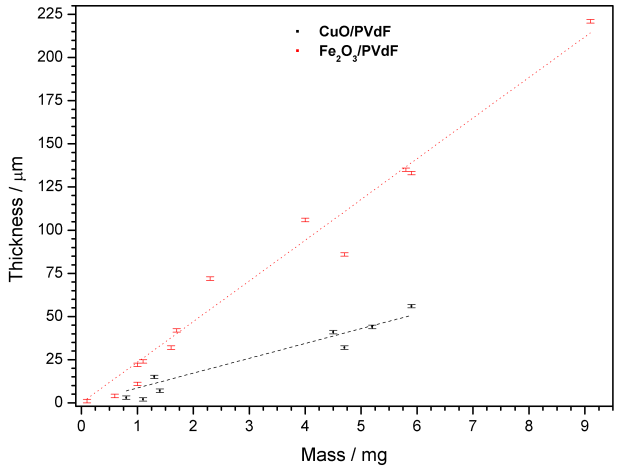

Figure 4.2 – Plot of the values of thickness vs. mass for the deposited electrodes of Cu/PVdF (open stars) and Fe_2O_3/ PVdF (solid stars) obtained for various sprayed volumes of the precursor solutions.

are shown in Figure 4.3(a) and (b), respectively.

Figure 4.3(a) shows that sub-micrometric deposits of CuO/PVdF have been formed. The observed elongated features are composed of smaller spherical-like structures merged together in agglomerates arranged in platelets. The surface morphology suggests that the pore size is similar to that of the particles. In Figure 4.3b) the surface of the Fe_2O_3/PVdF coating displays similar characteristics, showing, however, larger and more defined spherical deposits arranged in three dimensional agglomerates. The resulting pore size is comparable with that of the agglomerates. In both of the previous cases, the sub-micrometric deposits have been formed from the reacted droplets generated during electrospraying. It is worth noticing that all the deposits have a spherical-like shape, indicating that most of the evaporation of the solvent (i.e. NMP) and the precursor decomposition in the generated droplets practically occurred during their flight towards the heated substrate [47]. In this respect, each charged droplet acts as a sort of "microreactor" for the formation of the ultimate materials.

These results are in accordance with previous findings from our group, where precursor solutions containing cobalt or tin metal salts were electrosprayed to form CoO/PVdF or SnO_2)/PVdF nanocomopsites, respectively. In

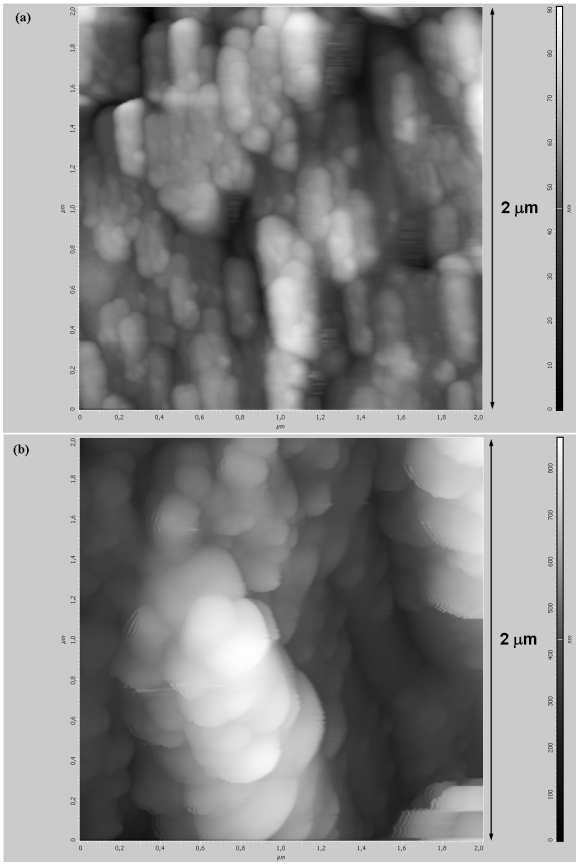

Figure 4.3 – AFM images of the surface morphology of the nanocomposites. a) scan of CuO/PVdF (height bar 0-90 nm) and b) Fe_2O_3/PVdF (height bar 0-850 nm). The scanned areas are 2 μm x 2 μm wide.

those experiments, we obtained matching spherical-like morphologies with sizes ranging from tens of nanometers to roughly 300nm. The outcome of this research has been carefully described in a dissertation [18] and recently published [48].

XRD was performed on samples synthesized under identical conditions to those described for the preparation of each oxide/PVdF electrode, but having a larger area coverage and a thicker coating. This is achieved by simply increasing spraying time. The underlying substrates were either aluminum or stainless steel.

In Figure 4.4(a), the diffraction pattern of the CuO/PVdF composite is presented. The sharpest peaks at 45°, 65° and 78°, correspond to characteristic diffractions related to the underlying Al foil support. The observed pattern indicates that monoclinic CuO (JCPDS: 80-1916) has been formed, as also confirmed by the black color of the coated material. Two broad peaks around 35° and 38° correspond to the strongest characteristic diffractions by the planes (-110) and (111) respectively. Four weak features can be also observed in the diffraction pattern around 33° (110), 49° (-202), 58° (202) and 62° (-113) respectively, confirming the presence of small crystallites of CuO. Moreover, the average crystallite size was evaluated by the Scherrer formula which yielded an approximate value of 12 nm for this material.

Figure 4.4(b) shows the diffraction pattern of the Fe_2O_3/PVdF layer. The only peaks that are clearly visible in the plot are those related to the stainless steel substrate, while the nanocomposite layer displays mainly amorphous characteristics. Nevertheless, the broad hump around 33° falls within the angular range where the strongest diffractions of Fe_2O_3 occur.

Indeed, characteristic diffractions by the planes (104) and (110) for α-Fe_2O_3 are respectively due at 33.15 and 35.61° (JCPDS no. 33-0664). Furthermore, α-Fe_2O_3 displays its strongest peak indexed (311) at 35.65° (JCPDS no. 39-1346). The reduced size of the nanoparticles and the relatively low temperature for the synthesis process are likely responsible for the observed diffraction pattern. Nevertheless, the dark reddish-brown color of the coatings clearly indicates that Fe_2O_3 has been formed, since other iron oxides with different stoichiometries have a distinctive black colour.

In the same manner, these XRD results are in agreement with our studies on SnO_2 and CoO, where the resulting metal oxide particles exhibit mainly amorphous-like features [48].

Investigation of the morphology and the intimate structure of the materials was performed by TEM. Figure 4.5(a) shows a bright field image of the deposited CuO/PVdF composite structure. Small CuO nanoparticles with sizes of roughly 4-7 nm are observed. The CuO nanoparticles, which correspond to

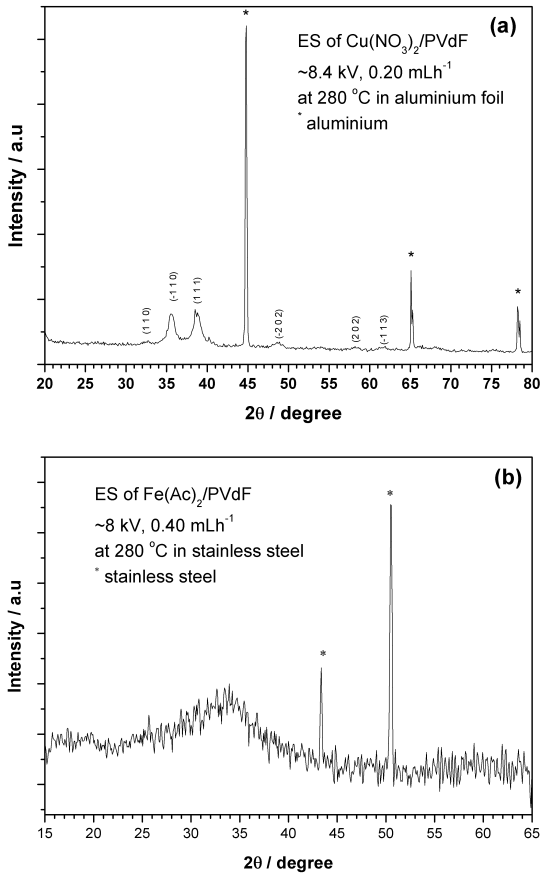

Figure 4.4 – XRD spectra of the nanocomposite electrodes by electrostatic spray pyrolysis of (a) $Cu(NO_3)_2.3H_2O$ /PVdF and (b) $Fe(C_2H_3O_2)_2$/PVdF at 280 °C. The peaks marked by an asterisk refer to the characteristic diffractions of the substrates used.

the dark dots in the image, are homogeneously interdispersed in the PVdF. The high resolution TEM image in Figure 4.5(b) shows the crystalline nature of the nanosized particles and lattice fringes are clearly observed (see the dotted circles). The data agree well with the calculated crystallite size derived from XRD. It can be further concluded that the nanoparticles are mainly nanocrystals.

Figure 4.6(a) shows the morphology of the Fe_2O_3/PVdF nanocomposite. It can be seen that the typical size of the remnants varies roughly from 20 nm up to 300 nm, matching well with the previous AFM analysis. The spherical shape of the deposits is caused by the drying process of the electrosprayed precursor droplets. Also in this case a fine interdispersion of the oxide particles in PVdF is achieved. Figure 4.6(b) presents a highly magnified image of one of these spherical-like relics, showing that Fe_2O_3 particles of about 5-7 nm are homogeneously distributed in these structures. Moreover, no lattices fringes are observed in this material, confirming the amorphous-like nature of the iron oxide, as previously derived from XRD analysis. The local chemical composition of these oxide particles was further investigated by Energy Dispersive X-rays analysis, yielding about 40 at.% of iron and 60 at.% of oxygen, matching with the Fe_2O_3 stoichiometry.

It is important to note that PVdF surrounds the particles in all the various nanocomposites in Figures 4.5(a,b) and 4.6(a,b), thus reinforcing the nanostructured material at a local nanometric level, while enhancing mutual adhesion of the deposits and improving the overall contact with the substrate at a macroscopic scale. At the same time, it can be expected that pores have been produced in the remnants during the processes of evaporation and pyrolysis, as it appears from the TEM micrographs. Porosity is particularly important in this type of electrodes, because apart apart from allowing direct access of the electrolyte to the active materials, it provides free space that can accommodate volume variations. Besides, the amorphous nanostructures undergo isotropic expansion and contraction upon cycling [49] and this circumstance helps the binder immobilizing the particles and preserving the integrity of the electrodes. These characteristics, as well as the pronounced presence of lattice deffects, can significantly contribute to improve cycleability, as well as Li^+ transport and storage in the electrodes. In this case, the PVdF layer that surrounds both the individual nanoparticles and the whole deposit is expected to exert an action similar to that of a "balloon" at both characteristic scales. On the one hand, it prevents agglomeraton and coalescence of the nanoparticles, on the other hand it helps holding the nanoparticles tight within the deposits, while buffering their volume changes upon cycling. It is important to mention

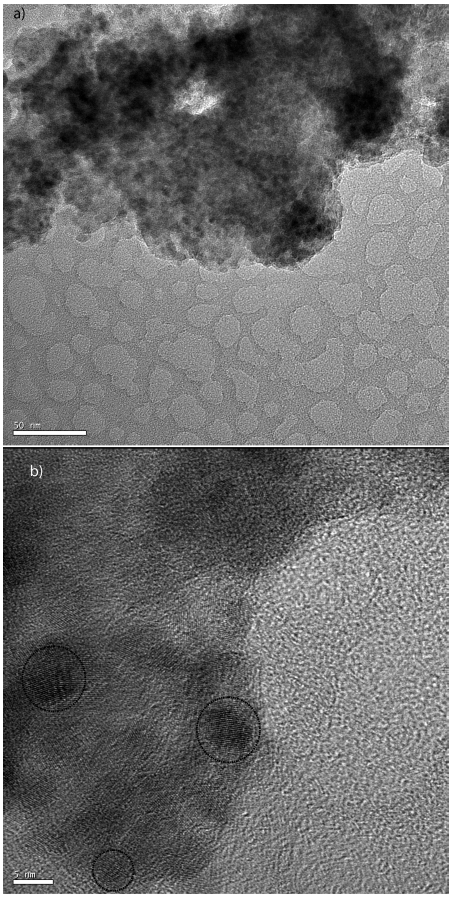

Figure 4.5 – TEM bright field images showing (a) morphology and size of the CuO/PVdF nanocomposites and (b) lattice fringes of CuO at high resolution.

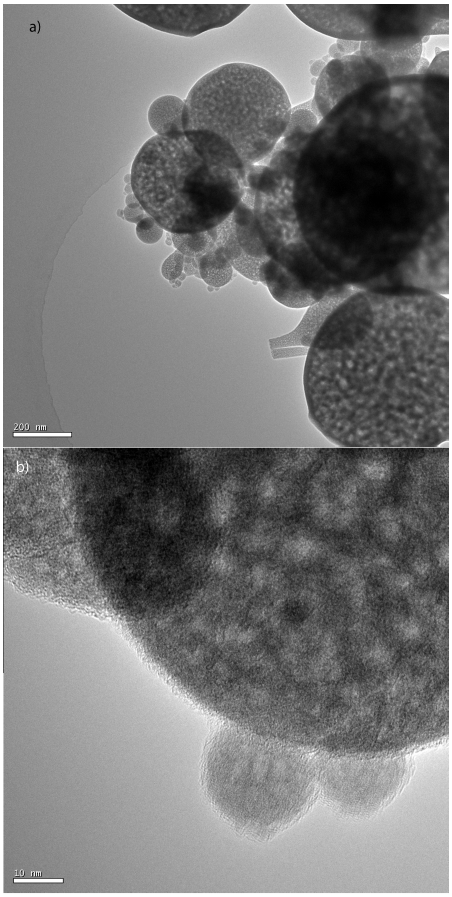

Figure 4.6 – TEM bright field images showing (a) morphology and size of the Fe_2O_3/PVdF nanocomposites and (b) local structure at high resolution showing the absence of lattice fringes.

that the grain size of the particles can be controlled by tuning the properties of the precursor solution and/or by changing the experimental parameters (i.e. flow rate, voltage, temperature, etc.).

4.3.3 Electrochemical performance

Figure 4.7 shows the CV plot of the CuO/PVdF electrode. The shape of the voltammogram and its respective peaks, are in accordance with previous reports [50] and [51]. During the first cycle, three cathodic peaks are observed at 2.4, 1.25 and 0.7 V and can be associated to a multistep reaction corresponding to:

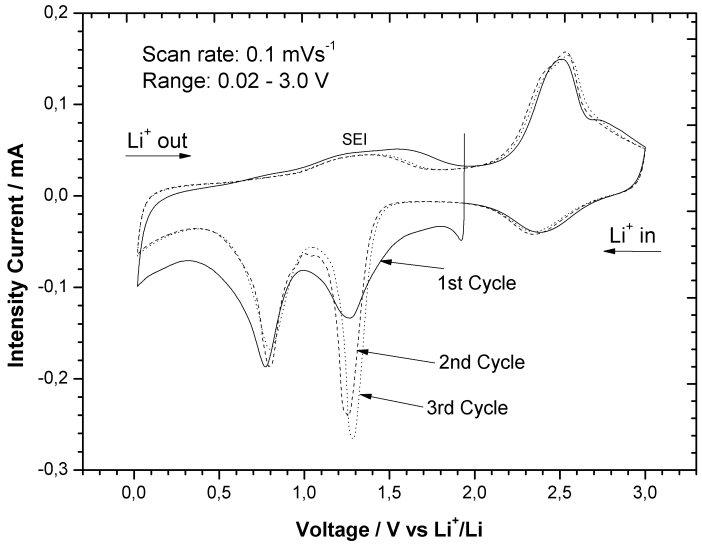

Figure 4.7 – CV plot for the CuO/PVdF electrode deposited by ESP.

- The creation of a $Cu^{II}_{1-x}Cu^{I}_{x}O_{1-\frac{x}{2}} (0 \leq x \leq 0.4)$ solid solution within the CuO phase and the formation of Li_2O as a separate phase, as suggested by Debart *et al.* [50]

$$CuO + xLi^{+} + xe^{-} \longrightarrow \left[Cu^{II}_{1-x}Cu^{I}_{x}\right] O_{1-\frac{x}{2}} + \frac{x}{2}Li_2O \qquad (4.3.1)$$

This process occurs when the starting material starts reacting with Li, causing a gradual reduction of Cu(II) in Cu(I), together with the creation of oxygen ion vacancies in the CuO structure, without affecting the overall configuration. The lost oxygen is then trapped by lithium ions to form a small quantity of Li_2O at the particle surface.

- The formation of a Cu_2O phase, which takes place when the strain, caused by the reaction with the extra lithium uptake, becomes strong enough so as to change the atomic arrangement of CuO into a Cu_2O-type structure with the formation of nanoparticles [51].

- The decomposition into metallic Cu nanoparticles embedded into a Li_2O matrix.

Furthermore, at high lithiation stages (i.e. between 0.02-0.3 V), another reduction process is present, which can be attributed to the reduction of the electrolyte solvent and hence the growth of an organic-type layer.

Conversely, during lithium removal, two anodic peaks appear at 2.5 V and 2.75 V, which are respectively due to the oxidation of metallic Cu to Cu(I) and to the partial oxidation of Cu(I) to Cu(II). The broad bump around 1.45 V could be associated to decomposition of the organic layer.

The CV peaks and their variations are consistent with the galvanostatic discharge-charge plots shown in Figure 4.8(a). The theoretical capacity of CuO is 674 $mAhg^{-1}$, according to the general reaction:

$$M_xO_y + 2yLi^+ + 2ye^- \longleftrightarrow yLi_2O + xMO^0 \tag{4.3.2}$$

where M represents the transition metal (e.g. Cu, Fe, Co, Ni, Ru, etc.) of interest. Three distinct potential slopes are visible in both the first discharge and charge curves, which are observed more clearly as peaks in the related differential capacity vs. voltage plot (see figure inset). Following the direction of the arrow in the plot, three different peaks are noticed at 2.4 V (wide bump), 1.3 V and 0.8 V, respectively. Similarly, a broad peak around 1.45 V followed by two other peaks at 2.35 and 2.7 V are observed in the upper curve corresponding to the charge process. It is important to observe that for this material a significant difference in the charge-discharge processes exists in terms of characteristic voltages at which the reactions take place. In this respect, it is necessary to charge the system above 2.0 V in order to extract most of the Li that has been stored during Li uptake. The CuO/PVdF electrode displayed a discharge capacity of about 800 $mAhg^{-1}$ in the first cycle at a gravimetric current density of 337 mAg^{-1}.

It is interesting to note that after the first cycle the subsequent discharge

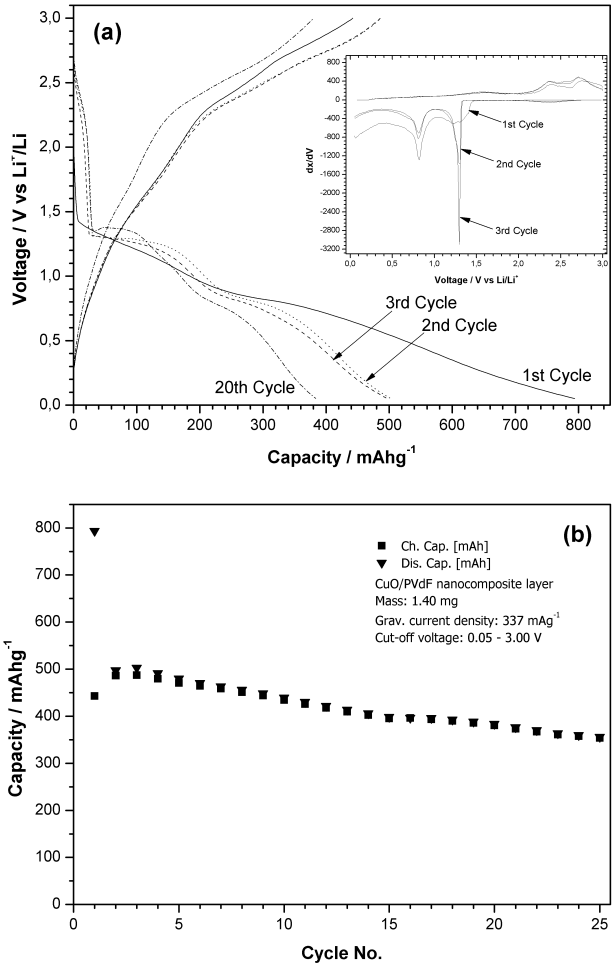

Figure 4.8 – Galvanostatic measurements of the composite CuO/PVdF electrode between 0.05 and 3.0 V at 337 mAg^{-1}: (a) charge-discharge voltage profiles. The inset is a graph representing the differential capacity. (b) Capacity retention upon progressive charge-discharge.

curves show a more pronounced step-like profile, with a typical upper shift of the voltage plateau around 1.3-1.4 V due to the enhanced tendency of dissolution of the regenerated nano CuO after initial reaction with Li, discovered for the CuO/Li primary battery [52]. Moreover, this rise in potential has also been observed in the case of CoO and it is an intrinsic characteristic related to the initial conversion of the CoO and its pulverization in the following cycles [48].

Figure 4.8(b) presents the evolution of charge and discharge capacities upon cycling. The first discharge curve yields a capacity of about 800 $mAhg^{-1}$. This indicates that a remarkable amount of Li is irreversibly consumed in the formation of the SEI layer and in the conversion reaction of the oxide to metallic Cu and Li_2O, yet this large contribution is not surprising, considering the large surface area of the nanostructured CuO and the peculiar texture of the deposits. The process is not fully reversible, since 2.4 lithium ions (800 $mAhg^{-1}$) react in the first discharge while only 1.3 (460 $mAhg^{-1}$) can be removed during the first charge, with subsequent capacity fading upon cycling. However, it should be noted that the CuO/PVdF electrode is able to cycle at a relatively high gravimetric current density, without the presence of any carbon additive and a non-negligible fraction of PVdF, which hinders electron conduction. The small CuO nanoparticles and their homogenous dispersion in the coating play a key role in the performance of the electrode, which shows a capacity of about 360 $mAhg^{-1}$ after 25 cycles.

The electrochemical behaviour of Fe_2O_3/PVdF electrode was investigated in a similar way. Figure 4.9 shows the CV plot for the first three cycles at a rate of 0.1 mVs^{-1}. In the first scan a cathodic peak around 0.67 V can be observed, which could be associated to the initial formation of the SEI layer and the conversion reaction of Fe_2O_3 into FeO and Li_2O [53]. In the following anodic part a clear oxidation peak is observed at about 1.50 V, accompanied by a broad shoulder around 1.75 V. During subsequent cycles these features do not shift but they gradually overlap, due to the width of the peaks. These two features can be associated to the decomposition of the SEI layer and the reversible oxidation of Fe^0-Fe^{3+} [5, 54]. In the subsequent cycles the cathodic and anodic peaks slightly shift to 0.70 V and 1.55 V, respectively. Furthermore, the intensity of the peaks, as well as their respective underlying areas decrease upon cycling indicating loss of capacity. The origin of the small reduction peak that appears around 1.30 V is unclear but it could be related to the reaction of the electrolyte with the nanoparticles left after the first cycle of conversion and regeneration.

The shape of the observed CV is consistent with the plot of the differential capacity, shown in the inset of Figure 4.10(a).

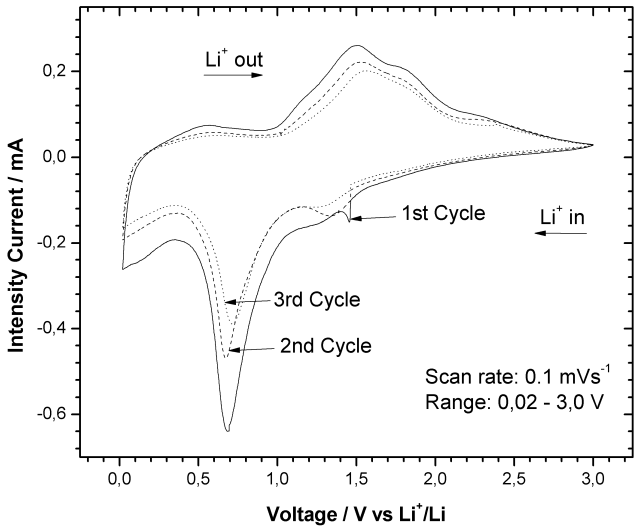

Figure 4.9 – CV plot for the Fe_2O_3/PVdF electrode deposited by ESP.

The discharge-charge curves of the Fe_2O_3/PVdF electrode in Figure 4.10(a) indicate that high capacities can be reached. Indeed, an initial discharge capacity of about 1550 $mAhg^{-1}$ is obtained at a gravimetric current density of 124 mAg^{-1}, while the first charge up to 3.0 V yields almost 1200 $mAhg^{-1}$, corresponding to a coulombic efficiency of approximately 77%. Considering that the theoretical capacity of Fe_2O_3 is 1007 $mAhg^{-1}$ (6 Li^+ exchanged per reaction), according to the general reaction described in equation (4.3.2), a considerable amount of lithium ions (9.3 during discharge and 7.1 during charge) is irreversibly consumed both in the formation of the SEI layer and in the conversion reaction of the oxide to metallic Fe and Li_2O. A certain loss of reversibility is visible in the subsequent discharge and charge curves, which shift towards lower capacities, maintaining profiles similar to those of the first cycle.

The discharge profile displays an initial slope with a slight inflection around 1.5 V and a definite plateau around 0.9 V, followed by another slope at lower voltages corresponding to the conversion reaction of the iron oxide. These values are close to the redox peaks found in the CV curves and there is a relation between the major peaks in the voltammogram and the definite plateaus in

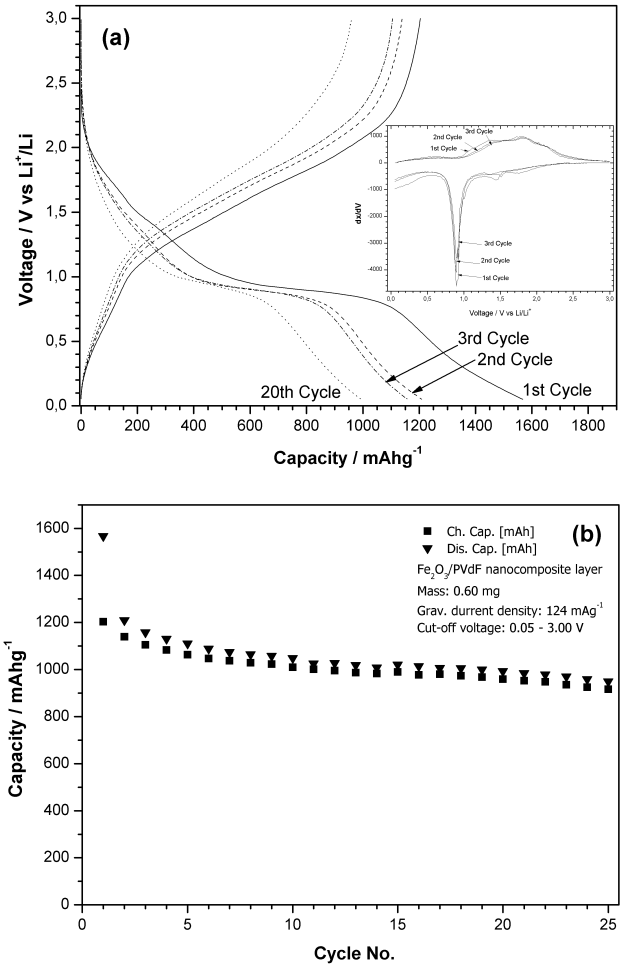

Figure 4.10 – Galvanostatic measurements of the composite Fe_2O_3/PVdF electrode between 0.05 and 3.0 V at 124 mAg^{-1}: (a) charge-discharge voltage profiles. The inset is a graph representing the differential capacity. (b) Capacity retention upon progressive charge-discharge.

the voltage profiles of discharge-charge. Interestingly, no rise in the potential of the "conversion plateau" is detected after the first discharge, indicating that the process of reaction with lithium is somehow different from that of CuO. Indeed, the particles of Fe_2O_3 are not directly decomposed upon reaction with lithium, while the initial formation of an intermediate $Li_xFe_2O_3$ compound has been reported [55].

The evolution of the charge and discharge capacities upon cycling is presented in Figure 4.10(b). Despite the irreversible loss in the first cycle and a slight fading of the capacity in the subsequent cycles, the electrode shows a remarkable capacity of about 950 $mAhg^{-1}$ after 25 cycles. Therefore, this electrode mainly suffers from capacity loss in the first cycles and no activation of the nanoparticles has been observed, suggesting that the formation and subsequent thickening of the SEI layer does not enable efficient charge transfer at the surface of the active material. The following cycles bring about only a moderate fading. The complete conversion of Fe_2O_3 to form 2FeO and $3Li_2O$ according to the general Eq. (4.3.2) causes a theoretical volume change of 93%, which needs to be sustained by PVdF and causes significant strain. Besides, the insulating properties of PVdF hamper efficient charge transport for Fe_2O_3, which is a poor electron conductor, especially when compared to other transition metal oxides, as, for example, RuO^2. In this respect, the effective transfer of electrons to and within Fe_2O_3 nanomaterials has been addressed in previous studies, showing that it is of utmost importance for sustaining high current densities and that it constitutes the rate limiting factor [56]. The reduction in size of the active particles in this case is only a pre-requisite to increase the performances of the nanocomposite. Still, it is not sufficient, since also the requirement of efficient electron/ion transport in the major steps of the kinetics (i.e. electron and ion transport from their "reservoirs" to the active particles, charge incorporation through their surface and transfer of the Li component inside their solid structure) of composite electrodes should be met [57]. It is relevant to insist that also in this case the nanocomposite electrode was able to cycle without any conductive additive and despite the poor electrical conductivity of iron oxide and the insulating properties of PVdF, not to mention the high gravimetric current density at which it was subjected, as compared with previous works on this material [4, 58, 59].

Finally, the influence of the thickness of the coatings on the capacity retention for the two different types of composite electrodes is presented in Figure 4.11.

Not surprisingly, from Figure 4.11(a and b) it is observed that for both oxide materials the best performances are obtained in correspondence of thinner electrode coatings. It is important to note that the electrode kinetics in

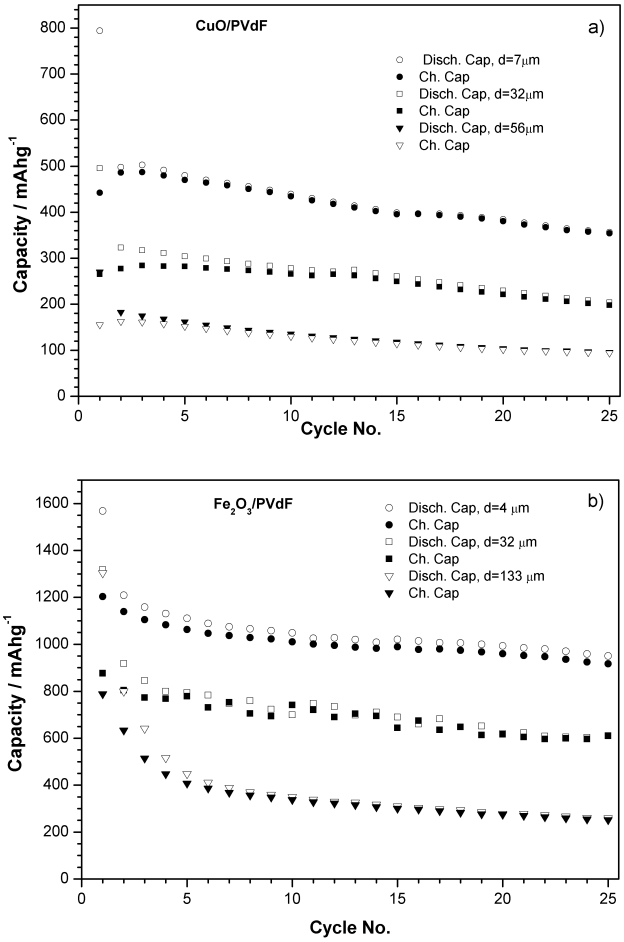

Figure 4.11 – Capacity retention upon repeated charge-discharge for electrodes with different thickness: (a) CuO/PVdF and (b) Fe_2O_3/PVdF.

composite electrodes can be divided into three steps [57]: (i) transport of the charge carriers (i.e., Li^+ and e^-) from their source to the active matter, (ii) charge incorporation reaction, involving the transfer of both charged species from the outside into the interior of the active particles and (iii) transport of the Li component inside the solid particles (diffusion). Herein CuO and Fe_2O_3 nanoparticles with size below 10 nm and narrow size distribution have been produced and homogeneously inter-dispersed with PVdF, therefore it is reasonable to expect that the characteristic times for steps (ii and iii) are much shorter than that related to step (i), due to the increased surface area of the nanoparticles and their extremely reduced size, respectively [6] and [8]. In this case, the electrode resistance is proportional to the electrode thickness (or, equivalently, the electrode mass, see Figure 4.2), since the thicker the electrode, the longer the average path of the charge carriers for step (i).

The absence of carbon black in both preparations limits the electron percolation between the nanoparticles and, at a certain point, with increasing electrode thickness, a conductive additive is needed to sustain the applied current density without losing capacity. In particular, a previous study [56] comparing bulk, nanoparticulate and mesoporous Fe_2O_3 addresses the various aspects that affect the rate of conversion electrodes, demonstrating that for this type of conversion reaction electron transport to and within the active particles is the limiting factor. Therefore, Figure 4.11 and the above considerations suggest that only thin layers in the range of micrometers, containing these nanoparticles, can cycle properly at the examined current densities. Indeed, in order to exploit the positive features of nanoparticles in these composite electrodes it is convenient either to have thin layers, where percolation is not an issue, or add a conductive additive to the precursors, in order to compensate for the growth of the overall resistance of the electrode as its thickness increases. Finally, in both cases it is also of paramount importance to optimize the ratio of the various components, depending on the specific requirements for their practical application and cycling conditions.

4.4 Conclusions

Nanostructured composite electrodes based on Fe_2O_3 and CuO were successfully fabricated by electrostatic spray pyrolysis of precursor solutions containing iron and copper salts dissolved in the presence of PVdF. Small oxide nanoparticles were directly synthesized and homogeneously dispersed with the PVdF binder to produce coated electrodes in one step. The small size of the generated Fe_2O_3 and CuO nanoparticles, as well as their homogenous distribution in the

composite coatings, enable electrochemical cycling of these electrodes even in the absence of conductive additives. Besides, the even inter-dispersion of the polymer binder on the nanoscale promotes the mutual adhesion of the nanoparticles in the deposits, acting at the same time as a barrier against their growth and agglomeration during both the synthesis process (i.e., inside the reacting droplets) and the electrochemical cycling, thus reinforcing the electrode and the overall contact with the current collector.

Initial discharge capacities are as high as 800 $mAhg^{-1}$ and 1550 $mAhg^{-1}$ for CuO and Fe_2O_3, respectively. The capacity retained after 25 cycles is about 360 $mAhg^{-1}$ for copper oxide and 950 $mAhg^{-1}$ for iron oxide in thin electrodes. These preliminary results indicate that this approach can be used for the direct production of nanocomposite electrode coatings, provided that the thickness of the grown layers does not hinder the electronic conduction in the whole electrode. In this respect, the deposition of thin films with a minimal amount of binder and no conductive additive is highly desirable to conveniently employ the features of the formed nanoparticles and to increase the overall energy density of the electrodes and improve their power delivery. Nevertheless, when thicker electrodes are required, it is likely necessary to include a conductive additive in the preparation, especially in presence of active materials that are poor e^- conductors.

In this way, some shortcomings of conversion materials, e.g., initial irreversibility, limited capacity retention and slow reaction kinetics in bulk powders, can be addressed by proper electrode preparation via ESP. Indeed, one can select dedicated precursor solutions/suspensions containing all the needed components and control the composition, morphology, texture and thickness of the deposited composite layers with the active nanoparticles. The large voltage hysteresis between charge and discharge displayed by conversion materials is an intrinsic drawback that has been related to the energy barrier which must be overcome to break the M-X bonds (where X can be: F, O, S, or P). As a matter of fact, this phenomenon is particularly pronounced for fluorides and oxides, while sulfides and phosphides suffer less from it. Therefore, substituting oxygen with phosphine in the proposed synthesis process could be a possible approach to address this main issue. Moreover, the process is simple and can be conveniently optimized.

Finally, it should be mentioned that this procedure, which has been carried out here on a lab scale (i.e. deposition on coin cell cans), has the potential to be implemented into a continuous, larger scale process for full fabrication of advanced nanocomposite electrodes in a roll-to-roll process [48] by convenient outscaling of electrospray via multiple nozzle systems [60] or equivalent equipments [31].

References

[1] K. Ozawa, "Lithium-ion rechargeable batteries with $LiCoO_2$ and carbon electrodes: the $LiCoO_2$/C system," *Solid State Ionics*, vol. 69, pp. 212–221, 1994.

[2] M. Lazzari and B. Scrosati, "A Cyclable Lithium Organic Electrolyte Cell Based on Two Intercalation Electrodes," *Journal of Electrochemical Society*, vol. 127, pp. 773–774, 1980.

[3] M. Winter, J. Besenhard, M. Spahr, and P. Novak, "Insertion electrode materials for rechargeable lithium batteries," *Advanced Materials*, vol. 10, no. 10, pp. 725–763, 1998.

[4] P. Poizot, S. Laruelle, S. Grugeon, L. Dupont, and J. Tarascon, "Nano-sized transition-metal oxides as negative-electrode materials for lithium-ion batteries," *Nature*, vol. 407, no. 6803, pp. 496–499, 2000.

[5] H. Liu, G. Wang, J. Wang, and D. Wexler, "Magnetite/carbon core-shell nanorods as anode materials for lithium-ion batteries," *Electrochemistry Communications*, vol. 10, pp. 1879–1882, 2008.

[6] P. Bruce, B. Scrosati, and J. Tarascon, "Nanomaterials for rechargeable lithium batteries," *Angewandte Chemie - International Edition*, vol. 47, no. 16, pp. 2930–2946, 2008.

[7] Y. Guo, J. Hu, and L. Wan, "Nanostructured Materials for Electrochemical Energy Conversion and Storage Devices," *Advanced Materials*, vol. 20, pp. 2878–2887, 2008.

[8] A. Arico, P. Bruce, B. Scrosati, J. Tarascon, and W. Van Schalkwijk, "Nanostructured materials for advanced energy conversion and storage devices," *Nature Materials*, vol. 4, no. 5, pp. 366–377, 2005.

[9] P. Balaya, H. Li, L. Kienle, and J. Maier, "Fully reversible homogeneous and heterogeneous Li storage in RuO_2 with high capacity," *Advanced Functional Materials*, vol. 13, no. 8, pp. 621–625, 2003.

[10] J. Maier, "Nanoionics: ion transport and electrochemical storage in confined systems," *Nature Materials*, vol. 4, pp. 805–815, 2005.

[11] J. Jamnik and J. Maier, "Nanocrystallinity effects in lithium battery materials Aspects of nano-ionics. Part IV," *Physical Chemistry Chemical Physics*, vol. 5, pp. 5215–5220, 2003.

[12] P. Balaya, A. Bhattacharyya, J. Jamnik, Y. Zhukovskii, E. Kotomin, and J. Maier, "Nano-ionics in the context of lithium batteries," *Journal of Power Sources*, vol. 159, no. 1 SPEC. ISS., pp. 171–178, 2006.

[13] J. Tarascon, S. Grugeon, M. Morcrette, S. Laruelle, P. Rozier, and P. Poizot, "New concepts for the search of better electrode materials for rechargeable lithium batteries," *C. R. Chemie*, vol. 8, pp. 9–15, 2005.

[14] P. Poizot, S. Laruelle, S. Grugeon, L. Dupont, and J. Tarascon, "Searching for new anode materials for the Li-ion technology: time to deviate from the usual path," *Journal of Power Sources*, vol. 97-98, pp. 235–239, 2001.

[15] Y. Li, B. Tan, and Y. Wu, "Mesoporous Co_3O_4 Nanowire Arrays for Lithium Ion Batteries with High Capacity and Rate Capability," *Nano Letters*, vol. 8, no. 1, pp. 265–270, 2008.

[16] L. Dupont, S. Laruelle, S. Grugeon, C. Dickinson, W. Zhou, and J. Tarascon, "Mesoporous Cr_2O_3 as negative electrode in lithium batteries: TEM study of the texture effect on the polymeric layer formation," *Journal of Power Sources*, vol. 175, pp. 502–509, 2008.

[17] N. Meethong, H. Huang, W. Carter, and Y. Chiang, "Size-Dependent Lithium Miscibility Gap in Nanoscale $Li_{1-x}FePO_4$," *Electrochemical and Solid-State Letters*, vol. 10, no. 5, pp. A134–A138, 2007.

[18] M. Valvo, *Electrospray-assisted synthesis methods of nanostructured materials for Li-ion batteries*. PhD thesis, Delft University of Technology, Delft, The Netherlands, November 2010.

[19] G. Derrien, J. Hassoun, S. Panero, and B. Scrosati, "Nanostructured Sn-C Composite as an Advanced Anode Material in High-Performance Lithium-Ion Batteries," *Advanced Materials*, vol. 19, pp. 2336–2340, 2007.

[20] R. Demir Cakan, M. Titirici, M. Antonietti, G. Cui, J. Maier, and Y. Hu, "Hydrothermal carbon spheres containing silicon nanoparticles: synthesis and lithium storage performance," *Chemical Communications*, vol. 32, pp. 3759–3761, 2008.

[21] R. Demir Cakan, Y. Hu, M. Antonietti, J. Maier, and M. Titirici, "Facile One-Pot Synthesis of Mesoporous SnO_2 Microspheres via Nanoparticles Assembly and Lithium Storage Properties," *Chemistry of Materials*, vol. 20, pp. 1227–1229, 2008.

[22] R. Yang, Z. Wang, J. Liu, and L. Chen, "Nano Co_3O_4 Particles Embedded in Porous Hard Carbon Spherules as Anode Material for Li-Ion Batteries," *Electrochemical and Solid-State Letters*, vol. 7, pp. A496–A499, 2004.

[23] G. Cui, Y. Hu, L. Zhi, D. Wu, I. Lieberwirth, J. Maier, and K. Mullen, "A One-Step Approach Towards Carbon-Encapsulated Hollow Tin Nanoparticles and Their Application in Lithium Batteries," *Small*, vol. 3, pp. 2066–2069, 2007.

[24] S. Chang, I. Leo, C. Liao, J. Yen, and M. Hon, "Electrochemical behavior of nanocrystalline tin oxide electrodeposited on a Cu substrate for Li-ion batteries," *Journal of Materials Chemistry*, vol. 14, pp. 1821–1826, 2004.

[25] N. Li and C. Martin, "A High-Rate, High-Capacity, Nanostructured Sn-Based Anode Prepared Using Sol-Gel Template Synthesis," *Journal of the Electrochemical Society*, vol. 148, no. 2, pp. A164–A170, 2001.

[26] N. Li, C. Martin, and B. Scrosati, "A High-Rate, High-Capacity, Nanostructured Tin Oxide Electrode," *Electrochemical and Solid-State Letters*, vol. 3, no. 7, pp. 316–318, 2000.

[27] J. Graetz, C. Ahn, R. Yazami, and B. Fultz, "Highly Reversible Lithium Storage in Nanostructured Silicon," *Electrochemical and Solid-State Letters*, vol. 6, no. 9, pp. A194–A197, 2003.

[28] L. Y. Beaulieu, T. D. Hatchard, A. Bonakdarpour, M. D. Fleischauer, and J. R. Dahn, "Reaction of Li with Alloy Thin Films Studied by In Situ AFM," *Journal of The Electrochemical Society*, vol. 150, no. 11, pp. A1457–A1464, 2003.

[29] C. Chan, X. Zhang, and Y. Cui, "High Capacity Li Ion Battery Anodes Using Ge Nanowires," *Nano Letters*, vol. 8, no. 1, pp. 307–309, 2008.

[30] C. Chan, R. Ruffo, S. Hong, and Y. Cui, "Surface chemistry and morphology of the solid electrolyte interphase on silicon nanowire lithium-ion

battery anodes," *Journal of Power Sources*, vol. 189, no. 2, pp. 1132–1140, 2009.

[31] U. Lafont, A. Anastasopol, E. Garcia-Tamayo, and E. Kelder, "Electrostatic spray pyrolysis of $LiNi_0.5Mn_1.5O_4$ films for 3D Li-ion microbatteries," *Thin Solid Films*, vol. 520, no. 9, pp. 3464–3471, 2012.

[32] L. Bazin, S. Mitra, P. Taberna, P. Poizot, M. Gressier, M. Menu, A. Barnabe, P. Simon, and J. Tarascon, "High rate capability pure Sn-based nano-architectured electrode assembly for rechargeable lithium batteries," *Journal of Power Sources*, vol. 188, no. 2, pp. 578–582, 2009.

[33] P. Taberna, S. Mitra, P. Poizot, P. Simon, and J. Tarascon, "High rate capabilities Fe_3O_4-based Cu nano-architectured electrodes for lithium-ion battery applications," *Nature Materials*, vol. 5, no. 7, pp. 567–573, 2006.

[34] C. Chan, H. Peng, G. Liu, K. McIlwrath, X. Zhang, R. Huggins, and Y. Cui, "High-performance lithium battery anodes using silicon nanowires," *Nature Nanotechnology*, vol. 3, no. 1, pp. 31–35, 2008.

[35] S. Kim, K. Choi, J. Eun, H. Kim, and HwangC.S, "Effects of additives on properties of MgO thin films by electrostatic spray deposition," *Thin Solid Films*, vol. 377-378, pp. 694–698, 2000.

[36] T. Nguyen and E. Djurado, "Deposition and characterization of nanocrystalline tetragonal zirconia films using electrostatic spray deposition," *Solid State Ionics*, vol. 138, pp. 191–197, 2001.

[37] C. Chen, E. Kelder, and J. Schoonman, "Electrode and solid electrolyte thin films for secondary lithium-ion batteries," *Journal of Power Sources*, vol. 68, pp. 377–380, 1997.

[38] A. A. van Zomeren, E. M. Kelder, J. C. M. Marijnissen, and J. Schoonman, "The production of thin films of $LiMn_2O_4$ by electrospraying," *Journal of Aerosol Science*, vol. 25, no. 6, pp. 1229–1235, 1994.

[39] C. Chen, E. Kelder, P. Van Der Put, and J. Schoonman, "Morphology control of thin $LiCoO_2$ films fabricated using the electrostatic spray deposition (ESD) technique," *Journal of Materials Chemistry*, vol. 6, no. 5, pp. 765–771, 1996.

[40] C. Chen, E. Kelder, and J. Schoonman, "Unique porous $LiCoO_2$ thin layers prepared by electrostatic spray deposition," *Journal of Materials Science*, vol. 31, no. 20, pp. 5437–5442, 1996.

[41] Y. Yu, J. Shui, and C. Chen, "Electrostatic spray deposition of spinel $Li_4Ti_5O_{12}$ thin films for rechargeable lithium batteries," *Solid State Communications*, vol. 135, no. 8, pp. 485–489, 2005.

[42] H. Ryu, J. Kim, Z. Guo, H. Liu, K. Kim, J. Ahn, and H. Ahn, "Electrochemical properties of Fe_2O_3 thin film fabricated by electrostatic spray deposition for lithium-ion batteries," *Physica Scripta*, vol. T139, p. 014066, 2010.

[43] M. Mohamedi, S. Lee, D. Takahashi, M. Nishizawa, T. Itoh, and I. Uchida, "Amorphous tin oxide films: Preparation and characterization as an anode active material for lithium ion batteries," *Electrochimica Acta*, vol. 46, no. 8, pp. 1161–1168, 2001.

[44] D. Munao, J. van Erven, M. Valvo, E. Garcia-Tamayo, and E. Kelder, "Role of the binder on the failure mechanism of Si nano-composite electrodes for Li-ion batteries," *Journal of Power Sources*, vol. 196, pp. 6695–6702, 2011.

[45] J. Hassoun, G. Derrien, S. Panero, and B. Scrosati, "A nanostructured Sn-C composite lithium battery electrode with unique stability and high electrochemical performance," *Advanced Materials*, vol. 20, no. 16, pp. 3169–3175, 2008.

[46] J. Lee, B. Kong, Y. Baek, S. Yang, and H. Jung, "Tin nanoparticle thin film electrodes fabricated by the vacuum filtration method for enhanced battery performance," *Nanotechnology*, vol. 20, p. 235203, 2009.

[47] Jaworek, A., "Electrospray droplet sources for thin film deposition," *Journal of Materials Science*, vol. 42, pp. 266–297, 2007.

[48] Valvo, M. and Garcia-Tamayo, E. and Lafont, U. and Kelder, E.M, "Direct synthesis and coating of advanced nanocomposite negative electrodes for li-ion batteries via electrospraying," *Journal of Power Sources*, vol. 196, no. 23, pp. 10191–10200, 2011.

[49] A. Timmons and J. Dahn, "Isotropic volume expansion of particles of amorphous metallic alloys in composite negative electrodes for li-ion batteries," *Journal of The Electrochemical Society*, vol. 154, no. 5, pp. A444–A448, 2007.

[50] A. Debart, L. Dupont, P. Poizot, J. Leriche, and J. Tarascon, "A Transmission Electron Microscopy Study of the Reactivity Mechanism of Tailor-Made CuO Particles toward Lithium," *Journal of Electrochemical Society*, vol. 148, no. 11, pp. A1266–A1274, 2001.

[51] F. Ke, L. Huang, G. Wei, L. Xue, J. Li, B. Zhang, S. Chen, X. Fan, and S. Sun, "One-step fabrication of CuO nanoribbons array electrode and its excellent lithium storage performance," *Electrochimica Acta*, vol. 54, pp. 5825–5829, 2009.

[52] D. Zhang, T. Yi, and C. Chen, "Cu nanoparticles derived from CuO electrodes in lithium cells," *Nanotechnology*, vol. 16, pp. 2338–2341, 2005.

[53] H. Liu, G. Wang, J. Park, J. Wang, H. Liu, and C. Zhang, "Electrochemical performance of α-Fe_2O_3 nanorods as anode material for lithium-ion cells," *Electrochimica Acta*, vol. 54, pp. 1733–1736, 2009.

[54] Y. Piao, H. Kim, Y. Sung, and T. Hyeon, "Facile scalable synthesis of magnetite nanocrystals embedded in carbon matrix as superior anode materials for lithium-ion batteries," *Chemical Communications*, vol. 46, pp. 118–120, 2010.

[55] Larcher, D. and Masquelier, C. and Bonnin, D. and Chabre, Y. and Masson, V. and Leriche, J.B. and Tarascon, J.M, "Effect of particle size on lithium intercalation into α-fe_2o_3," *Journal of The Electrochemical Society*, vol. 150, no. 1, pp. A133–A139, 2003.

[56] F. Jiao, J. Bao, and P. Bruce, "Factors Influencing the Rate of Fe_2O_3 Conversion Reaction," *Electrochemical and Solid-State Letters*, vol. 10, pp. A264–A266, 2007.

[57] M. Gaberscek, "Towards optimized preparation of cathode materials: How can modeling and concepts be used in practice," *Journal of Power Sources*, vol. 189, pp. 22–27, 2009.

[58] NuLi, Y. and Zeng, R. and Zhang, P. and Guo, Z. and Liu, H., "Controlled synthesis of α-fe2o3 nanostructures and their size-dependent electrochemical properties for lithium-ion batteries," *Journal of Power Sources*, vol. 184, no. 2, pp. 456–461, 2008.

[59] Hang, B.T. and Doi, T. and Okada, S. and Yamaki, J., "Effect of carbonaceous materials on electrochemical properties of nano-sized fe_2o_3-loaded carbon as a lithium battery negative electrode," *Journal of Power Sources*, vol. 174, no. 2, pp. 493–500, 2007.

[60] L. L. F. Agostinho, *Electrohydrodynamic Atomization in the Simple-Jet Mode*. PhD thesis, Delft University of Technology, Delft, The Netherlands, February 2013.

Chapter 5

Electrostatic spray pyrolysis of $LiNi_{0.5}Mn_{1.5}O_4$ films for 3D Li-ion microbatteries

> Information on how to handle the present so as to survive into the future is necessarily gleaned from the past. Non-random survival of DNA in ancestral bodies is the obvious way in which information from the past is recorded for future use, and this is the route by which the primary database of DNA is built up
>
> Richard Dawkins, *The Greatest Show on Earth*, 2009

Electrostatic spray pyrolysis has been used to produce high voltage $LiNi_{0.5}Mn_{1.5}O_4$ thin film electrodes for 3D Li-ion microbattery application. The influence of the synthesis parameters on the structure, texture and electrochemical behaviour of the produced electrode has been investigated using X-ray diffraction, scanning and transmission electron microscopies, cyclic voltammetry and galvanostatic measurements. A specific capacity of 135 $mAhg^{-1}$ can be achieved without any electronic conducting additive in the electrode. Moreover, a controlled de-

position on a flat and 3D architecture substrate has been demonstrated and discussed showing the potential of such a deposition technique in the production of 3D all solid state Li-ion batteries.

This chapter is based on the published article: U. Lafont, A. Anastasopol, **E. Garcia-Tamayo**, E.M. Kelder. "Electrostatic spray pyrolysis of $LiNi_{0.5}Mn_{1.5}O_4$ films for 3D Li-ion microbatteries". *Thin Solid Films 520 (2012) 3464-3471.*

5.1 Introduction

In Section 1.5 an in-depth discussion on the necessity, the advantages and the characteristics of solid-state, 2D and 3D (thin film) microbatteries was described. It is important to recall the interesting strategy of exploring novel architectures in 3D current collectors, as a mean to increase the surface area per footprint unit, therefore theoretically increasing the energy stored per footprint area, provided one could successfully deposit conformal thin layers of all battery components, namely: cathode, solid electrolyte, anode, current collectors and packaging film.
The present chapter will examine the results obtained during a project funded by the European Comission within the FP7 framework where, in summary, especially customized silicon wafers where used as current collectors for the development of novel 3D microbatteries. In the first part of the introduction an overall description, context and main objectives of this project will be briefly addressed. Naturally, a thorough discussion of my part in the project and the results obtained will be examined.

5.1.1 Context

Today's miniaturised systems go beyond monolithically integrated or hybrid systems which combine measurement, data processing and storage functions. The future will consist of integrated smart systems that will be able to sense and diagnose a situation, be predictive, and therefore be able to make decisions. According to experts, this market should have generated more than 25 billion euros revenues in 2011 [1].

According to the European strategic research agenda of the main technology platforms in these domains (ENIAC [2], EPoSS [3], and ARTEMIS [4]), the main functionalities that are often requested for these smart systems are: increased miniaturisation, high reliability, networking and communication capability, integration and energy - autonomous performance.

Therefore, considered as an R&D topic of high relevance for Smart Systems Integration (EPoSS Strategic Research Agenda [3]), the 'integration and energy-autonomous' aspects will be particularly investigated by the E-STARS (Efficient Smart sysTems with enhAnced eneRgy Storage) project [5]. During the past few years a lot of developments have been achieved to obtain new smart/remote micro device miniaturised with higher autonomy capacities. Today the miniaturisation of such devices is limited by the battery itself and particularly by the currently available micro power supply systems. In the major case, their autonomy is mostly limited by the low energy density of batteries.

The main request of the stakeholders is to get relevant microbatteries to enable further miniaturisation and enhanced sensing & communication capability of their smart devices.

5.1.2 Project Summary

Looking at the complete picture, the E-STARS project aims at developing enhanced sensing and communication capability on an autonomous smart micro system powered by a new 3D high capacity integrated microbattery.

The energy-management, scavenging and storing techniques aspects will be particularly investigated. 3D architecture microbatteries could significantly increase the battery capacity (i.e. from 100 μAhcm^{-2} to 1000 μAhcm^{-2}) and the power (i.e. from 5 mWcm^{-2} to 50 mWcm^{-2}) compared to traditional solutions. To do so, the consortium has investigated completely new deposition processes for microbattery layers such as Chemical Vapour Deposition (CVD), Electrospray (ES) and Electrodeposition (ED) in order to obtain 3D high aspect ratios.

The project has foreseen an increase of both energy capacity and power per cm^2, by a factor of 5 to 10 via texturing the substrate and thus increasing the volume of active material per footprint. To reach the strategic objective, two routes will be investigated: moderate and high aspect ratio 3D structuring. A drawing of this type of substrates is shown in Figure 5.1, but the project-specific substrates will be described in Paragraph 5.2.1.

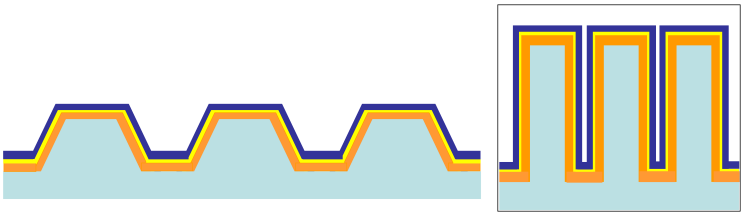

Figure 5.1 – Drawing of 3D Low Aspect Ratio (5:1) -left- and High aspect ratio (10:1) -right- substrates

5.1.3 TU Delft's aim

For certain applications microbatteries still suffer from low energy storage capabilities that are usually compensated by connecting microbatteries in series.

Another approach to tackle this issue consists in the increase of nominal cell voltage using high voltage (HV) type material as positive electrode. Among the HV material candidates the use of Ni substituted $LiMn_2O_4$ spinel and their derivatives as positive electrode material is really promising. Indeed, they present working voltage of 4.75 V vs Li/Li^+, a theoretical specific capacity of 150 $mAhg^{-1}$ and good electrochemical behaviour. Lithium nickel manganese oxide spinel, as it is also called, has been studied extensively and is obviously an attractive candidate due to its high operating voltage [6–15].

An all-solid-state microbattery construction involves layer-by-layer deposition techniques. These processes should be achieved without damaging the already existing layer providing a good inter-layer contact and, specifically in a 3D system, following a desired architecture. Pulsed laser deposition (PLD) [16, 17], RF-magnetron sputtering [18–21], chemical vapour deposition (CVD) [22], sol gel [23, 24], spin-coating [25] and electrolysis [26, 27] or electrodeposition [28] are common methods used to deposit thin films for solid state microbattery applications. Another suitable technique used to produce thin films is based on the atomisation of a liquid onto a heated substrate where it undergoes pyrolysis. It is referred to as Spray Pyrolysis and it is used for different applications [29, 30], including Li-ion (micro) batteries [31]. Electrohydrodynamic Atomisation (EHDA), Electrostatic Spray Pyrolysis (ESP) or Deposition (ESD) are, as thoroughly described in Chapter 3, similar methods where the atomisation of the liquid precursor is achieved by applying a high potential between the nozzle and the substrate. This produces a fine spray of sub-micrometric droplets which are conducted, under the action of the strong electric field, to the substrate where pyrolysis occur creating a nanostructured film [32–34]. In the same way as for Spray Pyrolysis, ESP is used for a wide range of applications [35–45] and, more important for our discussion, it has seen a remarkable increase of its use in the field of Li-ion (micro) batteries [31, 46–57]. ESP is cheap, easy to implement and presents a high deposition rate and efficiency compared to CVD and PLD. Due to the use of liquid precursor (i.e. metallic salts in solution) it is possible to produce a wide range of oxide based films (SnO_2 [43], CuO [56], Fe_2O_3 [56], ZnO [37], MgO [44], ZrO_2 [45], $LiTaO_3$ [35], $LiCoO_2$ [47] $LiMn_2O_4$ [46] and [31], $LiNi_{0.5}Mn_{1.5}O_4$ [58, 59]). Moreover, by controlling simple experimental parameters (flow rate, spraying times and modes, solvent type, concentration, distance nozzle to substrate, temperature) the morphology of the as-deposited film can be influenced and tuned [45, 60].

The role of TU Delft in this project, scope of my work and subject of this chapter, is the synthesis and deposition of $LiNi_{0.5}Mn_{1.5}O_4$ thin films as positive electrode material on previously designed substrates. ESP is used as a one-step deposition process. The influence of experimental parameters on

the film morphology and electrochemical performance will be described. Moreover, the feasibility of a controlled film deposition on a 3D micro architectured support will be highlighted.

5.2 Experimental

As described in Paragraph 3.1.2, illustrations of the equipments used for the production of the $LiNi_{0.5}Mn_{1.5}O_4$ nanostructured thin film electrodes are shown in Figures 3.2 and 3.3.

The precursor solutions were prepared from $LiNO_3$, lithium nitrate anhydrous (Sigma-Aldrich), $Mn(NO_3)_2$ $.4H_2O$, manganese nitrate tetrahydrate (Alfa Aesar) and $Ni(NO_3)_2$ $.6H_2O$, nickel nitrate hexahydrate (Alfa Aesar). These salts were dissolved in 2-propanol following the spinel stochiometry. The Li:Ni:Mn molar ratio in the solution is 2:1:3, respectively. No polymeric binder or conductive additive was added to the precursor solution. A precision dispense tip (EFD R Nordson) with inner diameter 0.25 mm was used in most of the experiments. The solutions were fed to the electrified nozzle in order to undergo electrospraying and direct reaction so as to form thin film electrodes on a stainless steel cap of CR2320 coin cell (Hohsen) or on E-STARS silicon substrates with flat or 3D architectured surfaces (STMicroelectronics). The temperature at which the film deposition was performed was chosen at 450°C following results recently published by our group [59], where we showed that cubic $LiNi_{0.5}Mn_{1.5}O_4$ spinel structure can be obtained at pyrolysis temperatures ranging from 300- 450°C and that the crystallinity increases as a function of the pyrolysis temperature, whatever the solvent used for the precursor solution (ethanol, propanol). All the experiments were performed in air and their suggestion of annealing the samples was followed. Hence, a brief study on the influence of the annealing temperature on the crystallinity of the structure, as well as on the electrochemical behaviour, was carried out and it will be described in Paragraphs 5.3.1 and 5.3.4, respectevely.

In a similar way as discussed in Section 4.2, the reaction that takes plaace during pyrolysis of the used precursors is simplified as follows:

$$Li\,(NO_3) + Mn\,(NO_3)_2 \cdot 4H_2O + Ni\,(NO_3)_2 \cdot 6H_2O + O_2 \xrightarrow{450^\circ C} LiNi_{0.5}Mn_{1.5}O_4 + 18H_2O \nearrow + CO \nearrow + ... + 3CO_2 \nearrow \quad (5.2.1)$$

As mentioned in Section 2.3 and Section 4.2, control of the morphology, thickness and texture (i.e. porosity) of the deposited layers can be achieved by adjusting the physical parameters of the ESP process. The electrode thickness

can be controlled, for example, by adjusting the deposition time on the substrate. The morphology and texture can be influenced by adjusting the flow rate, voltage, distance from nozzle to sample, as well as by taking into account properties of the solvent, like its temperature of evaporation, viscosity, conductivity, etc. These aspects have been widely addressed and reviewed, and several examples on different applications are available in the literature [60–63]. Moreover, morphological features like roughness and density of the layers are of great importance during the design of battery electrodes and are especially critical in that of all-solid-state-(micro) batteries because conformality within the subsequent layers (i.e. cathode, solid electrolyte, anode) need to be considered and carefully optimized.

In this respect, three parameters were varied in order to optimize film morphology: concentration, distance between the tip of the nozzle and the support, and injection flow rate. Additionally, a brief discussion will be made on the effects of different annealing temperatures on the crystallinity and morphology of the films. These results will be described in Paragraph 5.3.2.

Composition and crystalline structure of the as-produced films was studied by means of X-ray diffraction (XRD) using a Bruker (AXS D8 Advance) X-ray diffractometer with a Cu-K_α radiation source (α=1.5418 Å) in a Bragg-Brentano $\theta/2\theta$ configuration. The texture, morphology, particle sizes and thickness of the films have been investigated using a TECNAI TF20 transmission electron microscope (TEM) operated at 200 kV, a Philips XL20 scanning electron microscope (SEM) operated at 15 kV and a DekTak profilometer using 7x10^{-5} N as applied force. The electrochemical tests were performed using as cathode the as-deposited $LiNi_{0.5}Mn_{1.5}O_4$ film (directly deposited on the CR2320 coin cell can and/or on E-STARS substrate), a polyethylene separator (Solupor), few drops of 1 M $LiPF_6$ in ethylene carbonate/ dimethyl carbonate (2:1) as electrolyte and metallic Li as anode. It should be noted that no additives like binder or carbon were used for the electrode preparation. The cells were assembled in a Ar filled glove box (coin cells in the case of flat electrodes and pouch cells in the case of the LAR-3D architectured electrodes). Galvanostatic measurements between 3.5 and 4.9 V were performed on a MACCOR S4000 cycler using different gravimetric current densities and C-rates.

5.2.1 E-STARS substrate

ST Microelectronics, a crucial partner in the E-STARS consortium, developed and furnished two types of textured substrates: Low Aspect Ratio and High Aspect Ratio. Moreover, different masks were developed with specific traits so as to permit the layer-by-layer deposition of the different battery components.

The various specific items manufactured by ST Microelectronics are described below.

Moderate ratio (2:1)

ST Microelectronics manufactured these substrates using classical wet etching and allowing slopes of around 50°. Moderate aspect ratios (depth/opening > 2, Figure 5.1 -left-) should be accessible with the improvement of classical planar process (Physical Vapour Deposition). Nevertheless, it was of interest to develop alternative processes for these systems, which justifies the exploration with novel deposition techniques such as Electrospray.

High aspect ratio (10:1)

During the E-STARS project, ST Microelectronics developed additional process bricks for textured substrates. For the process bricks, one of the key necessary items was to overcome the scalloping on the sidewalls of the high aspect ratio features. Another point was to create an etch process that could taper the top and bottom edges of the features. These results have been made publicly available recently [64].

The investigation on high aspect ratios (depth/opening > 10, Figure 5.1 -right-) is completely new and it represents the actual breakthrough innovation of the E-STARS project. It requires the development of novel alternative deposition processes for microbattery layers such as Chemical Vapour Deposition (CVD), Electrospray and Electrodeposition.

Mask

For the deposition of the layers, metallic blade-like masks were made and used. They are put directly on the substrate and remain present during deposition allowing material to be coated only where there are holes in the mask. All these masks need to have fiducials (clear markers) in order to adjust the next mask for the following deposited layer.

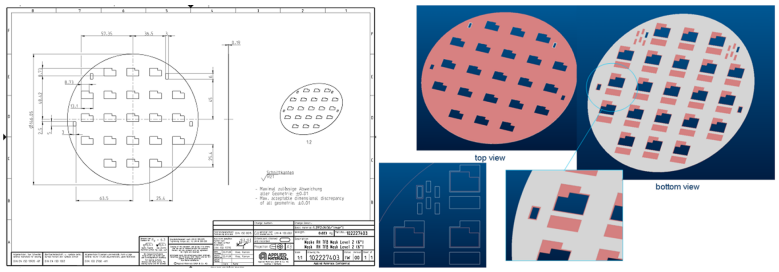

Figure 5.2 – Technical drawing of the metal mask (left hand image) for the deposition of the positive electrode (blue layer) on top of current collector layer (red layer) (right hand image)

Hence, the sample is aligned in such a way that the 3D textured patterns remain on the same area as where the electrode materials are deposited. Indeed, this is this area that is correlated to final capacity of the battery since these layers represent the volume of active materials capable of lithium insertion. For the subsequent layers (i.e. electrolyte, negative electrode, current collector and encapsulation), similar masks were used by the respective partners of the consortium in order to finish the stack.

5.3 Results and Discussion

5.3.1 Structural characterisation

The $LiNi_{0.5}Mn_{1.5}O_4$ spinel, where only the Li^+, Ni^{2+} and Mn^{4+} cations are present in the structure, belong to the $P4_332$ space group. This so called 'ordered' phase presents two types of octahedral sites (4a and 12d) and can be opposed to the 'disordered' phase (Space group $Fd3m$) in which only one type of octahedral site is present (16d) and where Mn cations present a mixed oxidation state (Mn^{3+}/Mn^{4+}) like in $LiMn_2O_4$ spinels. In most cases, synthesis of the pure ordered phase can only be achieved by combining annealing temperatures around 700 °C and slow cooling rates. The disordered phase is believed to be accompanied by a small amount of oxygen deficiency [65, 66].

In addition to the spinel reflections, the pattern in figure 5.3 shows a few weak reflections (marked with asterisks) corresponding to a rock salt impurity phase (attributed to Ni_xO or $Li_xNi_{1-x}O$ or $Li_xNi_yMn_zO$) with Bragg Peaks at 2θ 37°, 43° and 63° [65]. Because the X-ray scattering factors of Ni and Mn are similar, the super lattice peaks associated with the Ni /Mn ordering are

weak [66], which makes XRD not the method of choice to discriminate between the 'ordered' and 'disordered' structure. Nevertheless, a confirmation that the 'disordered' structure, corresponding to the F*d3m* space group of the spinel, has been prepared in this case is given later when the electrochemistry is discussed. In all the cases mentioned here, including the results presented in this chapter, the characteristic diffraction peaks of the cubic $LiNi_{0.5}Mn_{1.5}O_4$ structure were visible for all films. Even if the peaks belonging to the reflections (222), (331) and (531) seem be lost on the background noise, they become clearer after annealing as will be shown in Paragraph 5.3.2 (Figure 5.10). The average domain size is 12 nm, as deduced using the Scherrer formula.

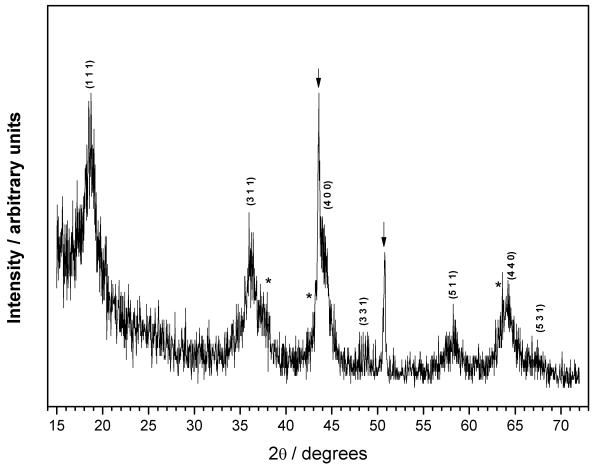

Figure 5.3 – XRD pattern of the $LiNi_{0.5}Mn_{1.5}O_4$ film synthesised at 450°C. The peaks marked with asterisks belong to impurities, while those with arrows to the support material

5.3.2 Film morphology and Optimisation

The texture, morphology, thickness and uniformity of the films have been investigated using SEM, TEM and profilometry. As it can be noticed on the SEM picture (Figure 5.4(a-b)), the film formation is related to the intrinsic characteristics of the deposition technique (i.e. ESP). Spherical droplets of solvent containing the precursors are feeding the film growth. When the charged droplets reach the heated substrate, the solvent evaporates and the

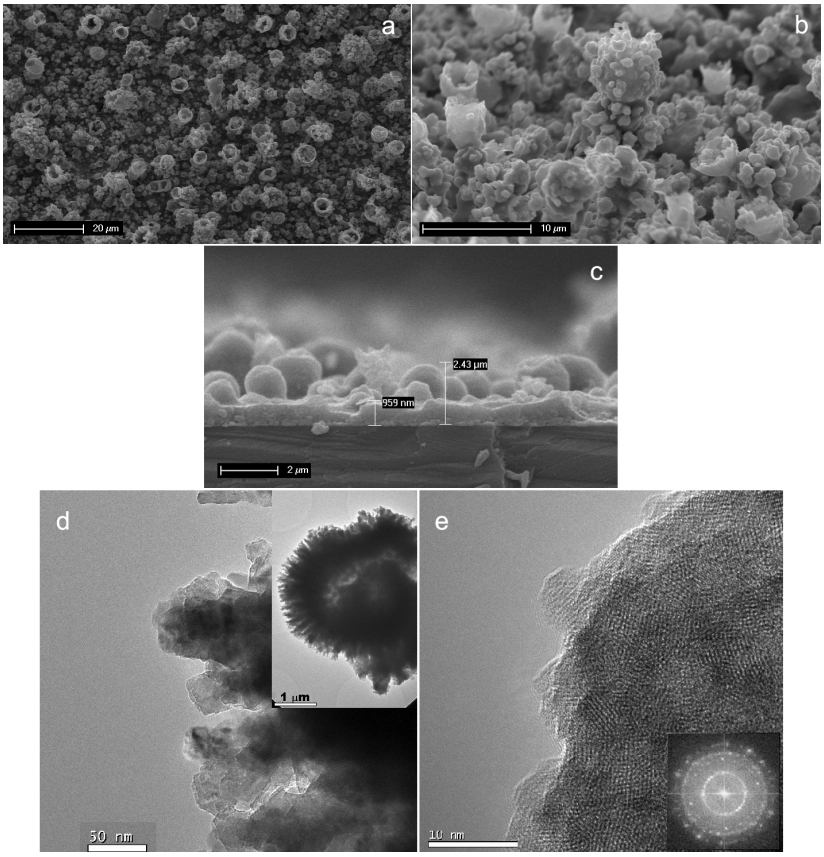

Figure 5.4 – (a and b) SEM micrograph of the film; (c) Cross section SEM; (d) TEM picture of the film texture (inset low magnification showing the fractal texture); (e) HR-TEM picture (inset Fourier Transform of the image)

crystallisation takes place within these micro containers. This fingerprint, due to the liquid precursor feeding process, is clearly seen in the solid film final texture [61]. The microtexture of the film is influenced by the solvent. The use of propanol as solvent involves an open structure presenting a macroporosity made of bridged spherical aggregates of 200 nm to 10 μm (Figure 5.4(a-b)). The film texture and constituting aggregates presenting fractal behaviour have been confirmed by TEM (Figure 5.4(d-e)). Moreover, the high resolution picture in Figure 5.4(e) clearly shows the crystalline nanoparticles being the main building blocks of the whole aggregates. It further is surrounded by amorphous domains or layers. The size of the crystallites spans from 5 to 20 nm and fits the one estimated by the Scherrer formula. The particle clustering implies polycrystalline behaviour.

The as-deposited film uniformity and thickness have been investigated using a 2cm x 1cm p-type silicon wafer as substrate. The film thickness has been tuned varying the spraying times from 10 to 40 min. For all experiments, the flow rate was fixed to 0.3 ml/h and the pyrolysis temperature to 450 °C. The setup configuration implies that, during the spraying process, the droplets will be positively charged whereas the support is connected to negative pole of the high voltage supply. The film morphology after 10 and 40 min of deposition is shown in Figure 5.5. After 10 min of deposition, the resulting film presents a maximum average thickness of 4.5 μm. After 40 min of deposition, the maximum film height is around 5.5 μm. It is clear that upon time, the film thickness has not been significantly increased.

The main influence of the spraying time resides in a better surface coverage and uniformity. This phenomenon has already been shown using ESP [67] and [68] and can be related to a combination of various phenomena: columbic interactions and preferential landing of droplets on the substrate, and, perhaps more important, the discharge and spreading of solution droplets on the surface (wettability). As soon as a charged droplet contacts with the surface of the substrate or the earlier formed layer, it starts to discharge by transferring the charge to the grounded substrate either immediately or through the layer to the substrate. In the cases of using insulating substrates or depositing insulating layers, the discharge may proceed slowly and, hence, it influences the morphology [59, 60].

As was clearly observed from the SEM micrographs in Figure 5.4, morphological features like roughness and density of the layers need improvements to obtain a better conformality with the subsequent layers. The parameters used in these studies included a flow rate of 0.7 mLh^{-1}, distance from the nozzle capillary to substrate was set to 20 mm and a precursor with a molar concentration of 0.05 M based on Li^{+}.

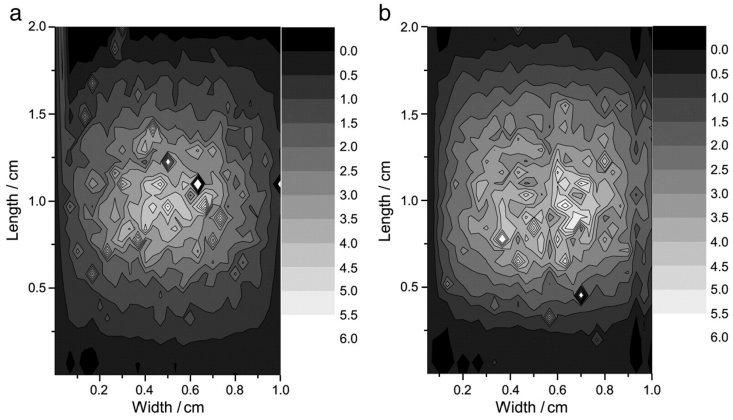

Figure 5.5 – Surface morphology of film on Silicon wafer sprayed for (a) 10 min and (b) 40 min. Scale-bar on the left is in μm.

Therefore, a study on the influence in the layers' morphology when varying a set of parameters in the electrospraying process was carried out. As mentioned in Section 2.3, the layer formation is a complex and multi-step process, and, therefore, numerous explanations can be met in the literature. The morphology of the layer depends, in general, on the gas and substrate temperature, the solvent used for spraying, and the time of solvent evaporation from the layer. Moreover, characteristics like film thickness, cristallinity, texture, and deposition rate can be easier controlled by varying the voltage, flow rate and molar concentration of the material to be deposited [60, 61, 69]. In this experiment, it was decided to study different distances from nozzle capillary to substrate (10, 15, 20, 25 and 30 mm), different flow rates (0.2, 0.3, 0.5, 0.9, 1.3 and 1.7 $\mathrm{mLh^{-1}}$) and different concentrations (0.01, 0.025, 0.05 and 0.1 M). The decision to choose this set of parameters was based on previous studies where different solvents (i.e. boiling temperature, conductivity, surface tension) and different substrate temperatures were tried [59].

The schema and picture of the experiment (variation of flow rate, distance and concentration) are shown in Figure 5.6 and a summary of the experimental parameters are described in Table 5.1.

Due to the versatility of the setup, it is possible to move the nozzle over an 'x, y, z' coordinate system. This allows for multiple experiments to be carried out on the same wafer, introducing in this way a novel tool for 'Scanning Electrospray'. Hence, this technique opens a space for important applications

Table 5.1 – Experimental parameters for optimisation of morphology.

	Distance[A] (mm)					Flow Rate[B] (mLh^{-1})							Molar Concentration[C] (M)			
	10	15	20	25	30	0.2	0.3	0.5	0.7	0.9	1.3	1.7	0.01	0.025	0.05	0.1
Voltage (kV)	6.01	6.32	8.5	8.8	9	9.52	9.41	9.2	8.5	8.4	8.0	7.6	5.49	6.72	8.55	8.81

[A]: Flow rate, 0.7 mLh^{-1}; Concentration, 0.05 M; Spraying time, 30 min; Temperature, 450°C
[B]: Distance, 20 mm; Concentration, 0.05 M; Spraying time, 30 min; Temperature, 450°C
[C]: Flow rate, 0.7 mLh^{-1}; Distance, 20 mm; Spraying time, 30 min; Temperature, 450°C

which are not completely foreseeable at present, but with obvious advantages like the optimisation of resources in terms of raw materials, substrates, time, growth rate, etc.

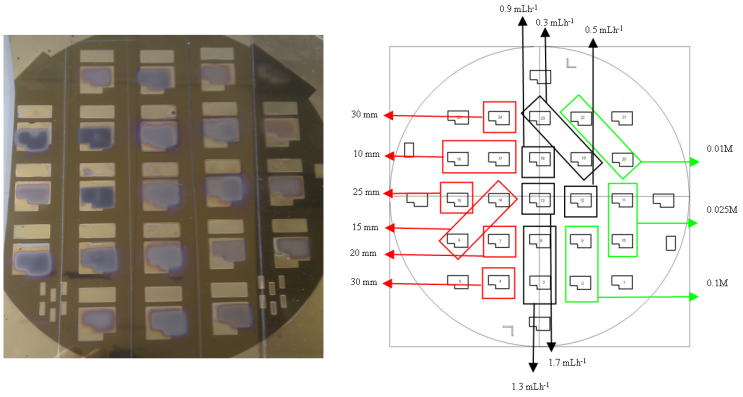

Figure 5.6 – Electrosprayed 6 inch E-STARS wafer with different parameters for the study of morphology

Influence of the Distance from nozzle-to-substrate (L)

Figure 5.7(a-e) displays how the variation of the distance between the tip of the nozzle and the substrate influences the morphology of the layer. Very rough

surfaces with variations in the size of the agglomerates in the order of a couple of micrometers can be clearly observed in Figures 5.7(c-e). Moreover, the layers present a certain degree of porosity as it is better observed in the cross section micrographs. In contrast, Figures 5.7(a-b) show better morphological properties regarding the features we are looking for, namely a good compromise between a smooth surface and a dense layer. Finally, and according to the expected characteristics described previously, it is evident that the layer sprayed at a 2.5 cm distance (Figure 5.7(b)) offers the best quality in morphological terms.

The reasons for these morphological changes taking place are, at least, twofold. First, the spraying mode at shorter distances was highly unstable, to the point that neither the cone-jet mode nor the relatively stable multi-jet mode were easily and consistently achieved. An unstable spray causes, as described in Chapter 3, the creation of large droplets with a wide range of diameters, which will contribute to the formation of polydisperse particles and, ultimately, of a non-homogenous film. It has been widely proven by many authors, and carefully reviewed by Jaworek, that the quality of the thin film strongly depends on the size of the particles or droplets forming the layer, their monodispersity, and their uniform distribution on the substrate. Smaller particles, having narrow size distribution, reduce the number and size of voids, flaws and cracks in the film. Uniform spatial dispersion of the droplets causes that the layer becomes more even and of the same thickness. All these properties affect the mechanical and electrical properties of the layer [61]. Second, the voltage required to form a semi-stable spraying mode needs to be decreased when L becomes smaller, as shown in Table 5.1, and the extent of particle agglomeration increases with decreasing electric field. Therefore, the layer from a stronger electric field looks denser (Figure 5.7(a-b)) than that from a weaker electric field (Figure 5.7(c-e)). This can be attributed to a shorter time of flight of the droplets under the stronger field according to eqns. 5.3.1 and 5.3.2 (which were previously explained in Chapter 3 but that are useful to recall since they will be used often in this discussion).

$$t \approx \left(\frac{2Lm}{qE_{sp}}\right)^{1/2} \tag{5.3.1}$$

or

$$t \approx \left(\frac{3\pi d\eta CL}{qE_{sp}}\right) \tag{5.3.2}$$

where m is the mass of the droplet, q is the droplet charge, E_{sp} is the electric field strength in the travelling space, L is the distance from nozzle-to-

substrate, η is the dynamic viscosity of air, d is the diameter of the droplet and C is a correction coefficient.

This then results in less solvent evaporation and larger incoming droplets at the substrate surface. Another reason might be a stronger preferential landing effect, existing in a stronger electric field [60].

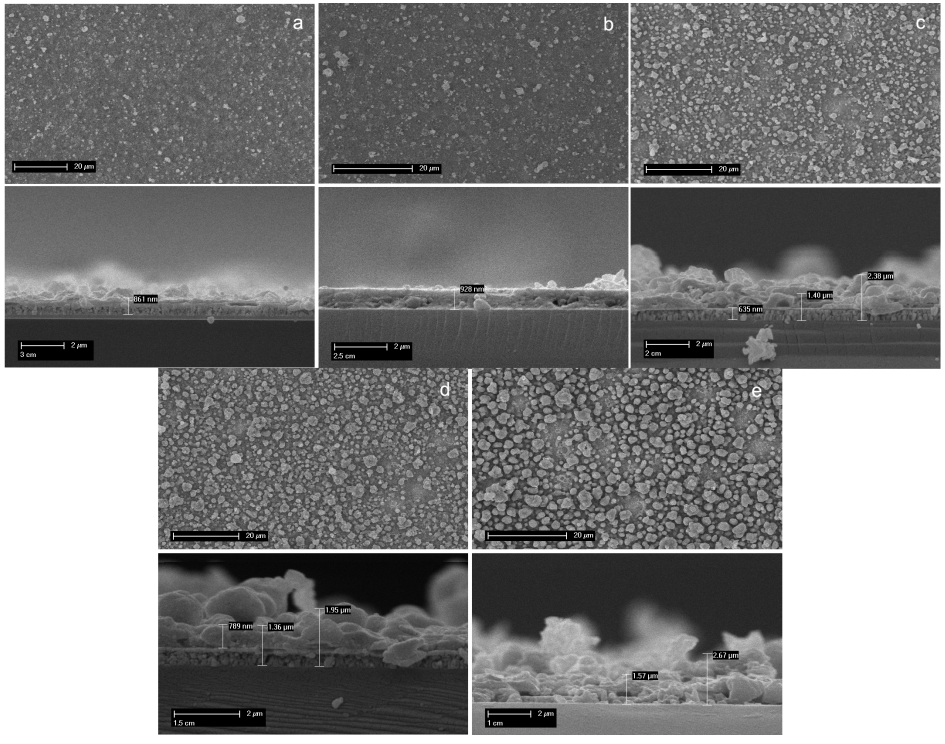

Figure 5.7 – SEM and Cross Section-SEM micrographs showing the influence of the distance in the morphology of the layers. (a) 3cm,; (b) 2.5cm; (c) 2cm; (d) 1.5cm; (e) 1cm

Influence of Flow Rate (Q)

Figure 5.8(a-g) shows SEM and XSEM micrographs for layers obtained using different flow rates. No clear difference or trend can be immediately appreciated among them from the top view, as they all present a dense layer with incorporated particles. However, by zooming in to make a closer inspection (left upper corner insets), although also noticeable when carefully studying it, one can observe a slight raise in the agglomerate and particle size when Q is increased. In most cases (Figure 5.8(a-e)), this range goes from 0.5-5 μm, while it ranges from 0.6-10 μm for higher values of Q (Figure 5.8(f-g)). Nevertheless, each layer presents a predominant average agglomerate size which goes from 0.8-1 μm for low Q (Figure 5.8(a-b)), 1.5-2 μm for mid-level Q (Figure 5.8(c-e)) and 2.5 μm for higher Q (Figure 5.8(f-g)). The effect on the particle size may be explained because the mean droplet diameter increases linearly as a function of the flow rate, according to scaling laws [70–72]. Furthermore, the agglomerates and lamellar particles are less scattered (i.e. more densely packed) for the last cases (Figure 5.8(f-g)). Films deposited using lower flow rates look slightly denser than those deposited using a higher flow rates. This can be attributed to a larger number of deposited droplets when the solution is fed using a higher Q. This results in faster formation of agglomerates. Therefore, films deposited with the low precursor Q contain less agglomerates and look denser than those deposited with the high Q [41].

On the other hand, the cross-section analysis shows comparable thicknesses between the different layers in spite of the larger volume of precursor solution sprayed at higher flow rates (the spraying time was the same for all layers, i.e. 30 min, as shown in Table 5.1). This may be due to the effects of preferential landing, discharge and spreading of solution droplets, causing that the excess of material in the case of larger Q is devoted to the homogenisation and flattening of the film instead of increasing its thickness, in agreement to what was described previously in this section (Figure 5.5). Additionally, from the scaling laws it can also be stated that the velocity of the droplets increases with the flow rate [71], therefore less solvent is evaporated and larger droplets arrive on the surface increasing wettability.

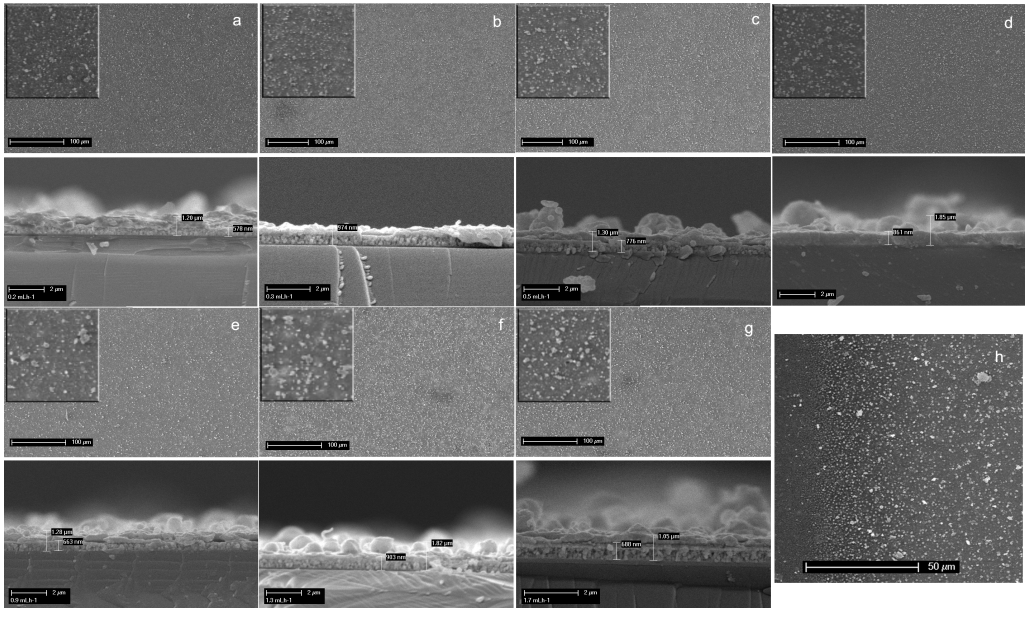

Figure 5.8 – SEM and XSEM micrographs showing the influence of the flow rate in the morphology of the layers. (a) 0.2; (b) 0.3; (c) 0.5; (d) 0.7; (e) 0.9; (f) 1.3; (g) 1.7mLh^{-1}. (h) image taken in the outer region of the sprayed section, 0.7mLh^{-1}. The left upper corner insets refer to a 10x higher magnification

Unlike the clear differences observed in Figure 5.7a-e, where a parameter choice was taken directly from the study of the micrographs, in this case the decision is not based solely on direct appreciation of Figure 5.8(a-g), but on the complete discussion carried out previously. Therefore, we conclude that the layer sprayed at Q=0.3 mLh^{-1} (Figure 5.8(b)) gives the most decent quality in terms of morphology.

Another effect taking place is that of the formation of secondary droplets being contributed by the raise of Q [71–73], which can be appreciated in the different particle sizes shown in Figure 5.8(h). This image was taken in the outer region of the sprayed section, where the boundary of the electrospray cone lands on the substrate.

Influence of Molar Concentration (c)

As discussed before, the morphology of a deposited layer is largely determined by several intrinsic and extrinsic parameters. However, the influence of the concentration had a minor effect. Figure 5.9(a-d) shows small changes on the morphology when the concentration of the dissolved salts in the precursor solution was varied. At high salt concentrations precipitation became more significant, leading to slightly rougher films in accordance with other studies [41, 60]. Slightly bigger agglomerates and larger particles are present in the film deposited using the 0.075 and 0.1 M solutions (Figure 5.9(c-d)) compared to the 0.01 and 0.05 M solutions (Figure 5.9(a-b)). Perednis et. al. [41] attributed this small difference to the spreading of droplets and to the fact that the particle size after drying increases with increasing concentration of the precursor solution. The spreading rate of the liquid droplet influences the roughness. Qualitatively, the spreading rate decreases with increasing viscosity. The spreading may not be completed if the simultaneous drying process proceeds rapidly and this will result in an increased roughness. It follows that the concentration should not be too high for the deposition of dense, smooth films. On the other hand, a high salt concentration is desired to achieve high deposition rates. However, it is not always favourable, because the surface roughness of the deposited film increases with increasing salt concentration in the precursor solution, as shown in Figure 5.9(c-d). Nevertheless it clearly shows the tunability of the system with respect to roughness.

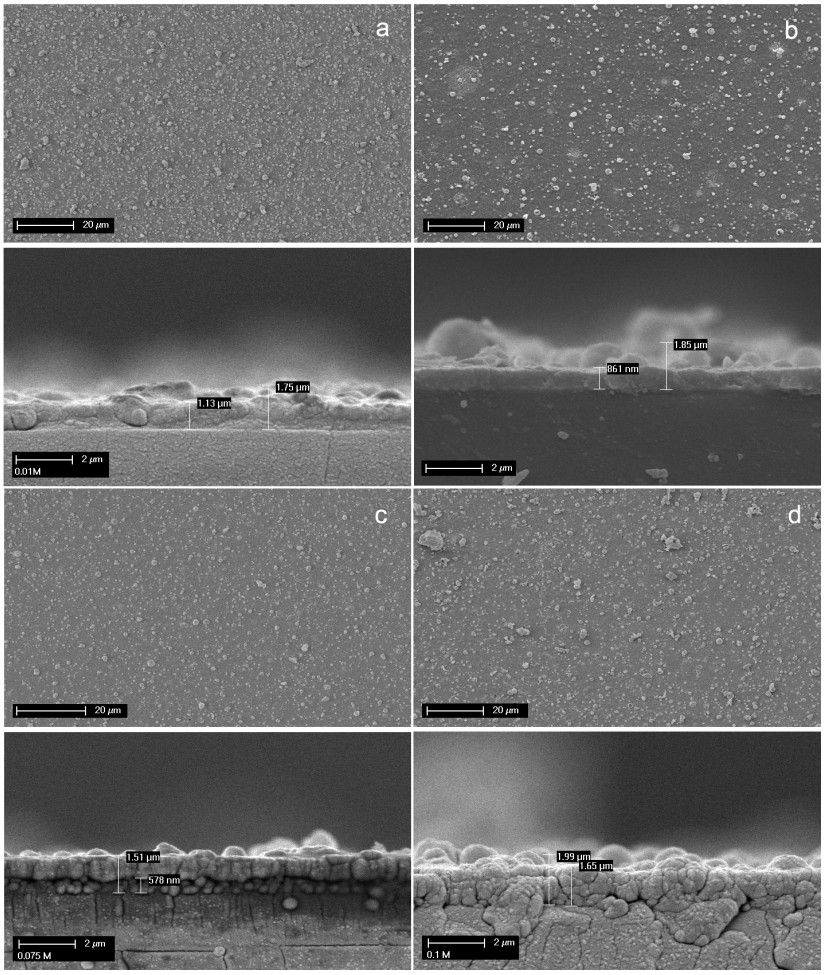

Figure 5.9 – SEM and XSEM micrographs showing the influence of the molar concentration in the morphology of the layers. (a) 0.01; (b) 0.025; (c) 0.05; (d) 0.1 M

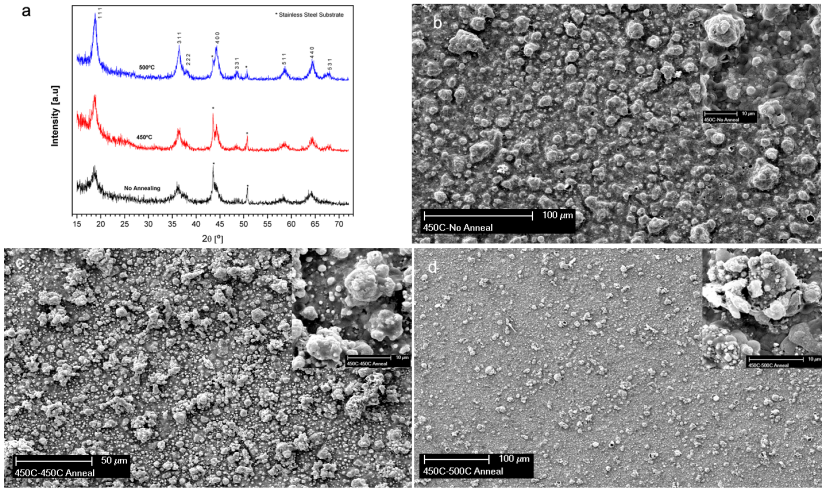

Figure 5.10 – Films synthesised at 450°C and annealed at different temperatures. The effect in cristallinity can be seen in (a) XRD pattern (the peaks marked with dotted lines belong to the support material); SEM micrographs of (b) non annealed; (c) annealed at 450°C; (d) annealed at 500°C.

Table 5.2 – Optimized set of experimental parameters

Voltage (kV)	Molar concentration (M)	Flow rate (mLh^{-1})	Nozzle (mm)	Temperature (°C)	Annealing temperature (°C)	Distance (cm)
8-9	0.05	0.3	20	450	450	2.5

Influence of Annealing Temperature

The XRD patterns presented in Figure 5.10(a) for the annealed samples exhibit the same 'disordered' phase structure (Space group F$d\bar{3}m$) as for the non-annealed sample shown in Figure 5.3. However, the intensity of the peaks increases with the temperature indicating a possible growth in the crystallite size and, as mentioned in Paragraph 5.3.1, the peaks belonging to the reflections (222), (331) and (531) become clearer after annealing. The SEM micrographs of Figure 5.10 show an increase in film density at higher annealing temperatures and confirm the increase of crystallite size as can be observed in the inset pictures, where the average crystallite size is almost two times bigger for the layer annealed at 500°C (Figure 5.10(d)) as compared to the non-annealed sample (Figure 5.10(b)).

5.3.3 Film deposition on 3D architectures and stacking

The next step in the E-STARS project was then to deliver flat, LAR and HAR substrates, with their respective electrosprayed cathode layer, to the partners for the completion of the stack. The parameters used for the creation of these films were then chosen from the layer optimisation study shown in the previous chapter and are summarized in Table 5.2.

The measured values of thickness and mass obtained in correspondence of different sprayed volumes for the precursors are shown in Figure 5.11. As expected, increasing the thickness of the coating results in a growth of the mass deposited on the coin cell cans following a linear trend.

The film deposition on a 3D LAR architecture Si wafer is presented in Figure 5.12. This 3D support presents 14.5μm x 33.3μm x 10μm (W x L x D) trenches periodically dispersed on the entire surface. After deposition, the film cross section shows that the thickness is homogeneous on the flat part of the support with an average value of 4 μm but gradually decreases in the trenches as seen in Figures 5.12(c-d). At the bottom of the trench, the film thickness

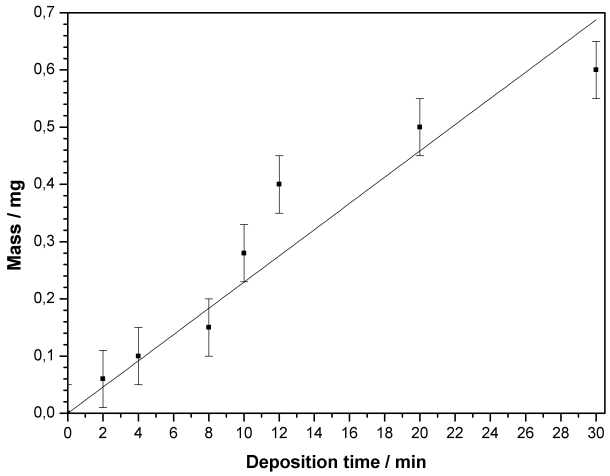

Figure 5.11 – Plot of the values of mass vs. time of deposition for deposited electrodes of $LiNi_{0.5}Mn_{1.5}O_4$ obtained for various sprayed volumes

has decreased to about 1 μm).

Similar experiments for a 3D HAR architecture were carried out and the results are presented in Figure 5.13. The layer shows to be quite dense both on the top flat part and inside the trench. The film cross section shows that the thickness is homogeneous in the first two regions of the trench, Figure 5.13(a and b), with an average value of 420 nm. As before, the film gradually decreases when moving to the bottom of the trench and, although a layer can be definitively observed (Figure 5.13(c)), a direct measurement of the thickness was difficult because proper cleavage of the wafer was not possible without destroying the layer. Using the ESP technique and the chosen set of experimental parameters, it was not possible to obtain a conformal coating of the 3D textured Si wafer.

From a quantitative point of view it means that the gain related to the amount of active material deposited on a 3D structure has not been maximized. Recently, a study on ionic transport in 3D battery presenting trenches has been modelled by Zadin et al. using finite element [74] and [75], where it is shown that ion diffusion in the trench is limited compared to the surface. The overall advantage, that is generally claimed to be gained by increasing the active surface area in 3D systems in order to increase energy density, is thus

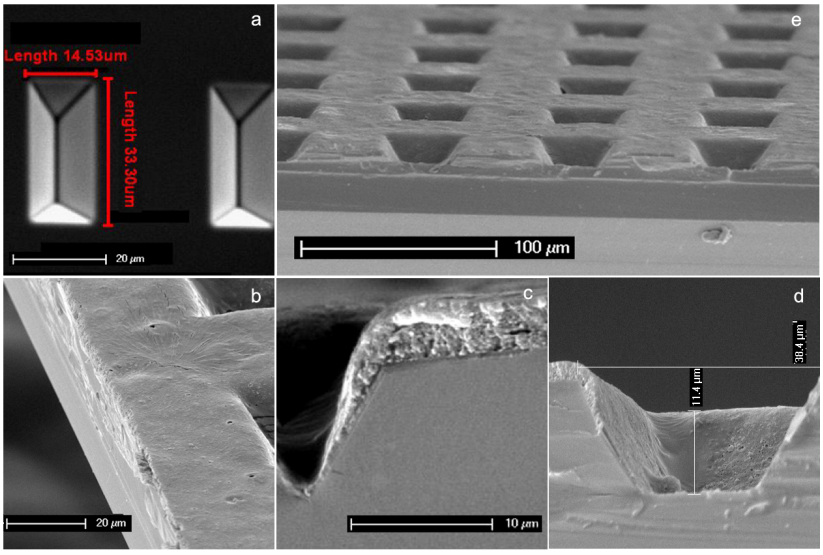

Figure 5.12 – SEM and XSEM images of the Si wafer presenting 3D LAR architecture (a) before and (b, c, d, e) after film deposition. (c, d) Cross section showing the film thickness.

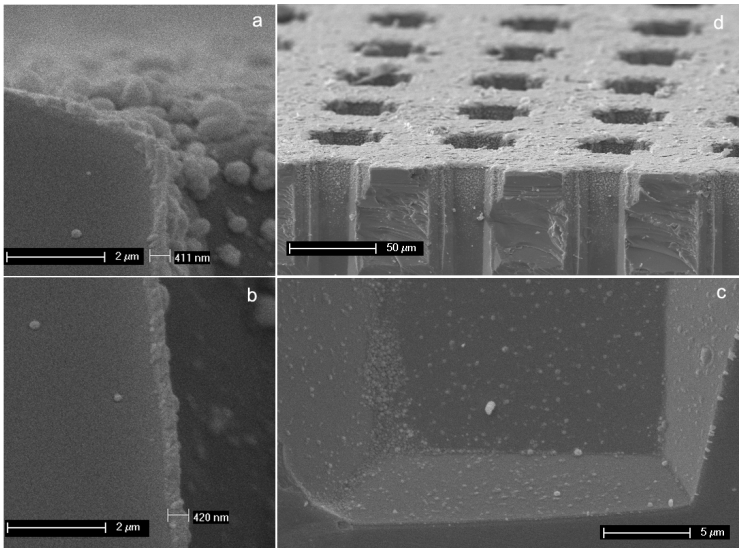

Figure 5.13 – SEM and XSEM images of the Si wafer presenting 3D HAR architecture. Cross section showing the layer on different parts of the trench (a) top (b) middle and (c) bottom. An overview of the film is shown in (d).

minimized. Moreover it can negatively affect the overall system efficiency compared to a flat electrode. From these recent theoretical findings, in order to get the full benefits of a 3D electrode, a gradual decrease of the film thickness in the trenches or valleys is thus preferred to a conformal film deposition. In this respect regarding the experimental results presented, ESP is a versatile technique to achieve suitable electrode deposition on 3D substrate presenting a homogeneous film thickness on flat surface together with a gradual decrease of this film thickness in trenches.

Flat, LAR and HAR substrates were sent to one partner in the E-STARS

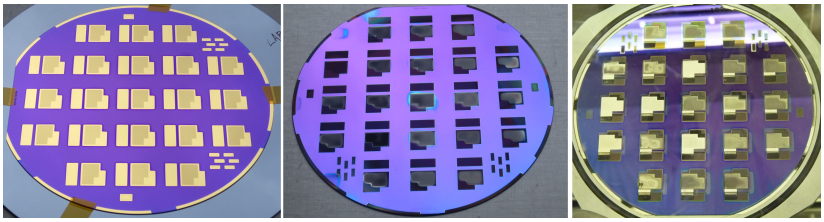

Figure 5.14 – 6" E-STARS wafers as received from partners (left), after cathode deposition (centre) and after completion of the stack by CEA (right).

consortium, 'Commissariat a l'énergie atomique et aux énergies alternatives (CEA)' in France, to complete the stack of the all-solid-state-battery. Figure 5.14 shows pictures of the silicon wafers as received from ST Microelectronics and Applied Materials (consortium partner who deposited the Ti-Au current collector appreciable in the image), after deposition of the high voltage spinel and after the complete stacking performed by CEA.

The steps performed by CEA consisted on film deposition of: 1.4 μm LiPON solid-electrolyte, 3 μm Li anode and a parafilm+glass encapsulation layer. A cross section of this stack is shown in Figure 5.15(a-f). A complete picture of all the components can be seen in Figure 5.15(b). A 1 μm thick, dense and relatively smooth $LiNi_{0.5}Mn_{1.5}O_4$ layer can be observed in Figure 5.15a-d. Overall, the obtained results are promising in terms of stacking of the different layers and confirm electrospraying as a suitable alternative thin-film method for the creation of 3D architectured solid state microbatteries. However, improvement is needed on the compatibility of the different layers. This can be obtained from Figure 5.15(a-b), where there is a visible delamination taking place from the Ti-Au / $LiNi_{0.5}Mn_{1.5}O_4$ interface. This may be caused by the subsequent layers' depositions which involve high vacuum processes (chemical vapour depo-

sition, CVD). Moreover, even if the films present a relatively small roughness, potential problems with impurities may occur introduced by the electrospray deposition or sample transportation. Figure 5.15(e-f) shows such an example where a large spherical core-shell feature which belongs, most likely, to a large droplet relic from the electrospray, but perhaps also to an adhered external contamination, was caught between processes. On top of that, a bad covering of the slopes by both the cathode and the electrolyte layer were present on the HAR stacks.

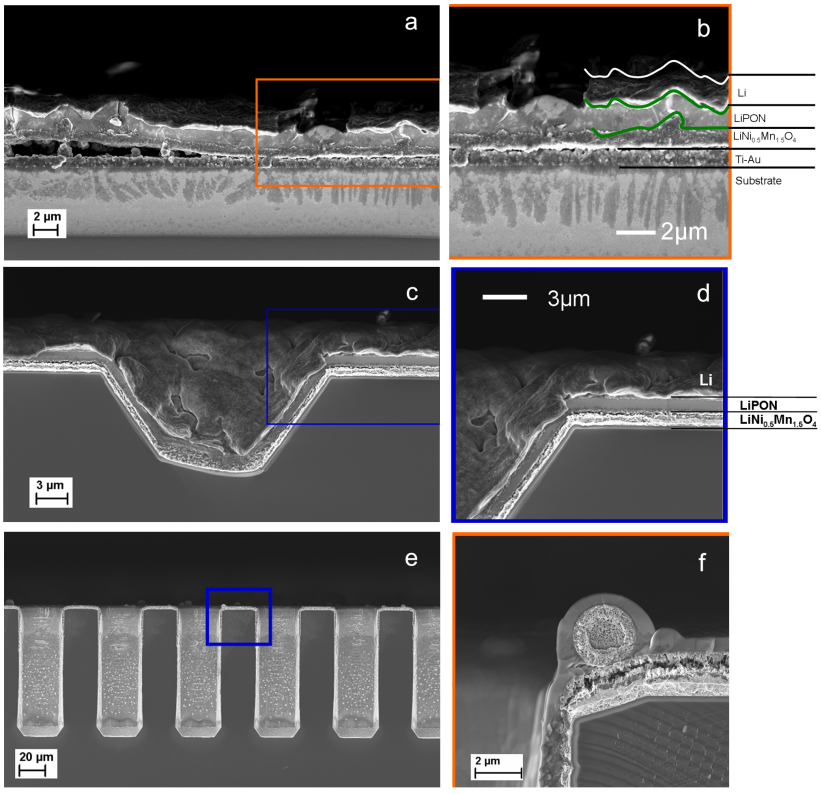

Figure 5.15 – Cross section SEM images of the complete stack on: flat substrate (a, b); LAR substrate (c, d); HAR substrate (e, f). SEM micrographs courtesy of CEA.

5.3.4 Electrochemical characterisation

The different films have been assembled in coin cells or pouch cells for electrochemical characterisation. This subsection consists in two parts. The first part will deal with the analyses performed in liquid electrolyte. The second involves preliminary results with solid electrolyte on a complete stack.

Results in liquid electrolyte

This paragraph will be, on its turn, separated in two subdivisions, namely: influence of annealing temperatures in the electrochemical behaviour, electrochemical proof test on flat stainless steel substrates and results on 3D architectured electrodes (LAR).

Influence of annealing temperature

Electrosprayed high voltage spinel was first tested on flat stainless steel substrates with commercial liquid electrolyte to assess the synthesis parameters studied in the previous section. The influence of annealing on the electrochemical performance was checked with galvanostatic cycling where the as-deposited $LiNi_{0.5}Mn_{1.5}O_4$ layers (those described in Figure 5.10) were tested directly as working electrodes while a lithium metal disk was used as a reference and counter electrode. The cells were charged and discharged at similar gravimetric current densities according to their measured mass.

It is clear from the differential capacity curves presented in Figure 5.16(b) that the materials present multiple redox processes. For the non annealed sample (black line) the profile shows two distinct peaks in the 4 V region clearly on the derivative curve. This is explained by the presence of Mn^{3+} ions, indicating the typical electrochemical characteristics of $LiMn_2O_4$. It is reported that the upper plateau region of discharge curve agrees with the two-phase equilibrium between λ-MnO_2 and $Li_{0.5}Mn_2O_4$, while the lower plateau represents a solid solution between $Li_{0.5}Mn_2O_4$ and $LiMn_2O_4$ [76, 77]. The peak appearing around 4.7 V belongs to the oxidation of Ni^{2+} cations. The behaviour of this material is in accordance to what we have recently published [59]. For the annealed samples the two major peaks appearing between 4.5 and 5 V during charge and discharge are due to the redox couples Ni^{2+}/ Ni^{3+} and Ni^{3+}/ Ni^{4+} probably governed by ordering of lithium and vacancies at x=0.5 [78–80]. Unfortunately, the small step around 4 V was still present for both annealed samples which, again, is associated with the Mn^{3+}/Mn^{4+} redox couple [7, 9, 81].

The galvanostatic tests presented in Figure 5.16(a-c) for the synthesised

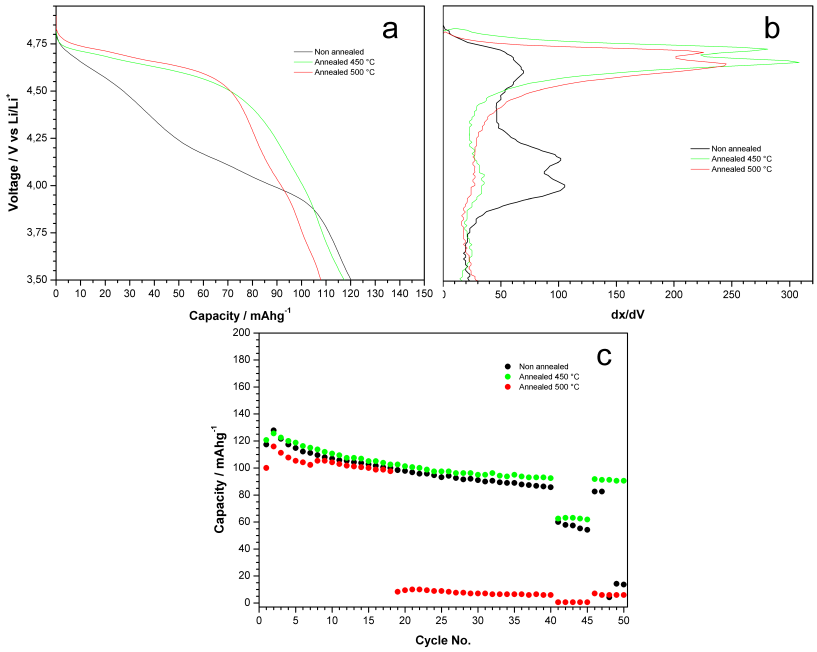

Figure 5.16 – Galvanostatic measurements of the high voltage spinel layers annealed at different temperatures: (a) charge-discharge voltage profiles; (b) differential capacity; (c) capacity retention upon progressive charge-discharge.

films using a pyrolysis temperature of 450 °C and different annealing temperatures do not exhibit a well defined plateau. It has been shown that the redox process upon Li insertion/removal involves oxidation reduction of both Mn and Ni cations. As it was demonstrated by TEM the as-synthesised spinel materials present very small crystallites as well as non-crystalline domains. The disappearance of a well defined plateau upon Li insertion/removal has been observed and explained for several materials were amorphous or nano domains are involved (amorphous [82] and nano [83] TiO_2, $Li_4Ti_5O_{12}$ [84], Sn [85]) as well as for $LiNi_{0.5}Mn_{1.5}O_4$ type nano spinels [14]. Thus, these pseudo plateaus are indeed related to the reversible oxidation reduction of Ni and Mn species combined with the presence of nanosized active domains and the presence of a poorly crystalline structure. The loss of capacity between the first charge and the first discharge is a common phenomenon related to irreversible surface reactions like a solid electrolyte interface formation [86]. Moreover, these irreversible reactions are amplified when the host material present high surface area and amorphous parts. Whereas the films do not contain extra electronic conductive material (e.g. carbonaceous materials) the polarisation effect is limited leading to a small difference between the charge and discharge. This may be attributed to the presence of nanosized crystallites and the hierarchical porous film texture involving smaller diffusion path for the Li ions and a better electrode-electrolyte contact area, respectively.

The discharge curves of Figure 5.16(a) show that through annealing the voltage plateaus at 4.7 become flatter and the voltage step around 4 V tends to disappear, which means that almost all the capacity is delivered at a high voltage. Apparently, the energy input during annealing enables a transition from the disordered $LiNi_{0.5}Mn_{1.5}O_4$ structure into a more ordered structure where most of the manganese is present as Mn^{4+}. Annealing at even higher temperature to further order the structure would damage the Si substrate and the preceding layers (Ti-Au current collector and passivation layer), therefore it was not attempted. As a partial conclusion, it is observed that the thermal treatment during the synthesis and/or annealing is the main factor influencing the electrochemical behaviour for the cells assembled in this study containing, as described before, commercial liquid electrolyte.

Therefore, if a thermal treatment is going to be applied to a layer of $LiNi_{0.5}Mn_{1.5}O_4$ deposited by ESD, in order to get a good electrochemical performance at high voltages, a temperature of 450 °C is suggested.

Proof test of the optimized set of parameters on flat stainless steel substrates

As a final proof test for this set of parameters, i.e. those summarized in Table 5.2, a final sample was prepared following that recipe with a deposition time of 25 min. Again, a CR2330-type coin cell cap was used as direct (flat) substrate. A half-cell battery with lithium metal as counter electrode and commercial liquid electrolyte was thus prepared. As it can be observed in Figure 5.17, the assembled battery presents a specific capacity of 125 mAh g^{-1}, during the first discharge, which corresponds to 50 μAh cm^{-2} per μm thickness of deposition. It increases to a maximum of 135 mAh g^{-1} (53 μAh cm^{-2}) in the second discharge. Based on the spinel density (4.4 g cm^{-3}), the area of deposition (1.5 cm^2) and mass (0.6 mg), a thickness of 1 μm was calculated. As described in Figure 5.11, the layer thickness can be controlled by increasing the volume of precursor being sprayed or, similarly, the time of spraying.

It is interesting to mention that the measured capacity doesn't come from

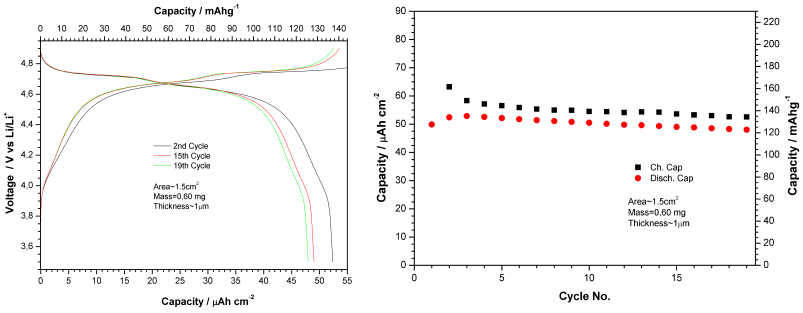

Figure 5.17 – Galvanostatic test using optimized parameters of Table 5.2 and a deposition time of 25 min.

the oxidation/reduction of Ni species only as it should be in the case of a perfect high voltage spinel $LiNi_{0.5}Mn_{1.5}O_4$, where all Mn atoms present a + 4 oxidation state. For this material during the first charge only 40% of the capacity can be attributed to Ni oxidation. This value increases and stabilizes to 81-83% directly after the first discharge and for the subsequent cycles. These values are presented in Table 5.3. The change on capacity of the various ions is due to irreversible redox reactions in this cycle. However, there is an amount of Mn related capacity which implies that a consequent amount of Mn cations exhibit a +3 oxidation state. It is stressed that from elemental analysis of the samples, the measured stoichiometry is similar to the expected stoichiometry

Table 5.3 – Contribution of Ni species to the total capacity of annealed samples using a deposition temperature of 450 °C.

	% of capacity related to Ni[a]					
	(1st cycle)		(2nd cycle)		(19th cycle)	
	Charge	Discharge	Charge	Discharge	Charge	Discharge
$LiNi_{0.5}Mn_{1.5}O_4$ Film	40	73	83	79	81	80

[a] Value extracted using the inflexion point as limit between Ni and Mn contribution.

with a Mn/Ni ratio of 3. The change in the voltage profile indicates that electrons are being stored after the first cycle at the Ni, making Ni^{2+}, rather than at the Mn, hence leaving Mn^{4+}. This indicates a change in the electronic distribution coming from the first and the second cycles. On the other hand, the presence of impurity phases with rock salt structure, for instance $Li_xNi_{1-x}O$, have been observed, as shown by XRD results in Figure 5.3, and might lead to the residual Mn^{3+}/Mn^{4+} plateau seen after the first cycle. However, numeric approximations (not shown here) show that this cannot be the only reason for that Mn^{3+}/Mn^{4+} plateau so, most likely, oxygen vacancies are also involved.

Proof test of the optimized set of parameters on LAR E-STARS substrates

Following the results presented for flat, stainless-steel substrates presented before, the material then deposited on low aspect ratio substrates. A pouch cell or coffee bag cell was prepared cleaving one of the batteries on the silicon wafer which was previously coated with the material following the above recipe. A polyethylene separator (Solupor) with few drops of as electrolyte was used as separator and metallic Li as anode. An aluminium strip was placed on top of the Ti/Au current collector and a copper strip was placed in contact with the lithium counter electrode. This sandwich type assembly was carefully introduced to the vacuum sealer. The contact between the elements is then provided by the vacuum pressure.

The electrochemical measurements are shown in Figure 5.18. As it can be observed, the assembled battery presents a specific capacity of 126 mAh g^{-1}, during the first discharge, which corresponds to 16.5 μAh cm^{-2}. It increases to a maximum of 130 mAh g^{-1} (17.2 μAh cm^{-2}) in the second discharge and then decreases and stabilizes at 117 mAh g^{-1} (15.2 μAh cm^{-2}) over the next

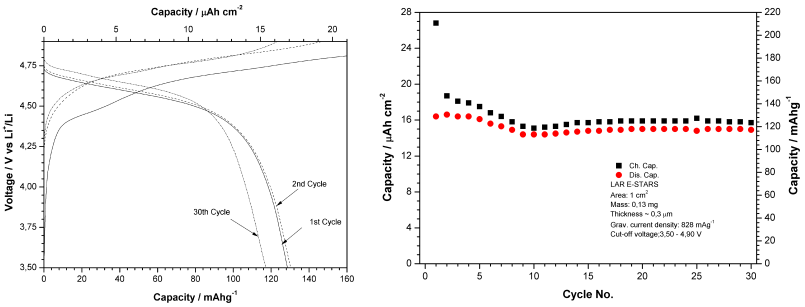

Figure 5.18 – Galvanostatic test on LAR E-STARS substrate with liquid electrolyte.

cycles. Based on the spinel density (4.4 g cm^{-3}), the area of deposition (1 cm^2) and mass (0.13 mg), a thickness of 0.3 μm was calculated. As mentioned before, the layer thickness can be controlled by increasing the time of spraying. Therefore the areal capacity of this example in particular raises to a value of 51 μAh cm^{-2} per μm thickness. Moreover, the electrode shows good capacity retention over the window studied and confirms the suitability of electrospray technology for the production of thin layers for 3D microbatteries.

Results in solid electrolyte

As mentioned in Paragraph 5.3.4, the steps performed by CEA consisted of film deposition of a LiPON solid-electrolyte, Li anode and a parafilm+glass encapsulation layer. In this case, none of the stacks (flat, LAR and HAR) yielded a functioning battery. However, the OCV mapping on the flat substrates gave several cells that did not show, at least, signs of short-circuiting. In fact, one of the cells with an OCV of 2.74 V was tested galvanostatically at a current density of 10 μm cm^{-2}. As shown in Figure 5.19, the cell begins with the expected electrochemical reactions during charging until about 4.6 V and then shows a drastic decrease in voltage. It is assumed that there was an induced short-circuit caused by cycling. These very preliminary results show at least the versatility of the methods applied within E-STARS, but also gives food for further optimisation.

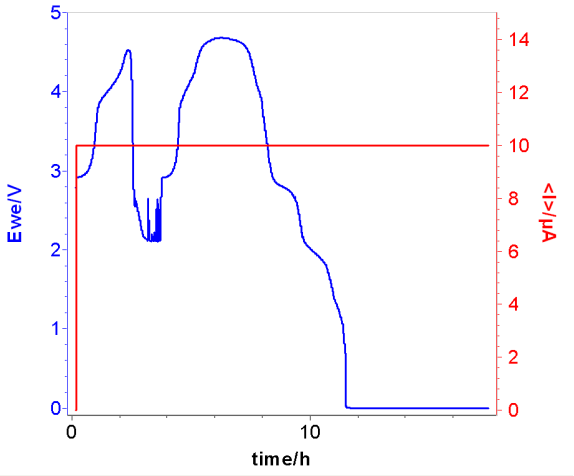

Figure 5.19 – Galvanostatic test on a stacked flat E-STARS substrate with solid-electrolyte.

5.4 Conclusions and prospects

The electrospraying technique has been used for the production of thin dense layers of the high voltage spinel $LiNi_{0.5}Mn_{1.5}O_4$ cathode on different substrates. The synthesis, deposition and film formation occur in a one step process. This technique opens the opportunity to control the morphology of a layer, by tuning the deposition parameters, for its use in a wide range of applications. For the production of all-solid-state-microbatteries, a specific requirement of smooth, dense layers is needed. Nevertheless, it is not trivial to obtain an optimum set of parameters, as they all present correlation between each other. At larger distances from nozzle to substrate (2.5 - 3 cm) the stability of the spraying was better, permitting the production of a more monodisperse jet. This parameter, together with a low flow rate and a low concentration, allows the wettability of the surface so as to obtain more density of the film. Annealing of the deposited layers at 450 °C improves both the cristallinity of the deposited films and the corresponding electrochemical behaviour. After this process, galvanostatic measurement yielded that the contribution to the capacity from the low voltage Mn^{3+}/Mn^{4+} redox couple is reduced, while the contribution from the high voltage Ni^{2+}/Ni^{4+} is increased.

The method allows the production of layers with capacities up to the re-

quired capacity per square centimetre, by adjusting its thickness. Besides, when having a low or high aspect ratio substrate surface, the thickness can be significantly reduced, according to the actual received surface area. The method in that respect also shows acceptable homogeneity within the "holes" or "grooves" of an etched Si wafer. Even if the spinel can be formed at low temperature, high pyrolysis and/or annealing temperatures are needed to enhance the material crystal structure and thus its electrochemical behaviour.

This method is not limited to the fabrication of the $LiNi_{0.5}Mn_{1.5}O_4$ cathode, but may be used for any other lithium transition metal oxide. The perspectives of the method are many fold. It has been shown in the mean time that electrospraying can be used to form (composite) layers as well as layers with polymers only. With regard to the composite layers basically two different approaches were shown and have been published yet, partly under the name of the E-STARS project, namely the spraying of an ink that contains similar salts as those used for the deposition of the $LiNi_{0.5}Mn_{1.5}O_4$ cathode, but with the addition of polymer binder PVdF, as described in the previous chapter; spraying of an ink that contains powders of relevant electrode material, e.g. silicon nanoparticles, together with a polymeric binder like PVdF or CMC, as recently published by our group.

Two different setups have been developed, one of which was solely designed for its use on the E-STARS project, as was described in Chapter 3. The other one has been built with the vision of a Roll-to-Roll system for electrode production. The employment of these two systems in several projects and the larger-than-laboratory samples used in this study, show that the method is scalable.

References

[1] S. Chatterjee, "Wireless Sensor Networks: Solutions and Market Opportunities," *Radio Frequency Identification Journal*, 2008.

[2] European Nanoelectronics Initiative Advisory Council, "Multi-annual strategic plan 2010." `http://www.eniac.eu/web/downloads/documents/masp2010.pdf`, November 2010. Accessed: 10 February 2013.

[3] European Technology Platform on Smart Systems Integrations, "Strategic research agenda." `http://www.smart-systems-integration.org/public`, March 2009. Accessed: 1 February 2013.

[4] Advanced Research & Technology for EMbedded Intelligence and Systems, "Strategic research agenda 2011." `http://www.artemis-ia.eu/sra`, April 2011. Accessed: 15 February 2013.

[5] Efficient Smart sysTems with enhAnced eneRgy Storage, "Newsletter I." `http://www.estars-project.eu/home/liblocal/docs/NewsletterI.-V0.pdf`, November 2009. Accessed: 26 May 2013.

[6] J. Arrebola, A. Caballero, M. Cruz, L. Hernan, J. Morales, and E. Castellon, "Crystallinity Control of a Nanostructured $LiNi_{0.5}Mn_{1.5}O_4$ Spinel via Polymer-Assisted Synthesis: A Method for Improving Its Rate Capability and Performance in 5V Lithium Batteries," *Advanced Functional Materials*, vol. 16, no. 14, pp. 1904–1912, 2006.

[7] M. Kunduraci, J. Al-Sharab, and G. Amatucci, "High-Power Nanostructured $LiMn_{2-x}Ni_xO_4$ High-Voltage Lithium-Ion Battery Electrode Materials: Electrochemical Impact of Electronic Conductivity and Morphology," *Chemistry of Materials*, vol. 18, no. 15, pp. 3585–3592, 2006.

[8] H. Xia, Y. Meng, L. Lu, and G. Ceder, "Electrochemical Properties of Nonstoichiometric $LiNi_{0.5}Mn_{1.5}O_{4-\delta}$ Thin-Film Electrodes Prepared by Pulsed Laser Deposition," *Journal of The Electrochemical Society*, vol. 154, no. 8, pp. A737–A743, 2007.

[9] S. Patoux, C. Daniel, C. Bourbon, H. Lignier, C. Pagano, F. Le Cras, S. Jouanneau, and S. Martinet, "High voltage spinel oxides for Li-ion batteries: From the material research to the application," *Journal of Power Sources*, vol. 189, no. 1, pp. 344–352, 2009.

[10] J. Arrebola, A. Caballero, L. Hernan, and J. Morales, "A high energy Li-ion battery based on nanosized $LiNi_{0.5}Mn_{1.5}O_4$ cathode material," *Journal of Power Sources*, vol. 183, no. 1, pp. 310–315, 2008.

[11] Z. Chen, H. Zhu, S. Ji, V. Linkov, J. Zhang, and W. Zhu, "Performance of $LiNi_{0.5}Mn_{1.5}O_4$ prepared by solid-state reaction," *Journal of Power Sources*, vol. 189, no. 1, pp. 507–510, 2009.

[12] K. Kanamura and W. Hoshikawa, "Electrochemical reaction of 5 V cathode $LiNi_{0.4}Mn_{1.6}O_4$," *Solid State Ionics*, vol. 177, no. 1-2, pp. 113–119, 2006.

[13] F. Ooms, E. Kelder, J. Schoonman, M. Wagemaker, and F. Mulder, "High-voltage $LiMg_{\delta}Ni_{0.5-\delta}Mn_{1.5}O_4$ spinels for Li-ion batteries," *Solid State Ionics*, vol. 152–153, pp. 143–153, 2002.

[14] U. Lafont, C. Locati, W. Borghols, A. Lasinska, J. Dygas, A. Chadwick, and E. Kelder, "Nanosized high voltage cathode material $LiMg_{0.05}Ni_{0.45}Mn_{1.5}O_4$: Structural, electrochemical and in situ investigation," *Journal of Power Sources*, vol. 189, no. 1, pp. 179–184, 2009.

[15] U. Lafont, C. Locati, and E. Kelder, "Nanopowders of spinel-type electrode materials for Li-ion batteries," *Solid State Ionics*, vol. 177, no. 35–36, pp. 3023–3029, 2006.

[16] R. Wartena, A. Curtright, C. Arnold, A. Pique, and K. Swider-Lyons, "Li-ion microbatteries generated by a laser direct-write method," *Journal of Power Sources*, vol. 126, no. 1–2, pp. 193–202, 2004.

[17] H. Xia, S. Tang, L. Lu, Y. Meng, and G. Ceder, "The influence of preparation conditions on electrochemical properties of $LiNi_{0.5}Mn_{1.5}O_4$ thin film electrodes by PLD," *Electrochimica Acta*, vol. 52, no. 8, pp. 2822–2828, 2007.

[18] J. Song, M. Cai, Q. Dong, M. Zheng, Q. Wu, and S. Wu, "Structural and electrochemical characterization of SnO_x thin films for Li-ion microbattery," *Electrochimica Acta*, vol. 54, no. 10, pp. 2748–2753, 2009.

[19] Y. Park and S. Park, "Preparation and electroactivity of poly(methylmethacrylate-co-pyrrolylmethylstyrene)-g-polypyrrole," *Synthetic Metals*, vol. 128, no. 2, pp. 229–234, 2002.

[20] S. Lee, H. Lee, T. Ha, H. Baik, and S. Lee, "Amorphous Lithium Nickel Vanadate Thin-Film Anodes for Rechargeable Lithium Microbatteries," *Electrochemical and Solid-State Letters*, vol. 5, no. 6, pp. A138–A140, 2002.

[21] H. Kim and Y. Yoon, "Characteristics of rapid-thermal-annealed $LiCoO_2$ cathode film for an all-solid-state thin film microbattery," *Journal of Vacuum Science & Technology A: Vacuum, Surfaces, and Films*, vol. 22, no. 4, pp. 1182–1187, 2004.

[22] K. Kim, M. Kim, S. Lee, K. Han, and S. Woo, "The Characterization of $LiMn_2O_4$ Thin Film Cathode for Lithium Rechargeable Microbattery Prepared by Liquid Source Misted Chemical Deposition," *Chemical Vapor Deposition*, vol. 9, no. 4, pp. 187–192, 2003.

[23] S. Lee, H. Kim, S. Choi, and S. Lee, "The production of $LiCoO_2$ cathode thick films for an all-solid-state microbattery," *Journal of Ceramic Processing Research*, vol. 8, no. 2, pp. 106–109, 2007.

[24] K. Dokko, J. Sugaya, H. Nakano, T. Yasukawa, T. Matsue, and K. Kanamura, "Sol-gel fabrication of lithium-ion microarray battery," *Electrochemistry Communications*, vol. 9, no. 5, pp. 857–862, 2007.

[25] Y. Park, J. Kim, M. Kim, H. Chung, W. Um, M. Kim, and H. Kim, "Fabrication of $LiMn_2O_4$ thin films by sol-gel method for cathode materials of microbattery," *Journal of Power Sources*, vol. 76, no. 1, pp. 41–47, 1998.

[26] D. Golodnitsky, M. Nathan, V. Yufit, E. Strauss, K. Freedman, L. Burstein, A. Gladkich, and E. Peled, "Progress in three-dimensional 3D Li-ion microbatteries," *Solid State Ionics*, vol. 177, pp. 2811–2819, 2006.

[27] L. Bazin, S. Mitra, P. Taberna, P. Poizot, M. Gressier, M. Menu, A. Barnabe, P. Simon, and J. Tarascon, "High rate capability pure Sn-based nano-architectured electrode assembly for rechargeable lithium batteries," *Journal of Power Sources*, vol. 188, no. 2, pp. 578–582, 2009.

[28] K. Edstrom, D. Brandell, T. Gustafsson, and L. Nyholm, "Electrodeposition as a Tool for 3D Microbattery Fabrication," *The Electrochemical Society Interface*, vol. 20, no. 2, pp. 41–46, 2011.

[29] Y. Xie, R. Neagu, C. Hsu, X. Zhang, and C. Deces-Petit, "Spray Pyrolysis Deposition of Electrolyte and Anode for Metal-Supported Solid Oxide Fuel

Cell," *Journal of The Electrochemical Society*, vol. 155, no. 4, pp. B407–B410, 2008.

[30] C. Chang, C. Hsu, and B. Hwang, "Unique porous thick $Sm_{0.5}Sr_{0.5}CoO_3$ solid oxide fuel cell cathode films prepared by spray pyrolysis," *Journal of Power Sources*, vol. 179, no. 2, pp. 734–738, 2008.

[31] A. Subramania, S. Karthick, and N. Angayarkanni, "Preparation and electrochemical behaviour of $LiMn_2O_4$ thin film by spray pyrolysis method," *Thin Solid Films*, vol. 516, no. 23, pp. 8295–8298, 2008.

[32] M. Valvo, U. Lafont, and E. Kelder, "An Aerosol-Based Route to Nanostructured Powders Synthesis in Liquids," *Journal of Nanoscience and Nanotechnology*, vol. 10, no. 9, pp. 5800–5809, 2010.

[33] J. Grace and J. Marijnissen, "A review of liquid atomization by electrical means," *Journal of Aerosol Science*, vol. 25, no. 6, pp. 1005–1019, 1994.

[34] R. Hartman, D. Brunner, D. Camelot, J. Marijnissen, and B. Scarlett, "Electrohydrodynamic Atomization in the Cone-Jet mode Physical modeling of the liquid Cone and Jet," *Journal of Aerosol Science*, vol. 30, no. 7, pp. 823–849, 1999.

[35] S. Youssef, R. Al Asmar, J. Podlecki, M. Abdallah, D. Zaouk, and A. Foucaran, "Preliminary study on pyroelectric lithium tantalite by a novel electrostatic spray pyrolysis technique," *Microelectronics Journal*, vol. 39, no. 5, pp. 792–796, 2008.

[36] D. Zaouk, R. Al Asmar, J. Podlecki, Y. Zaatar, A. Khoury, and A. Foucaran, "X-ray diffraction studies of electrostatic sprayed SnO_2:F films," *Microelectronics Journal*, vol. 38, no. 8-9, pp. 884–887, 2007.

[37] D. Zaouk, Y. Zaatar, R. Asmar, and J. Jabbour, "Piezoelectric zinc oxide by electrostatic spray pyrolysis," *Microelectronics Journal*, vol. 37, no. 11, pp. 1276–1279, 2006.

[38] K. Hwang, K. Jeon, Y. Jeon, and B. Kim, "Hydroxyapatite forming ability of electrostatic spray pyrolysis derived calcium phosphate nano powder," *Journal of Materials Science*, vol. 41, pp. 4159–4162, 2006.

[39] C. Hsu and B. Hwang, "Microstructure and Properties of the $La_{0.6}Sr_{0.4}Co_{0.2}Fe_{0.8}O_3$ Cathodes Prepared by Electrostatic-Assisted Ultrasonic Spray Pyrolysis Method," *Journal of The Electrochemical Society*, vol. 153, no. 8, pp. A1478–A1483, 2006.

[40] M. Consales, M. Pisco, P. Pilla, A. Cusano, A. Buosciolo, M. Giordano, R. Viter, and V. Smyntyna, "Influence of Layers Morphology on the Sensitivity of SnO_2-based Optical Fiber Sensors," *Proceedings of IEEE Sensors*, pp. 851–854, 2006.

[41] D. Perednis, O. Wilhelm, S. Pratsinis, and L. Gauckler, "Morphology and deposition of thin yttria-stabilized zirconia films using spray pyrolysis," *Thin Solid Films*, vol. 474, no. 1-2, pp. 84–95, 2005.

[42] H. Huang, X. Yao, X. Wu, M. Wang, and L. Zhang, "Morphology control of ferroelectric lead titanate thin films prepared by electrostatic spray deposition," *Thin Solid Films*, vol. 458, no. 1-2, pp. 71–76, 2004.

[43] D. Zaouk, Y. Zaatar, A. Khoury, C. Llinares, J. Charles, and J. Bechara, "Fabrication of tin oxide (SnO_2) thin film by electrostatic spray pyrolysis," *Microelectronic Engineering*, vol. 51-52, pp. 627–631, 2000.

[44] S. Kim, J. Kim, and H. Kim, "Deposition of MgO thin films by modified electrostatic spray pyrolysis method," *Thin Solid Films*, vol. 376, no. 1-2, pp. 110–114, 2000.

[45] C. Chen, F. Yuan, and J. Schoonman, "Spray pyrolysis routes to electroceramic powders and thin films," *European Journal of Solid State and Inorganic Chemistry*, vol. 35, no. 2, pp. 189–196, 1998.

[46] A. A. van Zomeren, E. M. Kelder, J. C. M. Marijnissen, and J. Schoonman, "The production of thin films of $LiMn_2O_4$ by electrospraying," *Journal of Aerosol Science*, vol. 25, no. 6, pp. 1229–1235, 1994.

[47] C. Chen, A. Buysman, E. Kelder, and J. Schoonman, "Fabrication of $LiCoO_2$ thin film cathodes for rechargeable lithium battery by electrostatic spray pyrolysis," *Solid State Ionics*, vol. 80, no. 1–2, pp. 1–4, 1995.

[48] X. Zhu, Z. Guo, P. Zhang, G. Du, R. Zeng, Z. Chen, S. Li, and H. Liu, "Highly porous reticular tin-cobalt oxide composite thin film anodes for lithium ion batteries," *Journal of Materials Chemistry*, vol. 19, pp. 8360–8365, 2009.

[49] D. Liu and G. Cao, "Engineering nanostructured electrodes and fabrication of film electrodes for efficient lithium ion intercalation," *Energy & Environmental Science*, vol. 3, pp. 1218–1237, 2010.

[50] H. Ryu, J. Kim, Z. Guo, H. Liu, K. Kim, J. Ahn, and H. Ahn, "Electrochemical properties of Fe_2O_3 thin film fabricated by electrostatic spray deposition for lithium-ion batteries," *Physica Scripta*, vol. T139, p. 014066, 2010.

[51] Y. Sun, X. Feng, and C. Chen, "Hollow Co_3O_4 thin films as high performance anodes for lithium-ion batteries," *Journal of Power Sources*, vol. 196, no. 2, pp. 784–787, 2011.

[52] X. Zhu, Z. Guo, P. Zhang, G. Du, C. Poh, Z. Chen, S. Li, and H. Liu, "Three-dimensional reticular tin-manganese oxide composite anode materials for lithium ion batteries," *Electrochimica Acta*, vol. 55, no. 17, pp. 4982–4986, 2010.

[53] P. Zhang, Z. Guo, S. Kang, Y. Choi, C. Kim, K. Kim, and H. Liu, "Three-dimensional Li_2O-NiO-CoO composite thin-film anode with network structure for lithium-ion batteries," *Journal of Power Sources*, vol. 189, no. 1, pp. 566–570, 2009.

[54] L. Wang, H. Xu, P. Chen, D. Zhang, C. Ding, and C. Chen, "Electrostatic spray deposition of porous Fe_2O_3 thin films as anode material with improved electrochemical performance for lithium-ion batteries," *Journal of Power Sources*, vol. 193, no. 2, pp. 846–850, 2009.

[55] S. Koike and K. Tatsumi, "Preparation and performances of highly porous layered $LiCoO_2$ films for lithium batteries," *Journal of Power Sources*, vol. 174, no. 2, pp. 976–980, 2007.

[56] E. Garcia-Tamayo, M. Valvo, U. Lafont, C. Locati, D. Munao, and E. Kelder, "Nanostructured Fe_2O_3 and CuO composite electrodes for Li ion batteries synthesized and deposited in one step," *Journal of Power Sources*, vol. 196, no. 15, pp. 6425–6432, 2011.

[57] Munao, D and van Erven, J.W.M and Valvo, M and Garcia-Tamayo, E and Kelder, E.M, "Role of the binder on the failure mechanism of si nano-composite electrodes for li-ion batteries," *Journal of Power Sources*, vol. 196, pp. 6695–6702, 2011.

[58] M. Mohamedi, M. Makino, K. Dokko, T. Itoh, and I. Uchida, "Electrochemical investigation of $LiNi_{0.5}Mn_{1.5}O_4$ thin film intercalation electrodes," *Electrochimica Acta*, vol. 48, no. 1, pp. 79–84, 2002.

[59] U. Lafont, A. Anastasopol, E. Garcia-Tamayo, and E. Kelder, "Electrostatic spray pyrolysis of $LiNi_{0.5}Mn_{1.5}O_4$ films for 3D Li-ion microbatteries," *Thin Solid Films*, vol. 520, no. 9, pp. 3464–3471, 2012.

[60] C. Chen, E. Kelder, P. Van Der Put, and J. Schoonman, "Morphology control of thin $LiCoO_2$ films fabricated using the electrostatic spray deposition (ESD) technique," *Journal of Materials Chemistry*, vol. 6, no. 5, pp. 765–771, 1996.

[61] A. Jaworek, "Electrospray droplet sources for thin film deposition," *Journal of Materials Science*, vol. 42, pp. 266–297, 2007.

[62] A. Jaworek and A. Krupa, "Jet and drops formation in electrohydrodynamic spraying of liquids. A systematic approach," *Experiments in Fluids*, vol. 27, pp. 43–52, 1999.

[63] J. Gaury, E. Kelder, E. Bychkov, and G. Biskos, "Characterization of Nb-doped WO_3 thin films produced by Electrostatic Spray Deposition," *Thin Solid Films*, 2013.

[64] Efficient Smart sysTems with enhAnced eneRgy Storage, "Newsletter III." `http://www.estars-project.eu/home/liblocal/docs/NewsletterIII-V0.pdf`, November 2009. Accessed: 26 May 2013.

[65] D. Pasero, N. Reeves, V. Pralong, and A. West, "Oxygen Nonstoichiometry and Phase Transitions in $LiMn_{1.5}Ni_{0.5}O_{4-\delta}$," *Journal of Power Sources*, vol. 155, no. 4, pp. A282–A291, 2008.

[66] K. Shajua and P. Bruce, "Nano-$LiNi_{0.5}Mn_{1.5}O_4$ spinel: a high power electrode for Li-ion batteries," *Dalton Transactions*, pp. 5471–5475, 2008.

[67] J. Jeong, Y. Jeon, K. Jeon, K. Hwang, and B. Kim, "Preparation of zinc oxide films by an electrostatic spray deposition process," *Ceramic Processing Research*, vol. 7, no. 1, pp. 70–74, 1993.

[68] N. Stelzer, A. Goossens, and J. Schoonman, "Synthesis of terbia doped yttria stabilized zirconia thin films by using the electrostatic spray deposition (esd) technique," *MRS Proceedings*, vol. 453, no. 6, pp. 429–438, 1996.

[69] A. Jaworek and A. Sobcyk, "Electrospraying route to nanotechnology: An overview," *Journal of Electrostatics*, vol. 66, pp. 197–219, 2008.

[70] A. Ganan-Calvo, J. Dávila, and A. Barrero, "Current and droplet size in the electrospraying of liquids. scaling laws," *Journal of Aerosol Science*, vol. 28, no. 2, pp. 249–275, 1997.

[71] E. Nijman, *Dynamic light scatteringat low concentrationand in turbulent flow*. PhD thesis, Delft University of Technology, Delft, The Netherlands, March 2002.

[72] O. Wilhelm, L. Madler, and S. Pratsinis, "Electrospray evaporation and deposition," *Journal of Aerosol Science*, vol. 34, pp. 815–836, 2003.

[73] D. Camelot, *The bipolar coagulation process for powder production. An application of the electrohydrodynamic atomization of liquids.* PhD thesis, Delft University of Technology, Delft, The Netherlands, May 1999.

[74] V. Zadin, D. Brandell, H. Kasemagi, A. Aabloo, and J. Thomas, "Finite element modelling of ion transport in the electrolyte of a 3d-microbattery," *Solid State Ionics*, vol. 192, no. 1, pp. 279–283, 2011.

[75] V. Zadin, H. Kasemagi, A. Aabloo, and D. Brandell, "Modelling electrode material utilization in the trench model 3d-microbattery by finite element analysis," *Journal of Power Sources*, vol. 195, no. 18, pp. 6218–6224, 2010.

[76] F. K. Shokoohi, J. M. Tarascon, B. J. Wilkens, D. Guyomard, and C. C. Chang, "Low Temperature $LiMn_2O_4$ Spinel Films for Secondary Lithium Batteries," *Journal of Electrochemical Society*, vol. 139, no. 7, pp. 1845–1849, 1992.

[77] C.-H. Lu and S.-W. Lin, "Influence of the particle size on the electrochemical properties of lithium manganese oxide," *Journal of Power Sources*, vol. 97-98, pp. 458–460, 2001.

[78] A. Van der Ven and G. Ceder, "Electrochemical properties of spinel Li_xCoO_2: A first-principles investigation," *Physical Review B.*, vol. 59, no. 2, pp. 742–749, 1999.

[79] A. Van der Ven, C. Marianetti, D. Morgan, and G. Ceder, "Phase transformations and volume changes in spinel $Li_xMn_2O_4$," *Physical Review B.*, vol. 135, no. 1-4, pp. 21–32, 2000.

[80] R. Santhanam and B. Rambabu, "Research progress in high voltage spinel $LiNi_{0.5}Mn_{1.5}O_4$ material," *Journal of Power Sources*, vol. 195, pp. 5442–5451, 2010.

[81] M. Kunduraci, J. Al-Sharab, and G. Amatucci, "Synthesis and Characterization of Nanostructured 4.7 V $Li_xMn_{1.5}Ni_{0.5}O_4$ Spinels for High-Power Lithium-Ion Batteries," *Journal of the Electrochemical Society*, vol. 153, no. 7, pp. A1345–A1352, 2006.

[82] W. Borghols, D. Lützenkirchen-Hecht, U. Haake, W. Chan, U. Lafont, E. Kelder, E. van Eck, A. Kentgens, F. Mulder, and M. Wagemaker, "Lithium storage in amorphous tio_2 nanoparticles," *Journal of The Electrochemical Society*, vol. 157, no. 5, pp. A582–A588, 2010.

[83] U. Lafont, D. Carta, G. Mountjoy, A. Chadwick, and E. Kelder, "In situ structural changes upon electrochemical lithium insertion in nanosized anatase tio_2," *The Journal of Physical Chemistry C*, vol. 114, no. 2, pp. 1372–1378, 2010.

[84] W. Borghols, M. Wagemaker, U. Lafont, E. Kelder, and F. Mulder, "Size effects in the $li_{4+x}ti_5o_{12}$ spinel," *Journal of the American Chemical Society*, vol. 131, no. 49, pp. 17786–17792, 2009.

[85] M. Valvo, U. Lafont, D. Munao, and E. Kelder, "Electrospraying-assisted synthesis of tin nanoparticles for li-ion battery electrodes," *Journal of Power Sources*, vol. 189, no. 1, pp. 297–302, 2009.

[86] K. Chung, W. Yoon, K. Kim, B. Cho, and X. Yang, "Formation of an sei on a $limn-2o_4$ cathode during room temperature charge-discharge cycling studied by soft x-ray absorption spectroscopy at the fluorine k-edge," *Journal of Applied Electrochemistry*, vol. 41, pp. 1295–1299, 2011.

Chapter 6

Effects of chromium oxide coating on the performance of $LiNi_{0.5}Mn_{1.5}O_4$ thin films

El mejor método de educación es la felicidad

Héctor Abad Faciolince, *El olvido que seremos*, 2006

$LiNi_{0.5}Mn_{1.5}O_4$ (LNMO) is currently one of the most interesting doping variants of $LiMn_2O_4$ due to its high stability and capacity. Higher power applications, however, require higher charge- and discharge rates. Lithium transfer inside the particle has been shown to be a fast process and, instead, ionic and electronic transference from the electrolyte into the bulk seem to be the rate limiting factor. In this chapter we propose the synthesis of pure LNMO thin films, employing the approach presented in the previous chapter, followed by the application of surface modification in the form of a Cr_2O_3 catalytic coating. Electrostatic Spray Pyrolysis (ESP) was used as synthesis technique for both materials. Appropriate settings to spray the chromia coating were found to be using 2-propanol as solvent with a 0.1 M concentration of precursor salts in the precursor, a 2.0 cm nozzle-to-substrate distance at a substrate temperaure of 400 °C. The flow rate was set at 0.6 mL h^{-1} and a voltage window between

6.5-8.5 kV was tuned to find a stable cone-jet spray mode. Variation on the spray time was used in order to get various surface coverage. The materials and the films produced were characterized by SEM, EDX, XRD, TGA, and electrochemical measurements. Although the coating did not alter the initial spinel structure of LNMO, a one minute Cr_2O_3 deposition exhibits better rate capability compared to bare LNMO.

6.1 Introduction

The market in portable electronics has matured Li-ion technology during the last 20 years to place it above other energy storage options for small applications and, in the past few years, also larger scale applications such as energy storage devices for power tools, EV and HEVs, military and aerospace applications. Moreover, the downscaling in the microelectronics industry complicates the assembly from their individual components and demand for the reduction in volume of the energy storage unit. The stored energy content of a (Li ion) battery can be optimized by increasing the specific capacity ($mAhg^{-1}$ and/or $\mu Ah\ cm^{-2}$) of the cell, maximizing the potential difference between positive (cathode) and negative (anode) electrodes and by reducing the amount of inactive material. As it was discussed in the pervious chapter in detail, LNMO is a high voltage cathode material in lithium-ion batteries and is currently one of the most interesting doping variants of $LiMn_2O_4$ due to its high stability, capacity and its intrinsic rate capability offered by the 3-dimensional lithium ion diffusion in the spinel lattice [1, 2]. Moreover, the 4 V $LiMn_2O_4$ exhibits serious capacity fading during charge and discharge due to the presence of Mn^{3+} ions which cause (i) Jahn-Teller distortions [3, 4]; (ii) spinel dissolution into the electrolyte [5–7] and (iii) electrolyte decomposition at the high potential regions [8]. Some of these factors have been circumvented in different ways.

In LNMO the Jahn-Teller distortion is mostly suppressed due to the presence of the majority of Mn as Mn^{4+} and Ni as Ni^{2+}. Spinel dissolution and corrosion reactions with the electrolyte at high voltages have been tackled by coating the active particles with materials such as ZnO [9–12], Bi_2O_3 [12, 13] and Al_2O_3 [12], which provided a stable surface chemistry in contact with the electrolyte. Additionally, much effort has been made to partially substitute Mn and Ni by other transition metals such as Li, Mg, Al, Ti, Cr, Fe, Co, Cu, Zn, and Mo, in order to improve the cyclability [11, 14–21]. One of the accepted conclusions for this improved cyclability is due to the smaller lattice parameter difference among the different cubic phases formed during the charge-discharge process.

Apart from this, electrochemical testing under high rates, for both ordered and disordered structure of LNMO, has been studied for nano- [22] and micron-sized [23] particles. Results for particle sizes around 50 nm showed high rate capability (120 mAh g^{-1} at 20C and 100 mAh g^{-1} at 40C for disordered LNMO; 80 mAh g^{-1} at 20C and 50 mAh g^{-1} at 40C for ordered LNMO), while those for average particle size around 3.5 μm showed better rate capability than both ordered and disordered nano-LNMO. By adding 65 wt% carbon in the electrode, capacities of 107 mAh g^{-1} at 83C and 78mAh g^{-1} at 167C,

which belongs to a high Li^+ diffusivity of 3 μm in 10 seconds. The fact that around 100-times larger particle shows higher rate capability strongly indicates that ion or electron transport in the particle is not the rate-limiting process; instead the performance of the material is mainly obstructed by the lithium transfer properties from the electrolyte into the bulk and viceversa. Hence, the surface plays a crucial role in the kinetics and the answer must come, then, from the electrode/electrolyte interface.

Although some efforts have been made to improve the cyclability through surface modification (i.e. coating), mainly, as described above, to impede corrosion between the high voltage spinel cathode and the electrolyte, no direct study, to our knowledge, has been devoted to explore the usage of a catalyst coating to facilitate Li-ion transfer. While some of the implemented strategies such as doping (substitution of cations) or coating of the LNMO have resulted in improved rate capability by lowering the surface resistance and charge-transfer resistance, and by the suppression of the SEI layer formation by the presence of cations in the surface [12, 24], the essential role of a surface coating has not been clearly understood and no direct study has been performed regarding the comprehension on the nature of this surrounding layer, i.e. if a partial or a full coating is needed.

Chromium oxides have been widely studied due to their importance in industrial applications, which includes coating of materials for high temperature uses [25], wear resistance [26], magnetic recording applications [27] and, of particular interest for this study, for their catalytic behaviour in terms of e^--transfer and conduction [28–34]. Moreover, it has been used in battery applications where Chromia (III)-coated $LiMn_2O_4$ increased Mn^{4+} concentration at the surface and prevented the direct contact between the active particles and electrolyte, reducing the dissolution of manganese and the oxidation of the electrolyte [7].

It is important to mention that in the case of a stable electrolyte, it wouldn't be neccesary to cover completely the LNMO electrode with Cr_2O_3 as the dissolution of metallic species and the degradation of the electrolyte at high voltages wouldn't be an issue.

Various techniques have been used to deposit Cr_2O_3 coatings, including sputtering [35–40], magnetron sputtering [41], electron-beam evaporation [42, 43], chemical vapour deposition [44, 45], electrochemical deposition [46], and chemical spray pyrolysis [47], based on different applications. Various deposition methods result in different chromium oxide coatings microstructure, which controls their properties, so it is important to know the microstructure of specimens prepared by different deposition methods.

In this chapter we propose the synthesis of pure $LiNi_{0.5}Mn_{1.5}O_4$ thin films,

employing the approach presented in the previous chapter, followed by the application of surface modification in the form of Cr_2O_3 catalytic active sites, or 'islands'. An improvement in rate capability is, thus, expected. ESP is used as synthesis technique for both materials. The film morphology and structural characterization will be discussed and special attention will be given to the electrochemical performance.

6.2 Experimental

As described in Chapter 3.1.2, a schematic drawing of the equipment used for the production of the Cr_2O_3-coated LNMO spinel layers is shown in Figure 3.2.

The steps at which these layers were synthesized consisted first on the production of the LNMO (by using the formula described in paragraph 5.3.4 of the previous chapter, specifically in Figure 5.17) followed by the deposition of the chromium oxide-based coatings, using different spraying times so as to obtain different partial coverings. The precursor solutions for the cathode layers were prepared following the recipe discussed in section 5.2. For the chromium oxide post-depositions, different solutions were prepared by dissolving chromium nitrate nonahydrate, $Cr(NO_3)_3$ $.9H_2O$ (Acros Organics) in ethanol or in 2-propanol, at a molar concentration of 0.1 M. A syringe containing the precursor liquid was attached to a syringe pump (KD Scientific KDS120). The pump fed the precursor liquid through a rubber hose into a dispensing tip (EFD R Nordson) with inner diameter 0.25 mm. The solutions were fed to the electrified nozzle in order to undergo electrospraying and direct reaction so as to form thin film electrodes on stainless steel flat disks and on caps of CR2320 coin cell (Hohsen). Moreover, to continue the discussion started in the previous chapter, the deposition of the chromium based precursor was also performed on ESTARS silicon substrates with 3D architectured surfaces (STMicroelectronics). All the experiments were performed in air.

The texture, morphology, particle sizes and thickness of the films have been investigated using a Philips XL20 scanning electron microscope (SEM) operated at 15 kV and atomic force microscope measurements using a NT-MDT NTEGRA scanning probe microscope in semi-contact mode by a Si cantilever and tip (NT-MDT, Silicon: NSG 03). Composition and crystalline structure was studied by means of X-ray diffraction (XRD) using a Bruker (AXS D8 Advance) X-ray diffractometer with a Cu-K_α radiation source (α=1.5418 Å) and by energy dispersive x-ray spectroscopy (EDX) which was coupled to the SEM system and was measured directly after morphology studies. Thermogravimet-

ric analysis (TGA) of the chromia produced was performed on a Perkin-Elmer TGA7, heated up from 25 °C to 700 °C under nitrogen atmosphere with a temperature increase of 10 °C per minute, in order to measure the mass or change in mass, as well as the oxidation state. The electrochemical tests were performed using as cathode the Cr_2O_3-coated LNMO films (directly deposited on the CR2320 coin cell can and/or on ESTARS substrate), a polyethylene separator (Solupor), few drops of 1 M $LiPF_6$ in ethylene carbonate/ dimethyl carbonate (2:1) as electrolyte and metallic Li as anode. No additives (i.e. binders or conductivity enhancers) were used for the electrode preparation. The cells were assembled in an Ar filled glove box (coin cells in the case of flat electrodes and pouch cells in the case of the LAR-3D architectured electrodes). Galvanostatic measurements between 3.5 and 4.9 V were performed on a MACCOR S4000 cycler using different gravimetric current densities and C-rates.

6.3 Results and Discussion

Chromium oxide is usually obtained by the thermal decomposition of its salts and, therefore, this decomposition process constitutes a decisive step in its production. Thermal studies of Chromium(III) Nitrate Nonahydrate (CNN), supplemented by IR and chemical analyses in the temperature range 20-500 °C, have concluded that the decomposition occurs in six stages [48]. As the synthesis procedure shown in this chapter was based in these studies, it is relevant to briefly describe their conclusions.

From the steps mentioned before, already between 100-150 °C there is oxidation of Cr^{+3} to Cr^{+6} although the content of this oxidation state in the obtained layer is minimum. The composition percentage of Cr^{+3} starts becoming relevant at temperatures between 300-420 °C, where thermal decomposition of chromium chromate to Cr_2O_3 occurs, and Cr^{+3} values range from 50-96%. This decomposition happens according to equation:

$$2Cr_2\left(CrO_4\right)_3 \rightleftharpoons 5Cr_2O_3 + O_2 \tag{6.3.1}$$

This conversion from $Cr_2(CrO_4)_3$ to Cr_2O_3 may be also described in the form of a gradual reduction of CrO_3 content and, upon increasing temperature up to 390 °C, that compound begins to lose its stability undergoing a loss of its original weight due to released oxygen [49]. In the final stage, at temperatures above 420 °C, there is the formation of α-Cr_2O_3 with a composition percentage of Cr^{+3}>98%.

Following these conclusions, the precursor solution was thus sprayed for one hour at different temperatures ranging from 300 to 450 °C. Preliminary

experiments were first conducted using ethanol as solvent. The flow rate was kept constant at 0.6 mL h^{-1} and the voltage was tuned looking for a stable spraying mode. Simple inspection by eye of the resulting layers proofed them to have poor adhesion to the substrate. Figure 6.1 shows examples of the material sprayed at two particular temperatures, 300 and 350 °C. The delamination of those deposited at higher temperatures was even higher. This effect may be caused by the low evaporation temperature of the ethanol. As a result, the droplets dry up before arriving on the substrate, lowering their wettability and lose their possibility to properly spread and adhere to the substrate surface. Moreover, no stable spraying mode (cone jet or multi-cone jet) was obtained which means that the droplet and particle sizes were not homogeneous and, as discussed in chapter 3 and as shown in chapter 5, this hinders the growth of a uniform film. Therefore the usage of ethanol was discarded and 2-propanol was chosen instead as its boiling temperature is higher.

Analogous experiments were then performed with the precursor salts dis-

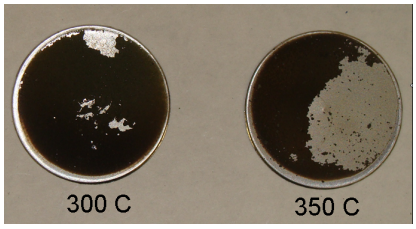

Figure 6.1 – As-deposited layers at different temperatures using ethanol as solvent

solved in 2-propanol, using the same parameters for temperature and flow rate mentioned above. A stable cone-jet mode was achieved in all the different samples at a voltage window between 6.5-8.5 kV. It is stressed again that the parameters in ESP are cross-related and each change may influence the electrohydrodynamic response of the system, see Chapters 2 and 5.

6.3.1 Morphology of Cr_2O_3 films

The texture and morphology of the as-sprayed materials have been investigated using SEM. Figure 6.2 shows different surface morphologies of chromia thin films deposited at different temperatures ranging from 300 to 450 °C using 2-propanol as solvent. As shown in Figure 6.2(a), the coating is cracked at 300 °C. This can be attributed to the stresses that have been developed during the

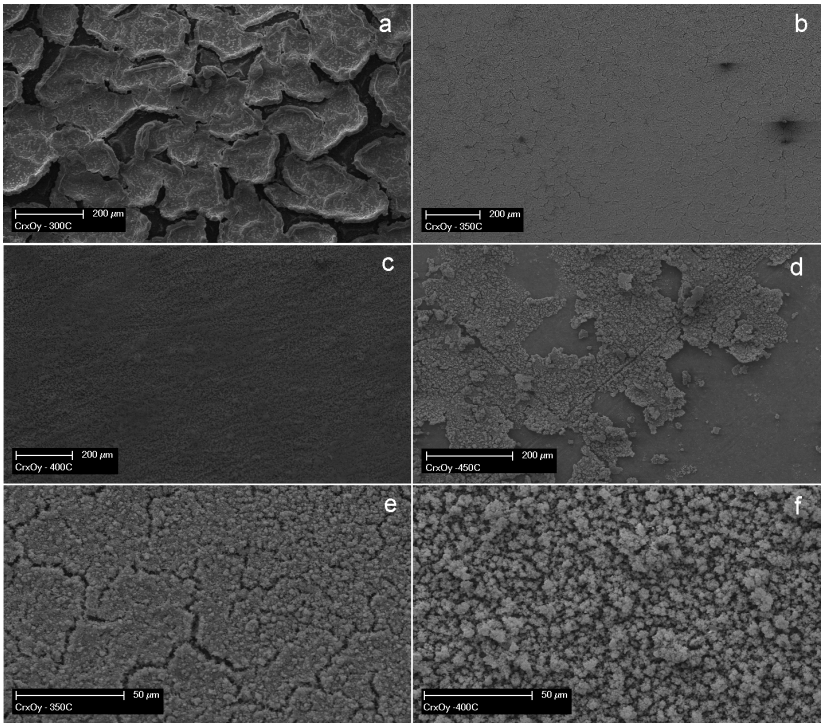

Figure 6.2 – SEM micrographs of the as-deposited layers using 2-propanol as solvent at different temperatures: (a) 300; (b, e) 350; (c, f) 400 and (d) 450 °C.

drying process of a large quantity of liquid on the substrate. Previous studies on $PbTiO_3$ [50] and zirconia [51] thin films fabricated with the same technique presented similar results and concluded that when the thickness of the film reaches a critical limitation, cracks will occur due to the accumulation of solvent on the surface of films deposited at lower temperatures. The crack formation mechanism was proposed by Chen et al. [52]. At too low substrate temperatures, the solvent evaporation is slow and too much of it remains within the film, but after its evaporation the cracks are formed due to mechanical stresses. In Figure 6.2(b) it can be observed that the film deposited at 350 °C still presents a dense bottom layer with some cracks (albeit smaller than those at 300 °C) covered by a reticular network of particles. In addition agglomerated particles are growing on top of this first layer (Figure 6.2e). When the temperature is increased to 400 °C (Figure 6.2c) a smooth layer with good adhesion to the substrate can be observed. The main point is that cracks have disappeared and some agglomerates are growing on top of a relatively dense layer (Figure 6.2f). At higher temperature the arriving droplets contain less solvent. Therefore, the drying step is more homogeneous and cracks disappear. The deposited particles agglomerate forming sponge-like structures that range in size between 200 nm and 2 μm. The individual particles are smaller as shown in chapters 4 and 5 for other electrosprayed materials such as Fe_2O_3 / CuO and $LiNi_{0.5}Mn_{1.5}O_4$, respectively. Samples sprayed at 450 °C (Figure 6.2d) presented poor adhesion to the substrate, similar to the samples where ethanol was used as solvent.

An interesting discussion is derived from the mathematical expression for the approximate voltage, V_{on}, needed to form a stable cone-jet, taken from the scaling laws [53]:

$$V_{on} \approx 2 \times 10^5 (\gamma r_c)^{1/2} ln(4d/r_c) \tag{6.3.2}$$

Where r_c is the inner radius of the capillary, γ is the surface tension of the liquid and d is the distance from nozzle to substrate.

With $\gamma = 20.9$ mN m^{-1} [54], $r_c = 0.00025$ m and $d = 0.02$ m, the theoretical minimum voltage to create a cone-spray would be around 8.3 kV, which lies very well between the voltage window used. It is emphasized that this calculation is a rough estimate of the voltage, since it is only based on the surface tension, nozzle diameter and distance to the substrate, and no measuring errors were taken into account. It is also possible that the dissolved precursor salts lower the surface tension of 2-propanol, leading to a lower applied voltage.

In conclusion, the optimized settings for the production of a thin coating of chromium oxide using the ESD method are: usage of 2-propanol as solvent with a 0.1 M concentration of precursor salts in the precursor; a 2.0 cm nozzle-to-substrate distance; 400 °C substrate temperature; a flow rate of 0.6 mL h^{-1}; and a voltage window between 6.5-8.5 kV.

6.3.2 Structure of Cr_2O_3 films

XRD was performed on samples synthesized under the similar conditions to those described before, but with a deposition time of 2 hours to increase thickness and to reduce background noise of the stainless steel substrate. The thin films obtained at 400 °C had a brown colour with a slight reddish hue, as can be observed in the inset of Figure 6.3. X-ray analysis shows that the film is amorphous (black pattern). Previous reports of chromium oxide films synthesised with spray pyrolysis at 420 °C on glass give similar results in terms of the colour of the layer. However, it is stated that reddish thin films are CrO_3, polycrystalline and orthorhombic in structure with no specific orientation. The fact that we did not see these results in our experiments may be due to the slight difference of the techniques used, and the difference in crystallographic orientation and thermal expansion coefficient of the substrates. Nevertheless, it has also been reported that polycrystalline phase of Cr_2O_3 is observed at substrate temperatures higher than 400 °C when employing sputtering as deposition technique [55]. Still, this temperature falls in the stage of thermal decomposition between 300-420 °C, mentioned in the previous paragraph, where chromium chromate is still present and the composition percentage of Cr^{+3} is not prevalent [48].

Annealing was thus performed for 1 hour at a temperature of 500 °C with a heating rate of 5°C per minute under air. In both cases, annealed and non-annealed, the thin films were quite uniform and hard. Figure 6.3 shows the XRD result of the produced layer (red pattern). The colour of the layer became greenish which is already a good indication for the formation of Cr_2O_3 (see inset in Figure 6.3). The obtained material has a crystalline Cr_2O_3 phase with a preferential growth on the 110 crystallographic plane. It further showed a rhombohedral structure belonging to the R-3c space group [56–58], which is similar to that of corundum (α-Al_2O_3), and is composed of a regular octahedral CrO_6 group. The Cr_2O_3 structure is approximately a hexagonal close packed array of Oxygen ions in which Cr^{3+} ions occupy two-thirds of the octahedral holes. The structure can be visualized more easily using a larger hexagonal unit cell [56].

Thermal gravimetric analysis of the non-annealed, amorphous chromium oxide is shown in Figure 6.4. As observed, the weight loss detected between 50 and 130 °C (3%) is attributed to the release of adsorbed water. Furthermore, from 300 to 430 °C there is a continuous loss of weight (18%) which can be associated with the decomposition of chromium chromate to chromium (III) oxide due to released oxygen. In fact, the mass of O_2 loss (0.536 mg) matches closely with that of the stoichiometric calculation (0.537 mg) suggested in equation

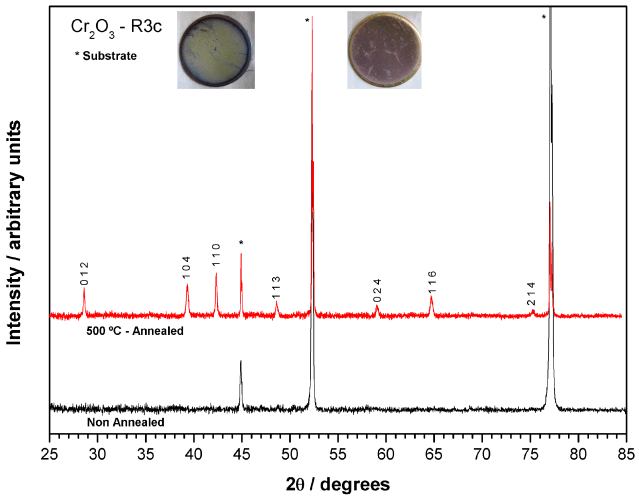

Figure 6.3 – XRD patterns of films synthesised by ESD at 400 °C (inset with pictures of the as-deposited materials). Black spectrum for the non-annealed sample (dark brown layer with reddish hue) and red pattern for the sample annealed at 500 °C (greenish layer). The peaks marked with asterisks belong to the support material.

6.3.1. The crystalline phase transition starts around 450 °C associated with no further weight loss. This is a higher temperature than previously reported for crystalline Cr_2O_3 nanoparticles synthesised by urea-methods [58, 59] and sonochemical techniques [56], but in close agreement with nanostructured thin films produced via spray pyrolysis [47] and RF-magnetron sputtering [55].

In conclusion, XRD and TGA analyses clearly show that the reaction at

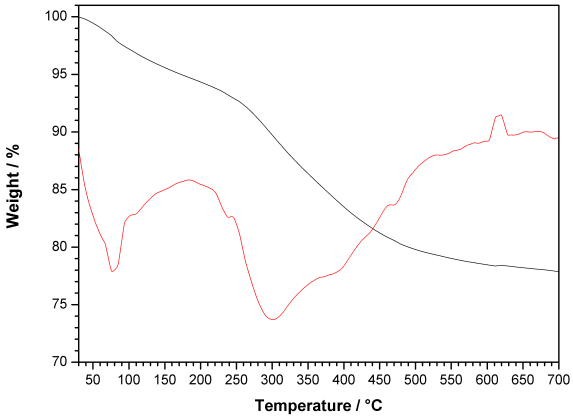

Figure 6.4 – Thermogravimetric analysis (and its derivative in red) obtained for the non-annealed sample synthesised at 400 °C

400 °C via the ESP method is not complete and an additional synthesis step is required to form the thermodynamically stable chromium (III) oxide by annealing the as-deposited film at 500 °C for 1 hour, so that the production of crystalline α-Cr_2O_3 is completed.

6.3.3 Cr_2O_3 coating on $LiNi_{0.5}Mn_{1.5}O_4$ thin films

The high voltage spinel layers were produced utilising the recipe described in paragraph 5.3.4. For the partial covering of these films, Cr_2O_3 'islands' were then deposited using different spraying times, specifically 1, 5 and 10 minutes. The spray parameters used were those defined in paragraphs 6.3.1 and 6.3.2, namely: 2-propanol based precursor with a 0.1 M concentration; 2.0 cm nozzle-to-substrate distance; 0.6 mL h^{-1} flow rate; 6.5-8.5 kV applied voltage; 400 °C substrate temperature; post-annealing at 500 °C for 1 hour in air.

Figure 6.5 shows SEM micrographs of the resulting samples. The sponge-

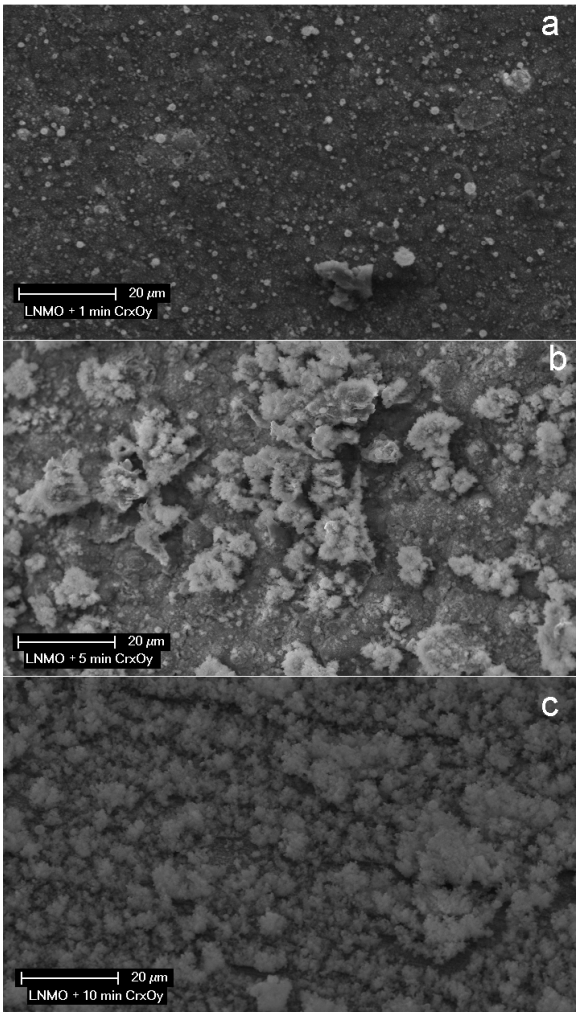

Figure 6.5 – SEM images of $LiNi_{0.5}Mn_{1.5}O_4$ films (dense background) with a Cr_2O_3 coatings (sponge-like on top) at different deposition times: (a)1 minute; (b) 5 minutes; and (c) 10 minutes

like nature of the Cr_2O_3 deposits can be observed over the flat and dense LNMO layer. When the spray time is augmented there is a clear increase in the size of the chromium oxide agglomerates, as well as on the density per area unit. In fact, after 10 minutes of spray time (Figure 6.5c) there is almost full coverage of the LNMO layer.

XRD analyses of the samples before and after coating, shown in Figure 6.6,

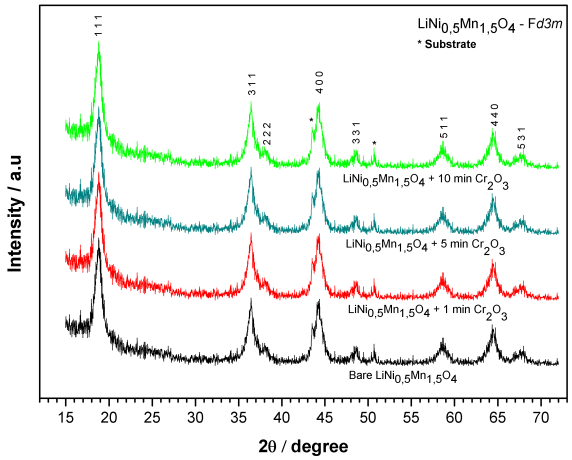

Figure 6.6 – XRD patterns of the non-coated and Cr_2O_3 partially-coated $LiNi_{0.5}Mn_{1.5}O_4$

exhibit reflection characteristics only of the LNMO cubic spinel structure for all samples, indicating that there is no coating at all, that it is amorphous or that the surface modification does not change the crystallographic structure of the initial cathode. Similar results have been observed for the latter case in previous studies where $LiNi_{0.42}Mn_{1.5}Zn_{0.08}O_4$ was coated with Al_2O_3, ZnO and Bi_2O_3 [12].

In order to confirm the presence of the coating, SEM coupled with EDX elemental mapping was performed. Figure 6.7 presents images of the Cr_2O_3-coated LNMO. The sample shows a homogeneous distribution of chromium throughout the surface of the LNMO film. This homogenous distibuted Cr then, did not indicate any individual particle with an increased amount of Cr. Clearly, Mn and Ni are well distributed all through the surface.

A recent study was performed by our group on Cr-coated and Cr-doped LNMO powders [60] comprising the analysis of the electrochemical behaviour

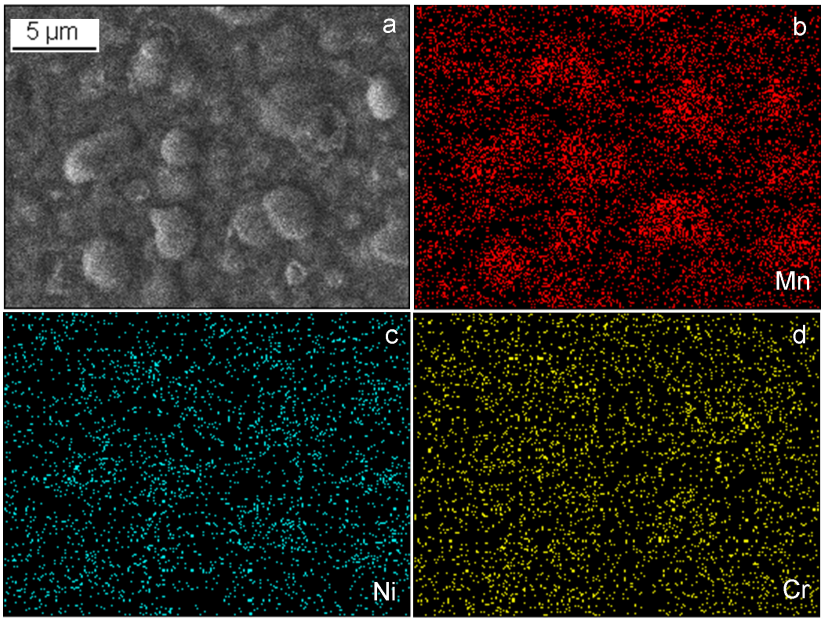

Figure 6.7 – (a) SEM image and corresponding EDX elemental mappings of (b) Mn, (c) Ni, and (d) Cr for the 1 min Cr_2O_3-coated $LiNi_{0.5}Mn_{1.5}O_4$

during charge and discharge while in-situ monitoring the change of the oxidation states of the various transition metal ions, the electronic structure and the local symmetry via X-Ray Absorption Spectroscopy (XAS). Cr K-edge X-ray Absorption Near Edge Structure (XANES) and O K-edge XANES were measured at the BM26 (DUBBLE) EXAFS beamline at the European Synchrotron Radiation Facility (ESRF) in Grenoble, France. It was found that the edge energy in the XANES region is the same for both the corundum and the surface modified LNMO spinel. To recall, the Cr_2O_3 coating was achieved by dip-coating the LNMO powders in a solution of chromium nitrate and annealing at 600 °C for 8 h. This means that, in all cases, chromium remains in a valence state of +3 throughout the electrochemical process. Furthermore, the EXAFS range clearly shows a difference in the environments for the Cr^{3+} ion in a corundum structure of the obtained coating. Actually, the Cr^{3+} ion environment for the coating is the same as for the Cr^{3+} in the LNMO, indicating that the Cr^{3+}-ion is in a spinel type structure. Hence, these observations in the XANES and the EXAFS regions, suggest that the chromium oxide forms a spinel structure, where the oxygen anions are arranged in a cubic close-packed lattice and the Cr cations occupy the octahedral sites in the lattice. Therefore it is concluded that there is an epitaxial growth of the Cr_2O_3 on the surface adopting the spinel structure of the underlying material, favouring the formation of this unusual phase.

6.3.4 Electrochemical behaviour

The various samples have been assembled in coin cells for electrochemical characterization. The so-called half-cells consisted thus of Cr_2O_3-coated $LiNi_{0.5}Mn_{1.5}O_4$ material directly deposited on CR2330-type coin cell caps with lithium metal as counter electrode and commercial liquid electrolyte. Neither conductive additive nor binder was included in the electrode preparation. A 1.5 cm^{-2} deposition area was selected by using a mask. The difference between cells consisted only in the amount of Cr_2O_3 present due to the variation in spray times, i.e. 1, 5 and 10 minutes.

Figure 6.8 compares the discharge profiles of LNMO at the highest discharge capacity value before and after surface modification with Cr_2O_3. These galvanostatic tests do not exhibit a well-defined plateau, analogous to what was described in chapter 5, most likely due to the presence of amorphous [61] or nano [62] domains. Thus, these pseudo plateaus -from now on, it will be referred to them simply as 'plateaus'- are indeed related to the reversible oxidation reduction of Ni and Mn species combined with the presence of nanosized active domains and the presence of a poorly crystalline structure. All profiles

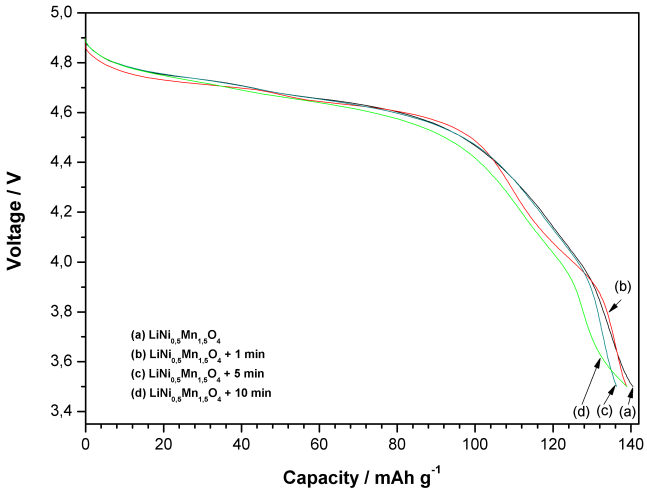

Figure 6.8 – Discharge curves of $LiNi_{0.5}Mn_{1.5}O_4$ before and after coating with Cr_2O_3. Discharge current density: 195 mA g^{-1}

exhibit three discharge plateaus. While the two plateaus at 4.7 V are due to the reduction of Ni^{4+} to Ni^{2+}, that at 4.0 V results from the reduction of Mn^{4+} to Mn^{3+}. It is interesting to note that the capacity value in all samples is practically the same. Moreover, the capacity of the 4 V plateau must basically be the same for all samples as the underlying LNMO layer is made in the same way. Although this might not be immediately seen as a result of the different kinetics of the samples. This actually is the main reason for coating the layer with Cr_2O_3, hence, to modify the charge transfer kinetics. In the case of the one-minute coating, a pronounced 4 V plateau becomes obvious, showing the improved kinetics, meaning charge transfer.

The obtained capacity depends basically on the internal resistance of the cell, including the coating. As the surface of the LNMO contains larger amounts of chromium, the obtained capacity decreases due to the thicker Cr_2O_3 insulating coating.

Figure 6.9 exhibits continuous discharge curves of the bare- and partially-coated $LiNi_{0.5}Mn_{1.5}O_4$/Li cells by applying different current densities (1C=195 mA g^{-1}) between 3.5 and 4.9 V versus Li. The cells were charged galvanostatically with 0.1 C, and then discharged at different C rates. To illustrate the rate capability, the discharge capacity values at various C rates are normalized to

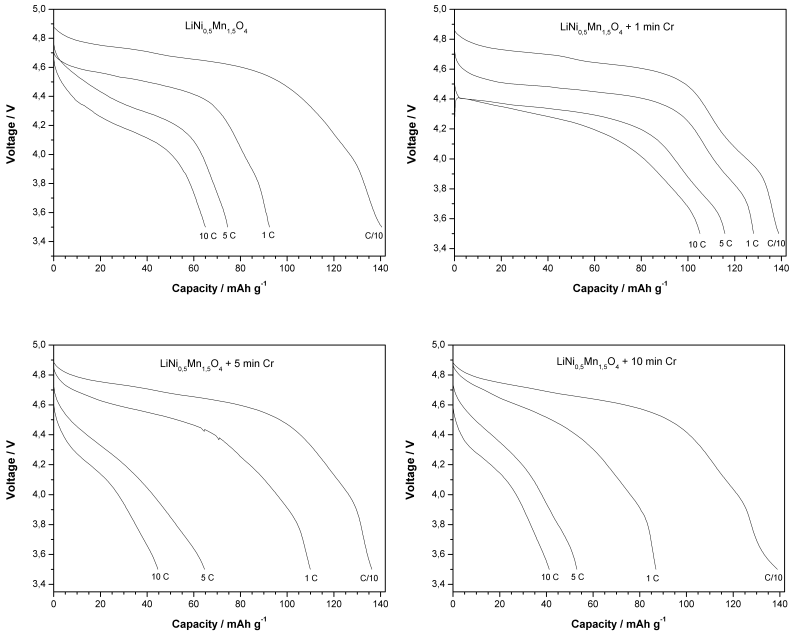

Figure 6.9 – Rate capability of Cr_2O_3 partial-coated and bare $LiNi_{0.5}Mn_{1.5}O_4$

the discharge capacity value at C/10 rate and plotted in Figure 6.10. Clearly, the one minute-spray-time sample delivers higher capacity at all currents than the pristine cathode and those sprayed for longer times.

Liu et. al. [12], performed surface modification of $LiNi_{0.42}Mn_{1.5}Zn_{0.08}O_4$

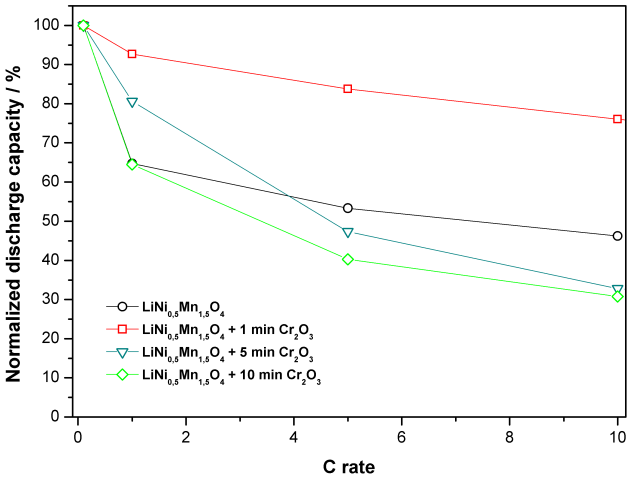

Figure 6.10 – Normalized discharge capacity values of $LiNi_{0.5}Mn_{1.5}O_4$ samples before and after surface modification at various C rates

by using Al_2O_3, ZnO and Bi_2O_3 as coatings and, after similar electrochemical analyses, demonstrated an increase in rate capability as well as rate capability retention for all cases. They suggest that the enhanced performance is due to a significant reduction on the surface-layer resistance and the charge-transfer resistance. The increase in charge transfer resistance upon cycling is related to the development of a less conductive SEI layer on the cathode surface. Normally, surface oxide coating would degrade the kinetics of the charge transfer reaction by partially blocking the surface of the material. However, they concluded, the improved charge transfer kinetics of the coated cathodes is partly due to the effective suppression of the SEI film growth on the cathode surface by the coating oxides. Al_2O_3 coating showed the best performance most likely due its stable surface chemistry suppressing or giving optimum SEI layers and to its porous structure facilitating the lithium-ion diffusion.

As to the influence of all the above presented results on the improved electrochemical behaviour of the Cr_2O_3-coated LNMO, in terms of faster ionic

and electronic transport on the interface, it is well known that the isotropic structure of spinel LNMO provides a 3D network for lithium-ion diffusion and, hence, this material is suitable for fast lithium insertion and de-insertion reactions [63–66]. Therefore an epitaxial growth of a Cr_2O_3 coating that adopts the spinel structure of the underlying cathode would act as a catalyst for electrochemical processes occurring at the interface [60] while, at the same time, as it is inactive towards the organic species in the electrolyte, it hinders the formation of an SEI layer improving the ionic exchange from the electrolyte into the active material. Nevertheless, an optimum amount of Cr_2O_3 surface modification must be present as a good relation is needed between its catalytic activity (while, at the same time, helps at suppressing SEI layer formation) and its insulating nature. Finally, a clear picture on the one minute partially

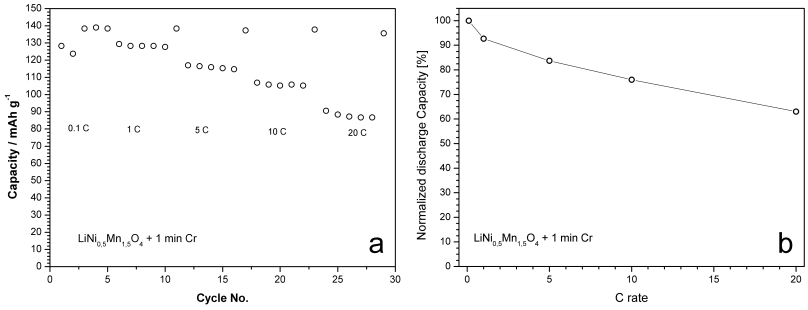

Figure 6.11 – Rate capability and rate capability retention of 1 min Cr_2O_3 partial-coated $LiNi_{0.5}Mn_{1.5}O_4$. 1C=195 mA g^{-1}

coated LNMO is shown in Figure 6.11. This sample delivers a capacity 140 mAh g^{-1} with a capacity retention of 98% in 30 cycles (Figure 6.11a) even after subjecting it at high rates. Moreover, it presents rate capability retention of 80% at 10C and 70% at 20C, as shown in Figure 6.11(b).

6.4 Conclusions

Electrostatic spray pyrolysis technique has been used to modify the surface of the spinel cathode LNMO via coatings of Cr_2O_3. By tuning the spray time, the covering of the underlying LNMO could be controlled and already after 10 minutes it presented almost full coverage of the cathode layer.

The structure of the samples before and after coating exhibit reflection

characteristics only of the LNMO cubic spinel structure for all samples, indicating that the surface modification does not change the crystallographic structure of the initial cathode. However, Cr_2O_3 seems to be present homogeneously throughout the surface of the cathode film, as suggested by elemental mapping, instead of the active sites initially intended. XRD and EDS results, together with XAS information from similar experiments, suggest the formation of an epitaxial Cr_2O_3 spinel type coating.

As this coating seems to be homogeneous, it opens the possibility of using LNMO-based cathodes with such modified surface together with conventional electrolyte.

The above mentioned surface modifications influence the electrochemical behaviour of the bare spinel cathode. Especially, the coating sprayed for 1 minute improves the rate capability and delivers a capacity of 140 mAh g^{-1} at C/10 rate and remarkably high capacities of 108 mAh g^{-1} at 10C and 90 mAh g^{-1} at 20C. The epitaxial growth of a Cr_2O_3 coating, that takes the spinel structure of the underlying cathode, act as a catalyst for electrochemical processes occurring at the interface while, at the same time, as it is inactive towards the organic species in the electrolyte, it hinders the formation of an SEI layer improving the ionic exchange from the electrolyte into the active material enhancing the battery performance. Nevertheless, an optimum amount of Cr_2O_3 surface modification must be present as a good relation is needed between its catalytic activity (while, at the same time, helps at suppressing SEI layer formation) and its insulating nature.

References

[1] K. Amine, H. Tukamoto, H. Yasuda, and Y. Fujita, "Preparation and electrochemical investigation of $LiMn_{2-x}Me_xO_4$ (Me: Ni, Fe, and x = 0.5, 1) cathode materials for secondary lithium batteries," *Journal of Power Sources*, vol. 68, no. 2, pp. 604–608, 1997.

[2] Q. Zhong, A. Bonakdarpour, M. Zhang, Y. Gao, and J. R. Dahn, "Synthesis and Electrochemistry of $LiNi_xMn_{2-x}O_4$," *Journal of the Electrochemical Society*, vol. 144, no. 1, pp. 205–213, 1997.

[3] R. Gummow, A. de Kock, and M. Thackeray, "Improved capacity retention in rechargeable 4 V lithium/lithium-manganese oxide (spinel) cells," *Solid State Ionics*, vol. 69, no. 1, pp. 59–67, 1994.

[4] M. Thackeray, Y. Shao-Horn, A. Kahaian, K. Kepler, E. Skinner, J. Vaughey, and S. Hackney, "Structural Fatigue in Spinel Electrodes in High Voltage (4 V) $Li/Li_xMn_2O_4$ Cells," *Electrochemical and Solid State Letters*, vol. 1, no. 1, pp. 7–9, 1998.

[5] D. Jang and S. Oh, "Effects of carbon additives on spinel dissolution and capacity losses in 4 V $Li/Li_xMn_2O_4$ rechargeable cells," *Electrochimica Acta*, vol. 43, no. 9, pp. 1023–1029, 1998.

[6] T. Aoshima, K. Okahara, C. Kiyohara, and K. Shizuka, "Mechanisms of manganese spinels dissolution and capacity fade at high temperature," *Journal of Power Sources*, vol. 97-98, pp. 377–380, 2001.

[7] H. Sahan, H. Goktepe, S. Patat, and A. Ulgen, "Effect of the Cr_2O_3 coating on electrochemical properties of spinel $LiMn_2O_4$ as a cathode material

for lithium battery applications," *Solid State Ionics*, vol. 181, no. 31-32, pp. 1437–1444, 2010.

[8] Y. Gao and J. R. Dahn, "Correlation between the growth of the 3.3 V discharge plateau and capacity fading in $Li_{1+x}Mn_{2-x}O_4$ materials," *Solid State Ionics*, vol. 84, no. 1-2, pp. 33–40, 1996.

[9] Y. Sun, K. Hong, J. Prakash, and K. Amine, "Electrochemical performance of nano-sized ZnO-coated $LiNi_{0.5}Mn_{1.5}O_4$ spinel as 5 V materials at elevated temperatures," *Journal of Power Sources*, vol. 4, no. 4, pp. 344–348, 2002.

[10] Y. Sun, C. Yoon, and I. Oh, "Surface structural change of ZnO-coated $LiNi_{0.5}Mn_{1.5}O_4$ spinel as 5 V cathode materials at elevated temperatures," *Electrochimica Acta*, vol. 48, no. 5, pp. 503–506, 2003.

[11] R. Alcantara, M. Jaraba, P. Lavela, and J. Tirado, "X-ray diffraction and electrochemical impedance spectroscopy study of zinc coated $LiNi_{0.5}Mn_{1.5}O_4$ electrodes," *Journal of Electroanalytical Chemistry*, vol. 566, no. 1, pp. 187–192, 2004.

[12] J. Liu and A. Manthiram, "Improved Electrochemical Performance of the 5 V Spinel Cathode $LiMn_{1.5}Ni_{0.42}Zn_{0.08}O_4$ by Surface Modification," *Journal of the Electrochemical Society*, vol. 156, no. 1, pp. A66–A72, 2009.

[13] T. Noguchi, I. Yamazaki, T. Numata, and M. Shirakata, "Effect of Bi oxide surface treatment on 5 V spinel $LiNi_{0.5}Mn_{1.5-x}Ti_xO_4$," *Journal of Power Sources*, vol. 174, no. 2, pp. 359–365, 2007.

[14] T. Arunkumar and A. Manthiram, "Influence of Lattice Parameter Differences on the Electrochemical Performance of the 5 V Spinel $LiMn_{1.5-y}Ni_{0.5-z}M_{y+z}O_4$(M = Li, Mg, Fe, Co, and Zn)," *Electrochemical and Solid-State Letters*, vol. 8, no. 8, pp. A403–A405, 2005.

[15] T. Arunkumar and A. Manthiram, "Influence of chromium doping on the electrochemical performance of the 5 V spinel cathode $LiMn_{1.5}Ni_{0.5}O_4$," *Electrochimica Acta*, vol. 50, no. 28, pp. 5568–5572, 2005.

[16] F. Ooms, E. Kelder, J. Schoonman, M. Wagemaker, and F. Mulder, "High-voltage $LiMg_\delta Ni_{0.5-\delta}Mn_{1.5}O_4$ spinels for Li-ion batteries," *Solid State Ionics*, vol. 152-153, pp. 143–153, 2002.

[17] K. Hong and Y. Su, "Synthesis and electrochemical characteristics of $LiCr_xNi_{0.5-x}Mn_{1.5}O_4$ spinel as 5 V cathode materials for lithium secondary batteries," *Journal of Power Sources*, vol. 109, no. 2, pp. 427–430, 2002.

[18] R. Alcantara, M. Jaraba, P. Lavela, and J. Tirado, "Structural and Electrochemical Study of New $LiNi_{0.5}Ti_xMn_{1.5-x}O_4$ Spinel Oxides for 5-V Cathode Materials," *Chemistry of Materials*, vol. 15, no. 12, pp. 2376–2382, 2003.

[19] G.-K. Fey, C.-Z. Lu, and T. Kumar, "Preparation and electrochemical properties of high-voltage cathode materials, $LiM_yNi_{0.5-y}Mn_{1.5}O_4$ (M=Fe, Cu, Al, Mg; y=0.0-0.4)," *Journal of power Sources*, vol. 115, no. 2, pp. 332–345, 2003.

[20] S.-H. Park, S.-W. Oh, S.-T. Myung, and Y.-K. Sun, "Mo^{6+}-Doped $Li[Ni(0.5+x)Mn_{(1.5-2x)}Mo_x]O_4$ Spinel Materials for 5 V Lithium Secondary Batteries Prepared by Ultrasonic Spray Pyrolysis," *Electrochemical and Solid State Letters*, vol. 7, no. 11, pp. A451–A454, 2004.

[21] J. Kim, S.-T. Myung, C. Yoon, S.-W. Oh, and Y.-K. Sun, "Effect of Ti Substitution for Mn on the Structure of $LiNi_{0.5}Mn_{1.5-x}Ti_xO_4$ and Their Electrochemical Properties as Lithium Insertion Material," *Journal of the Electrochemical Society*, vol. 151, no. 11, pp. A1911–A1918, 2004.

[22] K. Shajua and P. Bruce, "Nano-$LiNi_{0.5}Mn_{1.5}O_4$ spinel: a high power electrode for Li-ion batteries," *Dalton Transactions*, pp. 5471–5475, 2008.

[23] X. Ma, B. Kang, and G. Ceder, "High Rate Micron-Sized Ordered $LiNi_{0.5}Mn_{1.5}O_4$," *Journal of the Electrochemical Society*, vol. 157, no. 8, pp. A925–A931, 2010.

[24] J. Liu and A. Manthiram, "Understanding the Improved Electrochemical Performances of Fe-Substituted 5 V Spinel Cathode $LiMn_{1.5}Ni_{0.5}O_4$," *Journal of Physical Chemistry C*, vol. 113, no. 33, pp. 15073–15079, 2009.

[25] P. Berdahl, "Pigments to Reflect the Infrared Radiation From Fire," *Journal of Heat Transfer*, vol. 117, no. 2, pp. 355–358, 1995.

[26] H. Kitsunai, K. Hokkirigawa, N. Tsumaki, and K. Kato, "Transitions of microscopic wear mechanism for Cr_2O_3 ceramic coatings during repeated sliding observed in a scanning electron microscope tribosystem," *Wear*, vol. 151, no. 2, pp. 279–289, 1991.

[27] B. Bhushana, G. Theunissen, and X. Li, "Tribological studies of chromium oxide films for magnetic recording applications," *Thin Solid Films*, vol. 311, no. 1-2, pp. 67–80, 1997.

[28] B. Weckhuysen and R. Schoonheydt, "Olefin polymerization over supported chromium oxide catalysts," *Catalysis Today*, vol. 51, no. 2, pp. 215–221, 1999.

[29] R. Spitz, "Supported chromium oxide catalysts for olefin polymerization: IX. The nature of the narrow γ-phase ESR signal and its correlation with catalytic activity," *Journal of Catalysis*, vol. 35, no. 3, pp. 342–352, 1974.

[30] K. Miesserov, "Nature of active sites of supported chromic oxide polymerization catalysts," *Journal of Catalysis*, vol. 22, no. 3, pp. 340–346, 1971.

[31] S. De Rossi, M. Casaletto, G. Ferraris, A. Cimino, and G. Minelli, "Chromia/zirconia catalysts with Cr content exceeding the monolayer. A comparison with chromia/alumina and chromia/silica for isobutane dehydrogenation," *Applied Catalysis A: General*, vol. 167, no. 2, pp. 257–270, 1998.

[32] D. Myers and J. Lunsford, "Silica-supported chromium catalysts for ethylene polymerization: The active oxidation states of chromium," *Journal of Catalysis*, vol. 99, no. 1, pp. 140–148, 1986.

[33] B. Abu-Zied, "Structural and catalytic activity studies of silver/chromia catalysts," *Applied Catalysis A: General*, vol. 198, no. 1-2, pp. 139–153, 2000.

[34] S. Wang, K. Murata, T. Hayakawa, S. Hamakawa, and K. Suzuki, "Dehydrogenation of ethane with carbon dioxide over supported chromium oxide catalysts," *Applied Catalysis A: General*, vol. 196, no. 1, pp. 1–8, 2000.

[35] U. Rothhaar and H. Oechsner, "Temperature induced dissolution of Cr_2O_3 into polycrystalline tantalum," *Thin Solid Films*, vol. 302, no. 1-2, pp. 266–269, 1997.

[36] P. Hones, M. Diserens, and F. Levy, "Characterization of sputter-deposited chromium oxide thin films," *Surface and Coatings Technology*, vol. 120-121, pp. 277–283, 1999.

[37] F. Lai, C. Huang, C. Chang, L. Wang, and W. Cheng, "Ultra-thin Cr_2O_3 well-crystallized films for high transmittance APSM in ArF line," *Microelectronic Engineering*, vol. 67-68, pp. 17–23, 2003.

[38] G. Goodlet, S. Faty, S. Cardoso, P. Freitas, A. Simoes, M. Ferreira, and M. Da Cunha Belo, "The electronic properties of sputtered chromium and iron oxide films," *Corrosion Science*, vol. 46, no. 6, pp. 1479–1499, 2004.

[39] S. Hong, E. Kim, D.-W. Kim, T.-H. Sung, and K. No, "On measurement of optical band gap of chromium oxide films containing both amorphous and crystalline phases," *Corrosion Science*, vol. 221, no. 2-3, pp. 245–254, 1997.

[40] D. Gall, R. Gampp, H. Lang, and P. Oelhafen, "Pulsed plasma deposition of chromium oxide/chromium-cermet coatings," *Journal of Vacuum Science and Technology A*, vol. 14, no. 2, pp. 374–379, 1996.

[41] X. Pang, K. Gao, F. Luo, Y. Emirov, A. Levin, and A. Volinsky, "Investigation of microstructure and mechanical properties of multi-layer Cr/Cr_2O_3 coatings," *Thin Solid Films*, vol. 517, no. 6, pp. 1922–1927, 2009.

[42] J. Kruschwitz and W. Pawlewicz, "Optical and durability properties of infrared transmitting thin films," *Applied Optics*, vol. 36, no. 10, pp. 2157–2159, 1997.

[43] T. Seike and J. Nagai, "Electrochromism of 3d transition metal oxides," *Solar Energy Materials*, vol. 22, no. 2-3, pp. 107–117, 1991.

[44] J. Nable, S. Suib, and F. Galasso, "Metal organic chemical vapor deposition of Al_2O_3 and Cr_2O_3 on nickel as oxidation barriers," *Surface and Coatings Technology*, vol. 186, no. 3, pp. 423–430, 2004.

[45] V. M. Bermudez and W. J. DeSisto, "Study of chromium oxide film growth by chemical vapor deposition using infrared reflection absorption spectroscopy," *Surface and Coatings Technology*, vol. 19, no. 2, pp. 576–583, 2001.

[46] C. Sunseri, S. Piazza, and F. Di Quarto, "Photocurrent Spectroscopic Investigations of Passive Films on Chromium," *Journal of the Electrochemical Society*, vol. 137, no. 8, pp. 2411–2417, 1990.

[47] R. Misho, W. Murad, and G. Fattahallah, "Preparation and optical properties of thin films of CrO_3 and Cr_2O_3 prepared by the method of chemical spray pyrolysis," *Journal of Materials Science*, vol. 169, no. 2, pp. 235–239, 1989.

[48] L. Gubrynowicz and T. Strömich, "Study on the thermal decomposition of chromium(III) nitrate nonahydrate (CNN)," *Thermochimica Acta*, vol. 115, pp. 137–151, 1987.

[49] I.-H. Park, "Thermal Decomposition of Ammonium Salts of Transition Metal Oxyacids. III. Thermogravimetric Analysis of Ammonium Chromate," *Bulletin of the Chemical Society of Japan*, vol. 45, no. 9, pp. 2749–2752, 1972.

[50] H. Huang, X. Yao, X. Wu, M. Wang, and L. Zhang, "Ferroelectric $PbTiO_3$ thin films prepared by electrostatic spray deposition (ESD)," *Microelectronic Engineering*, vol. 66, no. 1-4, pp. 688–694, 2003.

[51] T. Nguyen and E. Djurado, "Deposition and characterization of nanocrystalline tetragonal zirconia films using electrostatic spray deposition," *Solid State Ionics*, vol. 138, no. 3-4, pp. 191–197, 2001.

[52] C. Chen, E. Kelder, M. Jak, and J. Schoonman, "Electrostatic spray deposition of thin layers of cathode materials for lithium battery," *Solid State Ionics*, vol. 86-88, no. 2, pp. 1301–1306, 1996.

[53] M. Ikonomou, A. Blades, and P. Kebarle, "Electrospray-ion spray: a comparison of mechanisms and performance," *Analytical Chemistry*, vol. 66, no. 18, pp. 1989–1998, 1991.

[54] B. Hoke Jr and J. Chen, "Binary aqueous-organic surface tension temperature dependence," *Journal of Chemical and Engineering Data*, vol. 36, no. 3, pp. 322–326, 1991.

[55] P. Qin, G. Fang, N. Sun, X. Fan, Q. Zheng, F. Chen, J. Wan, and X. Zhao, "Organic solar cells with p-type amorphous chromium oxide thin film as hole-transporting layer," *Thin Solid Films*, vol. 519, no. 13, pp. 322–326, 2011.

[56] N. Arul Dhas, Y. Koltypin, and A. Gedanken, "Sonochemical Preparation and Characterization of Ultrafine Chromium Oxide and Manganese Oxide Powders," *Chemistry of Materials*, vol. 9, no. 12, pp. 3159–3163, 1997.

[57] M. Banobre-Lopez, C. Vazquez-Vazquez, J. Rivas, and M. Lopez-Quintela, "Magnetic properties of chromium (III) oxide nanoparticles," *Nanotechnology*, vol. 14, no. 12, p. 318, 2003.

[58] H. Gulley-Stahl, W. Schmidt, and H. Bullen, "Characterization and reactivity of chromia nanoparticles prepared by urea forced hydrolysis," *Journal of Materials Science*, vol. 43, no. 22, pp. 7066–7072, 2008.

[59] M. Ocana, "Nanosized Cr_2O_3 hydrate spherical particles prepared by the urea method," *Journal of the European Ceramic Society*, vol. 21, no. 7, pp. 931–939, 2001.

[60] R. Fredon, A. Brownrigg, E. Kelder, M. Alfredsson, and A. Chadwick, "In Situ X-Ray Absorption Spectroscopy of Cr-doped $LiNi_{0.5}Mn_{1.5}O_4$ and Cr_2O_3-coated $LiNi_{0.5}Mn_{1.5}O_4$," *Submitted to Journal of Power Sources*, 2013.

[61] W. Borghols, D. Lützenkirchen-Hecht, U. Haake, W. Chan, U. Lafont, E. Kelder, E. van Eck, A. Kentgens, F. Mulder, and M. Wagemaker, "Lithium Storage in Amorphous TiO_2 Nanoparticles," *Journal of The Electrochemical Society*, vol. 157, no. 5, pp. A582–A588, 2010.

[62] U. Lafont, D. Carta, G. Mountjoy, A. Chadwick, and E. Kelder, "In Situ Structural Changes upon Electrochemical Lithium Insertion in Nanosized Anatase TiO_2," *The Journal of Physical Chemistry C*, vol. 114, no. 2, pp. 1372–1378, 2010.

[63] B. Hwang, R. Santhanam, and S. Hu, "Synthesis and characterization of multidoped lithium manganese oxide spinel, $Li_{1.02}Co_{0.1}Ni_{0.1}Mn_{1.8}O_4$, for rechargeable lithium batteries," *Journal of Power Sources*, vol. 108, no. 1-2, pp. 250–255, 2002.

[64] T. Ohzuku, M. Kitagawa, and T. Hira, "Electrochemistry of Manganese Dioxide in Lithium Nonaqueous Cell III. X-Ray Diffractional Study on the Reduction of Spinel-Related Manganese Dioxide," *Journal of The Electrochemical Society*, vol. 137, no. 3, pp. 769–775, 1990.

[65] S. Kobayashi, I. Kottegoda, Y. Uchimoto, and M. Wakihara, "XANES and EXAFS analysis of nano-size manganese dioxide as a cathode material for lithium-ion batteries," *Journal of Materials Chemistry*, vol. 14, no. 12, pp. 1843–1848, 2004.

[66] F. Shokoohi, J. Tarascon, and B. Wilkens, "Fabrication of thin-film $LiMn_2O_4$ cathodes for rechargeable microbatteries," *Applied Physics Letters*, vol. 59, no. 10, pp. 1260–1263, 1991.

Chapter 7

Modification of an Atomic Force Microscope for in-situ electrochemical characterization of Lithium-ion batteries

So long, and thanks for all the fish

Douglas Adams, *The Hitchhiker's Guide to the Galaxy*, 1979

$LiNi_{0.5}Mn_{1.5}O_4$ (LNMO) material is a cheap, non-toxic, high voltage alternative to the cathode material presently used. However, LNMO electrodes show poor capacity retention at high charging rates. In order to improve the power performance, surface modification via a catalytic partial coating, i.e. chromia, can be used to increase the rate of lithium (de)intercalation at the interface, as thoroughly described in Chapter 6.

The (de)intercalation at the electrode and coating are processes at the nanometre scale, and would preferably be imaged at this level. Atomic Force

Microscope (AFM) can image topography at the nanometre scale, and may, theoretically, be modified to measure ion transport at this range. In this chapter a brief description of some preliminary results will be given. In summary, the project consists on the development of a modified AFM that allows in-situ characterisation of lithium ion transfer at/from an electrode surface (i.e. LNMO).

For this purpose, the AFM probe will be used as electrode, i.e. a silicon probe is electrochemically (de)lithiated. The experimental setup consists of an electrochemical cell in which the probe can be mounted, and which can be attached to the AFM. Electrochemical experiments were performed using an external bipotentiostat. Most of the initial experiments were aimed at learning the electrochemical behaviour of the probe in the setup, with metallic lithium as counter electrode. These experiments were carried out under controlled argon atmosphere, and probes were later analyzed using Scanning Electron Microscopy (SEM). Next to this, LNMO samples with a Cr_2O_3 partial coating were topographically scanned in the AFM, at different conditions.

Preliminary results achieved include the possibility to control a two-electrode setup consisting of a silicon probe vs. metallic lithium in an electrochemical AFM cell; topographical scans of a LNMO sample in electrolyte; and scans of the same sample with a lithiated probe in a dry environment. Moreover, an adequate lithiation procedure was found, and some light on how to include an LNMO sample in a three-electrode setup will be shed.

Even if the present status of the system is incomplete, mostly due to engineering issues (i.e. connections, leakage of the electrochemical cell), we are convinced that this technique can be further developed to obtain a modified AFM for in-situ electrochemical experiments. Topographical data would be collected in the first run of the sample by a non-lithated tip. A second run, at a fixed distance from the surface with a lithiated tip, would then provide data on the rate of ion transport. The combination of these data should open the possibility to relate surface modifications, e.g. (partial) coatings, to locally increased ionic conductivity.

7.1 Introduction

A detailed description of LNMO as a very promising material was given in Chapter 5, together with an in-depth discussion on its synthesis and characterisation as a thin film for li-ion microbatteries. In Chapter 6, an account was carried on the drawbacks this material presents in terms of fast charging while preserving capacity and cycle life, and that lithium ion transport between electrode and electrolyte is the limiting factor. Moreover, it was shown how li-ion migration, and hence the kinetics, was increased by depositing active sites of Cr_2O_3, in the form of nanoparticles, on top of the cathode layer.

It would be very interesting to measure these sort of enhanced lithium ion transport kinetics of the surface, while making a topographic image of the interface. This could help in understanding the surface charge transfer mechanisms and could, for instance, image the type, and the coverage, of coating needed to improve transfer. Such study could be done with a combination of Atomic Force Microscopy (AFM) and Scanning Electrochemical Microscopy (SECM) techniques. AFM gives high-resolution topographic information, and is able to precisely control the distance between the sample and the probe, whereas SECM can provide detailed information of local electrochemical activities due to anodic and cathodic processes [1, 2]. The AFM probe is used as an electrode and charge transfer can be monitored in situ. This combination of techniques is being developed more often in the last decade, but modification for Lithium-ion battery electrodes has never been reported to our best knowledge [3, 4].

In this research project, an attempt will be made at building a modified AFM, for in situ electrochemical characterization of Lithium-ion battery electrode surfaces. The ultimate goal of this research is to obtain a characterization method with which it is possible to analyse the in situ kinetic performance of Lithium-ion batteries on a nanometre scale. Specifically, it is of particular interest to know if a partial chromium oxide coating on LNMO electrodes would render faster charge transfer.

7.1.1 Theoretical background

Besides the promising studies that could be carried out with the suggested in-situ AFM technique, there are several interface phenomena that are worth mentioning which could also profit of such system.

Typically, once an electrode is exposed to an electrolyte a layer is formed at the electrode/electrolyte interface. This layer is called a Solid Electrolyte Interface (SEI) or Solid Permeable Interface (SPI), depending on its perme-

ability. The layer and its behaviour is well studied for negative electrodes, but much less for positive electrodes is known, so far. Often the layers SEI or SPI are formed during the first cycle(s) and are constituted of different materials, depending on the electrode, electrolyte and, in this case, coating materials. The SEI or SPI usually is an insulating interphase[1], blocking the migration of charge carriers or molecules. However, it can therefore also block degradation of the electrode materials. Such is the case for Mn dissolution of $LiMn_2O_4$ (LMO). Beides, for carbonaceous electrodes it is a prerequisite to ensure significant Li-ion transfer. It is however also a barrier for lithium diffusion and electronic conduction [5–7], as was described in Chapter 6.

For LMO electrodes a model has been proposed by Edstrom et al. for the formation of different surface layers [7]. Both organic and inorganic layers are formed due to degradation of both the electrolyte and the electrode. The organic layer is mostly constituted of poly-ethylenecarbonate (PEC), which is formed by the oxidative polymerization of ethylene carbonate (EC) upon high voltage cycling [8]. Other organic solvents often used show less polymerizations, such as diethyl carbonate (DEC), ethyl-methyl carbonate (EMC) and dimethyl carbonate (DMC).

Despite the large amount of information regarding doped and coated LNMO and the discussions on the electrode/electrolyte interphase, no definite or clear model is described for this. Moreover, in most articles there is no clear description regarding the morphology of the coating. Whether the coatings are covering individual particles, agglomerates or just the interface is unclear, as is whether the coating fully or partially covers the active species. This is partly due to the unavailability of proper characterization techniques.

7.1.2 AFM, SECM and SECM-AFM combination

AFM is a type of Scanning Probe Microscopy (SPM) which can image the surface of both insulating and conducting substrates. An AFM probe consists of a sharp tip mounted on a flexible lever, fixed to a larger chip. The tip is scanned across the sample surface by means of piezoelectric translators. The tip can be in contact with the surface (contact mode), and then the force acting on the tip changes according to the sample topography, resulting in a varying deflection of the lever. The probe can also be vibrated at its resonance frequency by

[1] Note that once a material is exposed to any environment an interface region occurs due to charge carrier redistribution so as to level the Fermi levels (or electrochemical potential) of both. This then is actually called an interface. In the case this then will lead to an additional phase, an interphase occurs simultaneously.

means of a piezo oscillator, which is called tapping mode or semicontact mode (depending on the AFM manufacturer). During this oscillation, the tip slightly taps the sample surface and the amplitude signal is detected, which then can be translated to topography data. The deflection of the lever or the amplitude signal is detected by means of laser beam deflection induced by the cantilever and subsequent detection with a double-segment photodiode [9].

The AFM is most commonly used to scan the topography of samples. Because of the sensitive measurement of the cantilever deflection, resolutions on the order of fractions of a nanometer, in the direction orthogonal to the sample, can be obtained. Silicon nitride and single-crystal silicon cantilevers are commonly used in commercial instruments. Ideally the tip would end in a single atom, giving atomic resolution in both horizontal directions. However the tips available have a radius of curvature around 10 nm. Possible artifacts have to be considered when using this technique. These are for example convolution of the surface topography with the tip geometry (e.g., structures sharper than the tip result in an image of the tip) or destruction of sensitive samples by the load of the probe [9]. An important potential of AFM for surface chemistry is its capability to perform in-situ measurements under liquids and in air. This allows direct observation of surface processes by operating the microscope with a liquid cell. In this cell, both sample and cantilever can be immersed in the liquid while measurements are made. Such studies can also be performed with a bias voltage applied to the substrate, which opens up valuable opportunities for electrochemical AFM (EC-AFM). For instance topographic measurements of a cycling battery could be made using this technique [9, 10].

The AFM also has a number of configurations with which specific values of a substrate can be measured. One of them is the conducting or current sensing mode (C-AFM or CS-AFM). In this mode a metal-coated probe is scanned over the surface in contact mode while a fixed bias voltage is applied between the conductive probe and the substrate. This results in a local tip-surface current, typically dominated by the electronic component, with a resolution of 1-10 pA [11]. This method is used to scan the electronic conductivity of substrates and has been applied to LMO layers [12].

However, no AFM option exists to measure the ionic conductivity of substrates by applying a voltage between the probe and substrate. In the present research, a system is created to measure an electrochemical reaction in liquid at a constant distance from the surface, with a bias voltage applied between the probe and substrate. The probe would then be the counter electrode to the substrate. C-AFM measures in air and has direct contact between the probe and substrate which would, in the case of the system in interest, cause a short circuit. EC-AFM can only allow a voltage between the substrate and a refer-

ence electrode and not a voltage to the probe. But another SPM technique is able to measure the ionic conductivity of a substrate, namely Scanning Electrchemical Microscopy(SECM) [13].

SECM can image the reactivity of a surface at a microscopic scale, using an ultramicroelectrode (UME) instead of a cantilever for a probe. This probe consists of a metal core covered by glass, where only the top of the metal is exposed. A bias voltage is applied to the UME, resulting in a redox reaction at the exposed metal. Both the substrate and the probe are immersed in a solution containing an oxidizable species R. When a sufficiently positive potential is applied to the probe, R is oxidized to O, using electrons from the UME [1].

The current flow (i_t) resulting from the applied potential is time dependent. It also depends on the tip diameter and decays to a steady-state value $i_{t,\infty}$ at distances far from the substrate. The steady-state current is governed by the mass transfer of O to the UME and is given by Equation 7.1.1 where F is the Faraday constant, [O] is the concentration of O in the solution, D the diffusion coefficient and a the diameter of the tip. When the tip is closer to the surface's sample, the measured current is different from i_t. The current is then expressed relative to $i_{t,\infty}$ to obtain a normalized, time independent value [14].

$$i_{t,\infty} = 4n[O]FDa \tag{7.1.1}$$

When the tip is brought within a few tip radii of a conductive surface the O species formed in the reaction at the tip diffuses to the substrate where it can be reduced back to R. This process produces an additional flux of R to the tip and hence 'positive feedback', so the tip current increases. The shorter the tip to substrate distance (d), the larger the tip current [1].

If the substrate is an inert electrical insulator, the tip generated species, O, cannot react at its surface. At a small d the insulator blocks the diffusion of species R to the tip surface, giving lower tip current or 'negative feedback'. Overall, the rate of the mediator (R) regeneration at the substrate determines the magnitude of the tip current, which means the tip current vs. distance dependence provides information on the kinetics of the process at the substrate [1].

An SECM operates by scanning an electrode in a fixed plane without distance feedback. This means the UME tip can easily crash and the tip-substrate separation is not well-defined or constant. Next to this, the sizes of UME tips limit them to micrometer resolution. To obtain figures with sub-micrometer resolution at a constant and well controlled height, a combination of an AFM and SECM can be made [15].

The first SECM-AFM combination was described in 2000 by MacPherson and Unwin [16], and since this moment there have been several approaches at

combining these SPM methods [3, 4, 15]. They all involve specially designed AFM probes mounted in an AFM and operated with a bipotentiostat. Probe options include: 1) Hand-fabricated probes, made from an etched wire, not insulated at all but the tip end. 2) A commercial silicon nitride probe, coated in metal and an insulator, while using focused ion beam technology to reshape the probe so as to expose the electrode. 3) Batch microfabricated probes, made at the wafer level, which incorporate a triangular electrode at the very end of the probe. 4) Nanoelectrode probes based on the use of single-walled carbon nanotube bundles on AFM tips. All of these probe designs contain a small electrode and one of their main uses has been to carry out high resolution topographical and electrochemical imaging of surfaces [15].

For research in Lithium-ion batteries there is no need, in principle, for such complicated special tips, because a standard silicon tip can act both as probe and electrode. When lithiating it with enough lithium, the tip should remain intact and the tip diameter should not increase considerably. Lithium ions can then migrate from the tip to the surface, or the other way around, driven by an applied voltage. The resulting current can be measured and indicates the ease of lithium ion (de) intercalation on the substrate/electrolyte interface. This method would then be very similar to existing SECM/AFM combinations. To our knowledge, no one has attempted using standard silicon AFM probes for Li-ion battery SECM characterization yet.

A dual-mode AFM/SECM method described by Davoodi et al. could be used for collecting data. After a normal AFM linescan, to obtain a surface profile in the first pass, the feedback was stopped and the tip withdrawn to a desired distance from the surface. In the second pass, the probe followed the surface profile in the second linescan with a constant lift-up distance, and collected the local current. This distance should be optimized so the probe does not touch the surface, although not be too far because it would decreases the resolution [2]. An example of a combination of topographic and electrochemical data being collected, although using tapping mode, has been reported [17].

The image resolution with an AFM probe could be as high as the tip diameter, which ideally is small. Unfortunately, two aspects lead to strong limitations to the image resolution. First, measurable forces concentrated in a few atoms generate strong deformation of the tip and/or substrate. Secondly, long range forces (e.g. electrostatic forces) are sensitive to the overall shape of the tip. The second argument appears to be especially relevant in electrochemical systems in which variations of the applied potential may introduce substantial changes in the charge of the *diffuse layer* [4]. The diffusion profile of ions through the electrolyte should be taken into account as this strongly influences the obtained pictures. Most diffusion profile models are for cases where the

probe is insulated and only the tip is exposed [2, 18] only one model describes the case for an non-insulated probe [15]. To limit the diffusion distance of ions, short pulses were used here to obtain higher spatial resolution. In this diffusion limited case a time lag of the order $d^2/2D$ was found for the response (d=separation distance, D=diffusion constant). It is recommended that probes should be insulated when imaging conductive substrates. However, it would be more convenient if non-insulated probes can be used.

7.2 Experimental

In this section details of the experimental setup, materials and procedures used in this project will be given. However, a description of the complete electrochemical AFM combination (i.e. a system where morphological images can be taken while performing in-situ electrochemical measurements) won't be given, as this functionality is not possible at present. Ideas on the final system will be therefore discussed at the end of the results and discussion section.

7.2.1 AFM and Electrochemical Cell setups

The AFM used in this research is an NT-MDT Ntegra platform P9, controlled by Nova px software. For electrochemical experiments the SMENA liquid head was used. An optical microscope (Optem 2.0x mini) was available on top of the AFM setup.

When measurements in liquid are required, the SMENA liquid head is used instead of a standard AFM head. A picture of the electrochemical cell (EC) in the AFM setup with the SMENA head attached to it, is shown in Figure 7.1(a). By using the optical microscope (with a digital camera function) placed above the head, images of the probe, positioned under a transparent crystal, could be taken using mirrors. Such a picture of an immersed probe is shown in Figure 7.1(b). During liquid AFM experiments, the laser intensity is automatically lower because of absorption by the electrolyte and reflections through the crystal. In these types of measurements, contact mode is preferred as it is easier to carry out and the damage to the sample is less relevant.

For future application, there is the possibility to make a topographic line scan first and then follow the same path with the probe in a second run at a constant distance. This is the sort of strategy desired for electrochemical measurements. An optimal distance can be found by making slow approach curves and looking where the current starts to increase. Another option would be to scan at different points and, while the feedback loop is turned to off, the

probe is then retracted around 3 μm from the surface.

The full system and the connection layout are schematically shown in

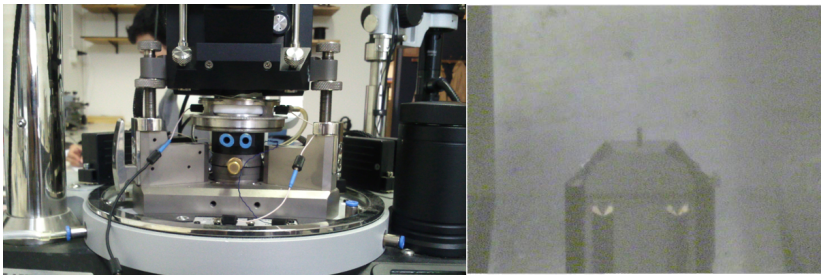

Figure 7.1 – Electrochemical cell in the AFM setup with SMENA head attached. (a) Side image and (b) digital microscope image (top) of immersed probe.

Figure 7.2(a). The EC is designed for electrochemical measurements with the Scanning Tunneling Microscope (STM) head of NT-MDT [13]. The sample (1) is placed at the bottom of the cell's chamber (5) which is filled with liquid electrolyte (4). The sample or working electrode (WE) is connected to the bipotentiostat (2). A reference electrode (3) is immersed in the electrolyte close to the WE. Finally, the scanner (6) is connected to the probe port of the bipotentiostat. The EC has three electrical connections, two of them are ports placed in the diameter of the chamber, while the third one rests at the bottom. An extra connection for the tip was added on top of the cell. The bipotentiostat delivered with the NT-MDT electrochemical cell package was not used as it has limited functionalities to what was needed, therefore a Maccor (model 2200) was used to perform the electrochemical tests, as it will be described in Subsection 7.2.2. . Figure 7.2(b) shows a schematic drawing where the cross-section of the EC and all the components are exposed.

A picture of the AFM probe holder can be seen in Figure 7.2(c). This holder is attached to the AFM head by means of a magnetic ring (localized at the top in Figure 7.2(b) and bottom in Figure 7.2(c)). A fork is used for the correct handling of the probe holder and it also helps to keep a distance of roughly 1 mm between the probe and the sample preventing tip crash. The fork is taken off only when the probe holder is correctly attached to the head, as the distance between probe and sample is then controlled by the AFM system. For pressurizing the working area and to make sure the cell is airtight, the probe holder is equipped with a silicon membrane. Between the membrane and the

base, a copper wire was coupled to provide a connection between the probe and the outside. The SMENA head has a crystal on the top through which the laser can see the probe while it is immersed in a liquid. The AFM (silicon) tip is placed on top of the crystal and will be used as an in-situ AFM electrochemical probe and as counter electrode.

Figure 7.2(d) shows a picture of the EC base. A Teflon®chamber, whose inner part has a stainless steel cover, is then filled with the electrolyte solution. The sample is placed on the bottom of the chamber and is mechanically held to it by a brass L-shaped hook (visible in the right side, Figure 7.2(b)), which also serves as a current collector. A second L-shaped brass hook, with a drilled hole in the extreme which is immersed in the electrolyte, holds a piece of metallic lithium that will act as reference electrode. These hooks fit in stainless steel clips (as seen in Figure 7.2(b)), which are in contact with wires to allow the connection with the bipotentiostat. The EC also features gas inlets.

7.2.2 Electrochemical procedures

All electrochemical measurements were done using the electrochemical cell. Most of them were carried out in the glovebox, where built-in ports permitted the connection to a Maccor S4000 cycler. For those electrochemical tests combined with the AFM (performed outside the glovebox), a Maccor S2200 was used.

Most of the experiments were in a two-electrode setup which consisted of silicon (AFM probe) as working electrode and metallic lithium as reference and counter electrode. The experiments performed are summarized in Table 7.1. All experiments started with a galvanostatic discharge. Samples were then either cycled further galvanostatically, or discharged potentiostatically. Galvanostatic cycling was done to observe the behavior after the first cycle. As mentioned in Subsection 7.1.3 a constant voltage is required. Therefore potentiostatic discharge is the most probable mode to be used in the final system. To prevent jumps in the voltage, the potentiostatic voltage has to be achieved by galvanostatic charge or discharge. Three-electrode experiments were also carried out, using LNMO (produced in the same as for Chapters 5 and 6) as third electrode. The Reference Control functionality available for the Maccor S4000, which gives the option of an auxiliary input, was used in this case. This scheme provides voltage control between the WE and the RE, while the current flows between the WE and CE. The channel output voltage is then WE vs. RE and the auxiliary voltage output gives WE vs. CE.

During most electrochemical test performed, there was electrolyte evapora-

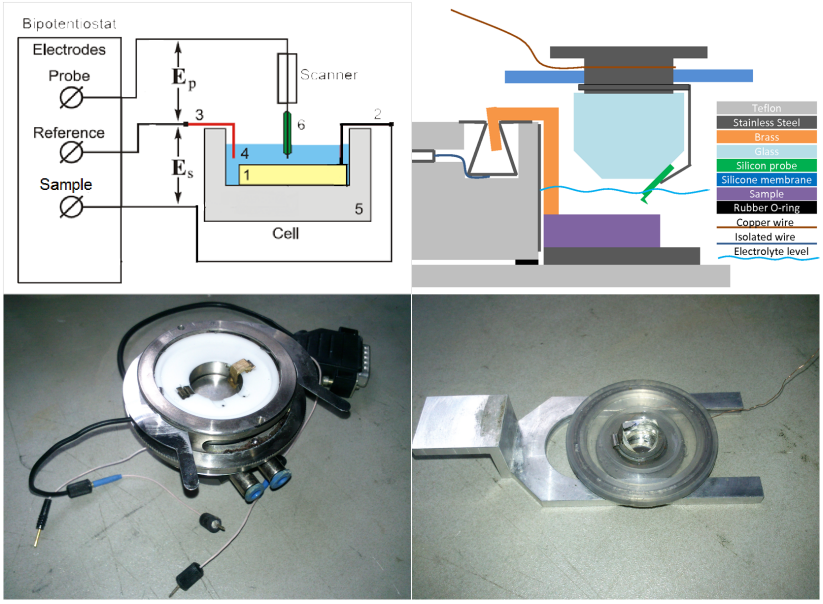

Figure 7.2 – (a) Scheme of the electrochemical setup with layout of connections: (1) sample (working electrode); (2) current-collector;(3) Li^0 reference electrode;(4) electrolyte; (5) cell housing; (6) Silicon SPM tip (counter electrode). (b) Cross-section schematic drawing of the liquid cell for the AFM; images of (c) bottom part; and (d) top part

Table 7.1 – Summary of electrochemical experiments

Experiment number	Probe previously used	Applied current/voltage (μA / V)	Voltage limits (V)	Number of cycles
A	Yes	10	0.05-1.5	5
B	Yes	3	0.05-1.5	10
C	Yes	3	0.05-1.5	1
D	No	3	0.05-1.5	10
E	No	3	0.01-1.5	1
F	No	3	0.05	1 discharge
G	No	1, 5, 1	0.05-1.5	30
H	No	3 / 0.3	0.3	1 discharge

tion because of leakage in the electrochemical cell. As a result, the electrolyte volume in the chamber was constantly changing during the reaction making it difficult to know what part of the probe was actually immersed. This gives rise to an intrinsic problem to calculate the C-rate as it is based on the electrode weight. Therefore, a fixed current of 3 μA was chosen for most experiments (as shown in Table 7.1) and will be more elaborately discussed in Subsection 7.3.1.

7.2.3 Materials Used

The AFM probes used were of the types NSG03 [19] and NSG30 [20]. These are probes fabricated by NT-MDT meant for non contact or semicontact scanning, but can also be used in liquid and in contact mode. They are made from single crystalline silicon (n-type) doped with antimony, with a bulk resistivity of 0.025 Ω cm. The chip sizes are 3.4 x 1.6 x 0.3 mm. The tips are 14-16 μm high and have a typical curvature radius of 10 nm. The cantilever dimensions are different for the two types of probe. For the NSG30 is 125$\pm$10 x 40$\pm$5 x 4.0$\pm$0.5 μm and for the NSG03 the size is 135$\pm$10 x 30$\pm$5 x 1.5$\pm$0.5 μm. The volume and mass of every part of an NSG30 probe is given in Table 7.2, using a density of 2.329 g cm^{-3}. The mass ratio between the probe components is given as well [19, 20].

Thin LNMO layers were electrosprayed, based on recipes described in Chapter 5. Spray times of 10 minutes, with fixed flow rates and concentrations, were chosen to achieve relatively flat layers. Aluminum foil and silicon

Table 7.2 – Volume and mass of NSG30 probe components

	Dimensions	Volume	Mass	Mass ratio
V_{chip}	3.4 x 1.6 x 0.3 mm	1.6 mm^3	3.8 mg	4 - 10^6
$V_{cantilever}$	125 x 40 x 4 μm	20 - 10^3 μm^3	47 ng	50
V_{tip}	$1/4 * 15$ x 10 x 11 μm	413 μm^3	0.96 ng	1

wafers (thickness 0.8 mm) were used as substrates. Some LNMO samples were coated with chromium oxide, following the details described in Chapter 6.

Experiments in the glovebox (MBraun) were performed under argon atmosphere. For most experiments outside the glovebox, the cell chamber was constantly flushed with helium so as to create an inert environment. Metallic lithium was used as negative electrode. The electrolyte solution used was 1.0 M $LiPF_6$ in ethylenecarbonate:dimethylcarbonate (EC:DMC) (1:1 by wt%). As DMC evaporates quickly at room temperature and EC subsequently crystallizes, DMC (Dimethylcarbonate, anhydrous, Merck) was often added to again dissolve the electrolyte.

7.2.4 Probes storage and characterisation

In order to decrease the waiting time of the first probe discharge (lithium insertion), using a probe which has been previously lithiated could be convenient. Therefore an investigation of whether the probes changed after a certain storage time was conducted. After the electrochemical experiments most probes were rinsed with different solvents: with DMC in the glovebox, with ethanol outside the glovebox, with both DMC and ethanol, and some were not rinsed at all. These probes were then stored.

Stored probes were characterized using a Phillips XL20 scanning electron microscope, operated at 15 kV. Moreover, a JEOL JSS-7500F SEM coupled to a NORAN System SIX, was used for energy dispersive x-ray spectroscopy (EDX) analysis.

7.3 Results and Discussion

In this chapter the results of both the experiments and the 'development process' will be discussed. The first section covers the electrochemical experiments. This is followed by some data on the storage of tips, and topographical images in the AFM. In Section 7.4.1 a discussion on the setup problems will be carried out and of some improvements that have either already been applied, or that should be applied to continue with this research. Finally, an important part will deal with how we think the modified AFM will look like, in the end.

7.3.1 Electrochemical experiments

Silicon probes were charged and discharged versus metallic lithium as described in section 7.2.2. Figure 7.3 shows the second cycle, as the first cycle usually involves SEI layer formation and also irreversible reduction of surface layers formed on silicon (SiO_x, Si-OR and Si-R) [21, 22]. The discharge plateau between 0.2 and 0.05 V and the charge plateau between 0.3 and 0.7 V gives a similar electrochemical behaviour to what has been previously reported in the literature [22]. From this electrochemical behaviour we can conclude that we have a working battery of silicon vs. lithium, which proves that the silicon probe can be lithiated. Some lithiated probes have been studied with Scanning Electron Microscopy. In Figures 7.4(a and b), a probe is shown which has been discharged to 0.05V (i.e. lithiated). When compared with the fresh tip in Figure 7.4(c), a change of the surface can be observed, although it is clear that the shape of tip is still intact. A probe which was discharged to 0.01V and charged again is shown in Figure 7.4(d). Here it is very clear that the deintercalation of lithium caused the silicon host to crumble. As this crumbling destroys the tip, making it unpractical for AFM measurements, the cut-off voltage for the discharge should not be very low.

Discharge curves from some of the probes previously used (including those shown in the SEM picture above) are shown in Figure 7.5. Probes A and C had been cycled earlier, while probes D, E and F were pristine, as described in Table 7.1. It can be immediately appreciated that the open circuit voltage of pristine tips is between 2 and 3 V and probes previously used have an OCV between 0.5 and 2 V. This is because of the reactions we see at higher voltages, suggesting that surface layers are reduced and an SEI is formed, as discussed in section 2.5. All probes show a voltage plateau at voltages between 0.5 and 0.05V, indicating lithium insertion in the silicon. The exact voltage levels and lengths of the plateaus differ significantly however, even though the setups and

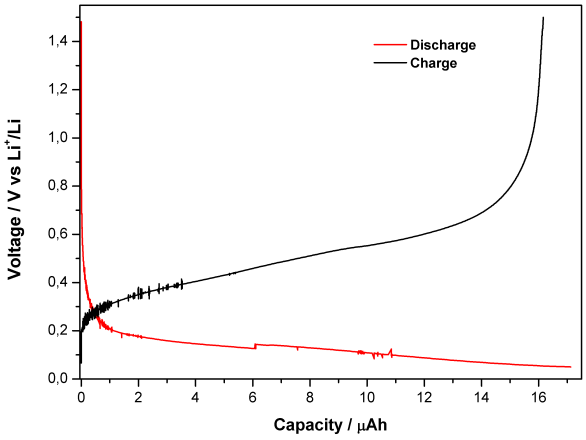

Figure 7.3 – Charge and discharge of silicon probe vs. metallic lithium (experiment B)

procedures are practically identical. In experiment A, a current of 10 μA instead of 3 μA was used, but this does not influence the Voltage-Capacity curves. Another noteworthy aspect is the noise and voltage jumps which are caused by poor electrical connections. This will be discussed in more detail in section 7.4.1.

As mentioned in sections 7.1.2 and 7.2.2, it is necessary to identify which voltage to use for potentiostatic measurements, in combination with the AFM. This voltage should be stable, i.e. at a plateau, to be able to measure for a significant amount of time at a constant voltage. However, it would be convenient if this voltage is as high as possible so that there is as little as possible lithium in the silicon in order to avoid too much volume expansion of the tip and, also, to minimize the waiting time until the voltage is reached. Still, lithium should be inserted at this voltage in any probe. Taking these above considerations into account, it is decided that 0.3V is the highest possible voltage.

Usually, the applied current in galvanostatic measurements is based on the electrode mass and expressed in C-rate. However, in this project a constant current was used (see section 7.2.2) because the mass of active silicon varies during the experiment as, due to electrolyte evaporation, the exposure of the

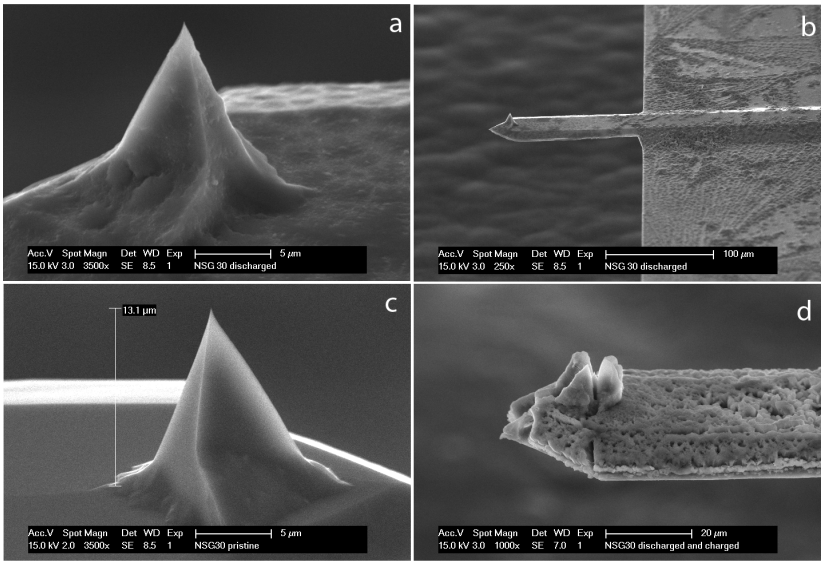

Figure 7.4 – SEM pictures of NSG30 tips; a) once discharged tip(in exp. E); b) once discharged tip and cantilever (in exp. E); c) pristine tip; d)once discharged and charged tip (in exp. F)

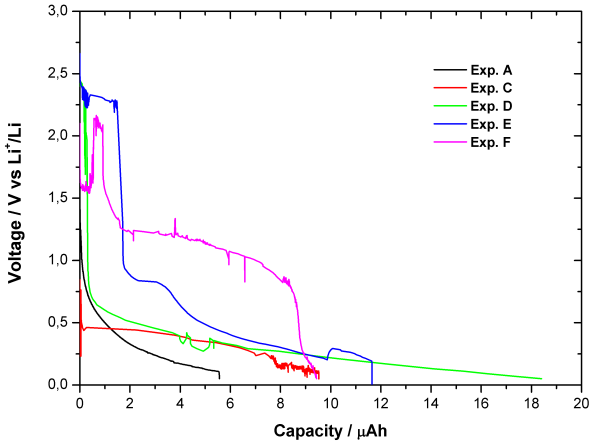

Figure 7.5 – Discharge curves of experiments A, C-F. Experiments E and F correspond to SEM pictures above

AFM's cantilever varies.

Potentiostatic experiments are preferred for the combination with the AFM, as previously discussed in this subsection. To obtain the desired voltage of 0.3V, the cell is discharged galvanostatically at a current of 3 μA, as depicted in Figure 7.6. When the voltage reaches 0.3V, 10 minutes of potentiostatic discharge followed, after which the cell was turned to a rest stage. In this case the voltage profile is flat, indicating perfect electrical connections. The current slightly fluctuates around 3 μA, as it does in every galvanostatic experiment, and decays in the potentiostatic mode. This is because there is a decreasing amount of silicon which can be lithiated at this voltage. A similar effect is described in section 7.1.2. An attempt was also made at doing three-electrode measurements, where a third electrode of LNMO was added. As described in Subsection 7.2.2,an auxiliary voltage input in the Reference Control mode of the Maccor was used. In this case, LNMO was acting as the working electrode (WE), Si as the counter electrode (CE) and Li as the reference electrode (RE). This means that the reaction between LNMO vs. Li could be controlled, while the current would actually run between LNMO and Si. Such measurement is shown in Figure 7.7. A very slow charging of the LNMO can be seen, and a

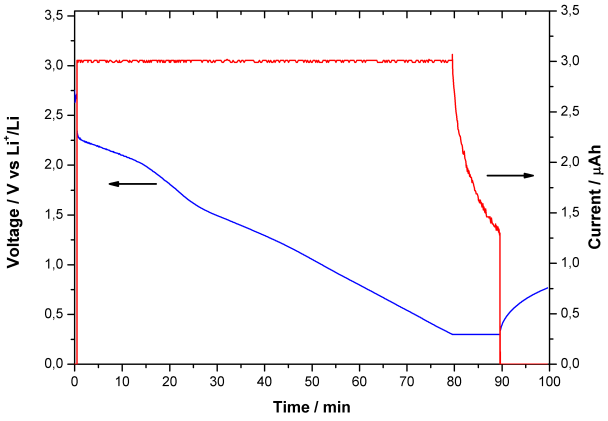

Figure 7.6 – Time profile of galvanostatic discharge (3 μA) to a voltage value of 0.3 V, followed by 10 min potentiostatic discharge (experiment H)

faster discharge of Si. The spike obtained at around 70 minutes is probably due to loss of contact for a very short time, leading to fast relaxation of LNMO and Si. Nevertheless, the system recovered and resumed charging and discharging. Finally, the voltage of Si vs. Li drops below 0 V, which could only indicate lithium plating on silicon. As the capacity of LNMO is higher than that of Si, because of the big difference in active masses, the LNMO is not fully charged while the Si is already fully discharged. Hence, the capacities should be better matched, or the control should be with regards to silicon and not to LNMO.

The ideal setup would use the Maccor cycler to control LNMO vs Si and Si vs Li simultaneously, as the probe is then constantly kept at the same level of lithiation avoiding a decreasing current vs. time due to the probe delithiating. Unfortunately, with this system, in its present form, it was not possible to perform such a measurement. This means that two devices have to be used for voltage control, one recording the reaction between LNMO and Si (preferably the Maccor), while the voltage of Si and Li could be kept stable by attaching, for example, a Si vs. Li battery, which is at the same voltage, with a very large capacity.

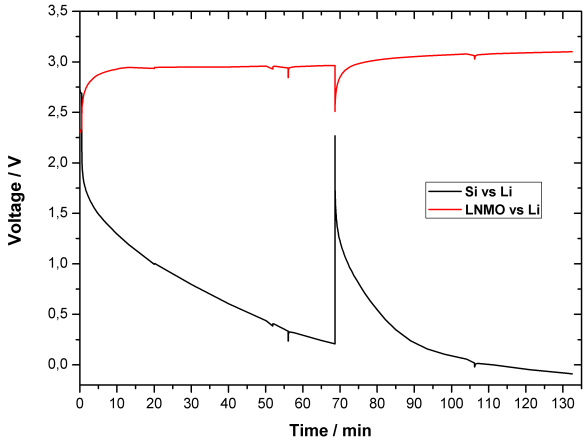

Figure 7.7 – Three-electrode measurements of LNMO (WE) vs Si (CE) and Li (RE)

7.3.2 Probe storage

The probes were stored at ambient conditions, so they could have reacted with air and moisture. Figure 7.8 shows SEM pictures of NSG03 probes under different circumstances. The tip and cantilever in Figure 7.8(a and b) are the same as the tip in Figure 7.8(c), but after being stored for two months. When comparing Figure 7.8(a) to Figure 7.8(c) the protrusion on the tip and the 'islands' on the cantilever seem to have decreased in size. During this time the lithium seems to insert further into the silicon, thereby distributing more evenly. Besides, after this period of time, the cantilever bends as seen in Figure 7.8(b). For a non-lithiated tip stored in exactly the same environment as the lithiated one, no bending of the cantilever is observed (Figure 7.8(d)). An explanation for this is that, most probably, lithium inserts further into the cantilever increasing its volume in certain spots causing mechanical stresses that makes it bend. This would mean that the bottom part of the cantilever (when mounted in the setup) reacts with more lithium than the top part. Note that in Figure 7.8 the tip is at the top in contrast to how it will be mounted in the AFM set-up. If the cantilever is bended too much, the laser spot in the AFM cannot be reflected in the right direction, leaving the probe useless.

After some storage time has passed, crystals are formed if the probe was

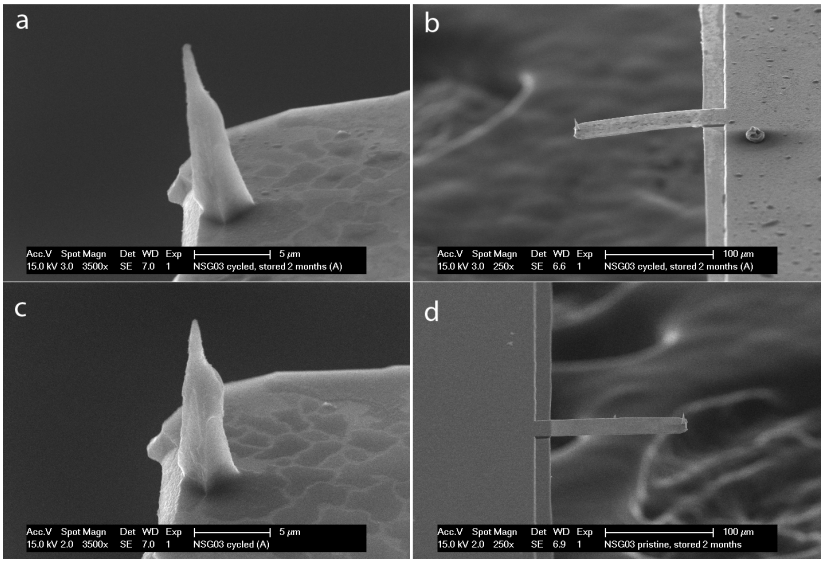

Figure 7.8 – NSG03 probes; (a) lithiated tip stored for 2 months; (b) bended cantilever, same as a; (c) same tip as a, directly after lithiation; (d) stored pristine probe, with no bended cantilever

not rinsed before storing it. Most of these crystals are cubic, as can be seen in Figure 7.9 and in the SEM micrographs shown in Figure 7.13, which will be described later. EDX images of a stored cantillever are shown in Figure 7.9. The tip is shown from above and a large crystal is laying next to it. In fact this is the same probe as in Figure 7.4(a and b), although these EDX pictures are made after a month of storage. The cantilever itself mostly consists of silicon, as expected, with traces of oxygen, nitrogen and sodium. The crystal is clearly formed from the electrolyte salt ($LiPF_6$), because it is mainly constituted of fluor and phospor.

7.3.3 Topographical AFM scanning of the sample

In order for the combined electrochemical AFM method to work, it should be possible to scan with a lithiated probe, as discussed in section 7.1.2. To prove that a lithiated probe can be controlled, a topographical scan in the contact

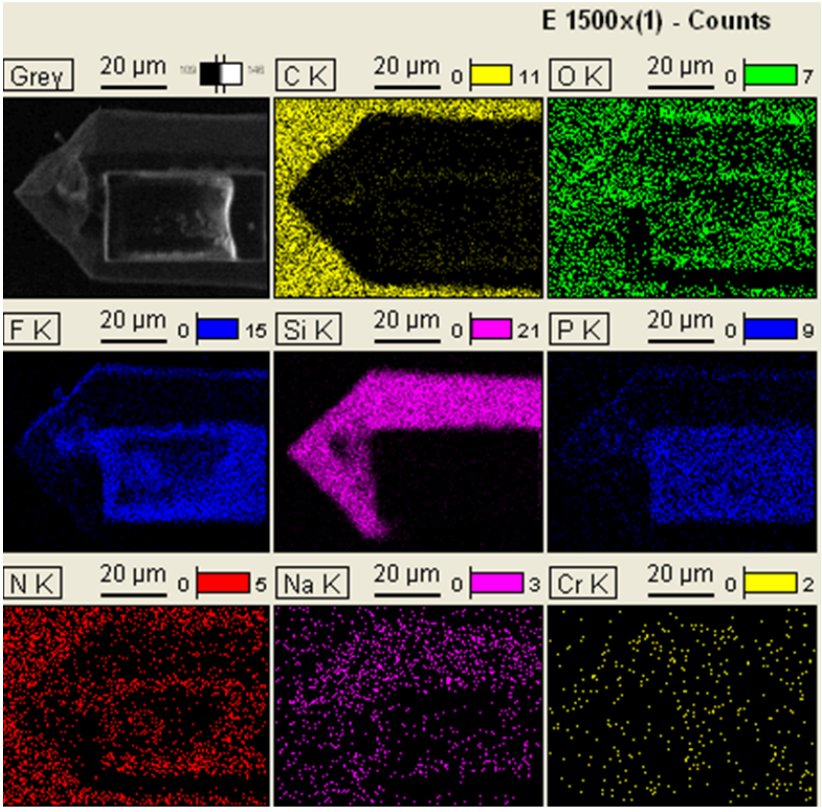

Figure 7.9 – EDX pictures of a probe cantilever and tip, from experiment F, taken one month after Figure 7.4(a and b). Color scales give the counts of elements in the picturer

mode was performed in a dry environment. Figure 7.10(a) shows an AFM image performed with a pristine tip on a sample of LNMO partially coated with chromium oxide, synthesized as described in Chapter 6. Figure 7.10(b), on its turn, shows a clear topographic image carried out with a lithiated tip. Therefore the feasibility of a scanned topography with a lithiated probe is demonstrated. To obtain this image, a tip force of approximetaly twice the one used in regular procedures was required.

Before the probe was used for AFM scanning it was observed under the

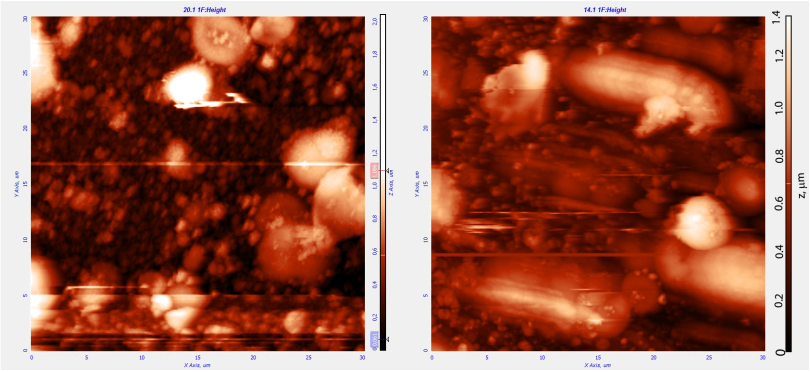

Figure 7.10 – AFM scan of LNMO with chromium oxide; (a) scanned with a pristine probe (30x30 μm); (b) scanned with a lithiated probe(30x30 μm)

SEM (Figure 7.11). The tip is shorter than the pristine one, which means it 'broke' during electrochemical measurements. However, for this purpose, it broke in a convenient way as there is still a relatively sharp tip with an approximate tip radius of 350 nm (Figure 7.11(b)). This corresponds quite well with the smallest artifacts observed in Figure 7.10(b), which are of the same order of magnitude, therefore the tip convolution is small enough. This probe had been stored for two weeks, and as discussed in the previous subsection, crystal formation of $LiPF_6$ can be seen on the chip and cantilever.

It is the aim of this research to make a topographic scan using a pristine (non-lithiated) tip in electrolyte, followed by a second scan made at a constant distance from the surface with a lithiated tip (see Subsection 7.1.2). Figure 7.12(a) shows an AFM scan done on a similar kind of smple as those shown in Figure 7.10, only this time performed in liquid electrolyte with a pristine tip. Scanning within the filled liquid cell is not straightforward, however,

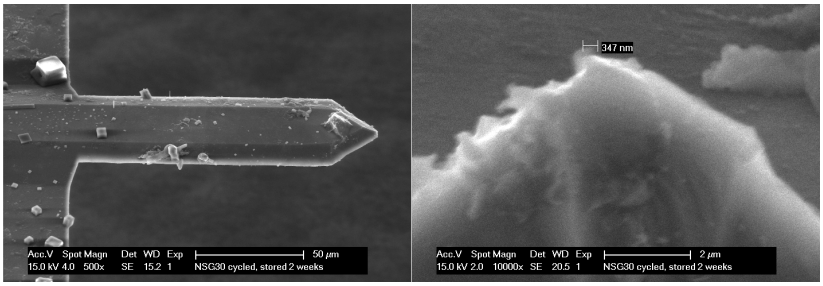

Figure 7.11 – Probe which was used to scan Figure 7.10(b); (a) cantilever (b) tip end

as will be discussed more elaborately in the next subsection. Simultaneous to AFM approaching and scanning, a voltage of 0.2V was applied between the probe and lithium. Unfortunately, no stable current flow was measured as shown by the voltage-and-current graph vs. time in Figure 7.12(b), most likely because of poor electrical connections.

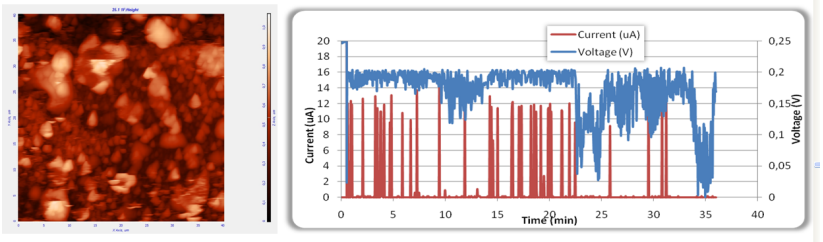

Figure 7.12 – (a) AFM scan of LNMO with chromium oxide, scanned in electrolyte (40x40 μm); (b) Electrochemical behaviour of Si vs Li during AFM scanning

7.4 Future research

As has been mentioned before, the techinique presents several unresolved issues at present. Because of this, it was hard to achieve reproducibility in the

experiments. Solutions have already been found and implemented for some issues. For others, further research is needed in order to optimize the setup, the technique and the procedure.

7.4.1 Setup improvement

The main problem in almost all the experiments was that the electrical connections were not stable, as it is clearly observed from the shape of the graphs in Figure 7.5, 7.7 and 7.12(b). In the schematic drawing of Figure 7.13 all the electrical connection points of the cell are shown. The points of which there were poor or no electrical connection are indicated in red circles.

- (1) The copper wire that is wound around the stainless steel crystal base oxidizes and unwinds with time. This was partly solved by placing the wire underneath the membrane ridge, preventing unwinding. It does, however, increase the chance of gas leakage.
- (2) The brass hook does not apply enough pressure on the sample to have a stable connection. Because of its shape, there is no mechanical force applied on the hook by the clip, so it 'floats' in the setup.
- (3) The wire underneath the clip is the most troublesome connection. The clip oxidizes with the electrochemical reactions, forming an insulating oxide layer. On top of this, the pressure the clip provides on the wire is not high enough, giving mechanical instability. Finally, the wire is very fragile and broke several times during the experiments. A solution for the issue with oxidation is that the wire, clip and hook should preferebly be made of platinum.
- (4) The electrolyte level drops during prolonged experiments, leaving the probe unimmersed in the electrolyte. This is mainly because DMC evaporates quickly at room temperature. The remaining electrolyte solution, EC, finally crystallizes (after more or less 10 h), as it does so at room temperature. Experiments could be done with the probe in crystalline electrolyte, however the cantilever would break when the cell was opened to add more DMC in order to dilute it. This could be prevented by arrying out short experiments in the cell (4 h). Moreover, low electrolyte levels were also due to leakage through the bottom, the side connections or the top, mainly caused by the constant (although needed) manipulation of the cell during experiments.

Another important aspect in these types of measurements is that the reactions should take place in an environment without moisture, oxygen or nitrogen.

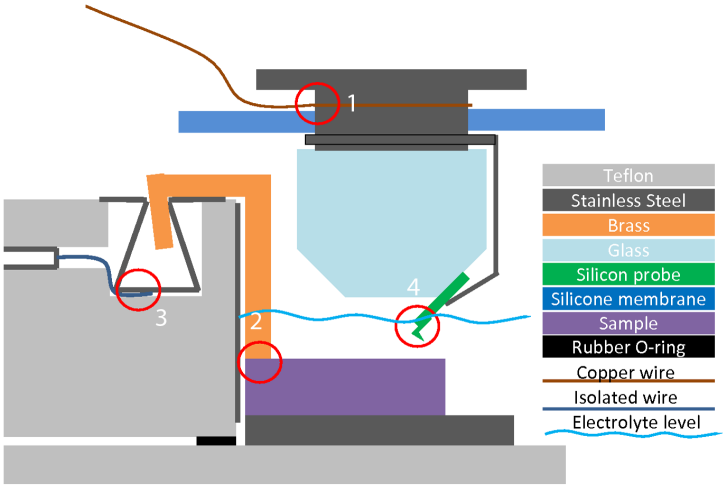

Figure 7.13 – Schematic of the faulty connections in the setup, half the cell is shown

Therefore a stable environment with inert gas should be used and all the leaks avoided.

- All the parts of the setup have to be dried, especially the AFM probe when used in the AFM setup. If this is not done properly, bubble formation (probably H_2) and layer formation (a $Li_xN_yO_z$ compound) occurred at the probe. Such artifacts can be seen in Figure 7.14. Beside reaction contamination, the bubbles blocked the laser and the formed layer decreased the reflected laser intensity. This stopped the laser feedback and the probe position could not be read or controlled by the AFM software. When experiments were carried out in the glovebox, probes which were not dried did not cause bubble or layer formation, therefore the environment where the measurement takes place also plays an important role.

- As the cell was not completely airtight, a balloon filled helium gas was connected during measurements performed outside the glovebox, to compensate for gas leakage. The main leak seemed to be at the top of the cell, between the stainless steel base of the crystal and the membrane.

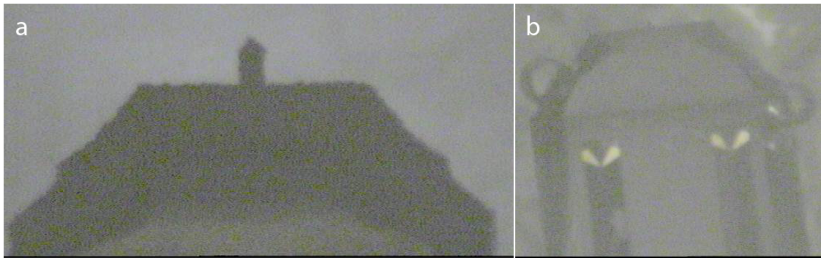

Figure 7.14 – Contaminated cell. (a) probe with layer formation in cell; (b) probe with bubbles and oxidized lithium foil.

7.4.2 Towards electrochemical experiments in a modified AFM system

Based on all the previously discussed results, a description will be made on how the modified AFM would work. For each step, a reference to the section where that part is discussed in detail will be given.

In the glovebox, the cell will be assembled with an LNMO sample (or any other active material) at the bottom, functioning as a working electrode (WE), and metallic lithium foil at the side, working as a reference electrode (RE), (Subsection 7.2.1). Before assembly, every part will be dried in the vacuum oven, including the probe to be used (Subsection 7.4.1). The cell will then be placed in the AFM. The gas flow and electrical connectors and the AFM head will be installed (Subsections 7.2.1 and 7.4.1). At this time the AFM and Maccor hardware/software are already operational.

A manual approach of the tip is done, followed by resonance and aiming and finally the computer drives the last part of the approach to the substrate (Subsection 7.2.1, Subsection 7.4.1). The probe will then make topographic line scans of the substrate and is subsequently retracted from the surface, so that it won't short circuit the system (Subsections 7.2.1 and 7.4.1). Now the probe can be prelithiated using the metallic lithium (RE), i.e. the cell of silicon vs. lithium will be discharged galvanostatically to 0.3V (Subsections 7.2.2 and 7.3.1). Right afterwards, the cell is switched to potentiostatic mode and the voltage between silicon and lithium is kept at 0.3V (Subsections 7.2.2 and 7.3.1).

A three-electrode setup is then made, in which the voltage of silicon vs. lithium is kept constant and LNMO can be cycled vs. silicon (Subsections 7.2.2 and 7.3.1). This could probably be done using the Maccor to control

LNMO vs. silicon and using a large silicon/lithium battery to control the probe voltage vs. lithium (Subsection 7.3.1). The tip can now repeat the scan lines previously made, but at a certain distance from the substrate (Subsections 7.2.1 and 7.2.1). At the same time, the current between LNMO and Si is being measured, as this provides information of the rate of lithium ion transfer in the cell (Subsection 7.2.1). In this manner the whole sample can be scanned. Afterwards the current data lines can be overlaid to obtain a 2D figure of the current at all the locations (Subsection 7.2.1). This image could then be compared to the topographic image to see if enhanced or reduced surface reactivity is related to objects, e.g. catalysts, at the surface (7.2.1).

In an even more advanced system the AFM will be connected to an Electrochemical Impedance Spectrometer.

7.5 Conclusions and Recommendations

In this research project, a silicon AFM probe was succesfully used as an electrode in a Lithium-ion battery setup. This was proven by electrochemical curves and SEM pictures. In two-electrode experiments of silicon vs. metallic lithium, it was found that the capacity of the probe was very low, hence discharge rates of 3 μA were used. A voltage of 0.3 V was chosen for potentiostatic operation, because most probes show a pseudo-plateau (due to Li alloying) at this voltage.

In AFM experiments, a three-electrode setup with a LNMO sample as working electrode would be prefered. Ideally, simmultaneous control of both LNMO vs. Si and Si vs. Li would be needed in this system. A working three-electrode setup with LNMO as WE, Si as CE and Li asRE was achieved, using the Reference Control mode of the Maccor (S4000) cycler.

It was found that it is possible to prelithiate probes and store them in ambient conditions, so as to use them in a later stage. However, for storage times in the order of a month, SEM pictures do show bending of the cantilever and formation of crystals on the probe.

The obtained electrochemical results were not very reproducible and showed significant noise. This resulted from poor electrical connections of the AFM cell. The initially observed side reactions with moisture and air could be prevented by predrying all the setup parts, including the probe, and controlling the environment with an inert gas.

A topographical scan of LNMO with a lithiated probe was also accomplished. This indicates that these probes can be used for further measurements.

Moreover, it was also possible to scan a similar LNMO sample immersed in liquid electrolyte with a normal (non-lithiated) probe in the AFM cell.

It is highly recommended to further improve the quality of the electrical connections when continuing with this research with the electrochemical AFM cell. This would make the results much more stable, reliable and reproducible. In more detail, the side wires should then be replaced by a stronger wire or metal strip. The hooks should be reshaped to apply more mechanical pressure on the sample. The clips should be thoroughly cleaned to remove oxidation or, better, new clips should be made. Ideally, all these parts should be made of platinum to produce a robust and corrosion-free system.

The ideal way to combine topographic and electrochemical data is to make topographic line scans and repeat these at a certain distance with a lithiated tip. A convenient distance for this has to be found.

As further proof that this system works (as it is expected to), it would be interesting to make an approach of Si vs. LNMO while measuring the current. There should be an increase in the current for short separation distances. Also it would be interesting to know what the electrochemical response is in the case of short circuiting, by touching the surface with the probe, while applying a voltage. This method can be used to study the safety of the various electrode materials on a nanometer scale.

When the system will be ready to work, the next step would be to increase the resolution. The tip size should remain as small as possible, while containing enough lithium. It might also be necessary to coat the tip with an insulating material, to obtain a better diffusion profile. Furthermore, it might be worth considering placing the AFM inside a glovebox or to put a portable glovebox around the AFM. This would significantly decrease the chance of contamination although, unfortunately, would make the handling of the system harder.

Nevertheless, we think it is possible to make a modified AFM for in situ electrochemical characterization. Topographical data would be collected in the first run of the sample by a non-lithated tip. A second run at fixed distance from the surface with a lithiated tip would then provide data on the rate of ion transport. By combining these data, we strongly believe it should be possible to relate surface artifacts, e.g. a coating, to increase the ionic conductivity.

References

[1] M. Mirkin, W. Nogala, J. Velmurugan, and Y. Wang, "Scanning electrochemical microscopy in the 21st century. Update 1: five years after," *Physical Chemistry Chemical Physics*, vol. 13, no. 48, pp. 21196–21212, 2011.

[2] A. Davoodi, A. Farzadi, J. Pan, C. Leygraf, and Y. Zhu, "Developing an AFM-Based SECM System; Instrumental Setup, SECM Simulation, Characterization, and Calibration," *Journal of The Electrochemical Society*, vol. 155, no. 8, pp. C474–C485, 2008.

[3] S. Kalinin and N. Balke, "Local Electrochemical Functionality in Energy Storage Materials and Devices by Scanning Probe Microscopies: Status and Perspectives," *Advanced Materials*, vol. 22, no. 35, pp. E193–E209, 2010.

[4] D. Fermin, "Nanoscale Probing of Electrode Surfaces by Scanning Force Microscopy," *CHIMIA International Journal for Chemistry*, vol. 60, no. 11, pp. 789–794, 2006.

[5] Y. Lee, J. Lee, H.-T. Shim, J. Lee, and J.-K. Park, "SEI layer formation on amorphous Si thin electrode during precycling," *Journal of the Electrochemical Society*, vol. 154, no. 6, pp. A515–A519, 2007.

[6] S. Zhang, K. Xu, and T. Jow, "Understanding formation of solid electrolyte interface film on $LiMn_2O_4$ electrode," *Journal of the Electrochemical Society*, vol. 149, no. 12, pp. A1521–A1526, 2002.

[7] K. Edstrom, T. Gustafsson, and J. Thomas, "The cathode-electrolyte interface in the Li-ion battery," *Electrochimica Acta*, vol. 50, no. 2-3, pp. 397–403, 2004.

[8] L. Yang, B. Ravdel, and B. Lucht, "Electrolyte Reactions with the Surface of High Voltage $LiNi_{0.5}Mn_{1.5}O_4$ Cathodes for Lithium-Ion Batteries," *Electrochemical and Solid State Letters*, vol. 13, no. 8, pp. A95–A97, 2010.

[9] R. Kellner, J. Mermet, M. Otto, M. Varcarcel, and H. Widmer, *Analytical Chemistry: A Modern Approach to Analytical Science, 2nd Edition*. Wiley-VCH Verlag BmbH & Co., 2004. ISBN 3527305904.

[10] R. Vidu, F. Quinlan, and P. Stroeve, "Use of in Situ Electrochemical Atomic Force Microscopy (EC-AFM) to Monitor Cathode Surface Reaction in Organic Electrolyte," *Industrial & Engineering Chemistry Research*, vol. 41, no. 25, pp. 6546–6554, 2002.

[11] Garcia, A. and Nguyen, T-Q., "Bruker: Nanoscale charge transport in LED materials using conducting AFM." `http://www.bruker.jp/axs/nano/imgs/pdf/AN127.pdf`, 2010. Accessed: 11 July 2013.

[12] Y. Matsuo, R. Kostecki, and F. McLarnon, "Surface layer formation on thin-film $LiMn_2O_4$ electrodes at elevated temperatures," *Journal of the Electrochemical Society*, vol. 148, no. 7, pp. A687–A692, 2001.

[13] NT-MDT, "Electrochemical measurements: Instruction Manual." `http://www.ntmdt.com/page/electrochemical`, 2011. Accessed: 2 July 2013.

[14] A. Bard, F.-R. Fan, D. Pierce, P. Unwin, D. Wipf, and F. Zhou, "Chemical Imaging of Surfaces with the Scanning Electrochemical Microscope," *Science*, vol. 254, no. 5028, pp. 68–74, 1991.

[15] M. Holder, C. Gardner, J. Macpherson, and P. Unwin, "Combined scanning electrochemical-atomic force microscopy (SECM-AFM): Simulation and experiment for flux-generation at uninsulated metal-coated probes," *Journal of Electroanalytical Chemistry*, vol. 585, no. 1, pp. 8–18, 2005.

[16] J. Macpherson and P. Unwin, "Combined scanning electrochemical-atomic force microscopy," *Analytical Chemistry*, vol. 72, no. 2, pp. 276–285, 2000.

[17] D. Burt, N. Wilson, J. Weaver, P. Dobson, and J. Macpherson, "Nanowire Probes for High Resolution Combined Scanning Electrochemical Microscopy-Atomic Force Microscopy," *Nano Letters*, vol. 55, no. 4, pp. 639–643, 2005.

[18] O. Sklyar, A. Kueng, C. Kranz, B. Mizaikoff, A. Lugstein, E. Bertagnolli, and G. Wittstock, "Numerical Simulation of Scanning Electrochemical Microscopy Experiments with Frame-Shaped Integrated Atomic Force Microscopy-SECM Probes Using the Boundary Element Method," *Nano Letters*, vol. 77, no. 3, pp. 764–771, 2004.

[19] NT-MDT, "AFM Tapping Mode Tips: NSG03 Series." `http://www.ntmdttips.com/noncontact/nsg03`, 2012. Accessed: 9 July 2013.

[20] NT-MDT, "AFM Tapping Mode Tips: NSG30 Series." `http://www.ntmdttips.com/noncontact/nsg30`, 2012. Accessed: 9 July 2013.

[21] N. Hochgatterer, M. Schweiger, S. Koller, P. Raimann, T. Wohrle, C. Wurm, and W. Winter, "Silicon/Graphite Composite Electrodes for High-Capacity Anodes: Influence of Binder Chemistry on Cycling Stability," *Electrochemical and Solid-State Letters*, vol. 11, no. 4, pp. A76–A80, 2008.

[22] D. Munao, M. Valvo, J. van Erven, E. Kelder, J. Hassoun, and S. Panero, "Silicon-based nanocomposite for advanced thin film anodes in lithium-ion batteries," *Journal of Materials Chemistry*, vol. 22, no. 4, pp. 1556–1561, 2012.

Summary

The remarkable physicist Richard P. Feynman once said, more than fifty years ago: "the principles of physics, as far as I can see, do not speak against the possibility of maneuvering things atom by atom. It is not an attempt to violate any laws; it is something, in principle, that can be done; but in practice, it has not been done because we are too big". Since then (1959), human creativity and innovation have led to a paramount number of developments, opening the possibility to study, design and fabricate novel materials not only with top-down techniques, but also with bottom-up methods.

Nanostructured materials and their applications to various technological fields (i.e. thin film production) are literally booming during the last decades. This is not surprising, because the search for new materials with special properties is a key point to overcome the limitations posed by conventional materials and their current technological use. Nanostructures are interesting systems, since their properties often vary strongly from those of the bulk. Their reduced size influences the physical and chemical properties of the original materials.

This thesis focuses on the deposition and (electro) chemical characterisation of electrode films synthesised via an aerosol-assisted route, based on electrospraying liquid precursors. Electrospray, also referred to as Electrospraying or Electrohydrodynamic Atomization (EHDA), is a versatile technique for the production of nearly-monodispersed, highly-charged droplets that, when coupled with a reaction mechanisms (i.e. pyrolysis), allows the production of a wide variety of nanostructured functional films and materials. When pyrolysis is used as reaction mechanism, the technique is usually referred to in the literature as Electrostatic Spray Pyrolysis (ESP) or Deposition (ESD), terms that will be used interchangeably throughout this thesis. Therefore, the main focus of this thesis is related to the synthesis and deposition of nanostructured thin films as electrode materials in Li-ion batteries. It will also deal with various aspects, including the effects of the deposition parameters on the properties of the deposited layers.

The structure of the thesis consists of seven chapters that describe the main ideas developed in this work, being the experimental ones (Chapters 4, 5, 6 and 7) the ones that form the heart of this thesis. They are all summarized below.

The aim of Chapter one is to put the research topic studied here into perspective. Thus, it presents some thoughts on sustainable energy in general and energy storage systems in particular, as well as where do they fit in the big picture of renewable energies. This discussion opens room to a brief historical overview of batteries, after which some generalities are explained and a comparison of the current available battery technologies are given. Finally, an introduction to the main topic of this thesis, namely thin film Li-ion batteries is discussed and some examples of materials readily available at the moment are highlighted. Chapter two describes the general theory of electrospraying and its modes of operation. The attractive features of generating charged, nearly-monodispersed droplets with tunable sizes, as well as the challenges related to the increase of their production rate are discussed. This chapter intends to show the interest in industrial and laboratory applications with regard to this technique, which allows the generation of sub-micrometric droplets while working in the cone-jet and multi-jet modes. The goal of this review is to provide a summary of electrospray applications in thin solid film deposition, as well as in the field of Li-ion batteries, i.e. cathode, anode and electrolyte materials.

One of the conclusions of this review, is that the temperature of the substrate, besides being needed as a synthesis parameter to obtain the desired material (i.e. by means of pyrolysis), is critical for the control of the layer uniformity and porosity. The porosity is a result of fast evaporation of the solvent, and increases with the substrate temperature. Optimal tuning of the temperature so as to obtain the desired structure without compromising the layer quality can be achieved by choosing a solvent with higher boiling temperature or by mixing several solvents.

It is clear that electrospray presents advantages of uniform coating of large areas, inexpensive equipment, operation at atmospheric conditions, and easy control of deposition rate and film thickness by adjusting voltage and flow rate. Utilisation of this technique in the field of thin film battery production will surely continue to rise, and new achievements in this field can be expected in the near future.

Chapter three provides an account of the different electrospray equipment used for the experiments that are described throughout this thesis, as well as which are their main differences. Moreover, a short description of a new experimental setup designed with the purpose of handling big substrates, i.e. silicon wafers, is illustrated.

Chapter four focuses on the synthesis and deposition of Fe_2O_3 and CuO nanostructured electrodes in one step via Electrostatic Spray Pyrolysis (ESP). It also offers some insight on possible shortcomings deriving from the conventional electrode fabrication, where the active materials (i.e. nanopowders) need to be processed in multi-step processes with polymeric binders/additives in order to cast laminated electrodes. During the processing, solutions containing precursor metal salts dissolved together with Polyvinylidene Fluoride (PVdF) binder are electrosprayed on a heated substrate where the generated submicron-sized droplets undergo pyrolysis. The oxide nanoparticles generated via pyrolysis of the metal precursors are in intimate contact with the binder contained in the emitted droplets during the electrospray process. The reacted droplets are at the same time directly driven on selected areas to form nanocomposite coated electrodes. The even inter-dispersion of the polymer binder on the nanoscale promotes the mutual adhesion of the nanoparticles in the deposits, acting at the same time as a barrier against their growth and agglomeration during both the synthesis process (i.e., inside the reacting droplets) and the electrochemical cycling, thus reinforcing the electrode and the overall contact with the current collector. Electrochemical tests demonstrate that the conversion reactions in these electrodes enable large initial discharge capacities, as high as 800 $mAhg^{-1}$ and 1550 $mAhg^{-1}$ for CuO and Fe_2O_3, respectively, but also reveal that capacity retention needs further improvements. It is, therefore, proposed that it is a viable approach to synthesize and assemble in one step thin nanocomposite coatings of negative electrodes at low temperature. Nevertheless, when thicker electrodes are required, it is likely necessary to include a conductive additive in the preparation, especially in presence of active materials that are poor e^- conductors.

One important remark from this chapter relate to the known shortcomings of conversion materials, e.g., initial irreversibility, limited capacity retention and slow reaction kinetics in bulk powders, can be addressed by proper electrode preparation via ESP. Indeed, one can select dedicated precursor solutions/suspensions containing all the needed components and control the composition, morphology, texture and thickness of the deposited composite layers with the active nanoparticles. The large voltage hysteresis between charge and discharge displayed by conversion materials is an intrinsic drawback that has been related to the energy barrier which must be overcome to break the M-X bonds (where X can be: F, O, S, or P). As a matter of fact, this phenomenon is particularly pronounced for fluorides and oxides, while sulfides and phosphides suffer less from it. Therefore, substituting oxygen with phosphine in the proposed synthesis process could be a possible approach to address this main issue. Moreover, the process is simple and can be conveniently optimized.

Finally, it should be mentioned that this procedure, which has been carried out here on a lab scale (i.e. deposition on coin cell cans), has the potential to be implemented into a continuous, larger scale process for full fabrication of advanced nanocomposite electrodes in a roll-to-roll process by convenient outscaling of electrospray via multiple nozzle systems or equivalent equipments like the one employed for the experiments described in Chapter 5. Chapter five examines the results obtained during a large European project which consisted on the synthesis and deposition of thin film cathodes of high voltage $LiNi_{0.5}Mn_{1.5}O_4$ on especially customized silicon wafers for the development of a novel 3D Li-ion microbattery. ESP, which is employed as synthesis and deposition technique, allows the production of layers with capacities up to the required capacity per square centimeter, by adjusting its thickness. Besides, when having a three-dimensional substrate surface, the thickness can be significantly reduced, according to the actual received surface area. The method in that respect also show acceptable homogeneity within the "holes" or "grooves" of an etched Si wafer and demonstrates its potential in the production of 3D all solid state Li-ion batteries. The influence of the synthesis parameters on the structure, texture and electrochemical behaviour of the produced electrode is investigated using different characterisation techniques.

For the production of all-solid-state-microbatteries, a specific requirement of smooth, dense layers is needed. As an important conclusion in this chapter, it is found that it is not trivial to obtain an optimum set of parameters, as they all present correlation between each other. At larger distances from nozzle to substrate (2.5 - 3 cm) the stability of the spraying was better, permitting the production of a more monodisperse jet. This parameter, together with a low flow rate and a low concentration, allows the wettability of the surface so as to obtain more density of the film. Annealing of the deposited layers at 450 Â°C improves both the cristallinity of the deposited films and the corresponding electrochemical behaviour. After this process, galvanostatic measurement yielded that the contribution to the capacity from the low voltage Mn^{3+}/Mn^{4+} redox couple is reduced, while the contribution from the high voltage Ni^{2+}/Ni^{4+} is increased. Even if the spinel can be formed at low temperature, high pyrolysis and/or annealing temperatures are needed to enhance the material crystal structure and thus its electrochemical behaviour.

Chapter six proposes the synthesis of pure $LiNi_{0.5}Mn_{1.5}O_4$ thin films followed by the application of surface modification in the form of Cr_2O_3 catalytic active sites, or 'islands'. ESP is used as synthesis technique for both materials. By tuning the spray time, the covering of the underlying $LiNi_{0.5}Mn_{1.5}O_4$ could be controlled and already after 10 minutes it presented almost full coverage of the cathode layer. The film morphology and structural characterisation is

discussed and special attention is given to the electrochemical performance. These measurements demonstrate that, although the coating does not alter the initial spinel structure of $LiNi_{0.5}Mn_{1.5}O_4$, it influences the electrochemical behaviour of the bare spinel cathode as it act as a catalyst for electrochemical processes occurring at the interface while, at the same time, improves the ionic exchange from the electrolyte into the active material enhancing the battery performance.

Structural analysis of the samples before and after coating exhibit reflection characteristics only of the LNMO cubic spinel structure for all samples, indicating that the surface modification does not change the crystallographic structure of the initial cathode. However, Cr_2O_3 seems to be present homogeneously throughout the surface of the cathode film, as suggested by elemental mapping, instead of the active sites initially intended. XRD and EDS results, together with XAS information from similar experiments, suggest the formation of an epitaxial Cr_2O_3 spinel type coating. As this coating seems to be homogeneous, it opens the possibility of using LNMO-based cathodes with such modified surface together with conventional electrolyte

The above mentioned surface modifications influence the electrochemical behaviour of the bare spinel cathode. Especially, the coating sprayed for 1 minute improves the rate capability and delivers a capacity of 140 mAh g^{-1} at C/10 rate and remarkably high capacities of 108 mAh g^{-1} at 10C and 90 mAh g^{-1} at 20C. The epitaxial growth of a Cr_2O_3 coating, that takes the spinel structure of the underlying cathode, act as a catalyst for electrochemical processes occurring at the interface while, at the same time, as it is inactive towards the organic species in the electrolyte, it hinders the formation of an SEI layer improving the ionic exchange from the electrolyte into the active material enhancing the battery performance. Nevertheless, an optimum amount of Cr_2O_3 surface modification must be present as a good relation is needed between its catalytic activity (while, at the same time, helps at suppressing SEI layer formation) and its insulating nature. Chapter seven describes some preliminary results at building a modified AFM for in situ electrochemical characterisation of Lithium-ion battery electrode surfaces on a nanometre scale. A specific application of such technique is to know if a catalytic active site on battery electrodes, like the ones that are described in Chapter six, would render faster charge transfer.

Although the machine is still far from its final aim, partial results include:

- The succesful implementation of a silicon AFM probe as an electrode in a Lithium-ion battery setup. This was proven by electrochemical curves and SEM pictures.

- In AFM experiments, a three-electrode setup with a LNMO sample as working electrode would be prefered. Ideally, simmultaneous control of both LNMO vs. Si and Si vs. Li would be needed in this system. A working three-electrode setup with LNMO as WE, Si as CE and Li as RE was achieved.
- It is possible to prelithiate probes and store them in ambient conditions, so as to use them in a later stage. However, for storage times in the order of a month, SEM pictures do show bending of the cantilever and formation of crystals on the probe.
- A topographical scan of LNMO with a lithiated probe was also accomplished. This indicates that these probes can be used for further measurements. Moreover, it was also possible to scan a similar LNMO sample immersed in liquid electrolyte with a normal (non-lithiated) probe in the AFM cell.

On the other hand, a series of suggestions in order to improve the system include:

- As the obtained electrochemical results were not very reproducible and showed significant noise, it is highly recommended to further improve the quality of the electrical connections.
- The initially observed side reactions with moisture and air could be prevented by predrying all the setup parts, including the probe, and controlling the environment with an inert gas.
- The ideal way to combine topographic and electrochemical data is to make topographic line scans and repeat these at a certain distance with a lithiated tip. A convenient distance for this has to be found.

It is thought, nevertheless, that it is possible to make a modified AFM for in situ electrochemical characterization. In such a setup topographical data would be collected in the first run of the sample by a non-lithated tip. A second run at a fixed distance from the surface with a lithiated tip would then provide data on the rate of ion transport. By combining these data, it is believed it should be possible to relate surface artifacts, e.g. a coating, to increase in ionic conductivity.

Samenvatting

De welbekende natuurkundige Richard P. Feynman zei reeds 50 jaar geleden: "Voor zover ik kan overzien, kunnen de wetten van de natuurkunde de mogelijkheid om dingen atoom voor atoom te verplaatsen niet weerleggen. Let wel, dit is geen poging om deze wetten te ontkrachten, het is gewoon weg een principe dat de mogelijkheid bevestigd. Dat het nog nooit gedaan is komt simpelweg doordat wij zelf te groot denken.". Nadien (1959) heeft 's mens creativiteit en innovatie geleid tot enorme ontwikkelingen, waarbij mogelijkheden zijn ontstaan om nieuwe materialen te bestuderen, te ontwikkelen en te produceren met behulp van zowel top-down als bottum-up processen.

Gedurende da laatste decennia is het veld van de nano-technologie, zoals bijvoorbeeld dunne-laag technologie, een booming markt. Dit is niet verbazingwekkend gezien de speurtocht naar nieuwe materialen met specifieke eigenschappen die met de standaard materialen niet bereikt kunnen worden. Nanostructuren zijn interessante systemen aangezien ze eigenschappen bezitten die veelal sterk verschillen van dezelfde materialen in bulkvorm, dit geldt zowel voor de chemische als fysische eigenschappen.

Dit proefschrift gaat in op de depositie en (elektro)chemische karakterisering van dunne-laag elektrodes gemaakt via een aerosol route, gebaseerd op het vernevelen van vloeibare uitgangsstoffen met behulp van een elektrische potential. De beoogde methode is Elektrospayen, ook wel "Electrohydrodynamic Atomization (EHDA)" genaamd. Het is een breed inzetbare techniek voor de productie van vrijwel-homogeen verdeelde, hoog-geladen druppeltjes, en indien gekoppeld aan een chemische reactie (pyrolyse) het mogelijk maakt om een breed scala aan nano-gestructureerde functionele dunne lagen en materialen te produceren. Bij gebruik van de combinatie met pyrolyse wordt de techniek Electrostatic Spray Pyrolysis (ESP) of Deposition (ESD) in de literatuur genoemd. Deze namen worden evenwel in dit proefschrift door elkaar gebruikt. De focus van het werk is de synthese en depositie van nano-gestructureerde dunne lagen voor gebruik als elektrodematerialen in Li-ionbatterijen. Tevens

wordt ingegaan op de invloed die de verschillende procesparameters hebben op de uiteindelijke eigenschappen van de elektrodes.

Het proefschrift bevat zeven hoofdstukken, waarbij de hoofdstukken 4-7 het experimentele gedeelte vormen en daarmee het hart vormen van het uiteindelijke werk. Hieronder worden alle hoofdstukken voorts kort toegelicht.

In hoofdstuk 1 zal besproken worden op waar het onderzoek in brede context staat. Hierbij wordt ingegaan op de plaats van het werk binnen duurzame energie en meer specifiek binnen energie-opslag en daarmee hoe het ingepast kan worden in het bredere perspectief van hernieuwbare energievormen. Hierbij wordt allereerst een historisch beeld gegeven van herlaadbare batterijsystemen, alvorens wordt ingegaan op de algemene principes van de huidige batterijen. Het hoofdstuk eindigt met een discussie aangaande het werk betreffende dunne-laag Li-ionbatterijen, en daaraan gekoppeld de materialen die daarvoor ontwikkeld zijn en worden.

Hoofdstuk 2 beschrijft de algemene theorie van elektrosprayen en de verschillende sprayvormen. Hierbij worden de attractieve mogelijkheden beschreven die gepaard gaan met het genereren van de vrijwel-homogeen verdeelde druppeltjes met controleerbare grootte, maar ook de uitdagingen die het verhogen van de productiesnelheid met zich meebrengt. Het hoofdstuk heeft ten doel om de potentie te laten zien voor industriële als ook laboratorium toepassingen Hierbij wordt gebruik gemaakt van een spray van submicron druppels in de zogenaamde cone-jet of multi-jet mode. Voorst geeft het een breed overzicht van de publicaties en mogelijkheden voor toepassingen aangaande vaste-stof dunne-laag depositie met name voor gebruik van deze lagen als elektrodes en elektrolyten voor Li-ionbatterijen.

Een van de conclusies uit dit overzicht is dat de temperatuur van het substraat de meest kritische parameter is voor de vorming van de micro- en/of nano-structuur van de laag en daarmee de porositeit en uniformiteit. De porositeit is een gevolg van de wijze en de snelheid waarop het oplosmiddel verdampt en wordt daarmee voornamelijk bepaald door de substraattemperatuur. Voor optimalisatie van de gewenste structuur van de elektrodes zal een adequaat oplosmiddel met een juist kookpunt gevonden moeten worden.

Een groot voordeel van deze vorm van elektrosprayen is dat gebruik maakt van eenvoudige en goedkope apparatuur waarmee uniforme lagen te maken valt over grote oppervlakken, waarbij de morfologie, de laagdikte, de depositiesnelheid, eenvoudig is te sturen door aanpassen van de procesparameters, zoals temperatuur, hoogspanning en vloeistofstroomsnelheid. Het uitnutten van deze techniek zal zeker groeien in het veld van Li-ionbatterijen, waarbij in de toekomst nieuwe resultaten zeker verwacht kunnen worden.

Hoofdstuk 3 laat de verschillede opstellingen zien die gebruikt zijn voor

de vorming van de dunne lagen voor dit proefschrift. Het gaat verder in op de verschillen tussen de opstellingen. Tevens wordt een nieuw en geavanceerd system beschreven voor het coaten van grote oppervlakken, zoals 10 inch siliciumwafers.

Hoofdstuk 4 beschrijft de depositie middels ESP in een eenstaps-proces van Fe_2O_3 en CuO nano-gestructureerde elektrodes. Daarbij laat dit hoofdstuk een aantal tekortkomingen zien bij de productie van commerciële elektrodes, waarbij de actieve componenten, zoals nano-poeders, in een multistaps-proces met bindermateriaal en additieven moeten worden gemengd en gelamineerd om de uiteindelijke elektrodes te vergaren. Gedurende het ESP proces worden de uitgangsstoffen, veelal zouten, tezamen met de binder Polyvinylidenefluoride (PVdF) gesproeid op een verwarmd substraat, waarbij de zouten in de microngrootte druppels worden gepyrolyseerd. De gevormde metaaloxide nano-deeltjes zijn hierbij in direct contact met de binder en de additieven die reeds in dezelfde druppel aanwezig waren. Dit leidt uiteindelijk tot een nano-composiet coating op het substraat. Het blijkt verder dat de toevoeging van bindermateriaal de groei en clustering van de nano-deeltjes tegengaat. Dit heeft een positief effect op de elektrochemische activiteit van de dunne laag. Testen laten dit duidelijk zien, waarbij de conversiereactie hoge initiële capaciteiten opleveren van 800 $mAhg^{-1}$ en 1550 $mAhg^{-1}$ voor respectievelijk CuO en Fe_2O_3. Het geeft tevens een sterke verbetering van de reversibele opslagcapaciteit. Het blijkt dus dat deze benadering leidt tot een dunne nano-composietlaag die geproduceerd kan worden in een stap bij relatief lage temperaturen. Even wel kan bij dikkere lagen worden uitgeweken naar extra toevoegingen van bijvoorbeeld een geleider zoals grafiet, met name indien we te maken hebben met slecht geleidende elektrodematerialen.

Een bijkomend resultaat is dat door een optimale elektrodepositie met ESP, een aantal problemen die bij bulkpoeders van conversiematerialen optreden, vermeden kan worden, zoals het initiële capaciteitsverlies, limitering van laad- en ontlaadcapaciteit en de langzame reactiekinetiek. Daarvoor is het nodig om de juiste oplosmiddelen met de gewenste uitgangsstoffen te kiezen samen met optimale procescondities om zo de samenstelling, morfologie, textuur en dikte van de lagen te controleren. Als gevolg van de energiebarrière die overwonnen moet worden om de verschillende M-X bindingen te verbreken, waarbij M het metaal is en X een van de elementen F, O, S of P, ontstaat een enorm hysteresegedrag tussen de laad- en ontlaadpotentiaal. Dit is met name het geval voor fluor en zuurstof en in mindere mate voor zwavel en fosfor. Om die reden zou introductie van fosfine in het reactieproces een mogelijkheid bieden om de hoeveelheid zuurstof in de materialen te verlagen. Al met al hebben we te maken met een eenvoudige productiemethode die daarbij ook nog simpel te

optimaliseren valt.

Hierbij zij aangetekend dat het werk alhier is beschreven voor laboratoriumschaal met elektrodes ter grootte van knoopcellen. In hoofdstuk 5 zal verder ingegaan worden op de mogelijkheid om een roll-to-roll systeem te maken met meerdere parallelle sproeimonden om zo een continueproces te creëren het depositieoppervlak te verbreden en de productiesnelheid te verhogen.

Hoofdstuk 5 beschrijft de resultaten met betrekking tot een Europees project, waarbij de synthese en karakterisering van dunne-laag hoog-voltage elektrodematerialen zoals $LiNi_{0.5}Mn_{1.5}O_4$ op specifieke siliciumwafers wordt onderzocht om zo een 3-dimensionale Li-ionmicrobatterij te fabriceren. ESP wordt hierbij gebruikt om zo een adequate capaciteit per oppervlak te verkrijgen van het gekozen kathodemateriaal door sturing van de laagdikte. Door tevens gebruik te maken van op voorhand aangeleverde 3-dimensionale siliciumoppervlakken van het substraat, waarin ofwel gaten dan wel sleuven zijn aangebracht in het silicium, kan de capaciteit per geometrisch oppervlak behoorlijk vergroot worden. Uiteindelijk zijn van deze systemen de structuur, de textuur en het elektrochemisch gedrag bepaald als functie van de depositieparameters.

Voor de productie van een volledige vaste-stof microbatterij worden specifieke eisen gesteld met betrekking tot de dichtheld en textuur van de lagen. Een belangrijke uitkomst van dit werk is dat het moeilijk is om een vaste set aan parameters te bepalen, aangezien ze allen met elkaar in verband staan. Bij grotere sproeimond tot substraatafstand (2.5 - 3 cm) wordt de stabiliteit van de spray beter. Deze afstand tezamen met een lage vloeistofstroomsnelheid met lage concentratie uitgangstoffen zorgt ervoor dat gedurende het sproeien het substraat bevochtigd blijft, zodat een dichte film verwacht mag worden. Het nadien uitstoken van de gevormde laag bij 450 °C verbetert voorts de kristallijniteit van de lagen en tevens het elektrochemische gedrag. Galvanostatische metingen tonen aan dat de contributie van het Mn^{3+}/Mn^{4+} redox niveau significant wordt verlaagd terwijl dat van Ni^{2+}/Ni^{4+} wordt verhoogd. Er wordt in dit hoofdstuk eveneens getoond dat een laag, gevormd bij lage depositietemperatuur, pertinent een uitstookprocedure zal moeten ondergaan om de juiste kristalstructuur en optimaal elektrochemisch gedrag te verkrijgen.

In hoofdstuk 6 worden dunne lagen van $LiNi_{0.5}Mn_{1.5}O_4$ gemaakt waarop een coating van Cr_2O_3 wordt afgezet met behulp van ESP, waarbij dit Cr_2O_3 gebruikt zal worden als katalytisch actieve plekken. De depositie van deze Cr_2O_3 lagen wordt geoptimaliseerd en na reeds 10 minuten is het mogelijk om een volledige coating te verkrijgen. Vervolgens worden van deze "dubbel"lagen de morfologie en structuur als ook het elektrochemisch gedrag geanalyseerd. Er blijkt dat de opslagcapaciteit van het materiaal niet wordt verhoogd, maar dat er wel een duidelijke verbetering optreedt in het vermogensgedrag van de

lagen. Dit betekent dat de additionele Cr_2O_3 laag niet deelneemt aan het intercalatieproces, maar wel zorgt dat het intercalatieproces wordt versneld en dat het materiaal een beschermende coating krijgt om degradatie in de elektrolyt tegen te gaan. Röntgendiffractieanalyse van de samples voor en na afloop van Cr_2O_3-coating laten geen verschil zien in de LNMO-laag, wat aangeeft dat er gedurende de vorming van de Cr_2O_3-coating geen verandering optreed met betrekking tot de LNMO-laag. Uit elementanalysemetingen van de Cr_2O_3-coating gemeten over het oppervlak, blijkt dat het gevormde Cr_2O_3 homogeen verdeeld is over de LNMO-laag en geen eilndjes van Cr_2O_3 vormt. Uiteindelijk kan geconcludeerd worden dat de gevormde Cr_2O_3-coating epiaxiaal gegroeid is op de LNMO-laag, wat mogelijkheden biedt om de LNMO-laag volledig te beschermen tegen nevenreacties met de elektrolyt.

De gevormde Cr_2O_3 coating beinvloed sterk het elektrochemisch gedrag van het LNMO. Met name in het geval van een coating aangebracht in een minuut sproeien levert een sterk verhoogd maximaal vermogen op van LNMO, waarbij tevens een hoge lithiumopslagcapaciteit wordt behaald. Deze resultaten laten waarden zien van een capaciteit van 140 $mAhg^{-1}$, 108 $mAhg^{-1}$ en 90 $mAhg^{-1}$ bij ontlaadsnelheden van respectievelijk C/10, 10C en 20C. Klaarblijkelijk werkt de epitaxiale Cr_2O_3-coating als katalysator om de ionen en elektronen versneld de LNMO-laag in en uit te krijgen, Daarbij beschermt het tevens de LNMO-laag voor vorming van een blokkerende zogenaamde Solid-Electrolyte Inteface. Optimalisatie van de laagdikte van de Cr_2O_3-coating is hierbij nog steeds van belang.

Hoofdstuk 7 beschrijft enkele initiële resultaten aangaande de gemodificeerde AFM opstelling voor in-situ elektrochemische analyse op nanometerschaal van Li-ionbatterij-elektrodes. De opstelling is zodanig opgezet om lokaal op nanometerschaal katalytische werking te zien van oppervlaktedeeltjes, zoals beschreven in hoofdstuk 6.

Ondanks dat het apparaat verre van optimal is, kan een aantal resultaten hier reeds vermeld worden:

- succesvolle implementatie van een silicium AFM-tip, zoals getoond met behulp van elektrochemische metingen en elektronmicroscoop-foto's.
- voor AFM experimenten is een drie-elektrode opstelling te prefereren. In het ideale geval is controle over zowel de werkelektrode als de siliciumtip mogelijk. In dat licht is een drie-elektrode system ontwikkeld met als werkelektrode LNMO, silicium als tegenelektrode en scanning tip en lithium als referentie-elektrode.
- het is mogelijk gebleken dat geprelithieerde sliciumtips een redelijke houdbaarheidsdatum hebben, zelfs onder normale omgevingcondities. Echter

bij langdurige opslag langer dan een maand verbuigen de cantilevers.

- topografisch scannen van LNMO met een gelithieerde tip is mogelijk, zodat de methode verder gebruikt kan worden voor vervolgstudies. Daarnaast was het mogelijk om evenzo een scan te maken van LNMO ondergedompeld in vloeibare elektrolyt met een niet-gelithieerde tip.

Naast de gerealiseerde resultaten wordt een aantal suggesties gedaan om het system verder te verbeteren, zoals:

- verbeteren van de elektrische aansluitingen, aangezien een aantal resultaten matig reproduceerbaar waren.
- controle over de gasatmosfeer tijdens de assemblage van de cel en het goed drogen van de onderdelen ervan, alvorens de cel in elkaar te zetten. Evenzo zal de gasatmosfeer gedurende de metingen gecontroleerd moeten worden.
- het opnemen van een topografische line-scan met een gelithieerde tip, indien topografische en elektrochemische metingen gekoppeld worden en herhaal deze meting bij verschillende tip-elektrode afstanden om zo de optimale afstand te bepalen.

Er wordt hoe dan ook niet getwijfeld aan het feit dat het mogelijk is om met deze gemodificeerde AFM methode in-situ elektrochemische metingen te doen. In zo'n topografische meting worden allereerst gegevens verzameld zonder een gelithieerde tip. In een tweede meting kan dan bij gefixeerde afstand van de tip tot de elektrode een elektrochemische meting gestart worden voor analyse van het lithiumtransport. Door combinatie van deze gegevens moet het mogelijk zijn om posities te bepalen die afwijkend elektrochemisch gedrag vertonen in ofwel positieve dan wel in negatieve zin.

Acknowledgments

It's been four intense years. Four intense years where I was able to pursue and follow one of my personal dreams and goals since I was a little child. Ever since I remember, and as I think the people closer to me would also do, this is what I wanted to do. But apart from this personal pursuit, and perhaps more importantly, these four years have been eye-opening in many aspects, one of which plays a crucial role: the wonderful people I have met, YOU, to whom this piece of my book is dedicated. All of you so different but at the same time so similar that I didn't even imagine there could be such amazing human beings everywhere in the world. There is a famous quote which is usually used with a negative connotation (and this is gladly and absolutely not my case) which goes something like: "you can choose your friends, but you can't choose your family". I would disagree with it or at least would like to rewrite it. The way I read it, is more like: "you can always choose new members to your family". That other family with which you share only a tiny bit less genetic information compared to your biological family, your friends. All this time in Delft wouldn't have been the same, and I dare to take it even to the next level, wouldn't have been possible, without the direct or indirect help, support and love of all of you people who shared moments with me during this time.

Erik, I think you don't even start to imagine how I have you in such a high esteem. Not only I respect you professionally but, more importantly, I have deep respect for you as a person. I am glad we could spend so much time together, share such wonderful experiences and achieved so many things. Believe me when I say that I have full confidence that the Bolivian Project will be something that will change the lives of many people in a good way, I think. Perhaps not exactly here in Delft, or The Netherlands, but for sure in that beautiful south american country. I hope you understand both the honour but also the responsibility this involves. I would like to thank you for all your trust, the freedom and the unconditional support you gave me during this years. Be confident that I learned a lot from you in terms of knowledge, but also from

life.

I would like to thank you Stephen not only for being my promotor and an important guide through all the procedure needed for this event to happen, but also for your valuable and expert input during my research.

To the members of the committee: Bernard, Kristina, Marc, Alan, Ekkes and Fokko, I give you my sincere gratitude for accepting my invitation to be part of this important day. I hope you appreciated the work I share with you as much as I did writing and producing it.

An important part of my PhD and quite significant time in my life I spent it at the office 1.017 in ChemE. It is not the space what is important but actually the people who came and went. Ugo, you were the first person who welcomed me in February 2009, just as I arrived for the first time there. I remember my English was not the best and it was the first time I faced an English speaking person with a (very strong) French accent. Moreover, you explained me everything related with batteries in 15 minutes. Thanks a lot for such reception and believe me when I say that I understood something (at least 5 %?). Mario, Boss, you were the person who guided me at the beginning of this journey and taught me a lot about one of my passions: beer. I'm glad we could spend some time as colleagues even if it was rather short. David, Chico, we built a strong relationship as we soon realized we shared a lot of things in common. I also consider you il mio fratello italiano and I'm very happy for all the things that are happening in your life. You are following a dream we both share by moving to Sicily. Even if it was a very scary and intense experience, I'm glad I was there when your accident happened. I admire your strength and perseverance because you overcame such event without serious consequences. Corradijn, my very dear swearing Italian. You taught me all the important words I need to know in Italian. I realized how many adjectives you can give to some mythological characters. Thanks a lot for all the scientific discussions, all the help with the autolab and for saving my sanity when I was about to lose my mind with LaTeX. Gianni, my Dutch counterpart in this Italian gang. We were both adopted and baptised as Gianni and Stefano. They made us become spoiled with food thanks to their pickyness (food nazis). Thank you for all the times we have shared together, for the 4 trendement and the awesome erwtensoup of your lovely mother (please thank her deeply, as well as your brother and father, for accepting us, your "international" friends). Even if I missed the last beerfest, I hope we can keep spending great times. Julien, thanks a lot for all the great moments we shared, not only at the office, but also at home organizing parties and dinners, or by going to Scheveningen during summer. I wish you all the success of the world for the completion of your PhD. Tobias, thanks a lot for those jokes that only you could understand (and, therefore, only you were

laughing), for all the beers we shared, the nice board game evenings and pub quizzes. Especial acknowledgement for the translation of the propositions! I wish you the greatest of success with the final part of your PhD (please give my sincere thanks to Kate as well). Raphael, you french bastard! We built a strong friendship in a short time mainly due to our similar taste for strong jokes. You, unlike me, are French...which is the only reason why I don't accept you as my brother. Thanks a lot my dear friend for all the nice moments we have shared and hope you enjoyed your visit to my beautiful homeland. Miguel, Chamo, en vos encontré un amigo y un hermano de forma inmediata. Es increíble lo similares que somos, Venezolanos y Colombianos, en muchos aspectos. Muchas gracias por estar ahí y mantener mis lineamientos políticos en regla. La cerveza en Holanda es bien sabrosa, pero cuando es mezclada con una conversación con alguien como vos, sabe incluso mejor. Muchas gracias por toda tu ayuda en todos los asuntos de la tesis, tanto en la parte científica como en la parte burocrática...sin mencionar tu ayuda como Paraninph. Manu, we have shared only a small amount of time but you are the best room mate ever. Thanks a lot for being so comprehensive with me hosting all the Colombian guests I had, and not only for not complaining but also for helping me and making them feel welcome. To all the other colleagues from the section, I would like to spend some lines on each of you but wouldn't finish. A big THANK YOU! Marco, Kostis, Anne, Giacomo, Anca, Marysia, Alper, Karol, Marilena.

A special part of these acknowledgements go to "my students", to whom I always preferred to refer to as colleagues, as the knowledge transfer was always bidirectional. Henk, you were the first student who wrote his thesis with me, based on the work we did together. Part of Chapter 5 wouldn't have been possible without your good work and effort, thank you! I hope you are still playing football. We still miss that football match we always mentioned we were going to play. Risang, your work also helped me in shaping Chapter 5, especially with your input on the fine-tuning of the big setup just after it was delivered to us. Without your help it would have taken me ages to reproduce the experiments we had performed on the small setup. Jeffrey, Chapter 6 is based on the work you carried out for your thesis. Thanks a lot not only for that but for the great mood you had, always willing to chat and joke around. Hope you keep that personality that defines you. Aletta, Chapter 7 is completely based on the great work you did. I am certainly aware of how challenging that project was and how without you taking part on it, wouldn't be even half of what it is. I'm sure you will have a great career. Thanks a lot for everything.

The technical work of this thesis wouldn't have been possible without the help of the technicians. Marcel, certainly Chapter 7 was possible because of you and your constant work and valuable input with AFM. A big thank you!

Ben, thank you for your help with the XRD and TGA measurements, not to mention for that great SAMBAL you always get for me. It has spiced my lunches for the past 2 years! To all the people involved on the development of the big electrospray setup: Duco, Bart, Alex, Nico, Piet. Chapter 5, and the work the TU Delft performed for the E-STARS project wouldn't have been possible without your great work.

Perhaps even more important that this technical work is the need of everything to run smoothly. Wil, Karin, you have been there helping me out in everything I needed. From VISA issues, contracts and travel arrangements, to housing. You made my stay in The Netherlands much easier. Even when I became "orphan" after the separation of the NSM section you continued to help me and guide me. An immense THANK YOU!

Especial acknowledgements go also to the wonderful "Dutch + One Colombian" team that went to that incredible experience in Bolivia. I was/am honored to participate in such an important endeavour and, more importantly, to share with such professional and easy going people as you. Thank you Ronald, Kees, Erik, Willem and Jaap for such an amazing memory. I hope we can continue in this project for the coming years and that everything keeps running as smooth as it has been in these years.

Apart from my life at work, there is also a group of people whose involvement in these years have helped me at making my life far from my beloved Colombia bearable. All of you, my great and dear friends, will have my sincere thanks for all the good times we spend together, not to mention all the memories that will always be with me.

Marcushof 5th floor. How to forget this crazy place with people like you: Stefi, Basti, Agnes, Klara, Kamil, Alvin, Salome, Mandy, Damian, Miren, Victor, Jaime, Augusto, Joel, Miquel, Joao, Beppe, Simone, Riccardo..and all of you I'm missing. Thanks for the dinners, parties, trips, football patchangas, winning all the football tournaments we participated in...

Binnenhof. We made a very strong bond that hasn't been lost to this day and that I hope it will never be. It's time to plan our next get together in Spain or Italy. Thank you guys for everything, for your friendship: Jelissa and Gabo (and now little lovely Matthias), Lukas, Leo, Gabriel, David, Marc, Marijita, Cristina, Vanessa, Pablo...

Marcushof 3rd floor. My last "erasmus" experience. Just as intense as the previous two. Full of incredible people eager to make friends for life. Dani (Barney), Victor, Federica, Dani (Barcelona), Ravi, Elenita, Estefania, Dani (Solo), Maite and all the rest I might be forgetting. Thanks a lot for your company and crazy moments.

Estos 5 años no hubieran sido lo mismo sin el pedacito de Colombia pre-

sente en Delft. Todos ustedes hicieron de aquellas fechas que siempre consideramos importantes, y que al estar lejos causantristeza, un poco más llevaderas y mantuvieron la nostalgia a raya, hasta donde fuera posible. Muchas gracias al "Combo Viejo" de Colombianos que siempre estuvo ahí durante todos estos años: Sebas, Fide, Juli, Andre, Jorge, Iván, Pablo (Venezolano adoptado ;)), cómo olvidar las comidas, cumpleaños, iditas a bailar salsa, empanadas, buñuelitos, frijoladas, ajíacos, etc. Muchas gracias por todos esos buenos momentos! Profe y Juan, ustedes me recibieron desde el primer día que pisé Holanda (tal y como hicieron con muchos otros compatriotas) y su casa siempre fue ese territorio que parecía Colombia y nos juntaba a todos. Fue un placer compartir con ustedes las vicisitudes del doctorado y ver como su hermosa familia crecía con el tiempo. Les deseo el mejor de los futuros!

Al "Combo Nuevo" de Colombianos, hicieron de este último año algo inolvidable. En momentos en los que quería tirar todo por la borda y salir corriendo, ustedes me distrajeron (influenciaron negativamente??) con sus invitaciones (in)oportunas a picnics, almuerzos, cenas, tomar cervecita, Bowpub, IO Cafe, Tango, etc. Cómo olvidar también este último verano lleno de actividades y conciertos en los que me autonombré su representante de "rifas, juegos y espectáculos". Muchas gracias Mauro, Damián, Lucho, Sara, Aleja Martínez, Alejita Arce, Santi De Francisco, Cata, Paulinha, Manu, Christian, Rami, Santi Ruiz, JuanCa, Dani, Nuci, César, Estefa, Cami, Tati, MariaCa,..., y todos ustedes que en este momento se me pasan. Conocerlos a ustedes influyó bastante en mi decisión de quedarme un tiempo más en Holanda y disfrutar de su compañía un poco más.

Desde la distancia estuvieron también ustedes, "Amigos de Toda la Vida", que siempre se aguantaron mis pataletas de lejanía, mis constantes quejas sobre mi país adoptivo. Fueron ustedes los que me hicieron 1000 despedidas y 1001 bienvenidas, además de siempre estar con la mejor disposición de parranda cada vez que regresaba y los hacía trasnochar. Como no mencionar también los partiditos de rigor o las jugadas interminables de rol (que ojalá nunca acabaran) o de las sesiones de juegos de mesa. Infinitas gracias Pablo, Susi, Guzmán, Linis, Aleja, Nati, Moni, Juli, Tati, Sebas Correa, Gordito, Flaca, Huffy, Cata, Sebas Peláez, Piratejo, Deivid, Tavo, Nico, Psychoman, Xavier, Caro Vargas, Enana Maldita, Salo,..., y todos los que se me pasen.

A very important part of my life that kept my brain working (partially) in order, an gave me always the energy to continue, was that of football/Futsal. How to forget all of you who have shared with me those wonderful times on the field. Tutor guys Wim, Roel, Ruud, Leon, Sybren, Jose, Jaap, Steven, Joris, Marijn, Eloi, Nuno.

How to miss the people from Doerak, the best bar in Delft, who have

quenched my thirst all these years, have accompanied me and have introduce me to such an immense amount of great beer. Thank you Marijke and husband (sorry, I forgot the name) and all the crew!

A mi familia grandota le debo todo ese cariño, amor y constante apoyo que me han brindado toda mi vida, pero especialmente estos últimos años que he estado lejos. Gracias Tías Tere, Patri, Pieda, Angie, Ceci, Mari. También tíos Mauri, Nano, Nacho. A todos los primos los incluyo en un sólo gran GRACIAS! porque me extendería más de lo que ya lo he hecho. Tía Alba, Perro Infeliz y Pablo: a ustedes especialmente va dedicada esta tesis. Gracias por ser esa segunda familia mía y por tratarme como un hijo y hermano. Los adoro a todos!

Quiero terminar con los agradecimientos más especiales para las personas más cercanas en estos últimos años y que sin ellas este viaje simplemente no hubiera sido posible. Querida Familia, gracias por ese apoyo y amor incondicional. Es increíble ese orgullo que nos brota y cómo los ojos nos brllan cada que hablamos los unos de los otros, Hermanos y Padres. Todo esto no hubiera sido posible sin ustedes y espero que eso lo tengan bien claro. Por eso este logro, como todos los demás que cada uno de ustedes ha alcanzado, es de todos. No alcanzan mis palabras para agradecerles. Pablo y Susi, qué haría yo sin ustedes? Son esas personas que cargan con la responsabilidad de conocer todo en mi vida y conocerme incluso mejor que yo mismo. Les agradezco su amor incondicional y esa voluntad de estar siempre juntos, incluso cruzando océanos. Estos 5 años de doctorado se hicieron más cortos por su hermosa compañía en esas tierras lejanas. Caro, mi Babes, eras importante en mi vida pero te convertiste en alguien indispensable. Eres mi amiga, confidente y familia en la lejanía (además mi asesora de imagen :)). Eres el apoyo diario en mi vida, la persona que comparte conmigo mis alegrıas y tristezas. Nunca bastarán mis agradecimientos para ti así que espero pagarte con mucha compañía por muchos años más, te adoro! Stefi...non so dove iniziare. Questa tesi è anche tua, come già ti avevo detto. Questi 5 anni sono stati i piu intensi della mia vita. E nessuno sa tutto quello che ho vissuto in questo tempo, come te. Tu eri la persona che mi ha evitato di diventare pazzo. Tu eri la persona che mi ha evitato di tornare di corsa in Colombia ogni giorno per gli anni passati. Grazie per essere come sei. Grazie per continuare a essere come sei, non importa le circostanze. Grazie per tutto quello che hai fatto per me e per tutto quello che continui a fare. Sono molto felice e mi sento onorato per il tuo contributo alla presentazione della mia tesi. Spero tu abbia capito che ti ho chiesto di farne parte come un modo per ringraziarti, anche se solo un po', di tutte le cose che hai fatto per me. Non voglio mai finire per ringrazi arvi. Damian, Primazo, Parcero, hemos estado juntos durante 5 años ya! Cuándo será que nos vamos

a largar de Delft? Nunca? A ti también van estos agradecimientos especiales por todo este tiempo. Gracias por compartirlo conmigo!

A sincere THANK TO ALL OF YOU!

Curriculum Vitae

Education

- 2009-2014. PhD in Chemical Engeneering: TU Delft, Delft, The Netherlands.
- 2004-2010. Diploma in Engineering Physics: EAFIT University, Medellín, Colombia.

Experience

- 2013. Consultant: Recursos Evaporíticos-COMIBOL, Bolivia
  Project: Elaboration of a Masterplan for the "Lithium Industrialization Project in Bolivia"
  Requested by: Dutch Ministry of Foreign Affairs
- 2009-2013. Researcher: TU Delft, Delft, The Netherlands
  Department of Chemical Engineering, Nanostructured Materials, Battery Lab. Advisor: Dr. Erik Kelder
- 2008. Visiting Research Assistant: CFATA-UNAM, Querétaro, México
  Thin Film Lab. Advisor: Dr. Luis M. Apatiga
- 2007. Undergraduate Research Assistant: EAFIT University, Medellín, Colombia
  Applied Electromagnetism Group, Advisor: Dr. Juan M. Jaramillo

Four year PhD Dissertation

- Title: *Advanced Thin Layer Deposition of Materials for Li-ion Batteries via Electrospray*
  Subject: Material Science, Nanostructured Materials, Electrochemistry.

- Teaching/Tutoring:
  - Summer 2012: *Characterization of electrode surfaces in Li-ion batteries using a novel AFM approach*, Aletta Kaas, MSc Thesis
  - Summer 2011: *Cr-Oxide Coating of $LiNi_{0.5}Mn_{1.5}O_4$ By Means of Electrostatic Spray Pyrolysis*, Jeffrey Ros, BSc Thesis
  - Winter 2010: *Fine-tunning of electrospray reactor for thin film battery materials*, Risang Mahendra, MSc Thesis
  - Summer 2010: *Synthesis of $LiNi_{0.5}Mn_{1.5}O_4$ by ESP as cathode material for thin film Li-ion batteries*, Henk Walpot, BSc Thesis

Conferences Attended

- **Colombia-US Workshop on Nanotechnology for Energy and Medical Applications**, Medellín, Colombia. March 11-13, **2013**. Presenter: "Synthesis of nanostructured thin films for Li-ion battery materials by means of Electrospray"
- **2012 ECS/PRIME'12**, Honolulu, HI, United States. October 7-12, **2012**. Presenter: "Effect of Cr-Oxide Partial Coating on the Electrochemical Behaviour of Thin Film HV-Spinel"
- **IMLB'12**, Jeju, South Korea. June 17-22, **2012**
- **IMLB'10**, Montreal, Canada. June 27-July 2, **2010**. Presenter: "Electrochemical Performance of Nanocomposite Fe_2O_3 and CuO Negative Electrodes for Li-ion Batteries" and "Synthesis and Deposition of Nanostructured Lithium Nickel Manganese Film as material for 3D microbatteries".

Publications

- U. Lafont, A. Anastasopol, **E. García-Tamayo**, E.M. Kelder. *Electrostatic spray pirolysis of $LiNi_{0.5}Mn_{1.5}O_4$ films for 3D Li-ion microbatteries.* Thin Solid Films 520 (2012) 3464 - 3471.
- D. Munao, M. Valvo, J. van Erven, **E. García-Tamayo**, E.M. Kelder. *Aerosol technology and Si nano-composite electrode assembly for Li-ion batteries.* Materials Research Society Symposium Proceedings 1313 (2011) 54-59.
- **E. García-Tamayo**, M. Valvo, U. Lafont, C. Locati, D. Munaó, E.M. Kelder. *Nanostructured Fe_2O_3 and CuO composite electrodes for Li ion batteries synthesized and deposited in one step.* Journal of Power Sources 196 (2011) 6425-6432.
- M. valvo, **E. García-Tamayo**, U. Lafont, E.M. Kelder. *Direct synthesis and coating of advanced nanocomposite negative electrodes for li-ion batteries via electrospraying.* Journal of Power Sources 196 (2011) 10191-10200.
- D. Munaó, J. van Erven, M. Valvo, **E. García-Tamayo**, E. Kelder. *Role of the binder on the failure mechanism of Si nano-composite electrodes for Li-ion batteries.* Journal of Power Sources 196 (2011) 6695-6702.